UNIVERSIDADE DE SÃO PAULO
INSTITUTO DE GEOCIÊNCIAS

Geologia e gênese dos depósitos de Zn-Pb de Shalipayco e Florida Canyon, centro-norte do Peru

SAULO BATISTA DE OLIVEIRA

Orientador: Prof. Dr. Caetano Juliani

Tese de Doutorado

Nº 595

COMISSÃO JULGADORA

Dr. Caetano Juliani

Dr. Peter Szatmari

Dr. Paulo César Boggiani

Dr. Nilson Francisquini Botelho

Dr. Rafael Rodrigues de Assis

SÃO PAULO
2019

Serviço de Biblioteca e Documentação do IGc/USP Ficha catalográfica gerada automaticamente com dados fornecidos pelo(a) autor(a) via programa desenvolvido pela Seção Técnica de Informática do ICMC/USP

Bibliotecários responsáveis pela estrutura de catalogação da publicação: Sonia Regina Yole Guerra - CRB-8/4208 | Anderson de Santana - CRB-8/6658

De Oliveira, Saulo Batista

Geologia e gênese dos depósitos de Zn-Pb de Shalipayco e Florida Canyon, centro-norte do Peru / Saulo Batista de Oliveira; orientador Caetano Juliani. -- São Paulo, 2018.

154 p.

Tese (Doutorado - Programa de Pós-Graduação em Recursos Minerais e Hidrogeologia) -- Instituto de Geociências, Universidade de São Paulo, 2018.

1. Florida Canyon. 2. Shalipayco. 3. Depósitos Mississipi Valley-type. 4. Grupo Pucará. 5. Evaporitos. I. Juliani, Caetano, orient. II. Título.

Agradecimentos

Caetano Juliani
Isaac Robles
Jose Diaz
Daniel Hinostroza
Nancy Tuanama
Carlos Silva
Jerry Huaman
Paulo Ravacci
Lucio Molinari
Jones Belther
Katherine Kutsumbos
Marcelo Rocha
Renato de Moraes
Rômulo Machado
Artur Almgren
Ivone Sonoki
Alyne Barros
Liliane Petronilho
Mariana Gazire
Paola Barbosa
Rafael Mota
Mauricio Pavan
Paulo Giannini
Lena Monteiro
Marianna Caran
Luis Felipe Batelochi
Paulo Boggiani
Jorge Betencourt
Colombo Tassinari
Helcio Prazeres
Marcelo Galé
Diego Gomez
Carlos Mario Misas
Mariangela Previato
Claudia Tokashiki
Lucas Cassini
Ronald Gutierrez
Paula Moura
Danielle Barbieri
Isaac Sayeg
Jonas Mota
David Dávila
Les Oldham
Claudia Passarelli
Jesus Valdivia
Dorie Chen
David Leach
Craig Johnson
Mark Cramer
Cayce Gulbransen
Thomas Monecke
Jim Reynolds
Cheryl Medford
Yuheng Liu
Vasco Loios
Marcio Sena
Maria Helena Bezerra
Giselle Magdaleno Enrich
Marcos Mansueto
Sandra Andrade
David Mann
Jens Gutzmer
Erin Marsh
Murray Hitzman
Simon Jowitt
Larry Meinert
Michele Silva
Gianna Garda
Janet Slate

E em especial à minha família, Lucas e Amanda, meu pais Ernesto e Lenice, e irmãos André e Ana

Resumo

De Oliveira, S.B., 2018, Geologia e gênese dos depósitos de Zn–Pb de Shalipayco e Florida Canyon, centro-norte do Peru, Tese de doutorado, São Paulo, Instituto de Geociências, Universidade de São Paulo, 154 p.

As mineralizações *Mississipi Valley-type* (MVT) dos depósitos de Zn–Pb de Shalipayco no centro do Peru e de Florida Canyon no norte do Peru, separados por centenas de quilômetros e hospedados na mesma sequência de rochas carbonáticas e evaporíticas de mais de mil quilômetros de extensão motivaram diversos questionamentos que vieram a compor esta tese. As questões fundamentais em que se basearam esta pesquisa são quais as possíveis conexões genéticas entre esses depósitos e como elas se relacionam com a evolução da bacia de Pucará. Assim o estudo enfoca os processos pré-, pós- e formadores do minério ocorrentes em ambos os depósitos, a idade das mineralizações, os controles estruturais e litológicos destas mineralizações, e as implicações para descoberta de novos depósitos neste contexto geológico. Estudos petrográficos, paragenéticos e de caracterização mineralógica, apoiados por análises isotópicas de carbono, oxigênio e estrôncio nos carbonatos e de enxofre, rubídio-estrôncio e chumbo-chumbo nos sulfetos permitiram identificação de fontes do fluido, de enxofre e de metal para mineralizações, a caracterização dos processos de interação fluido-rocha, das condições físico-químicas e dos mecanismos de deposição dos minérios nos depósitos de Florida Canyon e Shalipayco. As mineralogias de minério compostas por esfalerita, galena e pirita são as mesmas nos dois depósitos ocorrendo hospedadas em rochas denominadas dolomito poroso ou brecha dolomítica evaporítica. Estas rochas formam estratos permeáveis e porosos bem definidos, interpretados como fácies de ambiente deposicional sabkha intercalados em calcários finos da sequência do Grupo Pucará de idade Triássico Inferior a Jurássico Superior. Estes estratos originalmente de evaporitos provavelmente se tornaram dolomitos de granulação grossa durante diagênese de soterramento. Estes processos modificaram drasticamente as rochas originais e geraram porosidade e permeabilidade que tornaram estas rochas excelentes hospedeiras de hidrocarbonetos e mineralizações sulfetadas de Zn e Pb. Poros preenchidos por betume foram posteriormente preenchidos por esfalerita e galena e finalmente selados por dolomita tardia. Isótopos de carbono, oxigênio e estrôncio e imagens de catodoluminescência suportam a distinção de carbonatos de diagênese precoce, de diagênese de soterramento e tardios associados aos sulfetos de Zn e Pb, tanto em Florida Canyon quanto em

Shalipayco. Os isótopos de enxofre indicam mistura de fontes de enxofre reduzido (BSR, TSR e/ou degradação térmica de matéria orgânica) que teriam se acumulado nos estratos de dolomito poroso e de brecha evaporítica. A mineralização MVT é posterior à migração e acumulação de óleo, e ambas ocorrem nas mesmas rochas do Grupo Pucará. O reconhecimento de mesmas rochas hospedeiras, mesma mineralogia e em mesma paragênese, condicionada por mesmos controles estruturais nos depósitos de Shalipayco e Florida Canyon permitiu assumir mesmos processos atuantes na Bacia Pucará. Foi possível associar estes processos geradores de rocha, de estruturas, de fluidos mineralizantes e de migração destes fluidos aos principais eventos tectônicos descritos na literatura para evolução Andina peruana. A estrutura dômica de Florida Canyon provavelmente se formou por halocinese durante a orogênese Juruá (157–152 Ma); a migração de hidrocarbonetos deve ter ocorrido durante o evento Mochica (100–95 Ma); e as mineralizações MVT de Zn–Pb de Shalipayco e Florida Canyon provavelmente sincrônicas, devem ter ocorrido durante ou logo após a orogênese Peruvian (86–83 Ma). Em Florida Canyon a mineralização supergênica de Zn é dada por smithsonita, hemimorfita e goethita, tendo sido gerada predominantemente por substituição direta da mineralização hipogena. Por correlação com as mineralizações zincíferas supergênicas da Mina Grande e Cristal no mesmo distrito de Bongará, pode-se atribuir a idade do Mioceno superior à de Florida Canyon.

Palavras-chave: Florida Canyon, Shalipayco, Depósitos Mississipi Valley-type, Grupo Pucará, Evaporitos

Abstract

De Oliveira, S.B., 2018, Geology and genesis of the Zn-Pb deposits of Shalipayco and Florida Canyon, central-northern Peru, PhD thesis, São Paulo, Instituto de Geociências, Universidade de São Paulo, 154 p.

The Mississipi Valley-type (MVT) Zn-Pb deposits of Shalipayco in central Peru and Florida Canyon in northern Peru are separated by hundreds of kilometers and hosted in the same sequence of carbonate and evaporite-bearing rocks that span more than thousand kilometers in the Pucará basin motivated several questions that came to compose this thesis. Fundamental questions that underpin the research of this this study are what are the possible genetic connections between these deposits and how do they related to the evolution of the Pucará basin. This study focuses on the investigation of the pre-, post- and ore-forming processes that occurred in both deposits; the age of the ore forming events; the structural and lithological controls on mineralization; and the implications for the discovery of new deposits in the basin. Petrographic, paragenetic and mineralogical studies supported by isotopic analyzes of carbon, oxygen and strontium in carbonates and sulfur, rubidium-strontium and lead-lead in the sulfides allowed the identification of possible fluid, sulfur and metal sources for mineralization, characterization of the rock-fluid interaction processes, physicochemical conditions and ore deposition mechanisms in the Florida Canyon and Shalipayco deposits. The sphalerite, galena and pyrite mineral assemblages are the same in the two deposits and occurs in porous dolostone or evaporite dolomitic breccia. These rocks form well-defined porous and permeable strata interpreted as depositional sabkha facies intercalated with fine limestones of the Pucará Group sequence from the Lower Triassic to the Upper Jurassic. These former evaporite-bearing strata were probably altered to coarse-grain dolomite during burial diagenesis. These processes drastically modified the original rocks and generated porosity and permeability that made these rocks an excellent host for hydrocarbons and Zn and Pb mineralization. Pores filled with bitumen were later filled by sphalerite and galena and finally sealed by late dolomite. Carbon, oxygen and strontium isotopes and cathodoluminescence images support the distinction between carbonates from early diagenesis, burial diagenesis, and late Zn and Pb mineralization, both in Florida Canyon and in Shalipayco. The sulfur isotopes indicate a mixture of reduced sulfur sources (BSR, TSR and/or possibly thermal cracking of organic matter) that would have accumulated in the porous dolomite and evaporite breccia strata interpreted as sabkha facies.

The MVT mineralization occurred after the migration and accumulation of oil, in the same Pucará Group host rocks. The recognition of same host rocks, mineralogy and paragenesis, and same structural controls in the Shalipayco and Florida Canyon deposits suggests that the same processes of diagenesis and mineralization occurred on a basin-scale. It is possible to associate these processes of rock diagenesis, development of structural features and the generation and migration of the mineralizing fluids to the main tectonic events of the Peruvian Andean evolution. The Florida Canyon dome probably involved halokinesis during the Juruá orogeny (157-152 Ma). The migration of hydrocarbons probably occurred during the Mochica event (100-95 Ma) and the Shalipayco and Florida Canyon Zn-Pb MVT mineralization probably occurred during or just after the Peruvian orogeny (86-83 Ma). The supergene Zn mineralization in Florida Canyon deposit consists of smithsonite, hemimorphite and goethite which formed by direct replacement of hypogene sulfide mineralization. Supergene zinc mineralization in the Mina Grande and Cristal deposits in the Bongará district, occurred during the late Miocene, which may have also account for the supergene ores at the Florida Canyon deposit.

Keywords: Florida Canyon, Shalipayco, Mississipi Valley-type deposits, Grupo Pucará, Evaporites

Sumário

1 Introdução

A gênese de depósitos de Zn–Pb hospedados em rochas carbonáticas, denominados depósitos *Mississipi Valley-type* (MVT), tem intrigado diversos autores nas últimas décadas. Muito se avançou desde as primeiras descrições (Bastin, 1939) mas ainda existem muitas questões em aberto quanto a formação destes depósitos. A presente tese estudou dois depósitos de Zn–Pb denominados Florida Canyon e Shalipayco, hospedados na mesma sequência de rochas carbonáticas e evaporíticas do Grupo Pucará do Jurássico–Triássico, mas distando centenas de quilômetros entre si, localizados, respectivamente, nas regiões norte e central do Peru. Ambos os depósitos apresentam diversas características muito semelhantes às descritas em outros depósitos MVT ao redor do mundo. Além disso, com os resultados das novas observações de campo e em testemunhos de sondagem, e de análises de geoquímica isotópica foram possíveis novas interpretações que diferem dos modelos clássicos até então propostos para a geração dos depósitos MVT. Também são discutidos e comparados nos dois depósitos e em escala regional, a relação entre os eventos e processos geológicos formadores das mineralizações e antecessores a esta, durante a diagênese.

Nos dois depósitos a empresa Nexa Resources (anteriormente Votorantim Metais) conduz trabalhos de Exploração Mineral desde meados dos anos 2008 até o presente, dispondo de um grande acervo de dados de sondagens diamantadas ao longo dos corpos de minério. A aplicação de estudos metalogenéticos aprofundando o conhecimento de depósitos minerais em estágio de exploração mineral tem cada vez mais apresentado importantes contribuições a descoberta de novos recursos minerais e para a melhor interpretação e modelagem dos corpos de minério conhecidos. Esta tese foi desenvolvida em estreita cooperação entre a Universidade de São Paulo, a Colorado School of Mines e a empresa Nexa Resources, onde o candidato também desenvolve atividades profissionais como geólogo de exploração mineral.

Objetivos

O presente trabalho de pesquisa tem como objetivo entender a gênese e evolução dos depósitos de Zn–Pb de Shalipayco e Florida Canyon hospedados nas sequências carbonáticas e evaporíticas do Grupo Pucará. Os seguintes questionamentos foram propostos no início deste trabalho:

i) Como se formaram os depósitos de Zn–Pb de Shalipayco e Florida Canyon? Qual a natureza dos fluidos, mecanismos de precipitação, e fonte de enxofre e de metais em cada um deles?

ii) Os mesmos processos pré-, pós- e formadores do minério ocorrem em ambos os depósitos?

iii) Ocorre apenas um evento mineralizantes ou mais de um? Qual a idade da mineralização em Shalipayco e Florida Canyon? As mineralizações destes dois depósitos são sincrônicas?

iv) Qual o contexto tectônico e a sua influência na formação dos depósitos MVT do Peru?

v) Quais os controles das mineralizações de Zn–Pb presentes no Grupo Pucará? Quais são as implicações para descoberta de novos depósitos neste contexto geológico?

Hipóteses

Durante o início da pesquisa as seguintes hipóteses foram consideradas:

i) Para depósitos MVT as possíveis fontes de enxofre comumente apontadas são: água do mar conata, matéria orgânica, evaporitos, reservatórios de gás H_2S e/ou sulfetos diagnéticos, (Leach *et al*., 2005). Os principais mecanismos de precipitação dos sulfetos de zinco e chumbo normalmente são mistura de fluidos bacinais e fluidos meteóricos ou interação fluido–rocha (Sverjensky, 1986). O enxofre pode ter origem no próprio local de precipitação de sulfetos ou ser transportado. Os metais sempre são transportados a partir de diferentes fontes crustais externas à sequência carbonática, não existindo uma rocha fonte específica para sua origem (Leach *et al*., 2005).

ii) As observações de campo e descrições iniciais apontam muitas semelhanças entre os depósitos de Shalipayco e Florida Canyon. No entanto estes depósitos estão distantes aproximadamente mil quilômetros, e no distrito onde está localizado o depósito de Shalipayco, estão também presentes diversos outros depósitos de metais base relacionados a sistemas do tipo pórfiro e epitermal, levantando a hipótese de Shalipayco também ter uma possível origem magmática–hidrotermal, estando neste caso associado a um sistema do tipo *carbonate-replacement type* (CRD) (Megaw *et al*., 1988).

iii) Os depósitos MVT mundialmente conhecidos apresentam idades em geral em dois grandes períodos da história geológica, durante o Paleozoico e entre o Cretáceo e o Neógeno

(Leach *et al*., 2001). Depósitos MVT são epigenéticos por definição, com idades de formação variando de estágios diagenéticos iniciais a dezenas ou centenas de milhões de anos mais novos do que as rochas hospedeiras. A idade do Grupo Pucará é definida como do Triássico Superior a Jurássico Inferior pela presença de fósseis (Sanchez, 1995) e por idades $^{206}Pb/^{238}U$ em zircão de 201,58 ±0,17 Ma em cinzas vulcânicas intercaladas as sequências carbonáticas (Schaltegger *et al*., 2008). As relações de campo, como a ocorrência de mineralização de Zn–Pb posterior a sequências Cretáceas mais recentes que o Grupo Pucará na região de Bongará, próximo a localização de depósito de Florida Canyon, indicam idade mínima para a formação destes depósitos.

iv) A evolução tectônica dos Andes no Peru é dividida em três grandes ciclos: o ciclo pré-Andino (Pré-cambriano ao Paleozoico), um período transicional extencional no qual a Bacia Pucará se desenvolveu (Triássico Superior ao Jurássico Inferior), e o Ciclo Andino (Jurássico Inferior até o presente) (Mégard, 1987; Benavides-Cáceres, 1999). A evolução estrutural andina peruana segundo Mégard (1984) é caracterizada por sucessivos estágios orogênicos de deformação denominados: Mochica (Cenomaniano), Peruvian (Santoniano–Campaniano), Incaic (Eoceno Médio a Superior) e Quechua (Mioceno–Plioceno), aos quais a circulação de fluidos que geraram os depósitos MVT devem estar associados.

v) Os possíveis controles litológicos das mineralizações sulfetadas de Zn–Pb são os dolomitos, aos quais os corpos de minério ocorrem associados, e também as evidências de possíveis evaporitos que estiveram presentes nas sequências carbonáticas hospedeiras. Os controles estruturais por falhas são fundamentais para circulação de fluidos nas rochas encaixantes das mineralizações, ocorrendo diversas possíveis famílias de falhas com direções variadas NW, NE e N.

Com base nas amostras de afloramentos em campo e de testemunhos de sondagem disponíveis, elaborou-se um programa com objetivo de um estudo detalhado da geologia e metalogênese dos dois depósitos, buscando:

- A caracterização mineralógica da mineralização, enfocando texturas, associações paragenéticas e zoneamento metálico;

- O reconhecimento e distinção das alterações diagenéticas e hidrotermais, focando no condicionamento da mineralização;

- A aplicação de isótopos estáveis de oxigênio (O), carbono (C) e enxofre (S) buscando identificação de fontes do fluido e de enxofre a temperatura de deposição do minério por

geotermometria e a determinação das condições físico-químicas e mecanismos de deposição do minério;

- A aplicação de isótopos radiogênicos sistema Rb-Sr e sistema Pb-Pb, buscando a identificação da fonte de fluidos dos metais, a caracterização dos processos de interação fluido-rocha, e datação da mineralização.

- Atestar ao final um modelo integrado que sirva como base para um modelo de exploração para os distritos de Florida Canyon e de Shalipayco.

Estruturação da tese

Conforme previsto no regulamento do Programa de Pós-Graduação do Instituto de Geociências da Universidade de São Paulo, este doutorado será estruturado na forma de quatro artigos, sendo que dois primeiros foram submetidos para publicação em periódicos científicos internacionais especializados sobre os temas abordados, e encontram-se em revisão, enquanto que os dois últimos serão submetidos para publicação nos próximos meses.

Artigo 1

O artigo intitulado *The Zn–Pb mineralization of the Florida Canyon, an evaporite-related Mississippi Valley-type deposit in the Bongará District, Northern* Peru foi submetido ao periódico *Economic Geology* em Abril de 2018 e está em estágio de revisão no presente momento.

O objetivo deste estudo foi detalhar a mineralização sulfetada de Zn–Pb do depósito Florida Canyon, quanto a suas texturas, geoquímica, controles litológicos e estruturais e relações temporais entre elas. São apresentados dados geoquímicos isotópicos inéditos de C, O e Sr para os minerais carbonáticos e de S para os sulfetos, além dos modelos geológico e estrutural em 3D elaborado pelo autor e disponibilizado pela empresa. O texto traz novas interpretações com relação a estudos anteriores realizados no mesmo depósito para a origem da dolomitização que precede a mineralização sulfetada e também para o horizonte de rochas hospedeiras, sendo este um nível de rochas originalmente evaporíticas alteradas durante o soterramento e diagênese. O estudo ainda apresenta indícios que permitem traçar a relação temporal prévia de migração de hidrocarbonetos antes da mineralização de Zn–Pb, muitas vezes reconhecido em sistemas MVT mas ainda pouco compreendida.

Artigo 2

O artigo intitulado *Mineral characterization of the nonsulfide Zn mineralization of the Florida Canyon deposit, Bongará District, Northern Peru* foi submetido ao periódico *Applied Earth Science: Transactions of the Institutions of Mining and Metallurgy: Section B* em Abril de 2018, tendo sido aceito para publicação em Novembro de 2018.

Este texto traz a descrição inédita das mineralizações supergênicas de Zn presentes no depósito Florida Canyon. Foram utilizados neste artigo dados de caracterização mineralógica utilizando DRX e MLA–MEV para amostras de 65 sondagens. Com base em dados da literatura dos dois outros depósitos supergênicos de Mina Grande e Cristal, localizados no mesmo distrito de Bongará, no norte do Peru, foi possível estabelecer comparativos e discutir possíveis eventos recentes relacionados a gênese deste deposito.

Artigo 3

O artigo intitulado *Geology and Genesis of the Shalipayco evaporite-related Mississippi Valley-type Zn–Pb deposit, Central Peru: geological and C–O–S isotopic constraints* deve ser submetido ao periódico *Mineralium Deposita* no 1º semestre de 2019.

Este estudo aborda descrições inéditas do depósito Shalipayco em seus aspectos geológicos, geoquímicos, e no entendimento de sua origem, processo gerador e de deposição de fluidos hidrotermais mineralizantes. Contempla os dados de análises petrológicas, e de isótopos estáveis de oxigênio, carbono e enxofre para amostras selecionadas em campo de 8 sondagens e de afloramentos, além da base de dados litogeoquímicos (ICP-MS) disponibilizados pela Nexa Resources. É discutida uma possível origem da mineralização de Zn–Pb estar associada a fluidos magmáticas o que caracterizaria um depósito do tipo *Carbonate-replacement (CDR)*. O estudo revela que predominam características de sistemas MVT no depósito de Shalipayco e que estas estariam associadas a estruturas de direção principal norte. No entanto, ocorrências sulfetadas com calcopirita, galena e esfalerita aparentemente tardias, com associação geoquímica distinta (elevados valores de Ag, As, Cd, Cu, Hg e Sb), relacionadas a estruturas NW, puderam ser reconhecidas e são atribuídas a sistemas epitermais ocorrentes no distrito.

Artigo 4

O artigo intitulado *Structural control and timing of evaporite-related Mississippi Valley-type Zn–Pb deposits in Pucará Group, Northern Central Peru* deve ser submetido ao periódico *Journal of South American Earth Sciences* no 1º semestre de 2019.

Este artigo analisa as mineralizações em escala regional, apresentando uma compilação dos resultados dos estudos locais nos depósitos de Shalipayco e Florida Canyon, e também os disponíveis na literatura para a Mina de San Vicente, abordando assim os três maiores depósitos de Zn-Pb na Província MVT da Bacia Pucará. Traz como dados inéditos as análises de isótopos radiogênicos Rb-Sr e Pb-Pb e gerando assim um modelo geológico integrado útil para a geração de um modelo exploratório nestes distritos.

.

Referencias

Bastin, E.S., 1939, Contributions to a Knowledge of the Lead and Zinc Deposits of the Mississippi Valley Region, Geological Society of America, 156 p.

Benavides-Cáceres, V., 1999, Orogenic evolution of the Peruvian Andes: the Andean cycle: Geology and ore deposits of the Central Andes, v. 7, p. 61-107.

Leach, D.L., Bradley, D., Lewchuk, M.T., Symons, D.T., de Marsily, G., Brannon, J., 2001, Mississippi Valley-type lead–zinc deposits through geological time: implications from recent age-dating research: Mineralium Deposita, v. 36, p. 711–740.

Leach, D.L., Sangster, D.F., Kelley, K.D., Large, R.R., Garven, G., Allen, C.R., Gutzmer, J., Walters, S., 2005, Sediment-hosted Pb–Zn Deposits: a global perspective: Economic Geology, v. 100, p. 561–608.

Mégard, F., 1984, The Andean orogenic period and its major structures in central and northern Peru: Journal of the Geological Society, v. 141, p. 893–900.

Mégard, F., 1987, Structure and evolution of the Peruvian Andes, *in:* Schaer, J. P., Rodgers, J., (Eds)., The Anatomy of Mountain Ranges: Princeton, New Jersey, United States, Princeton University, p. 179–210.

Megaw, P.K.M., Ruiz, J., Titley, S. R., 1988, High-temperature, carbonate-hosted Ag–Pb–Zn–(Cu) deposits of northern Mexico: Economic Geology, v. 83, p. 1856–1885.

Sánchez, A., 1995, Geología de los cuadrángulos de Bagua Grande, Jumbilla, Lonya Grande, Chachapoyas, Rioja, Leimebamba y Bolívar: hojas 12-g, 12-h, 13-g, 13-h, 13-i, 14-hy 15-h, Instituto Geológico Minero y Metalúrgico Peru.

Schaltegger, U., Guex, J., Bartolini, A., Schoene, B., Ovtcharova, M., 2008, Precise U–Pb age constraints for end-Triassic mass extinction, its correlation to volcanism and Hettangian post-extinction recovery: Earth and Planetary Science Letters, v. 267, p. 266–275.

Sverjensky, D.A., 1986, Genesis of Mississippi Valley-type lead–zinc desposits: Annual Review of Earth and Planetary Sciences, v. 14, p. 177–199.

2 The Zn–Pb mineralization of the Florida Canyon, an evaporite-related Mississippi Valley-type deposit in the Bongará District, Northern Peru

Saulo B. de Oliveira[1,2], David L. Leach[3], Caetano Juliani[2], Lena V. S. Monteiro[2] and Craig A. Johnson[4]

[1]Nexa Resources, São Paulo, SP 04571-010, Brazil

[2]Institute of Geosciences, University of São Paulo, São Paulo, SP 05508-080, Brazil

[3]Center for Mineral Resources Science, Department of Geology and Geological Engineering, Colorado School of Mines, Golden CO 80401, USA

[4]U.S. Geological Survey, MS 963, P.O. Box 25046, Denver, CO 80225, USA

Abstract

The Florida Canyon evaporite-related Zn–Pb sulfide deposit, in northern Peru, is one of the largest Mississippi Valley-type (MVT) deposits in South America. Triassic carbonate and former evaporite-bearing rocks of the Pucará Group host the ore bodies that comprise two different styles: (i) predominantly stratabound ore associated with hydrocarbon-rich porous dolostones and evaporite dissolution breccias; and (ii) high-grade ore associated with evaporite breccias representing diapiric injections along faults. A dome structure defined by drillhole spatial data was likely facilitated by halokinetic processes during Andean thrusting controls the ore deposit. The NNE trending steeply dipping secondary faults linked to major northwest structures appear to control the distribution of ore grades in the deposit. The sulfide mineralization is linked to early and burial diagenetic carbonate stages that generated fluid circulation pathways, and created structural and hydrocarbon traps. The strontium, carbon, and oxygen data show isotopic signatures that support the distinction between carbonates from early diagenetic stages with no ore relations and the late carbonates associated with Zn–Pb sulfides. The MVT mineralization post-dates hydrocarbon migration and accumulation in the host rocks of the Florida Canyon deposit. The sulfur isotopic composition of ore suggest the mineralization fluid mixed with reduced sulfur derived from different sources in the basin that accumulated in the Florida Canyon dome. Local TSR within the Florida Canyon host rocks may have contributed to the reduced sulfur budget during mineralization.

Introduction

The most significant belt of Mississippi Valley-type (MVT) lead-zinc deposits in South America is hosted in the Mesozoic carbonate sequence of the Pucará Group in the central Andes. The most important deposits are San Vicente and Shalipayco, located in Central Peru, and Florida Canyon, located in the Bongará region of Northern Peru. The Florida Canyon deposit is located in the Eastern Cordillera of Peru within the boundary of the Shipasbamba community, 680 km north-northeast of Lima, in the Amazonas Department (Fig. 1). Previous work on these MVT deposits focused on the San Vicente mine (Fontbote and Gorzawski, 1990; Spangenberg et al., 1996; Spangenberg et al., 1999) and Shalipayco (Moritz et al., 1996) in the south portion of Pucará Group. For the north portion of Pucará in the Bongará District, there are studies on the hypogene and the supergene Zn mineralizations of Cristal deposit (Arfè et al., 2018; Mondillo et al., 2018a; Mondillo et al., 2018b) and on the Mina Grande supergene Zn deposit (Arfè et al., 2017a; Arfè et al., 2017b). Previous studies on Florida Canyon area include geology, mineralogy and isotope geochemistry for hypogene sulfide Zn–Pb mineralization (Reid, 2001; Basuki et al., 2008; Basuki and Spooner, 2009; Vega, 2018), and description of the nonsulfide Zn mineralization (de Oliveira et al., 2018).

The connections between evaporites and sediment-hosted Zn–Pb deposits have been mainly limited to the well-established links between the origin of the ore-forming brines from seawater evaporation and dissolved evaporite sequences (Leach et al., 2005; Leach et al., 2010 and references therein). Until recently, MVT deposits with a direct connection to evaporites and former evaporite-bearing rocks were limited to a small subset of MVT deposits. Well-known examples are the deposits of Canning Basin on the Lennard Shelf, Australia (Tompkins et al., 1994; Vearncombe et al., 1995; Warren and Kempton, 1997), Nanisivik, Canada (Ghazban et al., 1990), Gays River, Canada (Akande and Zentilli, 1984), and Pine Point district, Canada (Sasaki and Krouse, 1969). Mississippi Valley-type deposits associated with evaporite diapir and halokinetic structures are known in North Africa diapir belt, including Fedj el Adoum and Bou Jaber deposits, Tunisia (Charef and Sheppard, 1987; Bouhlel et al., 2016), Jbel Tirremi and Touissit-Bou Beker, Marocco (Bouabdellah et al., 2014; Bouabdellah et al., 2015), and in the Basque-Cantabrian Basin, Spain (Perona et al., 2018). Recent studies show that evaporite-related deposits are more important than previously recognized (Leach et al., 2014). China, for example, the world's largest producer of zinc, the resources are mainly from MVT deposits that are genetically related evaporites or former evaporites-rich rocks. These include 3 of the top 5

largest MVT deposits in the world (Huoshaoyun, Jinding, and Changba-Lijiagou) (Leach et al., 2017; Leach and Song, 2018).

Previous work on the Florida Canyon deposit did not recognize the importance of evaporites to the distribution of the mineralization (Reid, 2001; Basuki et al., 2008; Basuki and Spooner, 2009). We provide evidence that the Florida Canyon mineralization has a direct relationship with former evaporites, evaporative facies, and evaporite-related structures in the host sequence. The objective of this paper is to characterize the Zn–Pb sulfide mineralization to gain new understandings of the ore-forming processes based in part on the application of O, C and Sr isotope data for host rock carbonate minerals and S isotope data for sulfides. These data, together with the results of mineralogical, petrographic and field descriptions of the mineralization, provide a foundation for establishing the genesis of the Zn–Pb mineralization in the Florida Canyon deposit. Furthermore, the insights into the Florida Canyon deposit will contribute to a better understanding of similar deposits in the Pucará basin and provide guides for exploration targeting in the extensive carbonate sequence of the basin.

Geological Setting

Pucará Group sequence

The Florida Canyon deposit is hosted in carbonate rocks of the Pucará Group, a sedimentary unit that is more than 1,500 meters thick and extends in a NNW belt approximately 1,000 km from the Central to the North of Peru in the Sub-Andean fold and thrust belt (Mégard, 1984). The Pucará Basin developed during the first major period of the Andean Cycle, an extensional phase of the opening of the Atlantic Ocean from the Late Triassic to the Late Cretaceous (Mégard, 1984, 1987; Benavides-Cáceres, 1999). Detailed stratigraphic studies that mainly focused on the southern portion of the basin show the Pucará Group thickens progressively from west to east in the form of a half-graben within a continental margin rift basin (Fontboté, 1990; Rosas et al., 2007).

The oldest rocks in the Bongará region are Precambrian gneisses, mica schists, phyllites, and quartzites of the Marañon Complex. These rocks are covered unconformably by the Lower Triassic Mitu sequence, which consists of volcanic epiclastic rocks, red sandstones and polymictic conglomerates (Fontboté, 1990; Rosas et al., 2007). These units are the basement for the carbonate platform rocks of the Pucará Group. The Mitu volcano-sedimentary sequence

reflects the initial basin rifting linked to strike-slip fault-controlled subsidence that ceased by the Late Permian (Rosas et al., 2007). The Pucará phase of the basin formation comprises the first marine sequences with epicontinental evaporites and carbonate sedimentation during the Late Triassic–Early Jurassic (Benavides-Cáceres, 1999).

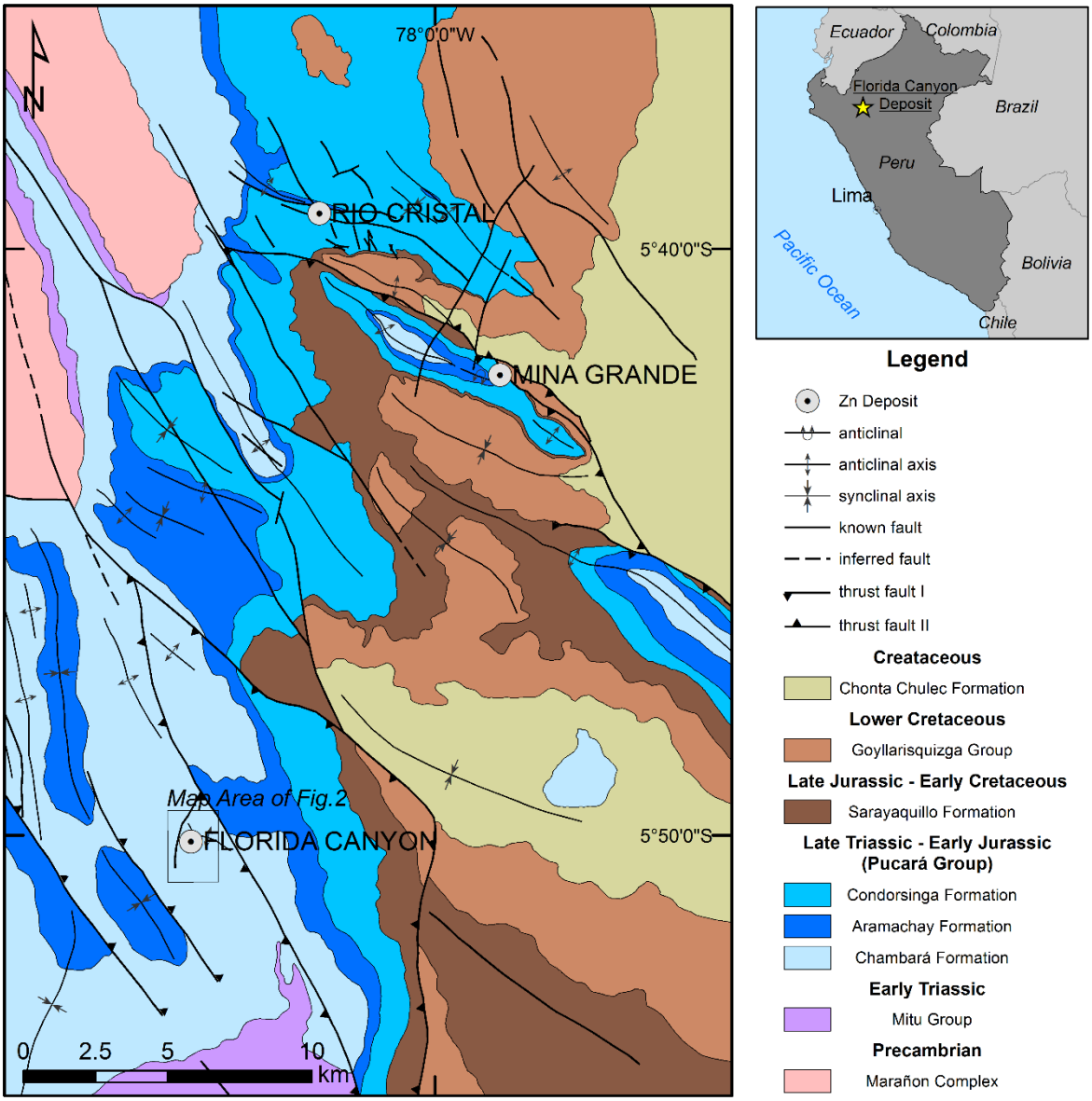

Fig. 1. Regional geologic map of Bongará District with the location of Zn–(Pb) deposits (modified from Wright, 2010). The location of the geological map of Florida Canyon deposit (Fig. 2) is shown the inset.

The Pucará Group comprises, from the base to the top, the Chambará, Aramachay, and Condorsinga formations that have angular unconformities in its lower contact with the Mitu Group and the upper contact with the Sarayaquillo Formation and Goyllarisquizga Group (Fontboté, 1990; Sánchez, 1995; Basuki et al., 2008) (Fig. 1). The Chambará Formation is composed of dolomitic rocks with locally interbedded limestones. Black argillaceous

limestones, sandstones, cherts, and shales of the Aramachay Formation are interpreted as deposited in a deeper-water setting. The Condorsinga Formation is dominated by limestones and shales with restricted lenses of dolostone deposited in a relatively shallow water environment (Sánchez, 1995; Rosas et al., 2007; Basuki et al., 2008).

The red beds, shales, and sandstones of Upper Jurassic to Lower Cretaceous Sarayaquillo Formation and the sandstones and siltstones of the Lower Cretaceous Goyllarisquizga Formation represent a continental depositional environment (Rosas et al., 2007). Covering this sequence is the gray limestone of the Cretaceous Chonta Formation (Sánchez, 1995). No intrusive magmatic rocks are described in the deposit region. The rocks of the Pucará Group were uplifted and deformed during post-Jurassic thrusting by the Andean tectonism (Benavides-Cáceres, 1999).

The ages of the Pucará sedimentary sequences were established by their fossil content. The fauna found in various levels of the Chambará Formation (mainly *monotis* fossils) assign a Norian depositional age for the carbonate rocks (Prinz, 1985 apud Sánchez, 1995). Schaltegger et al. (2008) determined $^{206}Pb/^{238}U$ zircon ages of 201.58 ±0.17 Ma (Rhetian–Hettangian) and 199.53 ±0.19 Ma (Hettangian–Sinemurian) from volcanic ash layers within the Aramachay Formation.

Geology of the Florida Canyon deposit

The Pucará Group in the Florida Canyon deposit contains the basal Chambará Formation limestone, dolostone, and former evaporitic rocks that overlay a fine-grained feldspar-rich sandstone of the Mitu Group with an erosional disconformity contact. The Chambará Formation is divided into three members designated: Chambará 1, 2, and 3, according to lithofacies defined by Reid (2001), Basuki et al. (2008), and Basuki and Spooner (2009).

The Chambará 1, the basal unit uncomformably overlies the Mitu clastic rocks, is composed of dark-gray to cream-color mudstones with thin intercalations of algal mats showing local wackestones layers. A finely laminated appearance is a characteristic feature of the Chambará 1. It is the thickest of the Chambará members varying between 60 m and 280 m. The depositional environment of the Chambará 1 was shallow water during a period of marine transgression or in a restricted bay in an estuarine environment (Reid, 2001; Basuki et al., 2008).

The Chambará 2 consists of relatively coarse-grained carbonates compared to the two adjacent members and include packstone, rudstone, and former evaporite. The Chambará 2

contains local fossiliferous markers, including star crinoids, sponges, coquina, and bivalve levels. The last two fossiliferous markers are the most consistent and preserved and are used as stratigraphic markers within the sequence. The upper and lower contacts of the Chambará 2 member are transitional. The intercalated layers of carbonate mudstone and former evaporite suggest deposition in a shallow hypersaline marine environment, such as a sabkha, intertidal, supratidal or saline lagoon environments. The former evaporative facies of the basal Chambará 2 member is basically dolostone in composition and is the host for the Zn–Pb mineralization. These sequences of rocks are 100 m to 180 m thick.

The Chambará 3 is composed of dark-gray lime mudstone locally with bitumen and thin interbedded shale layers with deposition in a deep basinal environment (Reid, 2001; Basuki et al., 2008). The Chambará 3 is the dominant member that crops out in the Florida Canyon deposit (Fig. 2) and has an approximate thickness between 100 m and 230 m in the studied area. The sedimentary structures of the Chambará 3 vary from laminated to turbiditic although the most dominant is a massive lime mudstone. Carbonate concretion-rich rock at the top of this member marks the contact with the Aramachay Formation.

The dominant structure in the Florida Canyon Deposit is a dome structure with a N50–60ºW trending axis defined by drilling (Figs. 3, 4). The dome is delimited by the Sam Fault in the west and by Tesoro Fault in the east. The Sam Fault has a north-northeast direction with a steep dip to the west (Fig. 5). This normal fault shows dip displacements that varies from 100 to 250 meters. The Tesoro Fault with a N15–30ºW direction is not as well known by drilling as the Sam Fault. However, the few existing data suggest a thrust fault dipping to the west with a possible posterior strike-slip component, as the contact between Chambará 2 and 3 was reached deeper in the eastern block. Vega (2018) describes that in addition to district-scale structural control of the Tesoro and Sam faults there is also a local-scale structural control with smaller N-S, SW-NE and SE-NW fault systems.

The Zn–Pb sulfide ore occurs mainly as stratabound mineralization that extends along the dome structure trending NNE with approximately two kilometers in extension (Fig. 4). The deposit can be spatially divided into four areas (Figs. 2, 3) according to geological features and dominance of different mineralization styles. The Sam Fault area is predominantly characterized by fault-controlled mineralization along its major structure (Fig. 5). The San Jorge area in the southern portion of the deposit contains the highest Zn–Pb grades in the Florida Canyon deposit (Fig. 5). The area also has the highest density of drillholes due to the presence of a short exploration gallery used for drilling access. The San Jorge area presents a northward

direction fault system that is parallel to the Sam Fault direction, with both stratabound mineralization and vertical fault-controlled mineralization (Figs. 5, 6). The Karen Milagros area in the northeast part of the deposit contains the highest concentration of stratabound mineralization. The sector between the Karen Milagros and San Jorge areas is called the Central area and is characterized by stratabound mineralization, but with fewer mineralized levels than in the Karen Milagros area.

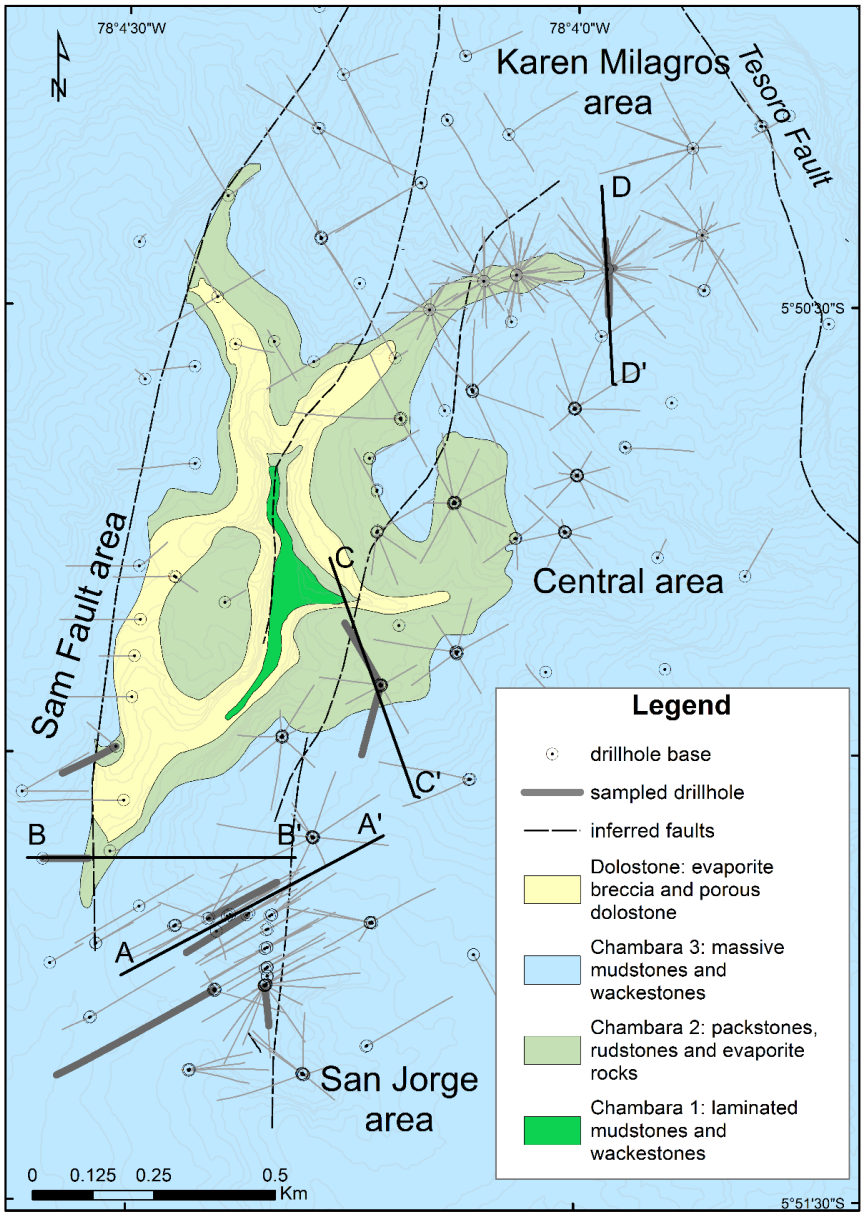

Fig. 2. Geologic map of Florida Canyon deposit with drillhole locations.

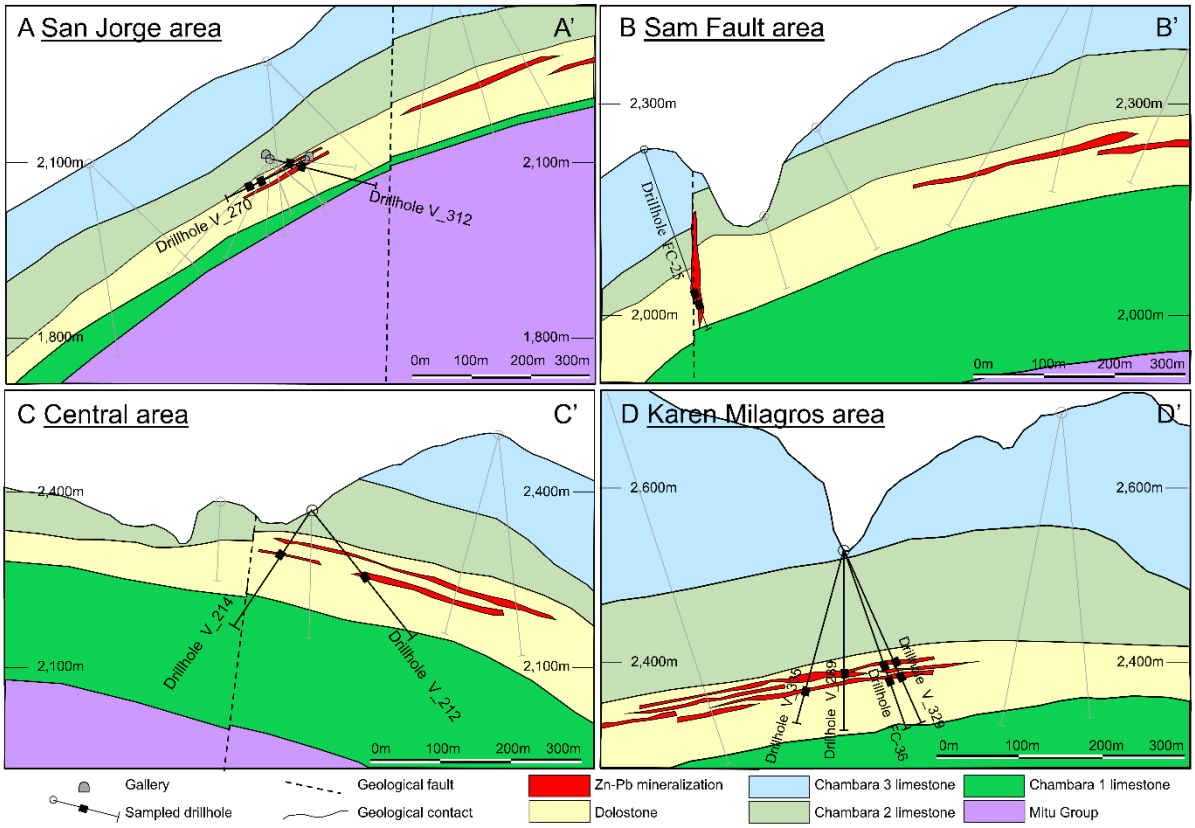

Fig. 3. Geological sections from San Jorge, Sam Fault, Central and Karen Milagros areas with sampling locations. Section locations in Fig. 2.

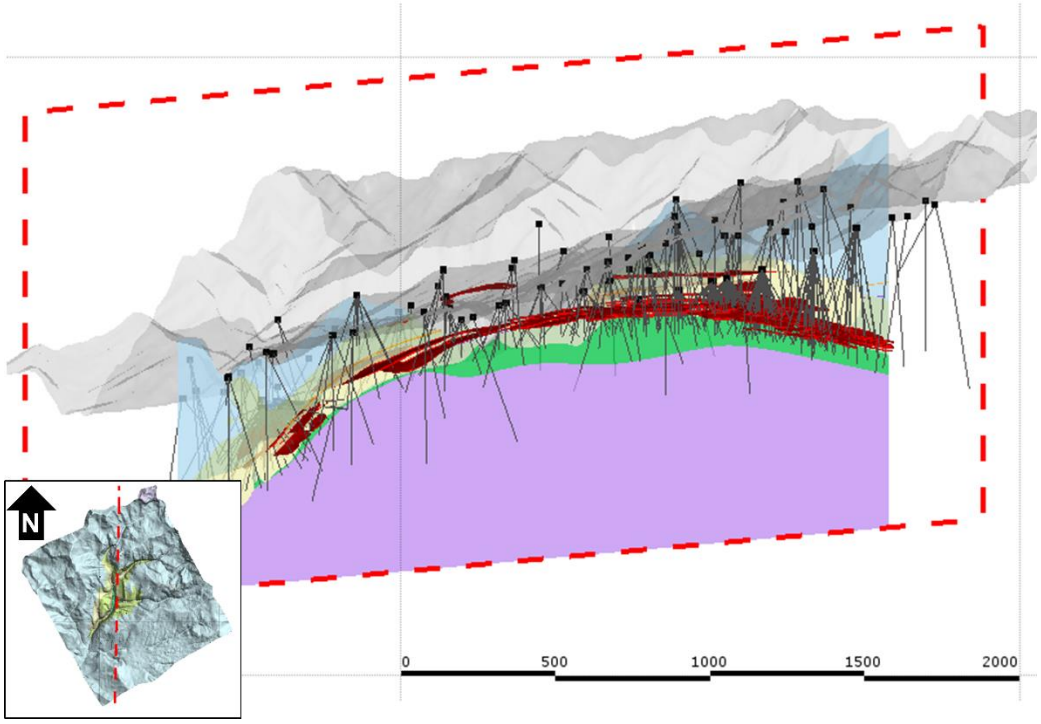

Fig. 4. Approximate N–S transversal section in a 3D view with digital terrain model and ore bodies in red color highlighting the general dome structure of the Florida Canyon deposit. Lithology color legend is the same as in Figures 2 and 3.

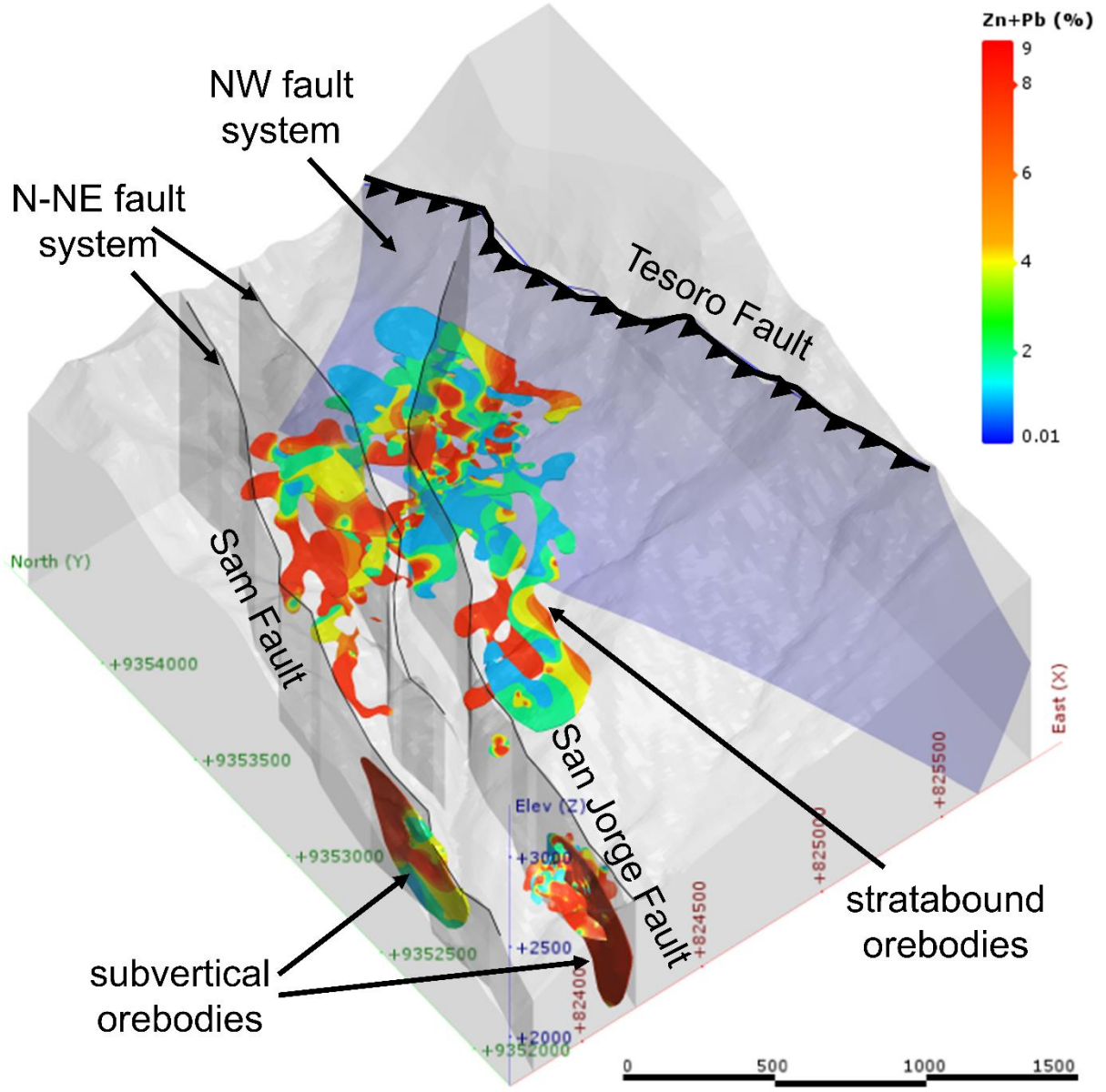

Fig. 5. Distribution of the combined zinc and lead grades along the Florida Canyon deposit with main structures in the 3D view.

Sampling and Analytical Procedures

This study is based on drill core samples selected from different areas in the Florida Canyon deposit that represent different textures, styles of mineralization and hydrothermal alteration. The sampling was designed with two main objectives: to characterize a vertical profile through the deposit stratigraphy and to reflect a general representation of the mineralization throughout the deposit. One of the deepest drillholes, V_46 with 750.50 m that covers all the local stratigraphic members, was sampled approximately every 50 m for carbon, oxygen, and strontium isotope analysis. For specific studies of the mineralization in each part

of the deposit 2 drillholes were selected in the Sam Fault area (FC-17 and FC-25), 3 drillholes in the San Jorge area (V_270, V_297 and V_312), 2 drillholes in the Central area (V_212 and V_214) and 4 drillholes in the Karen Milagros area (FC-36, V_289, V_329 and V_335) (Fig. 2).

The petrographic studies on 51 thin sections, 36 polished sections and, 39 polished thin sections were done using a Leica DM4500P optical microscope (transmitted and reflected light). For distinguishing the mineralogy and texture of different carbonate minerals the staining technique using the method described by Hitzman (1999) was applied. The carbonate thin sections were stained with a dilute hydrochloric acid solution containing both Alizarin Red S and potassium ferricyanide. Cathodoluminescence (CL) observations in carbon-coated thin sections used an HC5-LM hot-cathode microscope (14 kV and with a current density of ca. 10 $\mu A\ mm^{-2}$) coupled to a Lumic Special Microscope in the Cathodoluminescence Laboratory, at the Department of Geology and Geological Engineering, Colorado School of Mines, United States. Cathodoluminescence images were captured using a high sensitivity, double-stage Peltier cooled Kappa DX40C CCD camera.

Scanning electron microscope (SEM) images and chemical analysis were carried out on carbon-coated thin sections in a LEO 440I (Leo Electron Microscopy Ltd) platform equipped with an energy dispersive X-ray spectrometers (EDS), with Si(Li) solid-state detector Oxford Instruments Ltd, with operating conditions of 15 kV, in the Scanning Electron Microscope Lab of University of São Paulo, Brazil (LabMev-USP).

A selective sampling of different generations of carbonates was made using a diamond-drill device (Dremel 3000 model) generating mineral separate samples (mss) for grains of at least one decimeter or whole-rock samples (wrs) if the minerals were very fine grained and difficult to isolate, representing different generations of minerals. Carbon and oxygen isotope compositions of carbonate samples were determined by the continuous flow method using a Thermo Finnigan GasBench II coupled to a Delta V Advantage mass spectrometer at the Stable Isotope Laboratory, University of São Paulo, Brazil (LIESP-USP). Isotope ratios were determined on CO_2 gas released from carbonate minerals by reaction with orthophosphoric acid at 72 °C and corrected using the phosphoric acid fractionation factors given by Rosenbaum and Sheppard (1986) for dolomite. Results are reported in conventional per-mil notation (‰) relative to Vienna Pee Dee Belemnite (VPDB) and Vienna Standard Mean Ocean Water (VSMOW) standards for carbon and oxygen. The accuracy of the analysis was ±0.03‰ (1σ)

for $\delta^{18}O$ and ±0.04‰ (1σ) for $\delta^{13}C$, and the analytical precision was better than ±0.06‰ for $\delta^{18}O$ and $\delta^{13}C$ for 86 analyses of international standard NBS-19 during this study.

Strontium isotope analysis was done on splits of 44 selected carbonate samples used for stable carbon and oxygen isotope analysis at the Geochronology Center of the University of São Paulo, Brazil (CPGeo-USP). Chemical separation was conducted under clean laboratory conditions, all acids were distilled, and analysis by thermal ionization mass spectrometry (TIMS) was carried out using a Thermo Triton mass spectrometer. The precision of a single analytical result is given as two-standard errors of the mean (2σ). Mean values for $^{87}Sr/^{86}Sr$ ratio of NBS-987 Sr standard analysis during November/2015-August/2016 are 0.710237 ±0.000014 (n = 200). The $^{87}Sr/^{86}Sr$ isotope ratios were normalized to $^{87}Sr/^{86}Sr = 0.1194$.

Sulfur isotope analyses of sphalerite, galena, and pyrite were performed in the laboratories of the U. S. Geological Survey in Denver, Colorado, United States, following the procedures of Johnson et al. (2018). Isotopic compositions are reported in conventional per mil notation (‰) relative to Vienna Cañon Diablo Troilite (VCDT).

Evidence for Evaporite

In the Florida Canyon deposit there are several indicators for former evaporite being precursor to Zn-Pb mineralization such as 1) primary occurrence of evaporite in the Pucará sequence (Fig. 6); 2) pseudomorphs of evaporite minerals (Fig. 7A, B, C); 3) evaporite breccias (Fig. 7D, E); 4) porous dolostone (Fig. 7F); and 5) geometry and spatial extent of Zn–Pb ore bodies (Fig. 8).

Evaporites in the Pucará Basin

Although evaporites (gypsum, anhydrite, and halite) are present in the Pucará basin (Benavides, 1968) and the San Vicente deposit (Fontbote and Gorzawski, 1990; Spangenberg et al., 1996; Spangenberg et al., 1999), they have not been observed in the Florida Canyon deposit (Reid, 2001; Basuki et al., 2008) or in other deposits in the Bongará region (Arfè et al., 2017b; Mondillo et al., 2018a). However, the primary occurrence of evaporite minerals and sabkha facies are widely described in the carbonate sequence of the Pucará basin (Fernández Castañeda et al., 2002; Bertolotti and Moretti, 2009; Díaz and Ramírez, 2009; Moretti et al., 2013) (Fig. 6). Evaporites in the Pucará Group were first described by Benavides (1968) near

the top of the carbonate pile that could be attributed to the lower Sarayaquillo Formation or to the Pucará sequence. These evaporite-bearing layers were later confirmed by various authors (Mégard, 1978; Rosas et al., 2007; Bertolotti and Moretti, 2009; Moretti et al., 2013) to belong to both the Pucará Group and the Sarayaquillo Formation. Loughman and Hallam (1982) proposed Upper Triassic paleogeography for the evaporite-bearing sequence as a carbonate platform facing the paleo-Pacific Ocean in the west. Alternative paleogeography of the Pucará Basin placed the evaporite-bearing sequences and sabkha facies in a restricted sea that opened to the ocean in the northwest (Audebaud et al., 1973; Mégard, 1978; Fontbote and Gorzawski, 1990; Rosas et al., 2007) (Fig. 6). Evaporite was also described in the Mitu Group as originally present as thick layers that provided incompetent or lubricating layers to décollements and complex fold-thrust structures (Petersen, 1965; Mégard, 1987; Sempere et al., 2002). Mathalone and Montoya (1995), based on seismic data and inspections of petroleum exploration wells, reported the extension of the Pucará Group in the foreland basins of Marañon and Ucayali and confirmed the presence of evaporite intercalations in the sequence. Fernández Castañeda et al. (2002) reported that the upper part of the Pucará sequence is marked by evaporite sabkha deposits identified in outcrops and in the subsurface by drilling and seismic data. Jaillard et al. (2000) described Norian sequences in southern Bolivia and northern Chile begin with a basal clastic that is locally evaporitic, and evolves toward marine deposits similar to the Pucará Group.

Pseudomorphs after evaporites

Evaporites are usually rapidly removed from the rock record by dissolution and conversion of gypsum or anhydrite to carbonates during diagenesis or hydrothermal processes. Consequently, the evidence for the involvement of evaporites in the genesis of MVT mineralization can be problematic. Nevertheless, vanished evaporite minerals and ghosts of evaporite facies (Warren, 2006; 2016 and references therein) are preserved in the host rocks of the Florida Canyon deposit. Calcite pseudomorphs probable after anhydrite or gypsum occur in chicken-wire structures (Fig. 7A). Chicken-wire describes polygonal nodules of anhydrite or gypsum, typically 1-5 cm in diameter that is separated by dark stringers of other minerals, generally clays or carbonates (Dean et al., 1975). Chicken-wire nodular structures are widespread evaporite textures in both modern and ancient sabkha sediments (Hussain and Warren, 1989). Random oriented lenticular calcite laths probable after gypsum is the most

common pseudomorph texture in Florida Canyon deposit (Fig. 7B, C). Evaporite pseudomorphs are described in the Chambará Formation and evaporites are described in the Condorsinga and in the Sarayaquillo Formations in the San Vicente (Fontbote and Gorzawski, 1990; Spangenberg et al., 1996; Spangenberg et al., 1999) and Shalipayco deposits (Moritz et al., 1996).

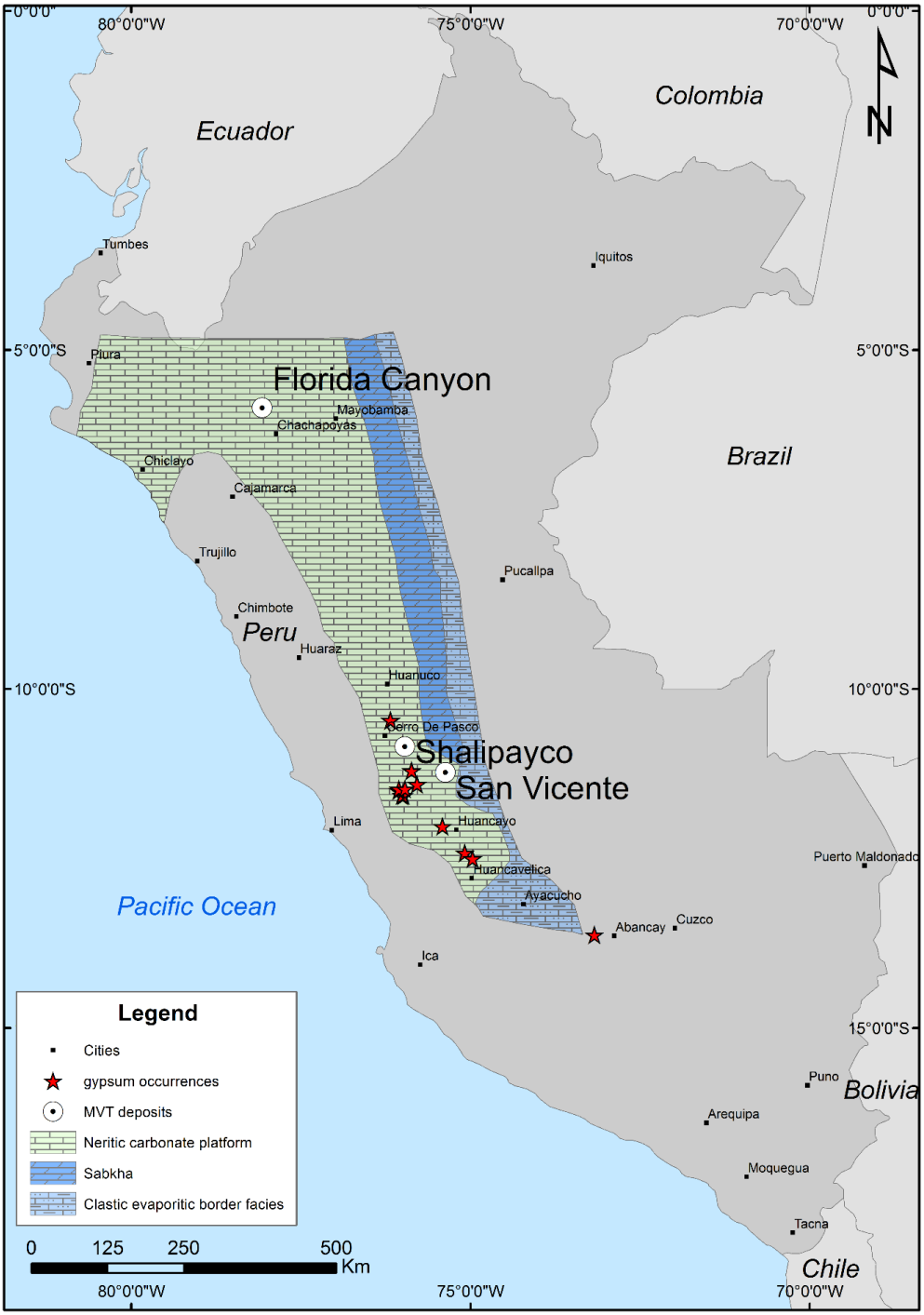

Fig. 6. Paleogeography of the Pucará basin during the Late Triassic (modified after Audebaud et al., 1973; Mégard, 1978; Fontboté and Gorzawski, 1990) with gypsum occurrences in Pucará Group (Díaz and Ramírez, 2009).

Evaporite breccia

The evaporite breccia in the Florida Canyon deposit is one of the most important hosts for Zn–Pb mineralization in the deposit and consists of two main types: bedded and halokinetic, according to the concepts of Warren (2000). The bedded evaporite breccia is characterized by sharp-edged and angular rock clasts (frequently dolostone) that appear to float with few clast-to-clast contacts in a matrix of white dolomite (Fig. 7D). The bedded evaporite breccia occurs as broad but discontinuous stratabound zones and can extend laterally for hundreds of meters. Bedded evaporite breccias are produced by the dissolution of evaporites and subsequence collapse of the enclosing dolostone host rocks. The open space created is subsequently filled by a coarse-grain carbonate matrix.

A variation of bedded evaporite breccia consists of small (centimeter-scale) host rock fragments in a sparry dolomite matrix that we interpret to have formed by the diagenetic alteration of a mixed evaporite-carbonate mud (Fig. 7G). This rock fabric has been called pseudobreccia in previous papers on the deposit (Basuki et al., 2008) and is not a true breccia in the sense of rock clasts and matrix, having been related to hydrothermal dolomitization and alteration. We do not use this term because it is a poorly defined term mainly applied to dolomitization and infrequently to mineral deposits. More detailed description of bedded evaporite breccias is given by Swennen et al. (1990), Friedman (1997), Warren (2016) and Leach and Song (2018).

The second type of evaporite breccia is the halokinetic breccia (or diapiric breccia) that is discordant to the host sequence and results from the migration of evaporites, with entrained rock clasts, along faults and structures (Hudec and Jackson, 2007). In addition to being discordant, the halokinetic breccia characteristically contains float breccia clasts that appear to have been rotated in a matrix of white dolomite and may contain clasts of rocks stratigraphically below. This texture is described as float breccia (Fig. 7E) (Warren, 2016 and references therein) and is diagnostic of halokinetic evaporite breccia and diapir zones. Halokinetic evaporite breccias are described by Hudec and Jackson (2007), and Warren (2016). The bedded and halokinetic evaporite breccias described in this paper for Florida Canyon deposit are almost equivalent to the stratigraphic and chaotic breccias described for Jinding deposit (Leach et al., 2017). Warren (2000) interpreted a pre-ore evaporite origin for these breccias for Gays River and San Vicente deposits. An evaporite origin is also attributed to ore-hosted rock in Nanisivik

(Ghazban et al., 1990) and Cadjebut deposits (Tompkins et al., 1994; Warren and Kempton, 1997).

Evaporite breccias could be misinterpreted as hydrothermal, hydraulic and karst breccias. Hydrothermal and karst breccias typically show dissolution or corrosion along the edges of the clast whereas evaporite breccia clasts are typically sharp-edged clasts (Fig. 7E). Zones of evaporite dissolution breccia have distinct or stratiform contacts with the enclosing rocks and small variations in the vertical to lateral dimensions relative to carbonate collapse breccia that can have extreme variations. Hydrothermal and karst breccias also contain abundant internal sediments derived from the dissolution of the host rocks and may have evidence of downward movement of the clasts and internal sediment (e.g., Kendall, 1960; Hill et al., 1971; Maslyn, 1977; Sangster, 1988; Kerans, 1993). Internal sediment is a clastic material derived from the dissolution of the carbonate rocks and in the case of karst breccias, material from the subareal weathering surface, which is not observed in Florida Canyon where evaporite breccia matrix is composed of massive white dolomite (Fig. 7D, E). Evaporite breccias contain little to no internal sediment. In a few MVT deposits (e.g., East Tennessee), the carbonate dissolution collapse breccia has clasts supported by internal sediment but may have limited areas where the clasts are supported by sparry carbonate matrix. These zones are limited in size, crosscut the early breccia and show unequivocal evidence that the breccias clasts were originally supported by internal sediment that was replaced by coarse carbonate (e.g., Davies and Smith, 2006). Hydraulic breccias in carbonate sequences are uncommon and are usually restricted to fault zones and was not observed in the Florida Canyon deposit.

Porous dolostone

An important host for the Zn-Pb mineralization in the Florida Canyon deposit is a hydrocarbon-rich porous dolostone. It is a coarse- to medium-grained dolostone with significant secondary porosity that typically contains abundant bitumen preserved in pores (Fig. 7F). The porous dolostone-hosted ore zones occur as stratabound bodies that are typically lenticular in shape with variable thickness and great lateral extent. Sphalerite fills porosity and occurs as a replacement of the dolostone and sparry dolomite matrix. The Florida Canyon mineralized porous dolostone resembles the host dolostone at the large MVT deposit at Huize, China (Leach and Song, 2018) and the Zn-Pb deposit of Dongmozhazhua, China (Liu et al., 2011). Similar porous dolostone also comprises important petroleum reservoirs that formed by the diagenesis

of organic-rich, evaporite-bearing carbonate sequences involving the dissolution of evaporites, conversion of the gypsum or anhydrite to calcite or dolomite, and maturation of organic matter (Sun, 1995; Zhao et al., 2014; Jiang et al., 2018).

Geometry and spatial extent of Zn–Pb ore bodies

The geological 3D implicit modeling (Cowan et al., 2002) based on approximately 117,200m of drilling in the Florida Canyon deposit, provided by the Nexa Resources Company, revealed important morphological and spatial aspects of the Zn-Pb ore bodies. The main ore bodies are stratabound and hosted within dolostone containing abundant evidence for former evaporites, evaporative carbonate facies and hydrocarbon-rich porous dolostone in the dome structure. The stratabound ore bodies follow the main dome structure that defines the deposit (Fig. 4). A NNE-striking fault system (e.g. Sam fault and San Jorge fault) confined within NW faults (Tesoro fault) cut the dome structure. There are also discordant diapiric breccia-hosted ore bodies directly associated with NNE striking faults (Fig. 8). The development of the dome could have been facilitated in part by salt tectonics (Hudec and Jackson, 2007) related to the lubricating effect of evaporites layers in the Pucará Group and in Mitu Group sequences. The discordant, sub-vertical geometry of the halokinetic breccia ore in the faults together with the stratabound mineralization reinforces the important roles of former evaporites in the Florida Canyon deposit. The ore geometry (Fig. 8) is very similar to the one proposed for Cadjebut (Fig. 16 in Warren and Kempton, 1997). The orebody geometry, occurrence, and distribution of the Zn–Pb mineralization constrain the time of the ore event to after the formation of extensive dolostone, the dome structure, and later than the extension of the ore-related NNE faults.

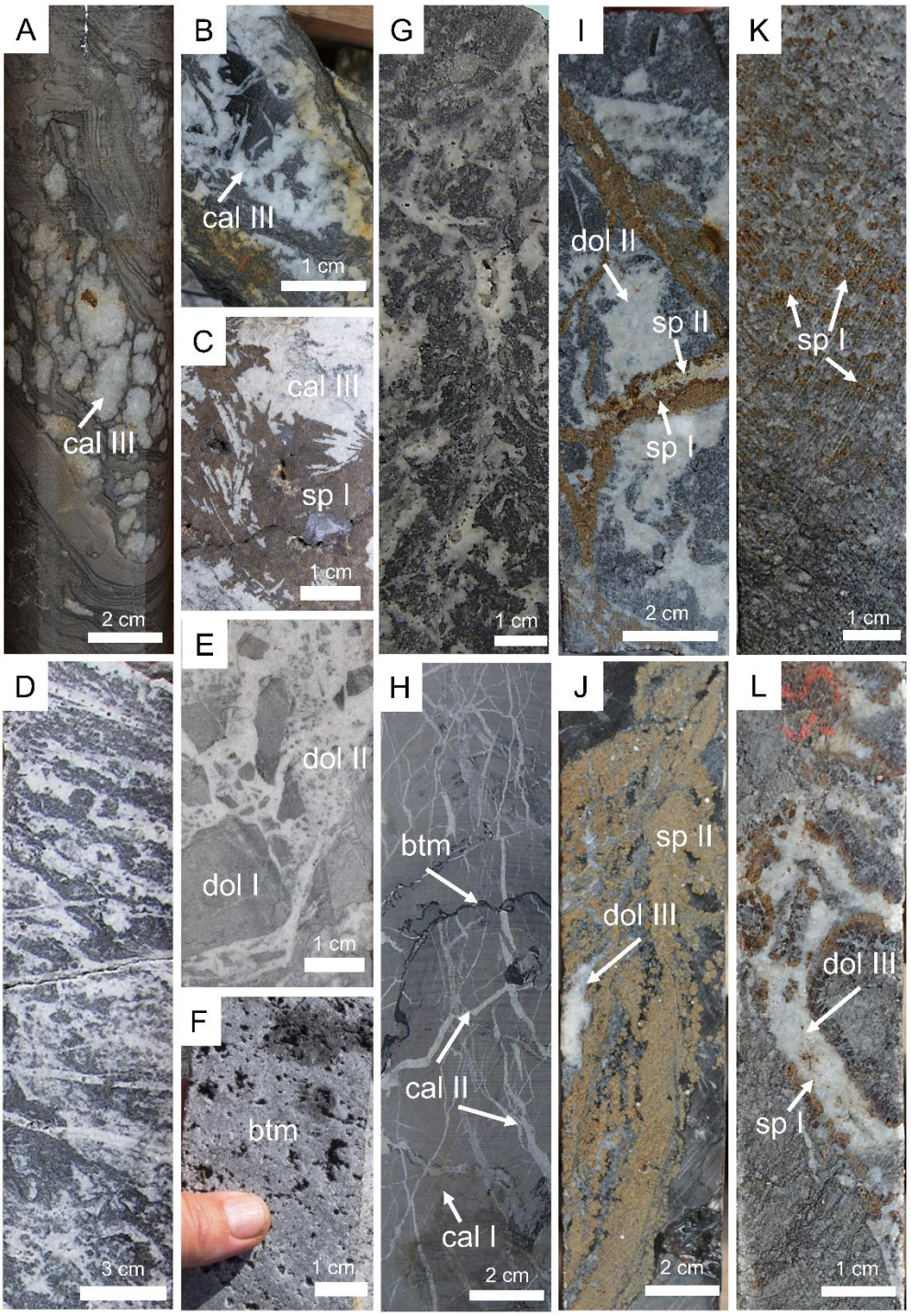

Fig. 7. Representative textures and strutures observed in drillcore. A. V_46-588.40: Calcite as evaporite pseudomorph after probable anhydrite in chicken-wire texture in limestone. B. V_46-486.40: Calcite as evaporite pseudomorph after probable gypsum. C. Calcite pseudomorph after probable gypsum or anhydrite engulfed by dark sphalerite. D. Stratabound evaporite breccia with intercalations of white and dark dolomite levels concordant with bedding. E. Halokinetic evaporite breccia, from San Jorge gallery, with angular clasts of host rock supported by dolomite matrix. F. Porous dolostone with abundant vuggy (large pores) with bitumen. G. V_297-199.10: Unmineralized evaporite breccia with dark and white dolomite in chaotic texture. H. V_46-377.20: Lime mudstone with calcite veins and stylolites containing organic matter and bitumen. I. V_297-226.40m: Dark-brown sphalerite on the edge and light-brown sphalerite in the center cutting an evaporite breccia. J. FC-28-134.10: Light-brown sphalerite in replacement texture in a former evaporite-bearing dolomite wackestone. K. FC-17-1987.70: Porous dolostone with sphalerite in pores. L. FC-23A-27.80: Sphalerite (sp I) with coarse white dolomite in open-space filling in evaporite breccia. Btm = bitumen, cal = calcite, dol = dolomite and sp = sphalerite.

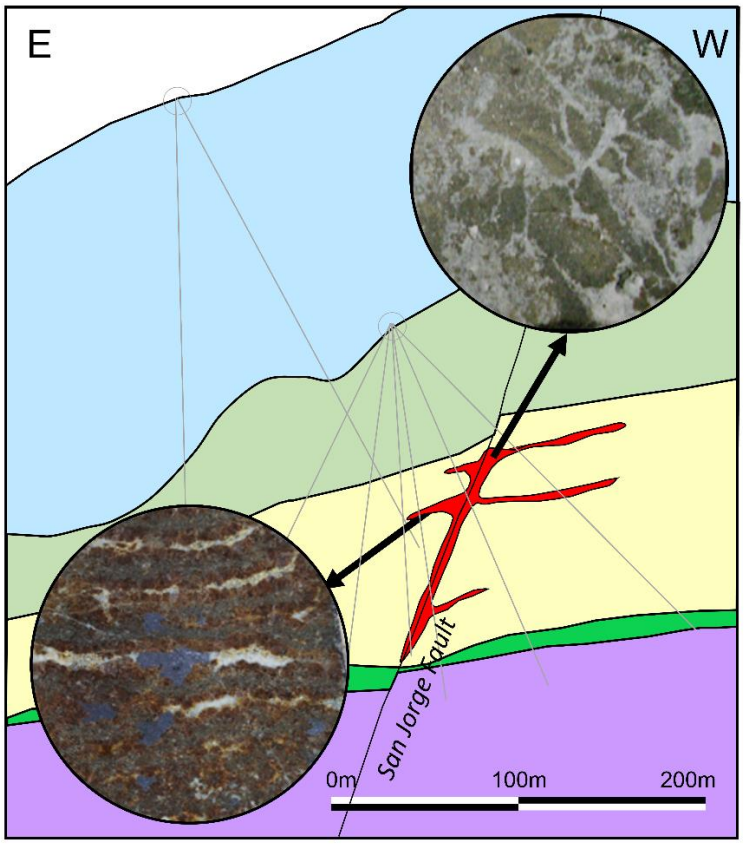

Fig. 8. Geological section from San Jorge showing the halokinetic evaporite breccia in a fault zone and stratabound evaporite breccia ore styles.

Mineralogy, Petrography and Paragenesis

The Florida Canyon deposit has a simple mineralogy in which the main host-rock minerals are dolomite, calcite, and trace quartz and the ore assemblage consists of sphalerite, galena, pyrite, and marcasite, in order of abundance. Four types of calcite, three types of dolomite, and two types of quartz, sphalerite, and pyrite were recognized. Drillcore sample descriptions and observations (Figs. 7, 9), together with mineralogy and textural relationships observed in cathodoluminescence (Fig. 10); optical mineralogy (Fig. 11); and in scanning electron microscope sections (Fig. 12) indicate three major paragenetic stages (Fig. 13).

The dark-grey limestones from the Chambará 1 and Chambará 3 members are composed of fine-grained calcite (cal I) that represent preserved sedimentary depositional textures consisting of micritic cement, bioclasts, and calcispheres. A second barren white calcite generation (cal II) occurs predominantly in millimeter to decimeter-thick veins in limestones (Fig. 7H). Calcite was identified by the strong reaction with dilute hydrochloric acid in hand samples and by pink to red color in stained thin section. A fine dark dolomite (dol I) occurs in

the Chambará 2 sabkha level as dark bands of stratabound evaporite breccia (Fig. 7D) and angular clasts in evaporite breccias (Fig. 7E). The second stage of dolomitization (dol II) is characterized by a pervasive alteration that resulted in recrystallization of the original carbonates to coarse-grained dolomite (Fig. 9) and probably was accompanied by diagenetic conversion of gypsum or anhydrite to calcite (cal III) (Fig. 7A, B, C) or dolomite (dol II) and dissolution of evaporite minerals that obliterated most of the original sedimentary structures (Fig. 11A, B). The coarse dolomite (dol II) typically has a white to beige color, occurring mainly as well-formed, coarse sparry crystals (~250 μm diameter in average) in replacement texture (Fig. 7I). This dolomite (dol II) occurs almost exclusively in the more porous and permeable carbonate and former evaporite rocks from the Chambará 2 member, described as evaporite breccia and porous dolostone. However, some dolomitization (dol II) occurred locally in the adjacent carbonate members (Chambará 1 and 3) especially in areas of fractures and faults. Quartz occurs as small crystal aggregates (< 50 μm) or as radial-fibrous chalcedony replacement within sedimentary textures or as intergrowths with second dolomite (dol II) in all the carbonate host rocks. The quartz shows euhedral hexagonal and elongated crystals associated with coarse dolomite (dol II) or occurs as fine inclusion in sphalerite.

Sphalerite and galena are the ore minerals in both stratabound and discordant orebodies. There are two types of sphalerite with different colors (Fig. 7I, J). The first is dark-brown (sp I) that commonly occurs in veins cutting evaporite breccias (Fig. 7I), as coarse grains filling pores in porous dolostone (Fig. 7K), in void filling texture (Fig. 7L), as masses and dissemination in evaporite breccias, and less frequently with replacement textures in carbonate matrix. In thin section, some dark-brown sphalerite crystals are larger than 200 μm in diameter but generally are ~100 μm on average (Fig. 9). The second type of sphalerite (sp II) has a light-brown color and is frequently associated with dark-brown sphalerite (sp I) as relatively fine grains along the borders of the sp I (Figs. 7I, 9A, 9B). The light-colored sphalerite (sp II) also occurs in replacement textures without being associated with other sulfides (Fig. 7J). The two sphalerite types clearly postdate the calcite pseudomorphs after evaporite minerals (cal III) (Fig. 7C) and the first two diagenetic dolomitization stages (dol I and dol II) (Figs. 7I, J, K, L, 9A, B).

Bitumen associated with some fine pyrite in thin veinlets are present in the mudstones of the Chambará 3 member (Fig. 9). These narrow veinlets (cal II) cut the earliest micritic calcite (cal I) and calcite vein (cal II) (Fig. 7H). Solid bitumen is also present in porous dolostone filling pores, which are cut by centimetric veins filled with dark sphalerite (sp I) and white

sparry dolomite (dol III) (Fig. 9). Sphalerite is also filling pores but there is no bitumen in the later dolomite vein (dol III) (Fig. 9B). The lack of any cement and presence of degraded hydrocarbons in the pores indicate that the burial digenetic dolomite (dol II) was the last diagenetic event before hydrocarbon emplacement and sphalerite deposition.

A third stage of dolomitization (dol III) is closely related to ore-sulfide phases (Figs. 8I, J, 9A, B). The white sparry dolomite (dol III) occurs after dark-brown sphalerite (sp I) and light sphalerite (sp II) in the open-space filling texture (Fig. 9B). This generation of sparry dolomite cuts the evaporite breccia (dol II) (Fig. 7L). Cathodoluminescence observations also show the non-luminescent sparry dolomite crystals (dol III) associated with sphalerite precipitated after the bright luminescent replacement dolomite (dol II) (Fig. 10). The vast majority of the sparry dolomite in Florida Canyon formed during diagenesis (dol II) although a minor amount, but the distinctly different stage of sparry dolomite is associated with mineralization (dol III). The burial dolomite (dol II) occurs predominantly as a replacement texture and is present throughout the Pucará basin. The ore-related sparry dolomite (dol III) occurs more frequently as fracture and void filling in the deposits and locally in the basin. White sparry calcite is present in veins ranging from few millimeters up to 1 cm in thickness, defining a fourth calcite stage (cal IV) (Fig. 11B). These calcite veins cut the dolomitized evaporite breccia. The temporal relationship of this late calcite stage (cal IV) with ore minerals may be attributed to the final mineralization stages.

Pyrite and marcasite are not restricted to the sulfide ore and can be found disseminated throughout the Chambará Formation (Fig. 11C, D). Different generations of pyrite occur (Fig. 11C, E). The most common pyrite (py I) occurs as crystals with cubic habits, granular aggregates and disseminated grains smaller than 50 μm on dolomite crystals and sphalerite. The presence of small inclusions of pyrite in late dolomite (dol III) and sphalerite (sp I) and replacement textures of sphalerite (sp I) after pyrite aggregates indicate a pyrite stage prior to mineralization (py I) (Fig. 11C). Marcasite precipitation appears to occur during and after pyrite (Fig. 11C, D) in the late mineralization stage. Another late pyrite generation (py II) is characterized by fine crystals in fractures and on edges of crystals of dolomite (dol III) and sphalerite (sp I) (Fig. 11E). Galena consists of coarse crystals associated with dark-brown sphalerite and sparry dolomite (Fig. 11F). The light-brown sphalerite (sp II) occurs along the borders of coarse sphalerite (sp I) and unlike the previous sphalerite is not associated with galena. The different colors in the two types of sphalerite could be apparently attributed to

variations of iron and zinc content (Fig. 12). The dark-brown sphalerite (sp I) contains more iron than the light sphalerite (sp II) (Fig. 12).

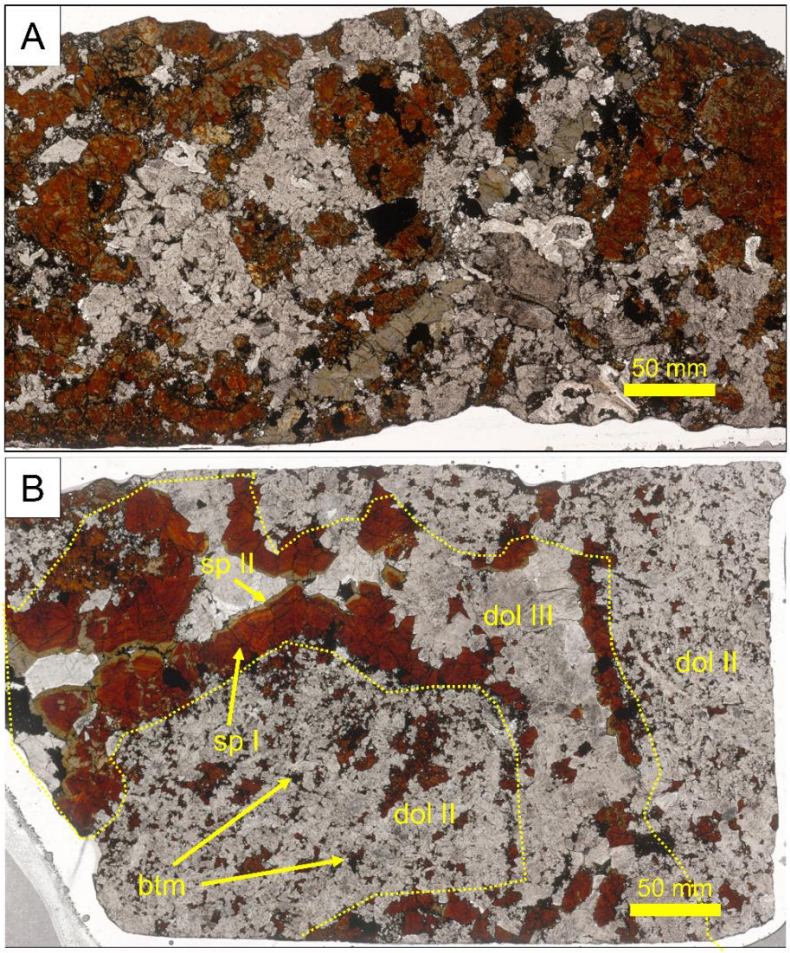

Fig. 9. Representative textures in thin sections of mineralized hydrocarbon-rich porous dolostone. A. FC-17-172.15: Porous dolostone with dark- and light-brown sphalerite and degraded hydrocarbons/bitumen (opaque), with some euhedral pyrite (opaque). B. FC-17-197.30: Porous dolostone formed during burial diagenesis (dol II) with abundant bitumen filling pores and fractures. Sphalerite I and II appear to replace former liquid hydrocarbons in pores and fractures. Hydrothermal dolomite (dol III) appears to be more closely associated with sphalerite (sp I) than burial dolomite (dol II). Btm = bitumen, dol = dolomite and sp = sphalerite

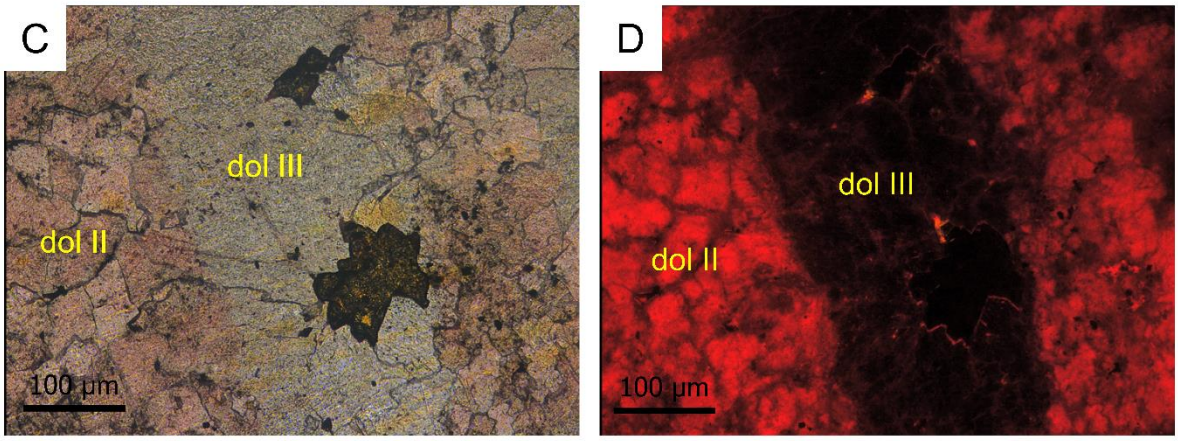

Fig. 10. Representative microscopic textures present in Florida Canyon deposit. A. V_297-226.40: Replacement dolomite (dol II) cut by white sparry dolomite (dol III) in association with sphalerite. B. V_297-226.40: Bright luminescent replacement dolomite (dol II) and non-luminescent sparry dolomite (dol III).

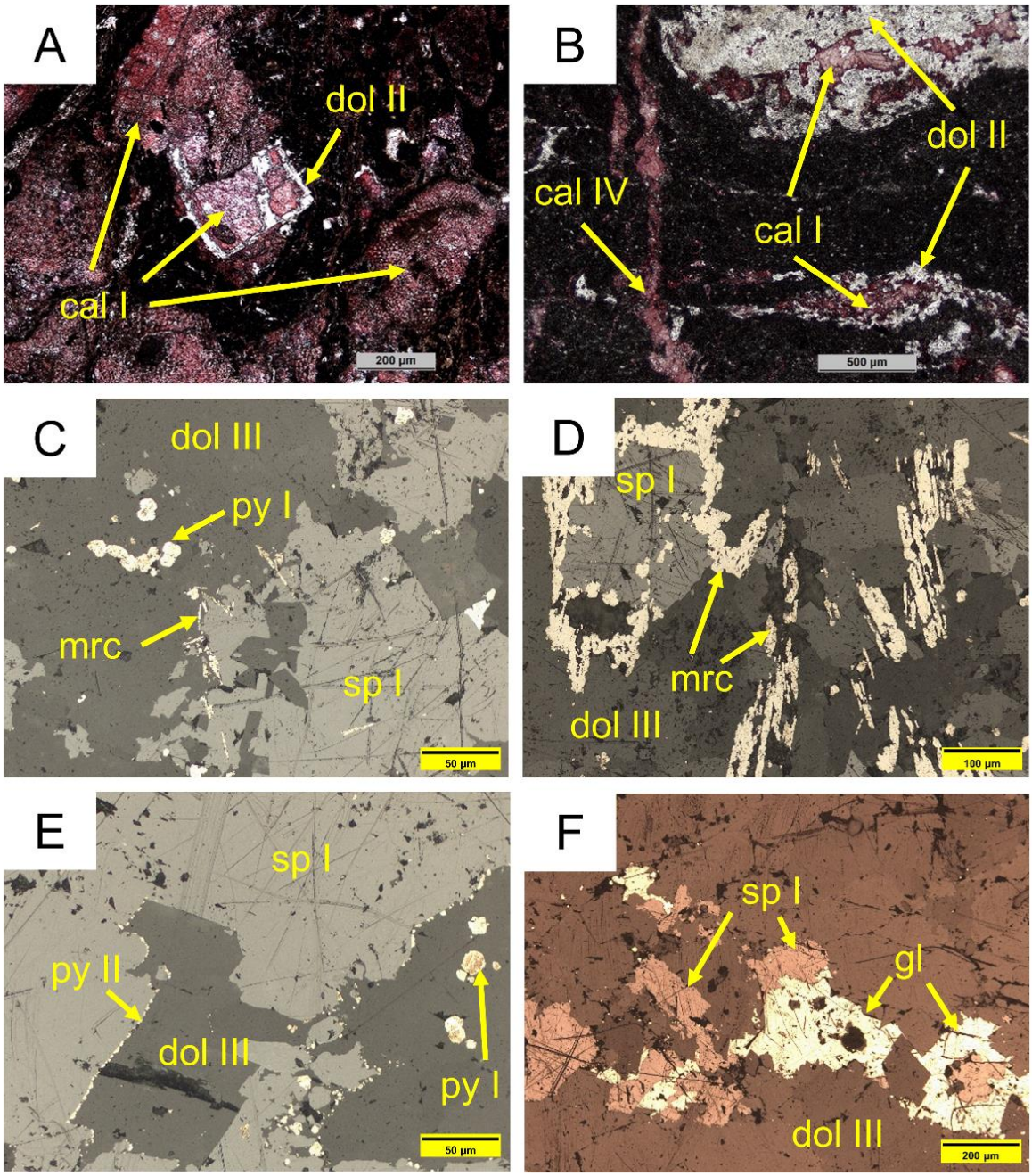

Fig. 11. Microscopic textures of host rocks and ores. A. V_46-103.30: Bioclastic lime rudstone with dolomite (dol II) replaced calcite (cal I) (stained thin section). B. V_46-588.40: Mudstone with late calcite vein (cal IV) cutting an early dolomite (dol III) vein with calcite (cal I) in the nucleus (stained thin section). C. V_199-307.00: Reflective light photomicrograph showing euhedral pyrite (py I) with dolomite (dol III) and marcasite laths associated with sphalerite (sp I). D. V_199-307.00: Marcasite laths after original pyrite bordering sphalerite (sp I). E. V_199-307.00: Early coarse euhedral pyrite and a fine-grained late pyrite in fracture filling or enveloping dolomite and sphalerite crystals. F. FC-18-97.50: Intergrowth of sphalerite (sp I) and galena in porous dolostone. Cal = calcite, dol = dolomite, gl = galena, mrc = marcasite, py = pyrite and sp = sphalerite.

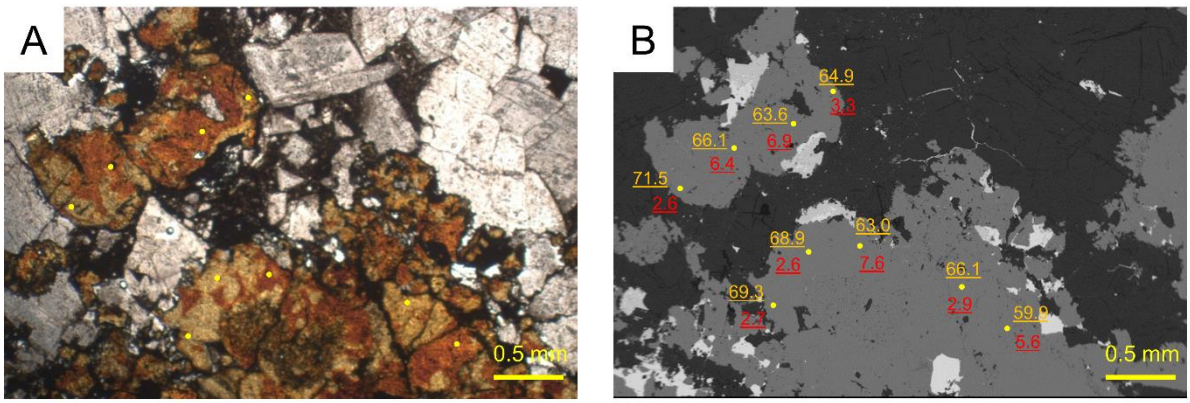

Fig. 12. A. FC-17-172.15: Thin section with dark-brown sphalerite (sp I) and light-brown sphalerite (sp II) B. Scanning electron microscope (SEM) image of the sphalerites (sp I and sp II) with EDS chemical analysis of Zn (in orange color) and Fe (in red color).

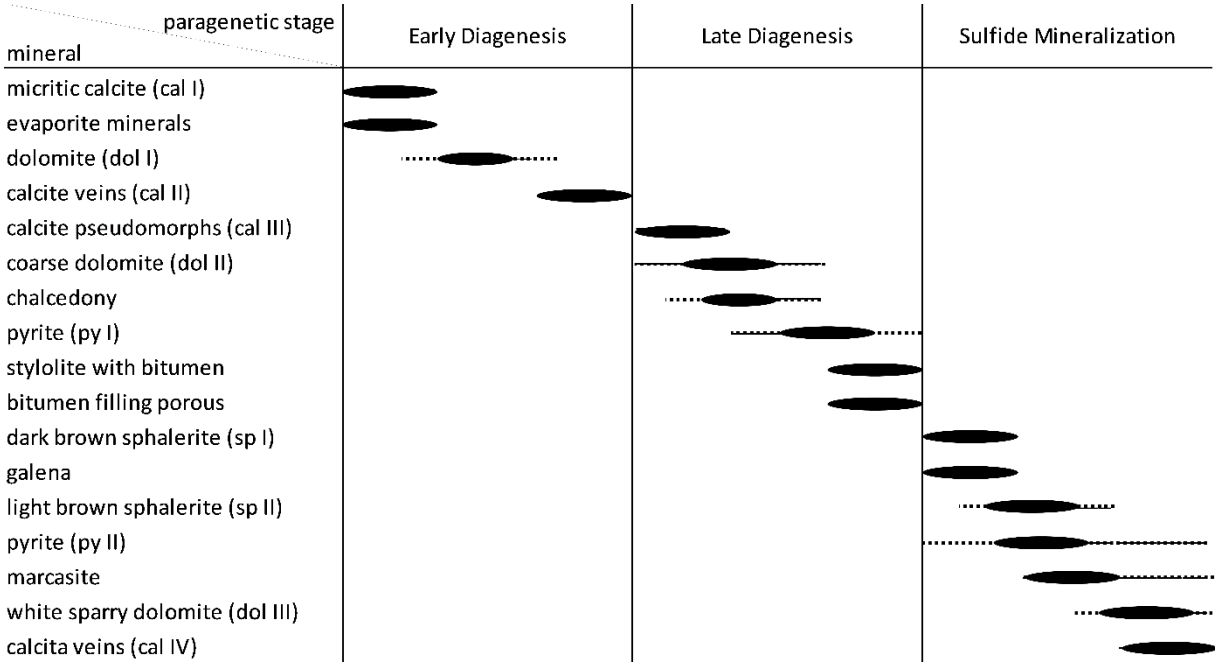

Fig. 13. Summary of the paragenetic sequence of diagenetic and ore-minerals from the Florida Canyon deposit.

Carbon and Oxygen Isotope Data

Results of carbon, oxygen, and strontium isotope analysis are given in Table 1 and shown in Figures 14 and 15. The isotopic analyses were carried out on host rocks and carbonate minerals from different stages. The host rocks comprise (1) dark-grey massive limestone, representing the least altered rocks (cal I; n = 14); (2) dolomitized evaporite breccia (dol II; n = 15); and (3) porous dolostone (dol II; n = 6), which is the altered dolostone representative of the regional dolomitization event (dol II; n = 6). The carbonate minerals include: (1) calcite

from early veins, related to early diagenesis (cal II; n = 6); (2) calcite as evaporite mineral pseudomorphs (cal III; n = 3); (3) replacement dolomite (dol II; n = 2); (4) white sparry dolomite (dol III; n = 8); and (5) late calcite in void-filling texture (cal IV; n = 6). The different carbonate generations show clustered carbon and oxygen isotope compositions in a plot of δ18O versus δ13C (Fig. 14A), which allow their separation into two groups with similar range values.

The least-altered limestone whole-rock (cal I) and calcite samples in early veins (cal II) have similar $\delta^{13}C$ (cal I = +1.0 to +2.8‰; cal II = +1.4 to +2.9‰) and $\delta^{18}O$ (cal I = +21.1 to +26.0‰; cal II = +21.8 to +25.1‰) values, forming the first group. This least-altered limestone from the Florida Canyon deposit displays $\delta^{18}O$ and $\delta^{13}C$ values that partially overlap those of the Triassic marine limestones (Veizer et al., 1999).

The second group is formed by samples of evaporite breccia, porous dolostone (dol II), replacement dolomite (dol II), calcite after evaporite minerals (cal III), dolomite associated with sulfides (dol III) and late calcite (IV). This set of samples has $\delta^{13}C$ values between –1.9 to +2.3‰ and $\delta^{18}O$ values between +14.7 to +21.9‰. The highest $\delta^{18}O$ and $\delta^{13}C$ values of +24.1‰ and +4.1‰, respectively, in a porous dolomite, refer to a partially supergene altered dolostone sample and represent an outlier. Among the three samples from calcite after evaporite (cal III), two samples show $\delta^{18}O$ values of +21.4 and +21.9‰ inside the range of the first carbonate group in terms of oxygen isotope composition but with $\delta^{13}C$ values more negative (-1.6 and -1.9‰), probably due to its occurrence in association with algal mats or to organic matter participation in sulfate reduction. The ore-related sparry dolomite (dol III) samples have $\delta^{18}O$ values between +17.2 to +19.3‰ and $\delta^{13}C$ values between -1.2 to +2.0‰. The data from late filling calcite (cal IV) samples have values of $\delta^{13}C$ (-0.7 to +0.2‰) and $\delta^{18}O$ (+17.7 to +19.5‰) among the lowest of all carbonates from the Florida Canyon deposit. In general, the ranges of $\delta^{13}C$ and $\delta^{18}O$ values are similar to the ranges reported by Reid (2001) for carbonates of the Florida Canyon deposit ($\delta^{13}C$ = -9.9 to +3.4‰ and $\delta^{18}O$ = +17.0 to +27.9‰), and by Mondillo et al. (2018a) for nearby Cristal deposit in Bongará District ($\delta^{13}C$ = -7.2 to +3.3‰ and $\delta^{18}O$ = +18.4 to +27.1‰).

Strontium Isotope Data

The two samples groupings defined by the oxygen and carbon isotope plot were also recognized in plots of $^{87}Sr/^{86}Sr$ versus $\delta^{18}O$ values (Fig. 14B) and $^{87}Sr/^{86}Sr$ versus $\delta^{13}C$ values (Fig. 14C). There is an overlap of $^{87}Sr/^{86}Sr$ values of the dark gray limestone samples, which

represent the least altered samples, and the dolostone that resulted from ground preparation alteration, represented by porous dolostone and evaporite breccia samples. The dark-gray limestone and early calcite samples (cal I and cal II) exhibit $^{87}Sr/^{86}Sr$ values from 0.707928 to 0.709433 and from 0.707990 to 0.708222, respectively, plotting partially in the Norian (Triassic) seawater field (0.7075-0.7082, Koepnick et al., 1990; Korte et al., 2003). All other carbonate generations have $^{87}Sr/^{86}Sr$ ratios more radiogenic than that of Norian seawater. Among these samples, strontium ratios increase through the paragenetic sequence. In addition to the two groupings, it was possible to identify new subgroupings within the first group: the least altered limestones of the Chambará 1 member (0.7090–0.7095) and of the Chambará 3 member (0.7078–0.7084), and within the second group: the ore-related carbonates (dol III and cal IV) from the pre-ore carbonates (dol II and cal III). The ore-related sparry dolomite (dol III) and void-filling calcite (cal IV) have mean $^{87}Sr/^{86}Sr$ values of 0.709562 and 0.70954, respectively. They are slightly more radiogenic than pre-ore carbonate generations, such as porous dolostone ($^{87}Sr/^{86}Sr$ = 0.708324), evaporite breccia (0.708678) and calcite from evaporite pseudomorph (0.708442), characterizing the two subgroups: 2a and 2b (Fig. 14B, C).

Sulfur Isotope Data

Results of sulfur isotope analysis of the ore-related sulfides, including dark-brown sphalerite (sp I), light-brown sphalerite (sp II), galena and pyrite (py II) are given in Table 2 and shown in Figure 16. The $\delta^{34}S$ values range between -5.8 and +10.4‰ for all Zn–Pb ore-related sulfides in the Florida Canyon deposit. The samples show a relatively wide $\delta^{34}S$ range within to the -13.7 to +17.6‰ interval reported by Basuki et al. (2008). No isotopic differences are observed among the four areas of the deposit. The average of $\delta^{34}S$ values for dark-brown sphalerite is +1.5‰ (n = 9), for light-brown sphalerite is +1.3‰ (n = 8), for galena is +0.8‰ (n = 8), and for pyrite is –1.7‰ (n = 2). The values of the Florida Canyon sulfides fall slightly below the $\delta^{34}S$ value of Triassic seawater (+12 to +16‰) (Claypool et al., 1980; Kampschulte and Strauss, 2004), and the $\delta^{34}S$ value of evaporite sulfate of the Pucará Group in the San Vicente deposit (+15.6 and 20.9‰) (Spangenberg et al., 1999).

Table 1. Carbon, oxygen, and strontium isotope composition of carbonates from Florida Canyon deposit.

Sample	Sector	Whole-rock sampe (wrs)	Mineral separate sample (mss)	Paragenetic stage	Description	87Sr/86Sr	2σ	$\delta^{13}C_{VPDB}$ (‰)	$\delta^{18}O_{VSMOW}$ (‰)
V_312-13.50-C	San Jorge	dark gray limestone		cal I	Dark grey mudstone with crackle breccia	0.708002	0.000019	2.8	22.0
V_46-59.80-C	San Jorge	dark gray limestone		cal I	Dark grey mudstone	0.708012	0.000023	2.8	25.9
V_46-103.30-C	San Jorge	dark gray limestone		cal I	Dark gray rudstone	0.708272	0.000016	2.0	26.0
V_46-212.50-C	San Jorge	dark gray limestone		cal I	Light grey breccia in mudstone	0.708016	0.000018	2.0	25.3
V_46-284.40-C	San Jorge	dark gray limestone		cal I	Dark grey mudstone with algal mats	0.707928	0.000024	2.3	25.6
V_46-317.10-C	San Jorge	dark gray limestone		cal I	Dark grey crackle breccia in mudstone	0.707994	0.000018	2.8	25.5
V_46-377.20-C	San Jorge	dark gray limestone		cal I	Dark grey mudstone	0.707966	0.000017	2.2	24.3
V_46-454.40-C	San Jorge	dark gray limestone		cal I	Dark grey mudstone	0.707958	0.000018	1.4	24.7
V_46-548.20-C	San Jorge	dark gray limestone		cal I	Light grey mudstone with criptalgal lamination	0.709433	0.000014	2.2	23.2
V_46-568.40-C	San Jorge	dark gray limestone		cal I	Light grey massive mudstone	0.708980	0.000015	2.1	24.7
V_46-588.40-C	San Jorge	dark gray limestone		cal I	Grey laminated limestone with algal mats	0.708975	0.000018	2.4	25.0
V_46-589.40-C	San Jorge	dark gray limestone		cal I	Light grey massive wackstone	0.709113	0.000019	2.3	24.9
V_46-665.05-C	San Jorge	dark gray limestone		cal I	Light grey laminated wackstone	0.708211	0.000019	1.6	21.1
V_46-727.00-C	San Jorge	dark gray limestone		cal I	Dark grey mudstone	0.709142	0.000019	1.0	23.6
V_46-59.80-D	San Jorge		early calcite vein	cal II	White calcite in decimetric veins in mudstone	0.707997	0.000017	2.1	25.1
V_46-103.30-D	San Jorge		early calcite vein	cal II	White calcite in decimetric veins in rudstone	0.707990	0.000019	1.5	22.8
V_46-212.50-D	San Jorge		early calcite vein	cal II	White calcite in mudstone	0.707994	0.000019	2.6	21.8
V_46-284.40-D	San Jorge		early calcite vein	cal II	White calcite in decimetric veins in mudstone	0.708222	0.000021	1.4	23.2
V_46-317.10-D	San Jorge		early calcite vein	cal II	White calcite in centimetric vein in mudstone	0.708141	0.000020	2.9	24.8
V_46-454.40-D	San Jorge		early calcite vein	cal II	White calcite in decimetric veins in mudstone	0.708141	0.000022	2.5	23.2
V_46-486.40-D	San Jorge		calcite as evaporite pseudomorph	cal III	White calcite pseudomorphs after evaporite minerals in dark mudstone	0.709079	0.000017	-0.4	19.0
V_46-588.40-D	San Jorge		calcite as evaporite pseudomorph	cal III	White calcite pseudomorphs after evaporite minerals in mudstone	0.708442	0.000019	-1.9	21.9
V_46-727.00-D	San Jorge		calcite as evaporite pseudomorph	cal III	White calcite in centimetric vein in grey limestone	0.708690	0.000019	-1.6	21.4
FC-17-150.90-C	Falha Sam	evaporite breccia		dol II	Light brown dolomitized evaporite breccia			-0.1	19.6
FC-25-229.20-C	Falha Sam	evaporite breccia		dol II	Light brown dolomitized evaporite breccia			0.6	18.3
FC-36-160.15-C	Karen Milagros	evaporite breccia		dol II	Medium gray packstone with fine disseminated dark brown sphalerite			1.6	17.7
V_212-118.50-C	Central	evaporite breccia		dol II	Light grey dolomitized evaporite breccia			1.8	17.0

Sample	Sector	Whole-rock sampe (wrs)	Mineral separate sample (mss)	Paragenetic stage	Description	87Sr/86Sr	2σ	$\delta^{13}C_{VPDB}$ (‰)	$\delta^{18}O_{VSMOW}$ (‰)
V_214-69.00-C	Central	evaporite breccia		dol II	Light brown dolomitized evaporite breccia			0.7	19.4
V_214-80.60-C	Central	evaporite breccia		dol II	Dolomitized evaporite breccia with light brown sphalerite			1.6	17.8
V_270-103.90-C	San Jorge	evaporite breccia		dol II	Dark grey breccia with coarse dark brown sphalerite			1.6	17.5
V_289-144.90-C	Karen Milagros	evaporite breccia		dol II	Light grey dolomitized evaporite breccia with dark brown sphalerite	0.708072	0.000017	-0.2	16.7
V_297-199.10-C	San Jorge	evaporite breccia		dol II	Dolomitized evaporite breccia	0.708764	0.000017	0.6	18.0
V_297-217.30-C	San Jorge	evaporite breccia		dol II	Light grey dolomitized evaporite breccia	0.708387	0.000018	-1.4	19.0
V_312-63.90-C	San Jorge	evaporite breccia		dol II	Dolomitized evaporite breccia with nonsulfide mineralization	0.709316	0.000018	0.1	18.7
V_329-154.90-C	Karen Milagros	evaporite breccia		dol II	Grey packstone with disseminated fine light sphalerite	0.709230	0.000019	1.5	18.0
V_335-174.60-C	Karen Milagros	evaporite breccia		dol II	Dolomitized evaporite breccia	0.708434	0.000017	1.0	17.5
V_46-478.40-C	San Jorge	evaporite breccia		dol II	Light grey dolomitized evaporite breccia	0.708286	0.000017	2.3	17.9
V_46-529.60-C	San Jorge	evaporite breccia		dol II	Light grey dolomitized evaporite breccia	0.708190	0.000015	2.0	17.8
V_270-95.40-D	San Jorge		replacement dolomite	dol II	Coarse replacement dolomite of evaporite breccia	0.708714	0.000019	0.5	17.8
V_297-226.40-D	San Jorge		replacement dolomite	dol II	Coarse replacement dolomite of evaporite breccia cutted by brown sphalerite vein	0.708992	0.000020	0.6	17.8
FC-25-229.00-C	Falha Sam	porous dolostone		dol II	Dark grey massive dolostone			0.7	18.2
FC-25-238.70-C	Falha Sam	porous dolostone		dol II	Dark grey massive packstone with porous			-1.4	14.7
FC-25-238.70-D	Falha Sam	porous dolostone		dol II	Light brown dolostone with porous			2.0	17.3
V_212-123.00-C	Central	porous dolostone		dol II	Light brown porous dolostone			1.6	17.4
V_312-60.50-C	San Jorge	porous dolostone		dol II	Light brown porous dolostone	0.708319	0.000018	0.0	18.5
V_329-146.00-C	Karen Milagros	porous dolostone		dol II	Light brown porous dolostone	0.708366	0.000019	4.1	24.1
FC-17-170.85-D	Falha Sam		white sparry dolomite	dol III	White sparry dolomite with coarse dark brown sphalerite in evaporite breccia			2.0	17.6
FC-17-197.30-D	Falha Sam		white sparry dolomite	dol III	White sparry dolomite in void-filling texture with fine brown sphalerite in evaporite breccia			1.9	17.6
FC-17-94.00-D	Falha Sam		white sparry dolomite	dol III	Coarse light brown dolomite of the center of the vein in mudstone			0.9	18.4
V_214-75.70-D	Central		white sparry dolomite	dol III	White sparry dolomite in massive sulfide interval			0.2	19.1
V_297-211.70-D	San Jorge		white sparry dolomite	dol III	White sparry dolomite with medium brown sphalerite in evaporite breccia	0.708810	0.000019	1.6	17.7
V_297-217.30-D	San Jorge		white sparry dolomite	dol III	White sparry dolomite with medium brown sphalerite in evaporite breccia	0.709732	0.000016	1.4	17.2
V_297-230.00-D	San Jorge		white sparry dolomite	dol III	White sparry dolomite with dark brown sphalerite in evaporite breccia	0.711206	0.000017	-1.2	19.3
V_46-478.40-D	San Jorge		white sparry dolomite	dol III	White sparry dolomite with organic matter and pyrite in evaporite breccia	0.708501	0.000016	2.0	17.6
FC-17-94.00-C	Falha Sam		late void-filling calcite	cal IV	Coarse white calcite of the edge of the vein in mudstone			-0.6	18.8

Sample	Sector	Whole-rock sampe (wrs)	Mineral separate sample (mss)	Paragenetic stage	Description	87Sr/86Sr	2σ	$\delta^{13}C_{VPDB}$ (‰)	$\delta^{18}O_{VSMOW}$ (‰)
FC-36-142.75-D	Karen Milagros		late void-filling calcite	cal IV	White sparry calcite in evaporite breccia			-0.5	17.7
V_214-69.00-D	Central		late void-filling calcite	cal IV	White sparry calcite in evaporite breccia			0.2	18.8
V_312-13.50-D	San Jorge		late void-filling calcite	cal IV	White calcite as crackle breccia cement in mudstone	0.708576	0.000018	-0.2	18.6
V_46-568.40-D	San Jorge		late void-filling calcite	cal IV	White calcite in centimetric vein in mudstone	0.710902	0.000017	-0.7	19.5
V_46-670.50-D	San Jorge		late void-filling calcite	cal IV	White sparry calcite in mudstone	0.710004	0.000019	-0.5	18.0
V_46-737.80-M	San Jorge	sandstone			Mitu Group feldspar-rich sandstone	0.758875	0.000045		
V_46-738.80-M	San Jorge	sandstone			Mitu Group feldspar-rich sandstone	0.732465	0.000020		
V_46-748.50-M	San Jorge	sandstone			Mitu Group feldspar-rich sandstone	0.750778	0.000020		

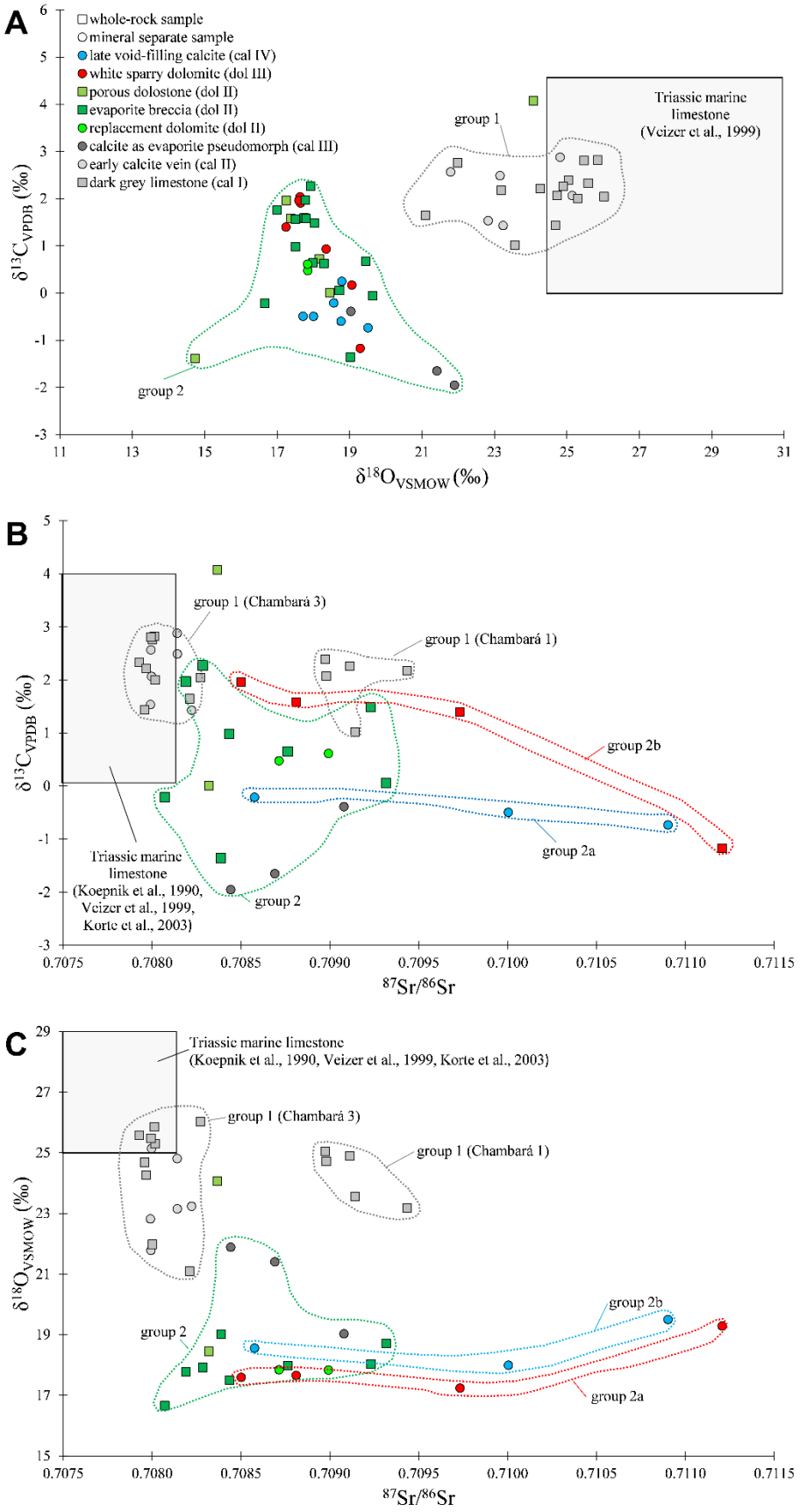

Fig. 14. Geochemical plots $\delta^{18}O$ vs $\delta^{13}C$ (A), $^{87}Sr/^{86}Sr$ vs $\delta^{18}O$ (B) and $^{87}Sr/^{86}Sr$ vs $\delta^{13}C$ (C) for various carbonates of Florida Canyon deposit.

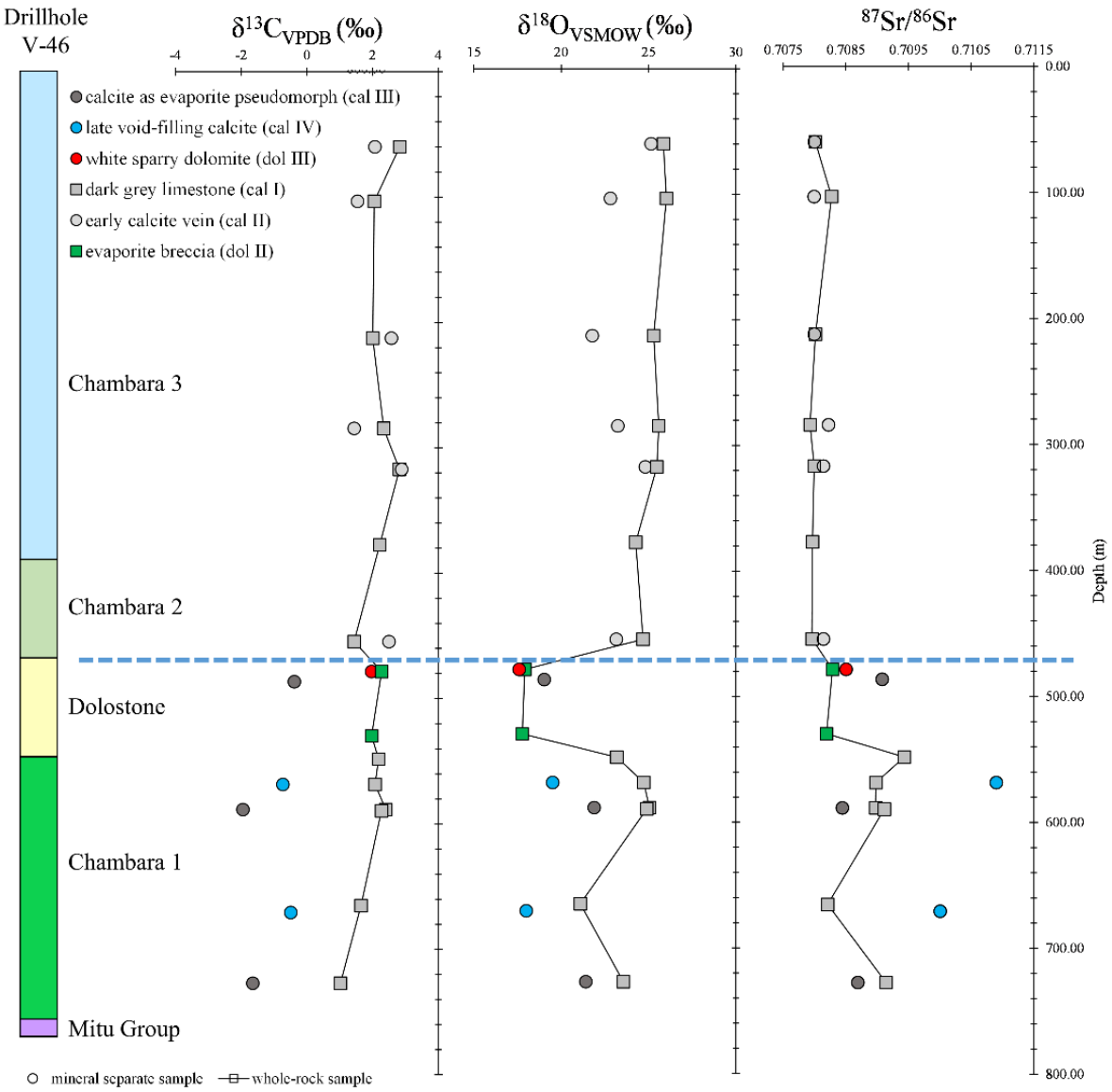

Fig. 15. Profile of V_46 stratigraphic drillhole with carbon, oxygen and strontium isotopic trends in the Florida canyon deposit.

Table 2. Sulfur isotope composition of sulfides from Florida Canyon deposit.

Sample	Sector	Mineral	$\delta^{34}S_{VCDT}$(‰)
V_212-120.00-E	Central	Sphalerite I	-2.8
V_214-80.60-E	Central	Sphalerite I	3.3
V_214-80.60-F	Central	Sphalerite II	-0.8
V_214-80.60-G	Central	Galena	-3.8
V_329-165.60-E	Karen Milagros	Sphalerite I	6.8
V_329-165.60-F	Karen Milagros	Sphalerite II	8.2
V_329-165.60-G	Karen Milagros	Galena	-1.6
V_329-165.60-H	Karen Milagros	Pyrite II	2.3
V_329-167.20-E	Karen Milagros	Sphalerite I	1.0
V_329-167.20-F	Karen Milagros	Sphalerite II	4.2
V_329-167.20-G	Karen Milagros	Galena	-1.7
FC-17-170.85-E	Sam Fault	Sphalerite I	-1.0
FC-17-170.85-F	Sam Fault	Sphalerite II	0.7
FC-17-170.85-G	Sam Fault	Galena	10.4
FC-17-198.70-E	Sam Fault	Sphalerite I	0.0
FC-17-198.70-F	Sam Fault	Sphalerite II	2.0
FC-17-198.70-G	Sam Fault	Galena	3.8
V_270-103.90-E	San Jorge	Sphalerite I	1.6
V_270-103.90-F	San Jorge	Sphalerite II	1.4
V_297-227.70-E	San Jorge	Sphalerite I	-1.8
V_297-227.70-F	San Jorge	Sphalerite II	-2.2
V_297-227.70-G	San Jorge	Galena	-2.8
V_297-227.70-H	San Jorge	Pyrite II	-5.8
V_297-250.10-E	San Jorge	Sphalerite I	2.2
V_297-250.10-F	San Jorge	Sphalerite II	-0.2
V_297-250.10-G	San Jorge	Galena	0.8
V_312-45.00-G	San Jorge	Galena	0.7

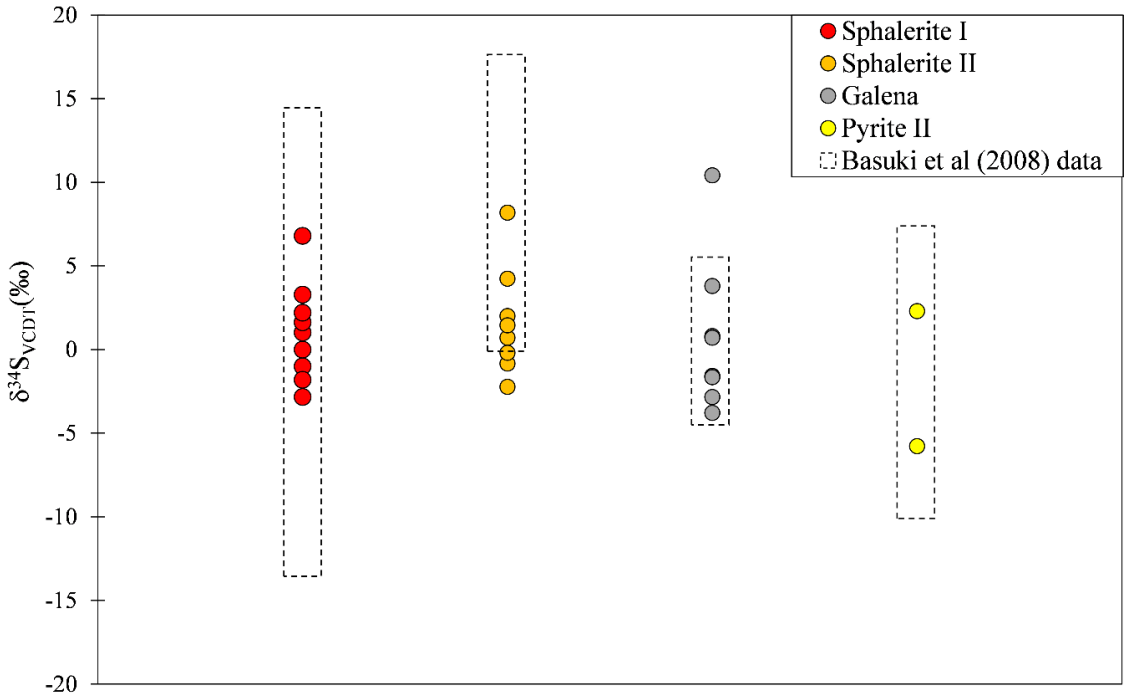

Fig. 16. Distribution of $\delta^{34}S$ values of sulfide minerals in Florida Canyon deposit.

Discussion

Nature and evolution of host carbonate and evaporite rocks

Prior to mineralization at Florida Canyon, diagenesis of the carbonate and evaporative platform rocks of the Pucará sequence played a key role in ground preparation for the ore-bearing fluids and localization of the ore deposit. Early to burial diagenesis of the carbonate rocks and evaporite units produced new carbonate phases, modified and created new fluid circulation pathways, and created structural and hydrocarbon traps that determined where ore deposits formed.

The diagenetic stages observed for the host rock sequence at Florida Canyon area are similar to those of other carbonate sequences around the world (e.g., Davies and Smith, 2006; Brigaud et al., 2009). The evolution of the host rock in the Pucará sequence can be divided into early diagenetic and burial diagenetic stages (Fig. 13). The early diagenetic stage includes the micrite calcite (cal I), early dolomite (dol I) and the early calcite veins (cal II) that formed during or after rock formation. Early dolomitization (dol I) of the calcareous sediments and (or) limestone probably occurred throughout Pucará sequence and could have been generated in near seawater evaporative environments. Burial diagenesis includes the recrystallization of early calcite (cal I) and dolomite (dol I) to coarse dolomite (dol II), dissolution of original evaporites and replacement of sulfate evaporite minerals by calcite (cal III) or dolomite (dol II) that locally created massive zones of secondary porosity that became the host for hydrocarbons generated by thermal maturation.

Dolomitization stage attributed to burial diagenesis in carbonate sequences around the world has been discussed by many authors (e.g., Davies and Smith, 2006; Nader et al., 2007; Brigaud et al., 2009; Zhao et al., 2014). Fontboté and Gorzawski (1990) attributed the generation of some carbonate phases in the San Vicente deposit to burial diagenesis. Dolomite precipitation in the Florida Canyon host rocks may have occurred under normal burial temperatures (e.g., Brigaud et al., 2009) or at higher temperatures by fluids migrating from deeper parts of the basin. The range of temperatures for early stage dolomite obtained by Basuki and Spooner (2009) is 93–173 °C. These temperatures are consistent with temperatures reflecting burial depth around 4–6 kilometers that are reasonable for the tectonic environment of the Pucará Group rocks in diagenetic stages.

The porous dolostone, which is an important host for mineralization, consists of burial dolomite (dol II) and abundant secondary porosity that is commonly filled with later former liquid hydrocarbons (bitumen) and ore sulfides. It is clear that burial dolomite (dol II) predated hydrocarbon generation and migration in the basin whereas sulfide deposition postdates both (Fig. 9B). We suggest that burial dolomite could have formed over a broad range of temperatures, perhaps up to at least the oil window (60–120 °C). Stylolitization occurs in response to tectonic stresses or increase in the overburden pressure (Norman, 2015). Suggestions for burial depth when stylolitization began has been presented and discussed by several authors varying from 300 to 900 meters (Dunnington, 1967; Alsharhan and Sadd, 2000). The presence of stylolites filled with bitumen after early carbonate stages (cal I and cal II) indicate burial diagenetic conditions for oil migration (Fig. 7H).

The Andean tectonism produced extensive thrust stacking and burial of the geological units that was accompanied by increasing burial diagenesis of the rock sequences, and extensive salt migration and halokinesis (Mathalone and Montoya, 1995). It is reasonable to propose that thrusting alone could have resulted in 4–6 kilometers of burial and produced thermal condition for dolomite (dol II) generation. The range of $\delta^{18}O$ values (+14.7 to +21.9‰) for evaporite breccia (dol II), porous dolostone (dol II), and replacement dolomite (dol II) samples are consistent with more elevated temperatures.

Equilibrium reaction-path calculations presented by Anderson and Garven (1987) show that reaction between organic carbon and calcium sulfate (gypsum or anhydrite) at low temperatures (~100 °C) leads to precipitation of dolomite analogous to the white sparry dolomite commonly described in MVT districts. This reaction also produces reduced sulfate as H_2S gas, which may have remained retained in the pores until later invasion by metal-bearing aqueous fluids. The native sulfur presence is an indicator that the carbonate replacement was accompanied by sulfate reduction (Anderson and Garven, 1987). In Florida Canyon, native sulfur was not observed; nevertheless, it is described in San Vicente deposit (Fontbote and Gorzawski, 1990; Spangenberg et al., 1999). Dolomite formed as a result of this mechanism is typically depleted in ^{13}C (Land, 1985; Anderson and Garven, 1987). The carbon-light calcites replacing evaporitic sulfates have the lowest $\delta^{13}C$ values in the deposit (-0.4 to -1.9‰), with a maximum difference of ~4.7 per mil against the least-altered limestones (Fig. 14A), suggesting the reduction of sulfate during diagenesis. The same sulfate reduction mechanism is proposed for San Vicente deposit with a minimum $\delta^{13}C$ value of -11.5‰ for calcite pseudomorph after evaporite minerals (Spangenberg et al., 1996; Spangenberg et al., 1999). Minimum $\delta^{13}C$ values

of -9.9‰ and -7.2‰ in calcite samples are reported for Florida Canyon (Reid, 2001) and Cristal deposits (Mondillo et al., 2018a), respectively.

The C and O isotope signature for ore-related sparry dolomite (dol III) overlap the range for burial dolomite (dol II) (Fig. 14A) indicating a buffering of the C–O isotopes in the fluids by the carbonates in the host sequence. A prolonged period of fluid-rock interaction should have approximated the values of carbon and oxygen isotopes from different carbonate stages. However, the Sr isotope data are quite distinct for the two distinguished carbonate stages reflecting different native fluids (Fig. 14B, C).

The dark-grey limestone samples (Chambará 1 and 3) show $^{87}Sr/^{86}Sr$ ratio ranges that plot partially in the Norian (Triassic) seawater field (0.7075–0.7082, Koepnick et al., 1990; Korte et al., 2003) and extend to a maximum value of 0.709433. The $^{87}Sr/^{867}Sr$ ratio values from early calcite vein (cal II) samples show a smaller range than their host rocks that also match with the Norian seawater composition (Fig. 14). This calcite occurs mainly as a filling in narrow short veinlets (cal II) that could be related to restricted fluid circulation in the Chambará 3 member during the early diagenetic stages, without incorporating radiogenic strontium external from the basin (Fig. 14B, C).

The strontium isotopic composition of the pre-ore phases, such as replacement dolomite (dol II), evaporite breccia (dol II), porous dolostone (dol II), and calcite as evaporite pseudomorph samples (cal III), exhibit $^{87}Sr/^{86}Sr$ values more radiogenic than the Norian seawater, but still within the range of dark-grey limestone samples (Fig. 14). Gorzawski et al. (1989) observed that minerals formed at the end of a diagenetic crystallization sequence are generally more radiogenic than those formed at the beginning. The small shift in the mean $^{87}Sr/^{86}Sr$ values from 0.7078 to 0.7086 for pre-ore alteration phases could represent late successive burial diagenetic stages without the involvement of external fluids. The shift between strontium data from burial diagenetic carbonates (cal III and dol II) and ore-related carbonates (dol III and cal IV) is much more significant (Fig. 14B, C), suggesting a basin exogenous strontium source.

Matrix dolomitization and replacement saddle dolomite followed by void-filling saddle dolomite precipitation is a common paragenetic sequence described in MVT deposits (Davies and Smith, 2006). Many authors believe that matrix replacement dolomite and void-filling saddle dolomite in many deposits are the product of the same fluid source, typically attributed to a hydrothermal origin (e.g. Spangenberg et al., 1996; Davies and Smith, 2006; Basuki et al., 2008; Mondillo et al., 2018a). Basuki et al. (2008) interpreted the two different stages of

dolomite (D1 and D2) in Florida Canyon as a hydrothermal alteration product of a single sequential ore-forming event. The same interpretation is proposed for dolomites from the Cristal deposit (dol1 and dol2, Mondillo et al., 2018a). We interpret the horizon formed by dolostone (porous dolostone and evaporite breccia) that occurs at the base of the Chambará 2 member and at the top of Chambará 1 (Figs. 3, 4) as a continuous layer of sabkha facies that should be separated as a new stratigraphic member. The widespread extension of dolostone along the Pucará Group and the fact that ore sulfide minerals do not always accompany dolomite argue with this interpretation, besides the differences between burial dolomite (dol II) and hydrothermal dolomite (dol III) shown by paragenetic relations (Figs. 7 and 9) and the cathodoluminescence analysis (Fig. 10).

Genesis of Zn–Pb mineralization

The Florida Canyon primary sulfide mineralization formed late in the diagenetic history of the marine carbonates and evaporites of the Pucará Group. Evidence that the mineralization postdates the diagenetic assemblage includes mineralization in diagenetic secondary porosity and voids, replacement textures and mineralization in small veins and fractures that cut burial dolomite (Figs. 7, 9). Sulfide minerals do not consistently accompany dolomitization, rather mineralization is closely associated with NNE tectonic structures that cut the diagenetic dolomitization assemblages. The hydrothermal ore event produced two generations of sphalerite, galena, pyrite, and marcasite and the subsequent late stage carbonates, including sparry dolomite (dol III) and late calcite (cal IV).

The ore zones of the Florida Canyon deposit consist of two distinct styles of ore: i) stratabound ore that fills open space in bedded evaporite breccias and porous dolostone. This style of ore is most abundant in the Central and Karen Milagros areas, ii) high-grade ore associated with halokinetic evaporite breccia that formed as halokinetic injections along faults and into stratabound zones (Table 3). This style of mineralization is common in San Jorge and Sam Fault areas.

The host sequence at Florida Canyon provides several essential requisites for the formation of the deposit. The Chambará 1 member is characterized by a laminated mudstone with fine intercalations and dark layers, which suggest abundant organic matter that could have contributed to the hydrocarbons trapped in the mineralized zones in the overlying Chambará 2. The Chambará 1 probably was an aquitard that may have helped confine ore fluid circulation

with hydrocarbon and reduced sulfur within the overlying permeable Chambará 2 rocks. Overlying the Chambará 2 are the Chambará 3 impermeable mudstones that likely provided a seal for the hydrocarbon reservoir with reduced sulfur and helped constrain fluid interactions within Chambará 2. In addition, reduction of the sulfate-bearing evaporite minerals in the Chambará 2 member was a likely contributor to reduced sulfur that precipitated sulfides in the deposit. However, it is probably not the only sulfur source. These interpretations are in agreement with the geochemical isotope behaviors of C, O, and Sr along the deposit stratigraphic profile (Fig. 15).

Table 3. Summary of the main characteristics of the two mineralization styles of Florida Canyon deposit

Area with dominant occurrence	**Styles of mineralization**	**Structural**	**Dominant host-rock**	**Mean grades**
Karen Milagros Central	stratabound	dome with N50-60ºW axis trending	porous dolostone bedded evaporite breccia	Zn 2.44% Pb 0.24%
San Jorge Sam Fault	structural-controlled (discordant to bedding)	secondary steeply deep faults with NNE direction	halokinetic evaporite breccia	Zn 15.24% Pb 0.48%

The San Vicente deposit is also hosted by the Chambará Formation but is located in a different stratigraphic level than the Florida Canyon deposit. Its Zn–Pb mineralization occurs in upper levels at the top contact of sabkha sequences in the Chambará Formation with the bituminous limestones of the Aramachay Formation (Spangenberg et al., 1996; Spangenberg et al., 1999). In all of the San Vicente mineralized zones, the pre-ore dolomite is similar to the replacement dolomite (dol II) described in Florida Canyon. The former evaporite-rich rocks in the Pucará Group interpreted as sabkha sequence at Florida Canyon and San Vicente may have undergone similar burial diagenetic processes and subsequent Zn–Pb mineralizing events. Mineralization in the Shalipayco and the Florida Canyon are located at the base of the Chambará Formation in contact with volcanoclastic rocks of the Mitu Group (Moritz et al., 1996). The Cristal deposit is hosted in dolomitized units in limestones of the upper Condorsinga Formation (Mondillo et al., 2018a).

The Florida Canyon deposit is located in a dome structure in the Sub-Andean thrust and fold belt that we interpret to have developed in Andean Cycle and possibly during a shift from strictly contractional to dextral shearing in Andean time. Complex and unusual structural

features are common in deformed rock sequences that contain evaporite units because of the low shear strength and density of evaporites relative to the brittle carbonates and siliciclastic rocks (Hudec and Jackson, 2007; Warren, 2016). The formation of the domal feature was possibly facilitated in part by salt halokinesis from the Pucará Group evaporites (Mathalone and Montoya, 1995) or more likely from the Mitu Group evaporites (Petersen, 1965). The abundance of discordant halokinetic breccia (Fig. 5) in faults in the Florida Canyon deposits is consistent with this suggestion. Dextral shearing affecting the Andean thrusts would likely produce steeply dipping extensional faults that may have been the pathway for the ascent of the ore-bearing fluid suggested by the distribution of zinc and lead grades in the ores (Fig. 5). The development of the dome structure was facilitated by halokinesis as indicated by abundant discordant halokinetic evaporite breccias in fault zones that also hosts some of the highest ore grades in the deposit (Fig. 5).

The faults that provided ascent of the metalliferous fluids should be extensional in nature (not faults in compression such as thrust faults) and sub-vertical and sufficiently deep to allow migration of hot metal-bearing brine from the Mitu Group rocks and/or from the basement, as indicated by strontium data and fluid inclusion temperatures (Basuki and Spooner, 2009). In this context, the late northward steeply dipping faults (Sam fault) may represent extensional fault linking strike-slip movements along the northwest trending Andean thrust faults (e.g. Tesoro fault) that could have served as vertical fluid pathways for the ore fluids. The distribution of zinc and lead grades in the deposit suggests that the Sam Fault and other parallel north directional faults in the San Jorge area were the main ascending pathways for mineralization fluids (Fig. 5). A fluid flow from southwest to northeast direction in Florida Canyon is also consistent with the decreasing homogenization temperatures trend obtained by Basuki and Spooner et al. (2009).

The age of the structures is still poorly constrained but could be related to early compressive and deformation stages of the Andean Cycle started in the Late Triassic (Mégard, 1984, 1987; Benavides-Cáceres, 1999). An upper age limit for Zn–Pb mineralization established by field relations indicates a Late Cretaceous or younger age for the Florida Canyon deposit (Reid, 2001). A thrust fault system with main NW direction are described in Peruvian (86–83 Ma), Mochica (100–95 Ma) and Nevadan (157–152 Ma) stages (Mégard, 1984; Mathalone and Montoya, 1995; Benavides-Cáceres, 1999).

The most consistent host units for mineralization are stratabound zones containing hydrocarbon-rich (bitumen) porous dolostone and bedded evaporite breccia that define former

evaporite-rich zones of a sabkha or marine evaporite lagoon setting. Diagenesis and dissolution of evaporites in the host sequence produced extensive lateral permeability in zones of evaporite breccia and porous hydrocarbon-rich dolostone. The dense and nearly impermeable limestones of the Chambará 3 provided a hanging wall seal for reduced sulfur and hydrocarbon fluids that are essential for sulfide deposition in many MVT mineralizing systems (Leach et al., 2005; Leach et al., 2010). We suggest that steeply dipping extensional faults that were active during the late Andean dextral shearing may have allowed deeply circulating metal-bearing fluids to ascend and interact with reduced sulfur and hydrocarbons in the dome.

The sulfur isotope values for ore sulfides ($\delta^{34}S$ = -5.8 to +10.4‰) suggest a predominant thermochemical sulfate reduction (TSR) process in Florida Canyon, as discussed by Basuki et al. (2008). Sulfide mineral precipitation may not have been limited by H_2S availability during the first sphalerite stage (sp I) ($\delta^{34}S$ = -2.8 to +9.4‰), but may have been locally limited by H_2S availability in the second stage (sp II) ($\delta^{34}S$ = -2.2 to +8.2‰). We suggest that only a component of the H_2S probably present in the pores and void spaces of evaporite breccias and porous dolostone could come from the diagenetic decomposition of organic matter and former evaporites due to a modest depletion in calcite ^{13}C. Another H_2S component could have been transported with the hydrocarbons as suggest by the variable scatter of sulfur isotope values. Nevertheless, minor contributions of reduced sulfur from BSR during diagenesis cannot be ruled out, due to the low values of the sulfur isotope in sulfides (minimum of $\delta^{34}S$ = -5.8‰). The sulfur isotope signature of the ore sulfides could also indicate a mixture of different sulfur sources, perhaps from different stratigraphic sources inside the basin. The interpretation of a pre-ore hydrocarbon reservoir hosted in the dolomitized dome could suggest a trap for accumulation of reduced sulfur from different sources.

Fontboté and Gorzawski (1990) interpreted the $\delta^{34}S$ values ($\delta^{34}S$ = +6.8 to +13.0‰) of San Vicente sulfides as reflecting TSR, and analogously Mondillo et al. (2018a) for Cristal deposit ($\delta^{34}S$ = +14.0 to +15.0‰). Spangenberg et al. (1999) and Schutfort (2001), with new sulfur isotope data ($\delta^{34}S$ = +2.5 to +14.2‰ and +1.1 to +12.7‰, respectively) for San Vicente, suggested a dominantly Middle Triassic to Late Jurassic marine evaporitic sulfate source. Sulfur isotope thermometry based on sphalerite-galena pairs indicates different ranges of temperature of precipitation for San Vicente ore, from 75 ° to 92 °C (Fontbote and Gorzawski, 1990); from 130 ° to 154 °C (data from Spangenberg et al., 1999 calculated by Schütfort, 2001), and from 93 ° to 187 °C (Schütfort, 2001). There are no published sulfur isotope data for the Shalipayco deposit.

Basuki and Spooner (2009) obtained high salinity values ranging from 12.1 to 23.5 wt.% $CaCl_2$ equivalent and homogenization temperatures (Th) from 93 ° to 187 °C in fluid inclusions of ore-stage dolomite and sphalerite from the Florida Canyon deposit. These fluid inclusion data are consistent with global MVT deposits (Leach et al., 2005) and considering the lack of magmatic rocks in the area, we assume the ore fluids were deeply circulating sedimentary brines. The $^{87}Sr/^{86}Sr$ ratio values for ore-associated dolomite (dol III) and late calcite stages (cal IV) show a significant shift away from values for the Mesozoic seawater. The $^{87}Sr/^{86}Sr$ maximum values of 0.710902 and 0.711206 are consistent exogenous metalliferous fluid and radiogenic strontium infilling into the carbonate sequence. The more radiogenic values of the ore-related carbonates do not show a depletion in carbon isotopes (Fig. 14B), suggesting an independent late mineralization event with no indication of in situ sulfate reduction during the ore-event.

The $^{87}Sr/^{86}Sr$ values of samples of feldspar-rich sandstone from the Mitu Group (0.732465 to 0.732465) are much more radiogenic than the values for the carbonates in the Florida Canyon deposit. The strontium isotope data implicate rocks from the Mitu Group as a possible strontium and metal source. However, other sources from a mixture with other basement sources cannot be excluded. Moritz et al. (1996) present the same strontium source interpretation for the Shalipayco deposit, although without strontium isotope data.

The fluid inclusion data from late dolomite and sphalerite in the Florida Canyon deposit (Basuki and Spooner, 2009) are consistent with the suggestion that the ore-forming fluid was a sedimentary brine. A common precipitation mechanism proposed for MVT deposits is fluid mixing, with metal-rich fluid encountering a source of reduced sulfur residing in other aquifers or in structurally defined chemical traps (Leach et al., 2005). For this scenario, the proposed hydrocarbon reservoir in the Florida Canyon dome could have also contained previously reduced sulfur produced through TSR of gypsum or anhydrite in the sabkha dolostone layer or elsewhere in the basin. In addition, reduced sulfur through TSR and BSR processes in other parts of the basin during diagenesis and burial could have been trapped in the dome prior to the arrival of the ore fluids. Mixing of a more radiogenic and metal-bearing brine with reduced sulfur retained in the porous dolostone and evaporite breccia from the sabkha facies layer may have resulted in precipitation of sulfides. The Table 4 summarizes the mineralogy and ranges of isotopic compositions of distinguished fluid migration events on Florida Canyon deposit.

The similarities of Florida Canyon host rock, mineral assemblages, paragenesis, and geochemical isotope data with the other MVT deposits of San Vicente, Shalipayco and Cristal

in Pucará Group suggest the same regional diagenetic and hydrothermal ore process acting at a province scale.

Table 4. Summary of mineralogy and ranges (minimum to maximum) of isotopic compositions of distinguished fluid migration events on Florida Canyon deposit.

Type of fluid	**Early diagenesis**	**Burial diagenesis**		**Sulfide mineralization**	
Source of fluid	basinal connate or formation water	basinal connate or formation water	basinal connate or formation water	exogenous formation brine	
Main carbonate phase	calcite	calcite	dolomite	dolomite	calcite
Main texture	veins	evaporite pseudomorph	replacement	void-filling	void-filling
Paragenetic stages	cal II	cal III	dol II	dol III	cal IV
Cathodo-luminescence	-	-	bright luminescent	non-luminescent	-
$\delta^{13}C_{VPDB}$(‰)	1.4 to 2.9	-1.9 to -0.4	0.5 to 0.6	-1.2 to 2.0	-0.7 to 0.2
$\delta^{18}O_{VSMOW}$(‰)	21.8 to 25.1	19.0 to 21.9	17.83 to 17.84	17.2 to 19.3	17.7 to 19.5
$^{87}Sr/^{86}Sr$	0.707990 to 0.708222	0.708442 to 0709079	0.708714 to 0.708992	0.708501 to 0.711206	0.708576 to 0.710902

Implications for mineral exploration

Based on the ore characteristics observed in the Florida Canyon MVT deposit, a prospective exploration model for the discovery of new Zn–Pb deposits in the Bongará region should consider the presence of evaporite breccias and porous dolostone in the sequence as a favorable factor for mineralization. The dolomitic former evaporite layer should be overlain by less porous and permeable units, such as the lime mudstones of the Chambará 3 member acting as hydrologic seals. The porous dolostone and evaporite breccia that formed during burial diagenesis could be used as one factor in a prospective program. However, the diagenetic ground preparation in Florida Canyon is much more extensive than the ore bodies and can occur in all Pucará Group sequence, not being a direct standalone ore identifier. All the Zn–Pb

mineralization is hosted in dolomites with associated vanished evaporites but not all dolomite from Pucará Group hosts mineralization.

Perhaps the most important factor that controlled the ore is the dome that provided a trap for hydrocarbons and reduced sulfur that was a chemical trap for ascending metalliferous fluids. The recognition of structures related to salt movements, such as domes as ore traps, and discordant vertical evaporitic breccia bodies that may have channeled the ascending ore fluids, must be considered. Finally, the critical/essential component of the exploration model is the steeply dipping extensional faults that may represent transtensional links between the main Andean thrust packages.

The application of carbon and oxygen isotopes in mineral exploration had been long used (Barker et al., 2013). In the case of the Florida Canyon region, their application together with strontium isotopes should be considered in the identification and differentiation of carbonates from early diagenetic stages with no ore relation and the carbonates from late hydrothermal stages that could be used as indicators of nearby mineralization.

Concluding Remarks

This study brings together field observations and information from exploration drillholes and petrographic studies together with detailed mineralogy studies, paragenetic descriptions and stable and radiogenic isotope data to better understand the Florida Canyon MVT deposit. The information from this study provides a framework of early to burial diagenesis to hydrothermal Zn–Pb mineralization recorded by the Pucará carbonate sequence at Florida Canyon.

1. The stratabound and structurally controlled Zn–Pb ore bodies are hosted in a hydrocarbon-rich porous dolostone and evaporite breccia in the Chambará 2 member, the most porous and permeable layer in the Pucará Group sequence. The ore-bearing dolostone is interpreted to be a former evaporite-bearing sabkha to evaporative lagoon sequence within limestones of the Chambará 2. These evaporite- and organic-rich rocks likely represent a former hydrocarbon reservoir.

2. The deposit is located in a dome that was facilitated by halokinetic processes during Andean thrusting. The involvement of halokinesis is shown by diapiric evaporite breccias along faults and abundant bedded evaporite breccias with evaporite pseudomorphs.

3. Within the dome, the distribution of ore grades reflects steeply dipping faults that appear to link the major faults of the northwest Andean thrust direction. This apparent control of high-grade ore in secondary fault zones that link to major regional faults is a common ore control globally for any kind of hydrothermal ore deposit.

4. Mineralization postdates migration of hydrocarbons in the Bongará region of the Pucará basin. Sphalerite and galena fill pores that were formally filled with liquid hydrocarbons (now bitumen).

5. This close association of mineralization with organic matter, together with the isotopic composition of sulfur and carbon, suggest that TSR processes were essential for the generation of reduced sulfur for sulfide deposition. TSR processes operated in the basin during burial diagenesis and presumably in situ in the Florida Canyon host rocks.

6. The results of this study illustrate the important roles that evaporites have in the genesis of some MVT deposits. MVT mineralization in the Florida Canyon deposit was largely controlled by carbonate-evaporite diagenesis, and halokinesis processes that made structures and chemical traps during deformation of the basin.

7. This study provides important constraints on the relative timing of MVT ore genesis relative to the evolution of the Pucará basin. The observations show that the MVT mineralization was late in the evolution of the basin. The ores were deposited after basin-scale diagenesis of the early carbonate and evaporite rocks during burial and formation of the Florida Canyon dome, and the maturation and migration of hydrocarbons (and reduced sulfur) into the dome. Finally, the ores were deposited in the dome as a consequence of a postulated change in Andean stress direction that produced the ore-controlling NNE steeply dipping faults that were secondary to the main Andean thrusts.

8. The similarities between the Florida Canyon host rocks, mineral assemblage, paragenesis, and geochemical isotope data with the other MVT deposits of San Vicente, Shalipayco and Cristal in the Pucará Group suggest the same regional diagenetic and hydrothermal ore processes operated on a basin scale.

Acknowledgments

The majority of the descriptions and characterizations came from the discussion and contribution of many field geologists involved with the exploration project. The authors would like to thank all field geologists, citing Isaac Robles and Jose Diaz Cardozo for the reception and discussions during the fieldwork, and Votorantim Metais Company (now Nexa Resources) in the name of Jones Belther, Lucio Molinari and Paulo Pires to permit the use of data and assistance with field arrangements and costs. We wish also to thank Cayce Gulbransen, for assistance during S isotope analysis, Thomas Monecke for discussions during cathodoluminescence analysis and Isaac Sayeg for SEM imaging. We appreciate the constructive reviews of the manuscript by Murray Hitzman and Jen Gutzmer. This paper is part of the first author's Ph.D. thesis (Geosciences Institute, University of São Paulo) and part of this work was conducted during a visiting scholar period at Colorado School of Mines, sponsored by the Capes Foundation within the Ministry of Education, Brazil (process 88881.135448/2016-01), that the authors would like to thank. Any use of trade, firm, or product names is for descriptive purposes only and does not imply endorsement by the U.S. Government.

References

Akande, S. O., and Zentilli, M., 1984, Geologic, fluid inclusion, and stable isotope studies of the Gays River lead-zinc deposit, Nova Scotia, Canada: Economic Geology, v. 79, p. 1187-1211.

Alsharhan, A. S., and Sadd, J. L., 2000, Stylolites in Lower Cretaceous carbonate reservoirs, United Arab Emirates: Society for Sedimentary Geology Special Publication, v. 69, p. 185-207.

Anderson, G. M., and Garven, G., 1987, Sulfate-sulfide-carbonate associations in Mississippi Valley-type lead-zinc deposits: Economic Geology, v. 82, p. 482-488.

Arfè, G., Mondillo, N., Balassone, G., Boni, M., Cappelletti, P., and Di Palma, T., 2017a, Identification of Zn-bearing micas and clays from the Cristal and Mina Grande zinc deposits (Bongará Province, Amazonas Region, Northern Peru): Minerals, v. 7, p. 214-231.

Arfè, G., Mondillo, N., Boni, M., Balassone, G., Joachimski, M., Mormone, A., and DiPalma, T., 2017b, The karst-hosted Mina Grande nonsulfide zinc deposit, Bongará District (Amazonas Region, Peru): Economic Geology, v. 112, p. 1089-1110.

Arfè, G., Mondillo, N., Boni, M., Joachimski, M., Balassone, G., Mormone, A., Santoro, L., and Medrano, E. C., 2018, The Cristal Zn prospect (Amazonas region, Northern Peru). Part II: An example of supergene enrichments in tropical areas: Ore Geology Reviews, v. 95, p. 1076-1105.

Audebaud, E., Capdevila, R., Dalmayrac, B., Debelmas, J., Laubacher, G., Lefevre, C., Marocco, R., Martinez, C., Mattauer, M., and Mégard, F., 1973, Les traits géologiques essentiels des Andes centrales (Pérou-Bolivie): Revue de Geologie Dynamique et de Geographie Physique, v. 15, p. 73-113.

Barker, S. L. L., Dipple, G. M., Hickey, K. A., Lepore, W. A., and Vaughan, J. R., 2013, Applying stable isotopes to mineral exploration: Teaching an old dog new tricks: Economic Geology, v. 108, p. 1-9.

Basuki, N. I., and Spooner, E. T. C., 2009, Post-early Cretaceous Mississippi Valley-type Zn-Pb mineralization in the Bongara Area, Northern Peru: fluid evolution and paleo flow from fluid inclusion evidence: Exploration and Mining Geology, v. 18, p. 25-39.

Basuki, N. I., Taylor, B. E., and Spooner, E. T. C., 2008, Sulfur isotope evidence for thermochemical reduction of dissolved sulfate in Mississippi Valley-type zinc-lead mineralization, Bongara area, northern Peru: Economic Geology, v. 103, p. 783-799.

Benavides-Cáceres, V., 1999, Orogenic evolution of the Peruvian Andes: the Andean cycle: Geology and ore deposits of the Central Andes, v. 7, p. 61-107.

Benavides, V., 1968, Saline deposits of South America: International Conference on Saline Deposits, 1968, 1968, p. 249-90.

Bertolotti, R., and Moretti, I., 2009, Deformation history and structural style in the North Ucayali basin: 10th Simposio Bolivariano - Exploracion Petrolera en las Cuencas Subandinas 2009, p. 8.

Bouabdellah, M., Castorina, F., Bodnar, R. J., Banks, D., Jébrak, M., Prochaska, W., Lowry, D., Klügel, A., and Hoernle, K., 2014, Petroleum migration, fluid mixing, and halokinesis as the main ore-forming processes at the peridiapiric Jbel Tirremi fluorite-barite hydrothermal deposit, northeastern Morocco: Economic Geology, v. 109, p. 1223-1256.

Bouabdellah, M., Niedermann, S., and Velasco, F., 2015, The Touissit-Bou Beker Mississippi Valley-type district of northeastern Morocco: relationships to the Messinian salinity crisis, Late Neogene-Quaternary alkaline magmatism, and buoyancy-driven fluid convection: Economic Geology, v. 110, p. 1455-1484.

Bouhlel, S., Leach, D. L., Johnson, C. A., Marsh, E., Salmi-Laouar, S., and Banks, D. A., 2016, A salt diapir-related Mississippi Valley-type deposit: the Bou Jaber Pb-Zn-Ba-F deposit, Tunisia: fluid inclusion and isotope study: Mineralium Deposita, v. 51, p. 749-780.

Brigaud, B., Durlet, C., Deconinck, J.-F., Vincent, B., Thierry, J., and Trouiller, A., 2009, The origin and timing of multiphase cementation in carbonates: Impact of regional scale geodynamic events on the Middle Jurassic Limestones diagenesis (Paris Basin, France): Sedimentary Geology, v. 222, p. 161-180.

Charef, A., and Sheppard, S. M. F., 1987, Pb-Zn mineralization associated with diapirism: fluid inclusion and stable isotope (H, C, O) evidence for the origin and evolution of the fluids at Fedj-El-Adoum, Tunisia: Chemical Geology, v. 61, p. 113-134.

Claypool, G. E., Holser, W. T., Kaplan, I. R., Sakai, H., and Zak, I., 1980, The age curves of sulfur and oxygen isotopes in marine sulfate and their mutual interpretation: Chemical Geology, v. 28, p. 199-260.

Cowan, E. J., Beatson, R. K., Fright, W. R., McLennan, T. J., and Mitchell, T. J., 2002, Rapid geological modelling: Applied Structural Geology for Mineral International Symposium, Kalgoorlie, 2002, p. 23-25.

Davies, G. R., and Smith, L. B., 2006, Structurally controlled hydrothermal dolomite reservoir facies: An overview: AAPG Bulletin, v. 90, p. 1641-1690.

de Oliveira, S. B., Juliani, C., and Monteiro, L. V. S., 2018, Mineral characterization of the nonsulfide Zn mineralization of the Florida Canyon deposit, Bongará District, Northern Peru: Applied Earth Science: Transactions of the Institutions of Mining and Metallurgy: Section B p. in press.

Dean, W. E., Davies, G. R., and Anderson, R. Y., 1975, Sedimentological significance of nodular and laminated anhydrite: Geology, v. 3, p. 367-372.

Díaz, A., and Ramírez, J., 2009, Compendio de rocas y minerales industriales en el Perú, INGEMMET, Boletín, Serie B: Geología Económica, 19, p. 482.

Dunnington, H. V., 1967, Aspects of diagenesis and shape change in stylolitic limestone reservoirs: World Petroleum Congress, Mexico, 1967, p. 726-737.

Fernández Castañeda, J., Martínez, E., Calderón, Y., and Galdos, C., 2002, The Pucara petroleum system and pre-Cretaceous sabkha regional Seal, a new hydrocarbon play in the Peruvian fold thrust belt, International Seminar INGEPET: Lima, Peru, p. 12.

Fontboté, L., 1990, Stratabound ore deposits in the Pucará basin, in Fontboté, L., Amstutz G. C., Cardozo M., Cedillo, E., and Frutos, J., eds., Stratabound Ore Deposits in the Andes, 8: Berlin Heildelberg, Springer-Verlag p. 253-266.

Fontbote, L., and Gorzawski, H., 1990, Genesis of the Mississippi Valley-type Zn-Pb deposit of San Vicente, central Peru; geologic and isotopic (Sr, O, C, S, Pb) evidence: Economic Geology, v. 85, p. 1402-1437.

Friedman, G. M., 1997, Dissolution-collapse breccias and paleokarst resulting from dissolution of evaporite rocks, especially sulfates: Carbonates and Evaporites, v. 12, p. 53-63.

Ghazban, F., Schwarcz, H. P., and Ford, D. C., 1990, Carbon and sulfur isotope evidence for in situ reduction of sulfate, Nanisivik lead-zinc deposits, Northwest Territories, Baffin Island, Canada: Economic Geology, v. 85, p. 360-375.

Gorzawski, H., Fonboté, L., Sureau, J. F., and Calvez, J. Y., 1989, Strontium isotope trends during diagenesis in ore-bearing carbonate basins: Geologische Rundschau, v. 78, p. 269-290.

Hill, W. T., Morrie, R. G., and Hagegeorge, C. C., 1971, Ore controls and related sedimentary features at the Flat Gap Mine, Treadway, Tennessee: Economic Geology, v. 66, p. 748-756.

Hitzman, M. W., 1999, Routine staining of drill core to determine carbonate mineralogy and distinguish carbonate alteration textures: Mineralium Deposita, v. 34, p. 794-798.

Hudec, M. R., and Jackson, M. P. A., 2007, Terra infirma: Understanding salt tectonics: Earth-Science Reviews, v. 82, p. 1-28.

Hussain, M., and Warren, J. K., 1989, Nodular and enterolithic gypsum: the "sabkha-tization" of Salt Flat playa, west Texas: Sedimentary Geology, v. 64, p. 13-24.

Jaillard, E., Hérail, G., Monfret, T., Díaz-Martínez, E., Baby, P., Lavenu, A., and Dumont, J. F., 2000, Tectonic evolution of the Andes of Ecuador, Peru, Bolivia and northernmost Chile, Tectonic Evolution of South America, 31st International Geological Congress, Publications Rio de Janeiro, p. 481-559.

Jiang, L., Worden, R. H., and Yang, C., 2018, Thermochemical sulphate reduction can improve carbonate petroleum reservoir quality: Geochimica et Cosmochimica Acta, v. 223, p. 127-140.

Johnson, C. A., Stricker, C. A., Gulbransen, C. A., and Emmons, M. P., 2018, Determination of δ13C, δ15N, or δ34S by isotope-ratio-monitoring mass spectrometry using an elemental analyzer, U.S. Geological Survey Techniques and Methods, 5, p. 19.

Kampschulte, A., and Strauss, H., 2004, The sulfur isotopic evolution of Phanerozoic seawater based on the analysis of structurally substituted sulfate in carbonates: Chemical Geology, v. 204, p. 255-286.

Kendall, D. L., 1960, Ore deposits and sedimentary features, Jefferson City mine, Tennessee: Economic Geology, v. 55, p. 985-1003.

Kerans, C., 1993, Description and interpretation of karst-related breccia fabrics, Ellenburger Group, West Texas, in Frits, R. D., Wilson, J. L., and Yurewicz, D. A., eds., Paleokarst Related Hydrocarbon Reservoirs, Special Publications of SEPM, Society for Sedimentary Geology, p. 181-201.

Koepnick, R. B., Denison, R. E., Burke, W. H., Hetherington, E. A., and Dahl, D. A., 1990, Construction of the Triassic and Jurassic portion of the Phanerozoic curve of seawater 87Sr/86Sr: Chemical Geology: Isotope Geoscience section, v. 80, p. 327-349.

Korte, C., Kozur, H. W., Bruckschen, P., and Veizer, J., 2003, Strontium isotope evolution of Late Permian and Triassic seawater: Geochimica et Cosmochimica Acta, v. 67, p. 47-62.

Land, L. S., 1985, The origin of massive dolomite: Journal of Geological Education, v. 33, p. 112-125.

Leach, D., and Song, Y., 2018, Sediment-Hosted Zinc-Lead and Copper Deposits in China, in Chang, Z., and Goldfarb, R., eds., Mineral deposits of China, p. in press.

Leach, D. L., Bradley, D., Lewchuk, M. T., Symons, D. T., de Marsily, G., and Brannon, J., 2014, Mississippi Valley-type lead–zinc deposits through geological time: implications from recent age-dating research: Mineralium Deposita, v. 36, p. 711-740.

Leach, D. L., Bradley, D. C., Huston, D., Pisarevsky, S. A., Taylor, R. D., and Gardoll, S. J., 2010, Sediment-hosted lead-zinc deposits in Earth history: Economic Geology, v. 105, p. 593-625.

Leach, D. L., Sangster, D. F., Kelley, K. D., Large, R. R., Garven, G., Allen, C. R., Gutzmer, J., and Walters, S., 2005, Sediment-hosted Pb-Zn Deposits: a global perspective: Economic Geology, v. 100, p. 561-608.

Leach, D. L., Song, Y.-C., and Hou, Z.-Q., 2017, The world-class Jinding Zn–Pb deposit: ore formation in an evaporite dome, Lanping Basin, Yunnan, China: Mineralium Deposita, v. 52, p. 281-296.

Liu, Y., Hou, Z., Yang, Z., Tian, S., Yang, T., Song, Y., Zhang, H., and Carranza, E. J. M., 2011, Formation of the Dongmozhazhua Pb–Zn deposit in the thrust-fold setting of the Tibetan Plateau, China: evidence from fluid inclusion and stable isotope data: Resource geology, v. 61, p. 384-406.

Loughman, D. L., and Hallam, A., 1982, A facies analysis of the Pucara Group (Norian to Toarcian carbonates, organic-rich shale and phosphate) of central and northern Peru: Sedimentary Geology, v. 32, p. 161-194.

Maslyn, R. M., 1977, Recognition of fossil karst features in the ancient record: A discussion of several common fossil karst forms, in Veal, H. K., ed., Southern and Central Rockies Exploration Frontiers, Rocky Mtn. Assoc. Geologists Guidebook, p. 311-319.

Mathalone, J. M. P., and Montoya, M. R., 1995, Petroleum geology of the sub-Andean basins of Peru, in Tankard, A. J., Suarez Soruco, R., and Welsink, H. J., eds., Petroleum Basins of South America, 62, AAPG Special Volumes, p. 423-424.

Mégard, F., 1978, Etude géologique des Andes du Pérou central: contribution à l'étude géologique des Andes n 1: Paris, Institut français d'études andines, 310 p.

Mégard, F., 1984, The Andean orogenic period and its major structures in central and northern Peru: Journal of the Geological Society, v. 141, p. 893-900.

Mégard, F., 1987, Structure and evolution of the Peruvian Andes, in Schaer, J. P., and Rodgers, J., eds., The Anatomy of Mountain Ranges: Princeton, New Jersey, United States, Princeton University, p. 179-210.
Mondillo, N., Arfè, G., Boni, M., Balassone, G., Boyce, A., Joachimski, M., Kang, J. S., and Villa, I. M., 2018a, The Cristal Zinc prospect (Amazonas region, Northern Peru). Part I: New insights on the sulfide mineralization in the Bongará province: Ore Geology Reviews, v. 94, p. 261-276.
Mondillo, N., Arfè, G., Herrington, R., Boni, M., Wilkinson, C., and Mormone, A., 2018b, Germanium enrichment in supergene settings: evidence from the Cristal nonsulfide Zn prospect, Bongará district, northern Peru: Mineralium Deposita, v. 53, p. 155-169.
Moretti, I., Callot, J.-P., Principaud, M., and Pillot, D., 2013, Salt pillows and localization of early structures: case study in the Ucayali Basin (Peru): Geological Society, London, Special Publications, v. 377, p. SP377-8.
Moritz, R., Fontboté, L., Spangenberg, J., Rosas, S., Sharp, Z., and Fontignie, D., 1996, Sr, C and O isotope systematics in the Pucará basin, central Peru: Mineralium Deposita, v. 31, p. 147-162.
Nader, F. H., Swennen, R., Ellam, R. M., and Immenhauser, A., 2007, Field geometry, petrography and geochemistry of a dolomitization front (Late Jurassic, central Lebanon): Sedimentology, v. 54, p. 1093-1120.
Norman, K., 2015, Stylolitization of limestone: a study about the morphology of stylolites and its impacts of porosity and permeability in limestone, 14, Department of Earth Sciences, Uppsala University, p. 24.
Perona, J., Canals, À., and Cardellach, E., 2018, Zn-Pb mineralization associated with salt diapirs in the Basque-Cantabrian Basin, Northern Spain: geology, geochemistry, and genetic model: Economic Geology, v. 113, p. 1133-1159.
Petersen, U., 1965, Regional geology and major ore deposits of central Peru: Economic Geology, v. 60, p. 407-476.
Reid, C. J., 2001, Stratigraphy and mineralization of the Bongara MVT zinc-lead district, northern Peru: Unpub. M.Sc. thesis, University of Toronto, 179 p.
Rosas, S., Fontboté, L., and Tankard, A., 2007, Tectonic evolution and paleogeography of the Mesozoic Pucará Basin, central Peru: Journal of South American Earth Sciences, v. 24, p. 1-24.
Rosenbaum, J., and Sheppard, S. M. F., 1986, An isotopic study of siderites, dolomites and ankerites at high temperatures: Geochimica et Cosmochimica Acta, v. 50, p. 1147-1150.
Sánchez, A., 1995, Geología de los cuadrángulos de Bagua Grande, Jumbilla, Lonya Grande, Chachapoyas, Rioja, Leimebamba y Bolívar: hojas 12-g, 12-h, 13-g, 13-h, 13-i, 14-hy 15-h, Instituto Geológico Minero y Metalúrgico Peru.
Sangster, D. F., 1988, Breccia-Hosted Lead—Zinc Deposits in Carbonate Rocks, in N.P., J., and P.W., C., eds., Paleokarst: New York, NY, Springer, p. 102-116.
Sasaki, A., and Krouse, H. R., 1969, Sulfur isotopes and the Pine Point lead-zinc mineralization: Economic Geology, v. 64, p. 718-730.
Schaltegger, U., Guex, J., Bartolini, A., Schoene, B., and Ovtcharova, M., 2008, Precise U–Pb age constraints for end-Triassic mass extinction, its correlation to volcanism and Hettangian post-extinction recovery: Earth and Planetary Science Letters, v. 267, p. 266-275.
Schütfort, E. G., 2001, The genesis of the San Vicente lead zinc rhythmite deposit, Peru: a petrologic, geochemical, and sulfur isotope study: Unpub. M.Sc. thesis, Oregon State University, 136 p.
Sempere, T., Carlier, G., Soler, P., Fornari, M., Carlotto, V. c., Jacay, J., Arispe, O., Néraudeau, D., Cárdenas, J., Rosas, S., and Jiménez, N., 2002, Late Permian–Middle Jurassic

lithospheric thinning in Peru and Bolivia, and its bearing on Andean-age tectonics: Tectonophysics, v. 345, p. 153-181.

Spangenberg, J., Fontboté, L., Sharp, Z. D., and Hunziker, J., 1996, Carbon and oxygen isotope study of hydrothermal carbonates in the zinc-lead deposits of the San Vicente district, central Peru: a quantitative modeling on mixing processes and CO2 degassing: Chemical Geology, v. 133, p. 289-315.

Spangenberg, J. E., Fontboté, L., and Macko, S. A., 1999, An evaluation of the inorganic and organic geochemistry of the San Vicente Mississippi Valley-type zinc-lead district, central Peru; implications for ore fluid composition, mixing processes, and sulfate reduction: Economic Geology, v. 94, p. 1067-1092.

Sun, S. Q., 1995, Dolomite reservoirs: porosity evolution and reservoir characteristics: AAPG bulletin, v. 79, p. 186-204.

Swennen, R., Viaene, W., and Cornelissen, C., 1990, Petrography and geochemistry of the Belle Roche breccia (lower Visean, Belgium): evidence for brecciation by evaporite dissolution: Sedimentology, v. 37, p. 859-878.

Tompkins, L. A., Rayner, M. J., Groves, D. I., and Roche, M. T., 1994, Evaporites; in situ sulfur source for rhythmically banded ore in the Cadjebut mississippi valley-type Zn-Pb deposit, Western Australia: Economic Geology, v. 89, p. 467-492.

Vearncombe, J. R., Dentith, M., Doerling, S., Reed, A., Cooper, R., Hart, J., Muhling, P., Windrim, D., and Woad, G., 1995, Regional-and prospect-scale fault controls on mississippi valley-type Zn-Pb mineralization at Blendevale, Canning Basin, Western Australia: Economic Geology, v. 90, p. 181-186.

Vega, I. M. R., 2018, Geologia y mineralizacion del deposito Mississipi Valley-type de Zn-Pb, proyecto Canon Florida, Norte de Peru: Unpub. M.Sc. thesis, Universidad Nacional de Huancavelica, 164 p.

Veizer, J., Ala, D., Azmy, K., Bruckschen, P., Buhl, D., Bruhn, F., Carden, G. A. F., Diener, A., Ebneth, S., Godderis, Y., Jasper, T., Korte, C., Pawellek, F., Podlaha, O. G., and Strauss, H., 1999, 87Sr/86Sr, δ13C and δ18O evolution of Phanerozoic seawater: Chemical Geology, v. 161, p. 59-88.

Warren, J. K., 2000, Evaporites, brines and base metals: Low-temperature ore emplacement controlled by evaporite diagenesis: Australian Journal of Earth Sciences, v. 47, p. 179-208.

Warren, J. K., 2006, Evaporites: sediments, resources and hydrocarbons: Berlin, Springer, 1036 p.

Warren, J. K., 2016, Evaporites: A geological compendium, Springer, 1813 p.

Warren, J. K., and Kempton, R. H., 1997, Evaporite sedimentology and the origin of evaporite-associated Mississippi Valley-Type sulfides in the Cadjebut Mine area Lennard Shelf, Canning Basin, Western Australia: Society for Sedimentary Geology Special Publication, v. 57, p. 183-205.

Zhao, W., Shen, A., Zheng, J., Qiao, Z., Wang, X., and Lu, J., 2014, The porosity origin of dolostone reservoirs in the Tarim, Sichuan and Ordos basins and its implication to reservoir prediction: Science China Earth Sciences, v. 57, p. 2498-2511.

.

3 Mineral characterization of the non-sulphide Zn mineralization of the Florida Canyon deposit, Bongará District, Northern Peru

Saulo Batista de Oliveira[1,2], Caetano Juliani[2] and Lena Virgínia Soares Monteiro[2]

[1] Nexa Resources, Av. Engenheiro Luís Carlos Berrini, 105, 6º andar, São Paulo, SP, 04571-010, Brazil

[2] Institute of Geosciences, University of São Paulo, R. do Lago, 562, São Paulo, SP, 05508-080, Brazil

Abstract

The Florida Canyon deposit hosted by a carbonate-evaporite sequence of the Pucará Group, Peru, has both Zn–Pb sulphide and Zn non-sulphide mineralisations. The Zn non-sulphide mineralisation has become increasingly important with the ongoing exploration. The mineralogical characterization of samples from the deposit enables the definition of a supergene assemblage dominated by smithsonite, in addition to hemimorphite, cerussite, and goethite. The main oxidation in in the study area involved the direct replacement of primary MVT stratabound sulphide ore. In comparison with other non-sulphide deposits of the Bongará District, the Florida Canyon deposit can be correlated with the Cristal deposit by means of the original sulphides preserved in the supergene textures, the similar hosting dolostone layer, lack of hydrozincite, and depth of emplacement, which are characteristics that contrast with those of the Mina Grande deposit, also inserted in the Pucará Group. The Florida Canyon supergene mineral assemblage is a paleoclimatic indicator suggesting a humid tropical climate during the late Miocene in the Peruvian Amazon region.

Introduction

The Florida Canyon deposit is one of the largest Mississippi Valley-type (MVT) deposits in South America with mineral resources of 12.1 million tons at a grade of 10.7% zinc and 1.2% lead (Hunt et al., 2017). The deposit is located in the northern portion of the carbonate and evaporite sequence of the Pucará Group, stretching out for more than 1,000 km extension along of Peruvian Andes (Fig. 1). Both Zn–Pb sulphide and Zn non-sulphide mineralisation are recognized in Florida Canyon. Previous research in this area, such as Reid (2001), Basuki et al. (2008) and Basuki and Spooner (2009), focused on the primary MVT sulphide mineralisation within the Florida Canyon deposit. The Pucará Group hosts other MVT Zn–Pb deposits, such

as San Vicente (Fontbote and Gorzawski, 1990; Spangenberg et al., 1996; Spangenberg et al., 1999) and Shalipayco (Moritz et al., 1996) and supergene non-sulphide Zn deposits, such as Mina Grande (Arfè et al., 2017a; Arfè et al., 2017b) and Cristal (Arfè et al., 2018; Mondillo et al., 2018a; Mondillo et al., 2018b).

This paper presents the first geological descriptions and mineralogical characterization of the Zn supergene mineralisation in the Florida Canyon deposit, so important for supporting the definition of metallurgical routes in a mining project. The results of petrography, mineralogical and textural characterization allow new insights for the genesis of the supergene mineralisation in the Pucará basin, thus contributing to the identification of new targets in this extensive carbonate sequence.

Exploration History

Zn–Pb sulphides occurrences in the Florida Canyon were first detected by Solitario Company in 1994. Cominco Ltd proceeded with the identification of sulphide mineralisation in drillholes through a joint venture partnership with Solitario Company during 1997 and 1999. In 2006, Solitario and Votorantim Metais (now Nexa Resources) constituted a new joint venture and conducted a new extensive diamond drilling campaign until 2014, which defined the current mineral resources (Hunt et al. 2017). The 1997-1999 campaign aimed to intercept the structure-controlled mineralisation and the main target was a major north-trending fault system that delimits the deposit in its western portion, which is called the Sam Fault sector. Until 2006, the mineralisation was considered to consist only of sulphide type with some few non-sulphide intervals. The new drilling campaign has shown that non-sulphide intersections are rather frequent, and currently non-sulphide mineralised intersections are known up to 500 m in depth. With the drilling advance over the years, Therefore, the supergene mineralisation represents an outstanding type of resource in the Florida Canyon and is a significant addition to the Zn resources, which is currently estimated as almost one-third of the total resource (Hunt et al., 2017).

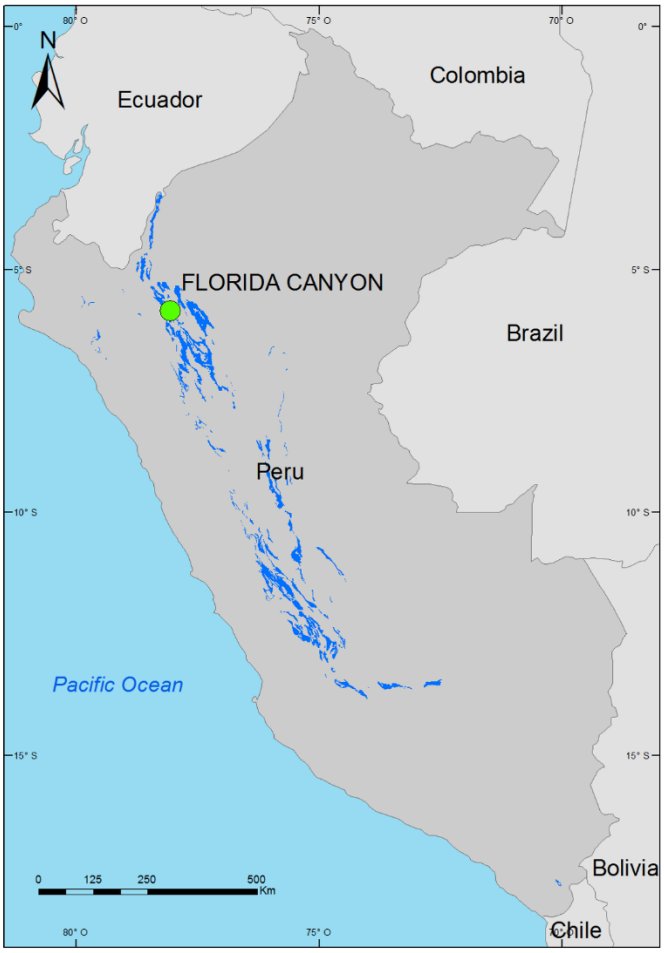

Fig. 1. Location of the Florida Canyon deposit in northern Peru. In blue the Upper Triassic to Lower Jurassic Pucará Group, modified from Sanchez et al. (1999).

Geological Background

The Pucará Group is an Upper Triassic to Lower Jurassic sequence of carbonate, evaporite rocks and shales, subdivided into the Chambará, Aramachay, and Condorsinga formations. It lies in angular unconformity on the Mitu Group volcano-sedimentary sequence (Szekely and Grose, 1972; Loughman and Hallam, 1982; Sánchez, 1995; Rosas et al., 2007). The Florida Canyon mineralisation is hosted by the Chambará Formation, which is locally subdivided in the Chambará 1, 2 and 3 members (Reid, 2001; Basuki et al., 2008; Vega, 2018). The Chambará 1 (basal member) and the Chambará 3 (top member) are mainly composed of limestones deposited in a shallow marine environment. Lamination is the predominant feature of the Chambará 1 lime mudstones whereas the Chambará 3 lime mudstones and lime wackestones are massive. The Chambará 2 comprises relatively coarse-grained dolostone and

former evaporite that suggests a sabkha environment. The main MVT Zn–Pb and supergene Zn mineralisations are hosted in the Chambará 2 member (Fig. 2).

The primary MVT mineralisation is dominantly stratabound and extends all along the dome structure that defines the deposit. The deposit is limited to the east by the steep N-trending Sam Fault and to the west by the NW-trending Tesoro thrust fault. Minor dip-slip faults are present and may be equally or more important as channels for the percolation of meteoric fluids (Fig. 2). Due to displacements of the order of 1 to 3 meters, these structures are not easily interpreted, as the average spacing between drill holes is 25 meters (Fig. 2).

The Florida Canyon deposit is divided into four sectors: San Jorge, Central, Sam Fault and Karen Milagros (Fig. 3). The San Jorge sector presents the highest zinc and lead grades both in the sulphide and in supergene mineralisations. Karst-related features are abundant in the San Jorge area (e.g. caves and conduits, attested by broken drill cores and reduced or no recovery) implying high non-sulphide Zn concentrations. Discordant Zn–Pb ore bodies with significant supergene contribution characterize the Sam Fault sector. In Karen Milagros, the mineralisation is dominantly stratabound and almost totally composed of sulphides. In the Central sector, supergene mineralisation predominates as stratabound ore bodies.

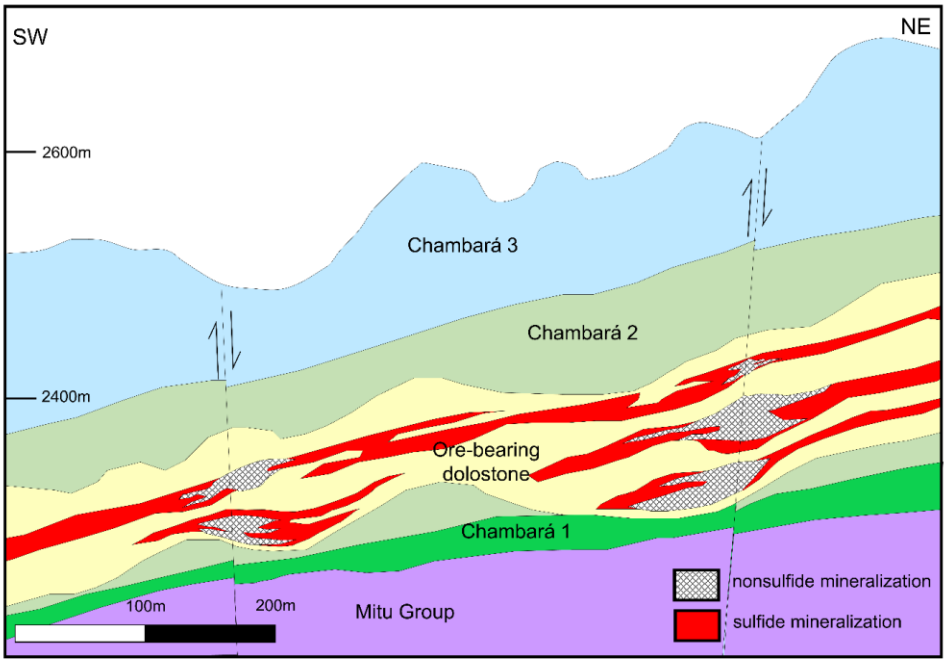

Fig. 2. Schematic NE–SW geological section highlighting the direct-replacement occurrence form of the Zn non-sulphide ore related to low heave-faults in the Florida Canyon deposit.

Methods

The sampling of drill cores took into consideration the distribution of the mineralisation throughout the deposit (Fig. 3). The mineral assemblages were characterized by means of the petrographic study of 36 polished sections and the automated Mineral Liberation Analysis (MLA) of 65 carbon-coated polished thin sections. MLA was performed using in a Quanta 650F FEG scanning electron microscope (SEM) equipped with two energy dispersive X-ray spectrometers (EDS) and a Bruker XFlash SDD-type silicon drift detector, under 25 kV operating conditions, at the Centre of Microscopy at the Federal University of Minas Gerais, Belo Horizonte, Brazil (CM–UFMG).

For carbon and oxygen stable isotope analysis, a selective sampling of the oxidation zone was made, seeking zones of massive smithsonite. Four samples were obteained using a Dremel 3000 diamond drill. The isotope compositions were determined using the continuous flow method and a Thermo Finnigan GasBench II equipment coupled to a Delta V Advantage mass spectrometer at the Stable Isotope Laboratory of the University of São Paulo, Brazil (LIESP-USP). Isotope ratios were determined on CO2 gas released from carbonate minerals by the reaction with orthophosphoric acid at 72 °C and corrected using the phosphoric acid fractionation factors given by Gilg et al. (2008) for smithsonite. Results are reported in conventional per mil notation (‰) relative to the Vienna Pee Dee Belemnite (VPDB) and the Vienna Standard Mean Ocean Water (VSMOW) standards for carbon and oxygen.

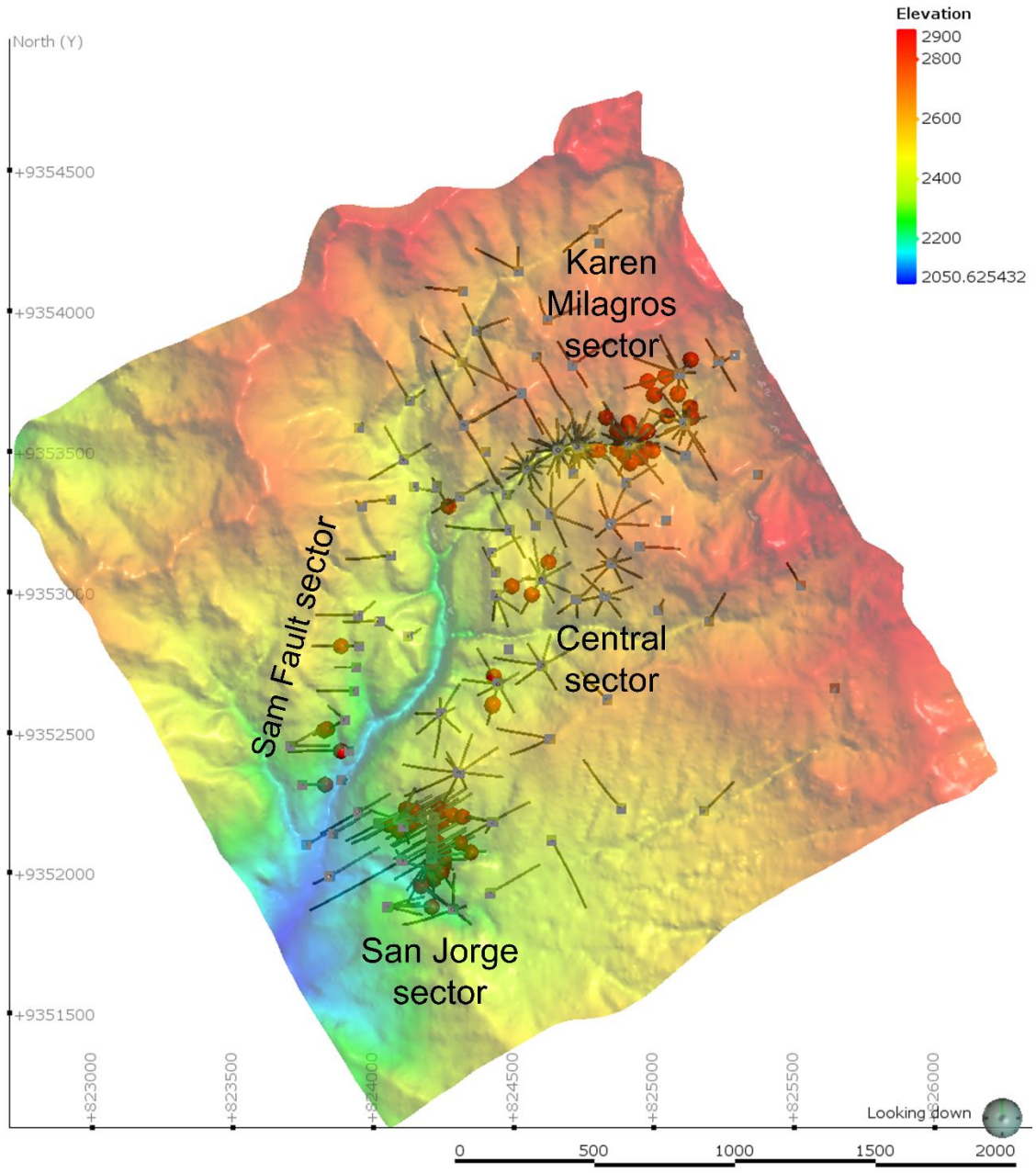

Fig. 3. Terrain elevation map with the spatial position of diamond drilling and sample location (red dots).

Results

Supergene ore mineralogy and SEM-MLA quantitative analyses

Smithsonite ($ZnCO_3$) and hemimorphite [$(Zn_4Si_2O_7(OH)_2.H_2O$] result from supergene alteration superimposed to the primary sulphide orebodies composed of sphalerite, galena, and pyrite. Supergene ore occurs predominantly in the Chambará 2 horizon (Fig. 3) and was formed from both stratabound and discordant sulphide ore in the Florida Canyon deposit. Smithsonite

and hemimorphite are earthy, colloform or form agglomerates, with colours varying from orange to medium brown (Fig. 4). The distinction of these minerals in hand specimens is not easy, being sometimes mistaken for cream dolomite. A possible identification can be made with "zinc-zap" solution (Hitzman et al., 2003), a chemical compound that in contact with zinc minerals turns into a vivid scarlet colour (Fig. 4e). Under the microscope, a common irregular replacement of sulphide minerals by zoned colloform smithsonite and remaining sphalerite lamella are observed (Fig. 4g). Smithsonite (from 0.1 to 63.4 wt %, average 4.5 wt %) usually predominates over the hemimorphite (from 0.1 to 8.1 wt %, average 1.3 wt %) being *ca.* three times more abundant (Table 1). These minerals are frequently accompanied by relict sphalerite (Figs. 4h, 5). In turn, cerussite ($PbCO_3$) is associated with relict galena (Fig. 4b).

The results of the mineral quantitative analysis by EDS are presented in Table 1. The Florida Canyon deposit has simple mineralogical composition in which the host rock-forming minerals are dolomite, calcite, and quartz. The maximum contents of these minerals quantified by the combined SEM/EDS-MLA analysis are 98.9 wt %, 58.1 wt %, and 24.6 wt %, respectively. The primary sulphide ore assemblage consists of sphalerite, galena, and pyrite, the maximums contents being 86.9 wt %, 3.7 wt %, and 48.0 wt %, respectively. Supergene assembalges are dominated by smithsonite with a maximum of 63.4 wt %, and hemimorphite, with a maximum of 8.1 wt %. In addition, cerussite occurs at a maximum of 0.7 wt % and goethite (FeO.OH) at a maximum of 2.0 wt %. These ten mineral phases, in different proportions, comprise almost totality of the 65 samples analysed by SEM/EDS-MLA.

Table 1. Mineral Liberation Analysis (SEM-MLA) chemical and mineral quantitative analysis for selected drill core samples. Dol = dolomite, cal =calcite, qtz = quartz, sp = sphalerite, gl = galena, py = pyrite, sm = smithsonite, hm = hemimorphite, gth = goethite, cer = cerussite.

Sample	Sector	Mineral quantitative analysis										Chemical analysis						
		Dol	Cal	Qtz	Sp	Gl	Py	Sm	Hm	Gth	Cer	Ca	Mg	Fe	Si	S	Zn	Pb
V_232-344.60	Karen Milagros	98.0	0.1		0.4		0.2					21.35	12.95	0.13	0.26	0.00	0.25	0.02
V_232-351.90	Karen Milagros	97.9	0.1				0.1					21.41	12.97	0.09	0.09	0.00	0.03	0.00
V_232-354.10	Karen Milagros	90.8	1.2	0.2	3.2	0.4	0.7					20.43	11.99	0.35	1.49	0.00	2.12	0.41
V_233-356.70	Karen Milagros	92.7	0.1		3.3	0.1	0.3	0.2	0.2	0.1		20.26	12.31	0.33	1.26	0.00	2.38	0.08
V_235-349.20	Karen Milagros	97.2	0.1				0.7					21.28	12.84	0.36	0.40	0.00	0.00	0.00
V_235-356.20	Karen Milagros	95.9	0.2	0.1			0.2					20.96	12.93	0.24	0.11	0.00	0.00	0.00
V_235-370.30	Karen Milagros	88.5	0.2	8.2	0.1		0.5					19.36	11.69	0.23	0.27	0.00	0.04	0.00
V_235-374.90	Karen Milagros	63.7		0.1	23.6	3.6	1.6				0.3	14.02	8.41	0.73	9.07	0.00	15.81	3.45
V_237-384.60	Karen Milagros	84.6	0.1	7.2	3.7		0.2					18.54	11.19	0.11	1.33	0.00	2.50	0.04
V_237-385.30	Karen Milagros	97.3		1.8								21.22	12.87	0.04	0.01	0.00	0.00	0.01
V_257-39.90	San Jorge	85.8	0.1		10.6	0.3	1.4		0.1			18.80	11.32	0.68	4.30	0.00	7.17	0.42
V_270-52.20	San Jorge	71.0		12.6	2.5		0.1	6.0	2.1			15.51	9.38	0.13	0.85	0.00	6.03	0.00
V_270-53.20	San Jorge	89.9	0.5	0.3	5.5		0.9					19.93	12.19	0.54	0.53	2.27	3.67	0.00
V_273-58.30	San Jorge	55.7		24.6				4.9	2.5	0.1		12.44	7.62	0.10	11.54	0.01	4.03	0.00
V_277-71.70	San Jorge	76.0	0.5	2.0	16.8	0.1	0.8	0.3	0.9	0.2		16.87	10.20	0.65	0.95	5.97	11.92	0.06
V_279-245.90	Karen Milagros	95.6	0.1	0.3		0.1		0.9	1.7	0.1		20.88	12.71	0.18	0.50	0.03	1.48	0.13
V_288-264.20	Karen Milagros	50.6	42.9	0.4			1.2			0.1		29.11	6.96	0.74	0.65	0.00	0.01	0.00
V_298-131.70	San Jorge	25.3		0.1	54.7	2.8	6.9				0.1	5.70	3.34	3.28	0.04	22.07	36.71	2.49
V_299-82.10	San Jorge	60.9	0.1	1.4	21.5	1.3	0.6				0.2	13.44	8.01	0.27	0.66	7.57	14.46	1.34
V_299-84.00	San Jorge	77.6	1.8	0.1	7.6	0.1	0.4					20.27	10.25	0.21	0.10	2.74	5.11	0.05
V_301-132.60	San Jorge	54.7			26.4		2.1					11.95	7.20	0.99	0.01	9.79	17.66	0.01
V_302-101.90	San Jorge	5.6			86.9	1.2	0.2	0.9	0.4			1.32	0.74	0.10	0.05	28.88	59.04	1.06
V_303-154.80	San Jorge	66.4		0.2	22.3		0.2	0.6	0.2			14.37	8.67	0.13	0.11	7.50	15.47	0.00
V_304-135.70	Karen Milagros	97.2	0.1	0.3				1.1	0.4			21.22	12.90	0.06	0.02	0.00	0.79	0.01
V_304-136.70	Karen Milagros	48.3		9.1	28.5	0.8	1.0	0.2	1.2		0.1	10.62	6.55	0.53	9.99	0.00	19.92	0.79
V_317-155.20	Karen Milagros	84.5	1.4	2.2	3.0	0.3	0.4	0.4	0.6			19.17	11.22	0.24	1.24	0.00	2.57	0.33
V_329-147.60	Karen Milagros	74.9	2.3	2.1	2.1	0.2		1.2	0.6	2.0		17.33	9.90	1.42	1.07	0.73	2.33	0.21
V_329-151.20	Karen Milagros	84.9	1.0					6.1				18.93	11.20	0.01	0.02	0.00	3.20	0.00
V_329-154.50	Karen Milagros	97.0	0.2	0.2	0.3		0.3					21.25	12.90	0.19	0.26	0.00	0.20	0.02
V_329-164.40	Karen Milagros	98.9	0.2						0.1	0.1		21.62	13.08	0.11	0.00	0.00	0.03	0.01
V_333-99.80	Karen Milagros	87.9	0.1	0.2				9.5	1.2			19.18	11.68	0.10	0.37	0.01	5.69	0.02
V_334-108.50	Karen Milagros	89.8	1.3	0.2	2.3	0.1	0.4		0.5			20.11	12.36	0.45	0.86	0.98	1.81	0.09

Sample	Sector	Mineral quantitative analysis										Chemical analysis						
		Dol	Cal	Qtz	Sp	Gl	Py	Sm	Hm	Gth	Cer	Ca	Mg	Fe	Si	S	Zn	Pb
V_335-177.30	Karen Milagros	10.3	0.5	1.0	10.1	0.6	48.0			0.1		3.20	1.37	22.15	0.47	28.77	6.80	0.55
V_335-179.60	Karen Milagros	97.9	0.1	0.4			0.4					21.41	12.97	0.20	0.20	0.00	0.02	0.00
V_336-86.80	Karen Milagros	88.4	0.5						6.4	0.1		19.69	11.68	0.09	0.84	0.00	3.77	0.00
V_336-97.00	Karen Milagros	87.6	0.6	0.1	0.2	0.2		3.2	1.5		0.1	19.52	11.57	0.03	0.24	0.11	2.68	0.20
V_337-183.50	Karen Milagros	94.6	0.4	0.4			0.5					20.79	12.59	0.31	0.37	0.29	0.00	0.00
V_337-188.00	Karen Milagros	86.8	4.5	1.4						0.1		21.35	11.68	0.14	0.00	0.00	0.00	0.03
V_339-136.10	Karen Milagros	80.9	0.2	10.3	0.1		0.1	1.7	3.6	0.3		17.71	10.70	0.25	0.07	0.00	3.06	0.05
V_339-154.90	Karen Milagros	98.8					0.2					21.56	13.04	0.13	0.13	0.00	0.02	0.01
V_339-164.00	Karen Milagros	97.9	0.2	0.7			0.5					21.43	12.94	0.27	0.28	0.00	0.02	0.00
V_340-148.00	Karen Milagros	24.7	48.9				0.2					33.44	3.82	0.34	0.09	0.00	0.00	0.00
V_340-150.00	Karen Milagros	87.3	0.1	0.1	3.1	0.5	1.1		0.1			19.08	11.53	0.55	1.70	0.00	2.11	0.53
V_340-163.50	Karen Milagros	69.8	0.1	0.2	14.5	0.8	0.3	0.1	0.1		0.1	14.67	8.51	0.13	0.11	5.35	10.43	0.88
V_340-164.70	Karen Milagros	83.7	1.1	0.6	0.7			0.1	0.5			19.28	11.04	0.03	0.37	0.25	0.87	0.04
V_346-108.60	San Jorge	83.9	0.1	1.6	8.7		0.5	1.2	0.1			18.44	11.40	0.38	1.23	3.13	6.57	0.00
V_346-109.60	San Jorge	86.6	0.1	1.4	5.3		0.2	3.6	0.4	0.1		19.00	11.60	0.20	0.97	1.81	5.60	0.00
V_349-172.10	Karen Milagros	88.9	0.2		1.5		0.1	0.3				19.61	11.69	0.04	0.01	0.53	1.13	0.03
V_351-200.80	Karen Milagros	90.4	0.2		6.2		0.1					19.81	12.21	0.20	0.43	2.11	4.16	0.03
V_352-141.30	Karen Milagros	97.8		0.2					0.4			21.28	13.10	0.10	0.42	0.00	0.26	0.00
V_354-37.10	San Jorge	19.6	58.1	7.7	2.3		2.2	0.1	0.2	0.3		27.27	3.58	1.53	4.65	1.92	1.72	0.00
V_355-118.00	San Jorge	58.5	4.2	3.5	9.8	1.6	5.9	0.6	8.1	0.1	0.7	14.24	7.48	2.90	3.46	6.71	11.82	2.24
V_356-212.90	San Jorge	26.3	0.6	0.1				63.4	6.7	0.3		6.02	3.58	0.73	1.05	0.02	37.18	0.00
V_360-154.70	Karen Milagros	90.1	0.4	0.6				2.6	1.0			19.81	11.97	0.08	0.03	0.00	1.97	0.07
V_360-209.90	Karen Milagros	70.2	0.1	10.9			0.3		0.1			15.29	9.26	0.17	0.24	0.00	0.09	0.03
V_361-154.20	Karen Milagros	27.5	55.1	2.9			0.1					32.90	3.85	0.14	1.69	0.04	0.00	0.01
V_361-154.90	Karen Milagros	93.1	1.5	0.7					0.1			20.92	12.54	0.14	0.72	0.01	0.03	0.00
V_361-157.30	Karen Milagros	74.3	0.1	0.8	15.1	3.7	0.8		0.3		0.2	16.45	9.83	0.41	0.50	5.89	10.31	3.46
V_361-157.60	Karen Milagros	90.5	0.2	3.1	0.1		0.1					19.79	12.44	0.30	2.16	0.11	0.06	0.04
V_361-160.30	Karen Milagros	97.6	0.3	0.1			0.1					21.34	12.97	0.12	0.19	0.07	0.00	0.00
V_361-172.70	Karen Milagros	94.6	1.1							0.2		21.20	12.52	0.12	0.00	0.00	0.01	0.00
V_361-173.50	Karen Milagros	78.4	0.4	16.7			0.5					17.28	10.36	0.22	7.83	0.25	0.01	0.02
V_361-174.80	Karen Milagros	96.1	0.5	0.3			0.1			0.1		21.30	12.74	0.16	0.23	0.06	0.01	0.00
V_363-181.00	Karen Milagros	76.2	0.5		14.3	0.1	0.6					17.29	10.06	0.28	0.03	5.02	9.59	0.05
V_363-187.90	Karen Milagros	89.3	0.2	4.7	2.2	0.1	0.2		0.2			19.54	12.09	0.24	2.68	0.82	1.57	0.05

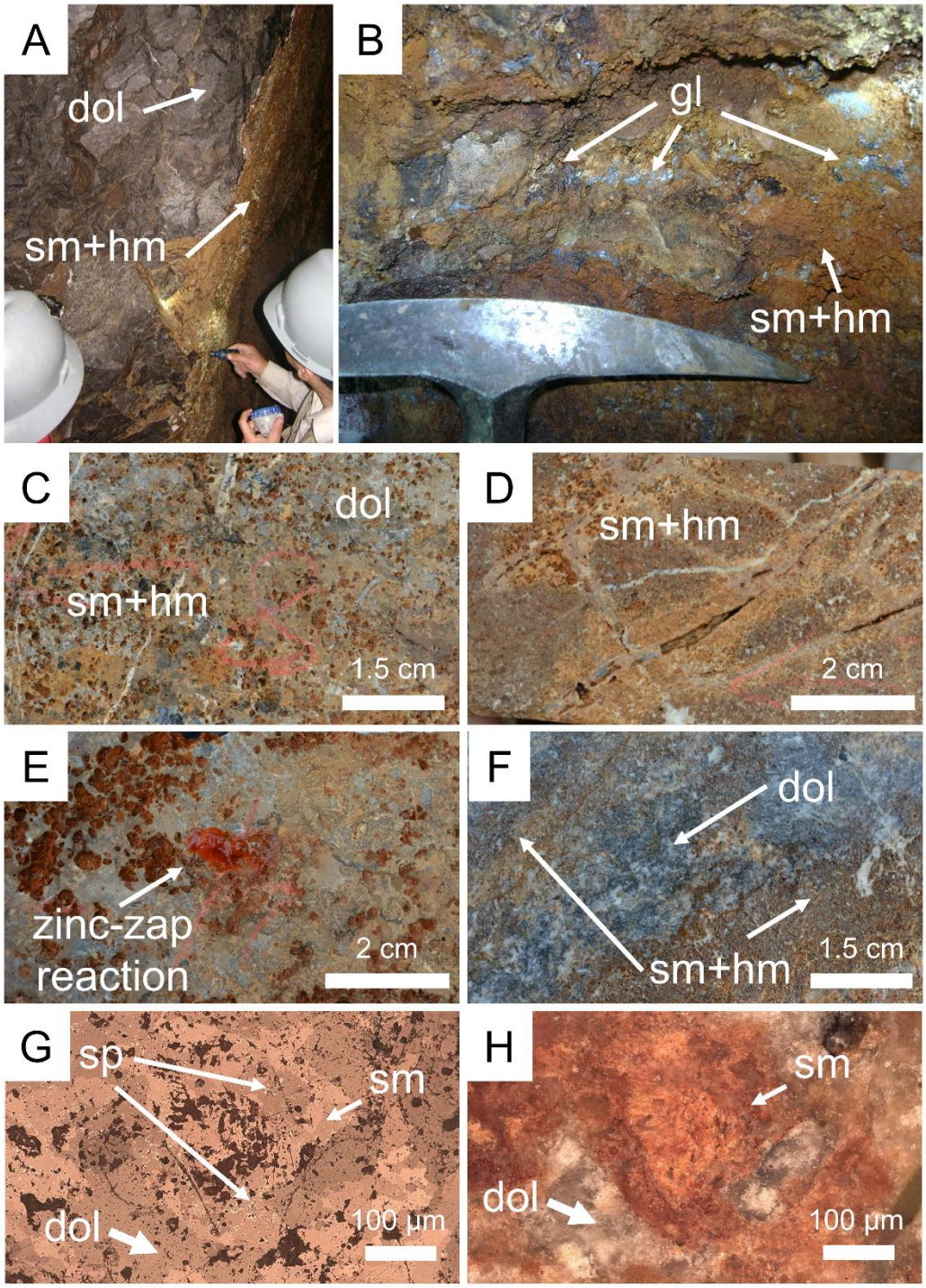

Fig. 4. Most representative non-sulphide samples. (a) Research gallery wall photo with non-sulphide mineralisation as wall-rock replacement type. (b) Research gallery wall photo of non-sulphide mineralisation with galena relicts. (c) Drillcore sample V_270-47-70: Porous dolostone with smithsonite and hemimorphite. (d) Drillcore sample V_270-45.00: Preserved stockwork texture with non-sulphide mineralisation. (e) Drillcore sample V_270-77.10: Reaction of zinc zap solution in porous dolostone with non-sulphide mineralisation. (f) Drillcore sample V_312-63.90: Gradational supergene alteration associated with fractures. (g) Photomicrograph of sample V_329-151.80: Smithsonite in collomorph to crustiform texture. (h) Photomicrograph of sample V_199-223.80: Fine sphalerite relicts associated with smithsonite. Dol = dolomite, hm = hemimorphite, sm = smithsonite and sp = sphalerite.

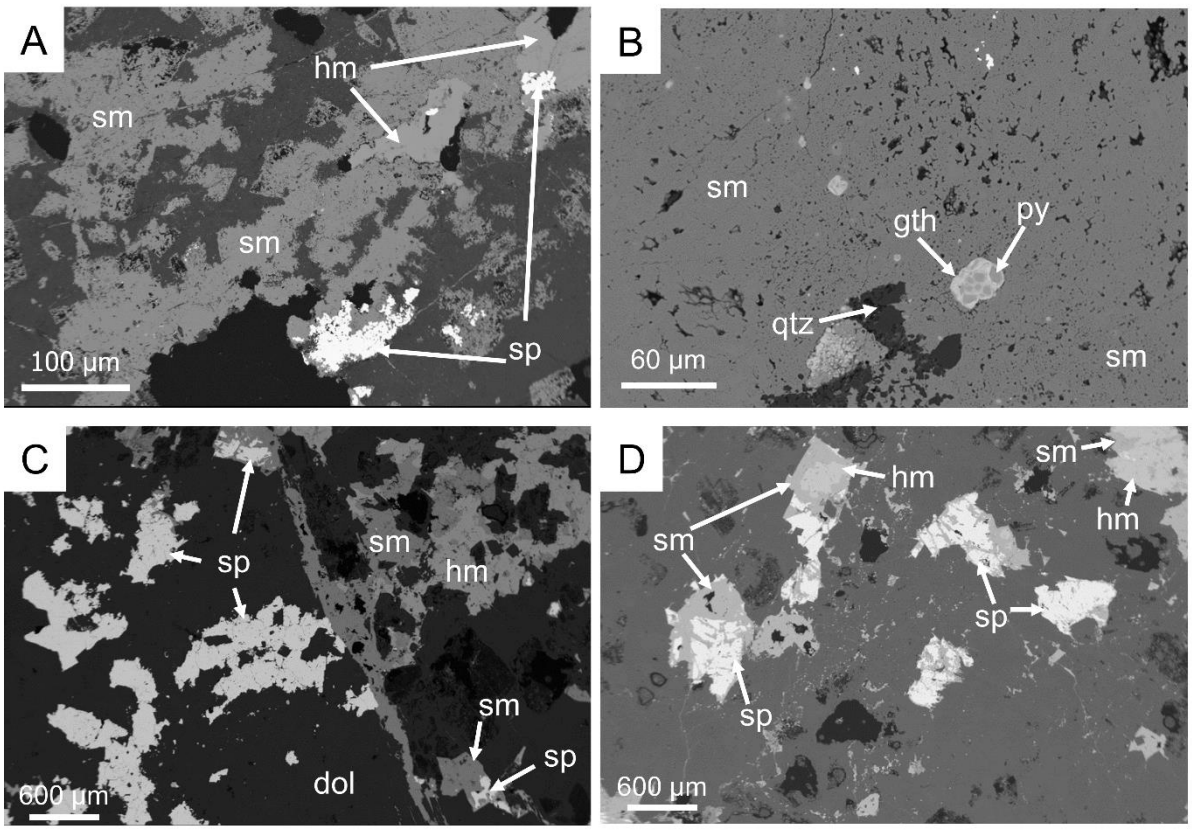

Fig. 5. Scanning electron microscope (SEM) images of the non-sulphide minerals. (a) V_270-47.70: Sphalerite as relict both in smithsonite as in hemimorphite. (b) V_270-47.70: Pyrite cores with an alteration border of goethite. (c) V_312-45.00: Smithsonite in veins and bordering sphalerite. (d) V_312-63.90: Sphalerite as relict both in smithsonite as in hemimorphite. Dol = dolomite, hm = hemimorphite, qtz = quartz, sm = smithsonite and sp = sphalerite.

Forty-two samples are from the supergene zone and contain at least one of the following minerals: smithsonite, hemimorphite, goethite or cerussite. Eleven samples contain only primary sulphide minerals such as sphalerite or galena, and the remaining twelve samples are composed only of the main rock-forming minerals (dolomite, calcite or quartz).

In general, all sectors show the same ore mineral assemblage but in different proportions. The San Jorge sector shows greater average contents of sphalerite (13.2 wt. %), galena (1.1 wt. %); smithsonite (7.6 wt. %) and hemimorphite (1.3 wt %) than the Karen Milagros sector (maximum sphalerite, galena, smithsonite and hemimorphite contents of 6.0; 0.8; 2.0 and 1.0 wt %, respectively), indicating higher amounts of Zn and Pb concentrations in the San Jorge sector relatively to the northern region.

The non-sulphide mineralisation reflects different stages of oxidation (Fig. 4) sometimes with the complete alteration of primary sulphide minerals and could be assigned to a direct-replacement type of supergene mineralisation (Hitzman et al., 2003). The supergene ore shows predominantly features of in situ oxidation and replacement of previous zinc and lead-bearing

sulphides due to the constant presence of remnant minerals (Fig. 4b, h). However, some local occurrences of non-sulphide mineralisation in a metric cave wall found in the metre-sized research gallery in the San Jorge sector indicate the wall-rock replacement type (Fig. 4a). Gradational supergene alteration associated with fractures also occurs (Fig. 4c, d, f).

Carbon and oxygen isotopes

Smithsonite samples yielded $\delta^{18}O$ values ranging from +19.6 to +26.2‰ and $\delta^{13}C$ values ranging from –0.9 to +0.7‰ (Table 2). Three samples plot in the Florida Canyon ore-related dolomite field of Reid (2001) and a sample plots in the global supergene smithsonite field (Gilg et al., 2008) (Fig. 6). It is worth mentioning that the supergene mineral phases are very-fine grained and difficult to separate from one another. In all 24 samples analysed by SEM-MLA that contain smithsonite (0.1 to 63.4 wt %), dolomite also occurs in different proportions (5.6 to 97.2 wt %, Table 1). It seems that the smithsonite samples also conatin dolomite (Fig. 6), resulting in a mixture of smithsonite with dolomite isotope compositions. Thus, these are only preliminary data and more carbon and oxygen isotope data is needed for further discussion.

Table 2. Carbon and oxygen isotope composition of supergene carbonates, predominantly smithsonite, from Florida Canyon deposit.

Sample	$\delta^{13}C_{VPDB}$(‰)	$\delta^{18}O_{VSMOW}$(‰)
V_270-45.00-C	+0.7	+19.6
V_270-47.70-C	-0.9	+26.2
V_312-45.00-C	0.0	+19.6
V_312-63.90-D	-0.9	+21.5

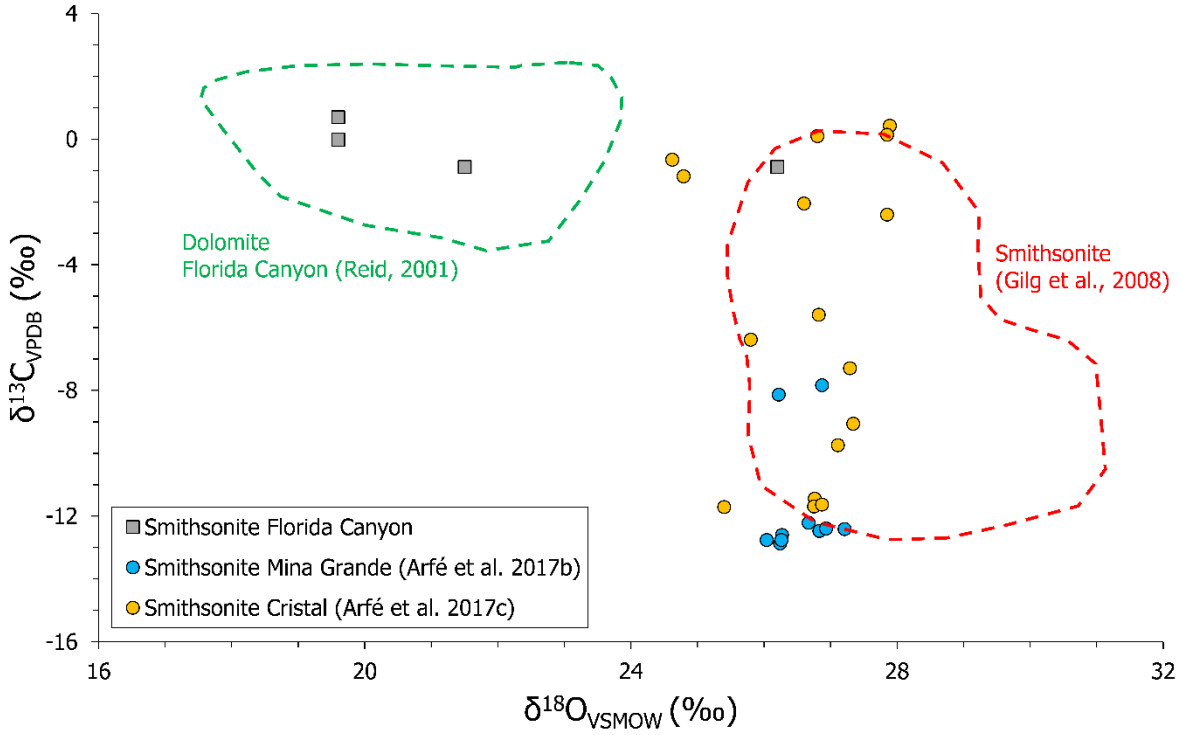

Fig. 6. Geochemical plot $\delta^{18}O$ vs $\delta^{13}C$ for smithsonite of Florida Canyon deposit compared with smithsonites from Mina Grande (Arfè et al., 2017b) and Cristal (Arfè et al., 2018). Florida Canyon ore-related sparry dolomite field (Reid 2001). Global supergene smithsonite field (Gilg et al. 2008).

Discussion

Supergene mineralization

The non-sulphide Zn mineralisation in the Florida Canyon deposit is frequently accompanied by relicts of the primary sulphide mineralisation (Fig. 3), taking place in the same sequence of host rocks. Sphalerite occurs associated with smithsonite or hemimorphite in 22 out of 34 SEM/EDS-MLA samples (Table 1). The identified non-sulphide assemblage of smithsonite, hemimorphite, and cerussite in Florida Canyon is typically found in non-sulphide deposits derived from MVT deposits (Hitzman et al., 2003). The presence of remnant sulphides indicates an in situ alteration assigning it to direct replacement, with local wall-rock replacement, according to the classification of Sangameshwar and Barnes (1983), reviewed by Hitzman et al. (2003). During the development of a research gallery in the San Jorge sector, a metre-sized karst cavern was intercepted. The gallery is located outside the main known Zn ore bodies. However, local stratabound ore occurrences were intercepted with supergene direct replacement (Fig. 4b) and also a wall-rock mineralisation type on the cave wall (Fig. 4a). The

walls of the cavity are covered by concretionary aggregates of smithsonite, hemimorphite, and goethite. The ore texture indicates that the cavity was initially formed and then Zn supergene minerals precipitated into the cavern wall (Fig. 4a). This wall rock type feature occurs locally and is not predominant throughout the deposit.

The spatial position of the supergene mineralisation in Florida Canyon does not define a clear level near the surface as in other deposits located in tropical areas, such as the Lough Keng deposit, Myanmar (Hitzman et al., 2003). Instead, the Florida Canyon non-sulphide mineralisation occurs at depths ranging from a few meters from the surface down to hundreds of meters, which suggests groundwater percolation in hydrologic systems developed along minor offset faults or fractures and discontinuities in the carbonate rocks (Fig. 2).

Galena seems to be more resistant to the oxidising groundwater than sphalerite and thus could occur in association with smithsonite and hemimorphite (Fig. 4b). The total replacement of sulphide minerals by non-sulphide minerals was observed in only 10 SEM/EDS-MLA samples. However, there is relict galena in the eight samples where cerussite occurs (Table 1). The sphalerite relicts are better observed in thin sections (Fig. 4g, h) and BSE images (Fig. 5a, c, d), as well as the alteration of pyrite to goethite (Fig. 5b). The oxidation of pyrite makes the percolating water more acidic and consequently the replacement of sulphides by supergene minerals is more effective. The frequent occurrence of original sulphide relicts in Florida Canyon may be linked to the original low pyrite contents (1.8 wt. % on average, Table 1).

The first mineral that is commonly produced by sphalerite oxidation is smithsonite (Reichert and Borg, 2008). In natural conditions, subsurface water pH ranges from 6 to 8, which is in agreement with the the smithsonite precipitation field at 25 °C (Takahashi, 1960). The precipitation of minor hemimorphite and cerussite in Florida Canyon is conditioned to pH decreases. One of the main agents that lead to pH decrease is the oxidation of pyrite (Hitzman et al., 2003). As seen in the previous paragraph, pyrite contents in Florida Canyon are low, thus explaining the low hemimorphite and cerussite contents and partial sphalerite and galena oxidation.

Takahashi (1960) determined experimentally the stability fields of the common paragenesis of supergene Zn deposits (smithsonite, hemimorphite, and hydrozincite) simulating supergene conditions when the minerals were contacted with meteoric water (approximately 25 °C and 1 atm pressure). The conversion of smithsonite to hydrozincite [$Zn_5(CO_3)_2(OH)_6$] is controlled by pH and CO_2 partial pressure. Takahashi (1960) shows that in arid climate

conditions, hydrozincite predominates over smithsonite on the surface, but the relationship reverses with depth.

Hydrozincite is not abundant under tropical climatic conditions, and smithsonite predominates (Takahashi, 1960). Hemimorphite is more stable than hydrozincite and smithsonite under lower pH conditions, and it is not expected to be formed under near-neutral pH climatic conditions (Hitzman et al., 2003). In other words, for the formation of hemimorphite, sufficiently acidic conditions are required to reach and maintain lower pH, which is usually achieved when large quantities of pyrite are present and sulfuric acid is generated (Sangameshwar and Barnes, 1983). The predominance of smithsonite with minor hemimorphite and absence of hydrozincite suggests a tropical climate environment for the formation of Zn supergene mineralisation in Florida Canyon deposit.

A comparison with other non-sulphide Zn deposits in the Bongará District

The nearby non-sulphide Zn deposits of Mina Grande (Arfè et al., 2017b) and Cristal (Arfè et al., 2018), also located in the Bongará district, despite presenting similar mineral composition similar to that of Florida Canyon, contain hydrozincite. Although Mina Grande, Cristal, and Florida Canyon supergene deposits are related to the primary MVT-sulphide mineralisation hosted in the Pucará Group, they occupy different stratigraphy positions. The Zn mineralisation in Mina Grande and Cristal is hosted in the Condorsinga Formation, whereas the Florida Canyon Zn supergene and sulphide mineralisations types are hosted in the Chambará Formation. There are no descriptions of Zn supergene occurrence in the San Vicente and Shalipayco MVT deposits also related to the Pucará Group rocks. A brief comparison of the three supergene Zn deposits of the Bongará District (Mina Grande, Cristal, and Florida Canyon) is presented in Table 3.

Almost all supergene SEM/EDS-MLA samples from the Florida Canyon deposit show the smithsonite ± hemimorphite assemblage, not evidencing different types of supergene mineralisation as observed in the Cristal deposit (Arfè et al., 2018). Out of 34 samples, 22 contain smithsonite and hemimorphite, 10 hemimorphite only, and 2 smithsonite only (Table 1). Out of 32 hemimorphite-bearing SEM/EDS-MLA samples, 27 also contain quartz, suggesting that hemimorphite formed in lithotypes richer in silica, as also described in the Cristal deposit (Arfè et al., 2018).

Table 3. Summary comparison of Zn supergene deposits data from the Bongará District, Northern Peru, with the Florida Canyon, Mina Grande (Arfè et al., 2017a; Arfè et al., 2017b) and Cristal deposits (Arfè et al., 2018; Mondillo et al., 2018a).*Classification for nonsulfide zinc deposits from Hitzman et al. (2003).

Deposit	Mineralization type	Host stratigraphic unit	Supergene deposits classification*	Main Zn supergene minerals	Other supergene minerals
Florida Canyon	sulphide, non-sulphide	Chambará Fm.	direct replacement, (wall-rock replacement)	smithsonite >> hemimorphite	goethite, cerussite, calcite
Cristal	sulphide, non-sulphide	Condorsinga Fm.	direct replacement	smithsonite >> hemimorphite, hydrozincite	goethite, greenockite, siderite, chalcophanite, synchysite, sauconite, hendricksite, calcite
Mina Grande	nonsulphide	Condorsinga Fm.	residual and karst-fill	hydrozincite >> smithsonite, hemimorphite	geothite, desclozite, otavite, fraipontite, zaccagnaite, calcite

The Florida Canyon supergene paragenetic sequence is characterized by initial smithsonite with later hemimorphite replacing minerals or filling spaces (Fig. 5). Arfè et al. (2017b) and Arfè et al. (2018) interpreted the evolution of the supergene mineralisation in the Mina Grande and Cristal deposits, based respectively on the South American events of mega-wetland ecosystems (Hoorn et al., 2010) and tectonic uplifts that affected the Bongará District (Pfiffner and Gonzalez, 2013). Arfè et al. (2018) attribute the main smithsonite stage in Cristal to a Mid to Late Miocene uplift (ca. 10–7 Ma) during the Pebas mega-wetland ecosystems (Hoorn et al., 2010). On the other hand, Arfè et al. (2017b) attribute the first generation of smithsonite in the Mina Grande deposit to Miocene-Early Pliocene (ca. 7 Ma) during the switch from the Pebas to the Acre mega-wetland ecosystems (Hoorn et al., 2010) and the Quechua II tectonic event (Pfiffner and Gonzalez, 2013). The distinction between the two stages of smithsonite generation is based on their different oxygen isotopic compositions (Arfè et al., 2018). However, preliminary oxygen isotope data for the Florida Canyon must be dealt with caution, because of the mixing of fine smithsonite with dolomite during preparation. A later development of a karstic system with a second smithsonite stage associated with the Pliocene-Early Pleistocene uplift is interpreted in the Mina Grande deposit (Arfè et al., 2017b). The Florida Canyon non-sulphide Zn ore correlates better with the Cristal supergene deposit in terms of the predominance of direct-replacement mineralisation style, with the presence of original sulphides, similar dolostone host rock, scarce hydrozincite and the depth of the supergene enrichment, which allows assuming a Miocene age for both deposits. .

Concluding Remarks

1. The mineral characterization of the Florida Canyon zinc and lead deposit showed that the ore minerals comprise both sulphides – sphalerite, galena and pyrite –, and non-sulphide – smithsonite (mainly), hemimorphite, cerussite, and goethite –, which are hosted by carbonate rocks composed of dolomite, calcite, and quartz.

2. The genesis of Florida Canyon non-sulphide mineralisation is associated with fault structures reaching up to hundreds of meters in depths. This supergene assemblage is a paleo-climatic guide, suggesting tropical climatic conditions for its generation. By analogy to the Cristal non-sulphide Zn deposit, also located in the Bongará District, a late Miocene age is assumed for the Florida Canyon supergene Zn mineralisation.

3. The ore minerals (sulphide and non-sulphide) occur in different proportions in the four sectors of the Florida Canyon deposit. Therefore, a concentration plant with different routes for the different ore types should be considered in the economic evaluation of the deposit.

Acknowledgments

The authors would like to thank Votorantim Metais (now Nexa Resources) and Solitario Resources for allowing the use of the data and the field geologist team for the discussions and assistance during fieldwork. We would like to thank the two anonymous reviewers for their suggestions and comments, which surely improved the quality of the paper.

References

Arfè, G., Mondillo, N., Balassone, G., Boni, M., Cappelletti, P., Di Palma, T., 2017a. Identification of Zn-bearing micas and clays from the Cristal and Mina Grande zinc deposits (Bongará Province, Amazonas Region, Northern Peru). Minerals 7, 214-231.

Arfè, G., Mondillo, N., Boni, M., Balassone, G., Joachimski, M., Mormone, A., DiPalma, T., 2017b. The karst-hosted Mina Grande nonsulfide zinc deposit, Bongará District (Amazonas Region, Peru). Economic Geology 112, 1089-1110.

Arfè, G., Mondillo, N., Boni, M., Joachimski, M., Balassone, G., Mormone, A., Santoro, L., Medrano, E.C., 2018. The Cristal Zn prospect (Amazonas region, Northern Peru). Part II: An example of supergene enrichments in tropical areas. Ore Geology Reviews 95, 1076-1105.

Basuki, N.I., Spooner, E.T.C., 2009. Post-early Cretaceous Mississippi Valley-type Zn-Pb mineralization in the Bongara Area, Northern Peru: fluid evolution and paleo flow from fluid inclusion evidence. Exploration and Mining Geology 18, 25-39.

Basuki, N.I., Taylor, B.E., Spooner, E.T.C., 2008. Sulfur isotope evidence for thermochemical reduction of dissolved sulfate in Mississippi Valley-type zinc-lead mineralization, Bongara area, northern Peru. Economic Geology 103, 783-799.

Fontbote, L., Gorzawski, H., 1990. Genesis of the Mississippi Valley-type Zn-Pb deposit of San Vicente, central Peru; geologic and isotopic (Sr, O, C, S, Pb) evidence. Economic Geology 85, 1402-1437.

Gilg, H.A., Boni, M., Hochleitner, R., Struck, U., 2008. Stable isotope geochemistry of carbonate minerals in supergene oxidation zones of Zn–Pb deposits. Ore Geology Reviews 33, 117-133.

Hitzman, M.W., Reynolds, N.A., Sangster, D.F., Allen, C.R., Carman, C.E., 2003. Classification, genesis, and exploration guides for nonsulfide zinc deposits. Economic Geology 98, 685-714.

Hoorn, C., Wesselingh, F.P., Hovikoski, J., Guerrero, J., 2010. The development of the amazonian mega-wetland (Miocene; Brazil, Colombia, Peru, Bolivia). Amazonia, landscape and species evolution: a look into the past, 123-142.

Hunt, W., Pennington, J.B., D.H., S., Poeck, D.H., Osborn, J., Gilbertson, J., Tinucci, J., 2017. NI 43-101 Technical Report Preliminary Economic Assessment Florida Canyon Zinc Project Amazonas Department, Peru. SRK Consulting (U.S.), Inc., p. 217.

Loughman, D.L., Hallam, A., 1982. A facies analysis of the Pucara Group (Norian to Toarcian carbonates, organic-rich shale and phosphate) of central and northern Peru. Sedimentary Geology 32, 161-194.

Mondillo, N., Arfè, G., Boni, M., Balassone, G., Boyce, A., Joachimski, M., Kang, J.S., Villa, I.M., 2018a. The Cristal Zinc prospect (Amazonas region, Northern Peru). Part I: New insights on the sulfide mineralization in the Bongará province. Ore Geology Reviews 94, 261-276.

Mondillo, N., Arfè, G., Herrington, R., Boni, M., Wilkinson, C., Mormone, A., 2018b. Germanium enrichment in supergene settings: evidence from the Cristal nonsulfide Zn prospect, Bongará district, northern Peru. Mineralium Deposita 53, 155-169.

Moritz, R., Fontboté, L., Spangenberg, J., Rosas, S., Sharp, Z., Fontignie, D., 1996. Sr, C and O isotope systematics in the Pucará basin, central Peru. Mineralium Deposita 31, 147-162.

Pfiffner, O., Gonzalez, L., 2013. Mesozoic–Cenozoic evolution of the Western margin of South America: case study of the Peruvian Andes. Geosciences 3, 262-310.

Reichert, J., Borg, G., 2008. Numerical simulation and a geochemical model of supergene carbonate-hosted non-sulphide zinc deposits. Ore Geology Reviews 33, 134-151.

Reid, C.J., 2001. Stratigraphy and mineralization of the Bongara MVT zinc-lead district, northern Peru. University of Toronto, p. 179.

Rosas, S., Fontboté, L., Tankard, A., 2007. Tectonic evolution and paleogeography of the Mesozoic Pucará Basin, central Peru. Journal of South American Earth Sciences 24, 1-24.

Sánchez, A., 1995. Geología de los cuadrángulos de Bagua Grande, Jumbilla, Lonya Grande, Chachapoyas, Rioja, Leimebamba y Bolívar: hojas 12-g, 12-h, 13-g, 13-h, 13-i, 14-hy 15-h. Instituto Geológico Minero y Metalúrgico Peru.

Sanchez, A., Chira, J., Romero, D., De la Cruz, J., Herrera, I., Cervante, J., 1999. INGEMMET Serie A: Carta Geológico Nacional 1: 100000. Boletin no 132.

Sangameshwar, S.R., Barnes, H.L., 1983. Supergene processes in zinc-lead-silver sulfide ores in carbonates. Economic Geology 78, 1379-1397.

Spangenberg, J., Fontboté, L., Sharp, Z.D., Hunziker, J., 1996. Carbon and oxygen isotope study of hydrothermal carbonates in the zinc-lead deposits of the San Vicente district, central Peru: a quantitative modeling on mixing processes and CO_2 degassing. Chemical Geology 133, 289-315.

Spangenberg, J.E., Fontboté, L., Macko, S.A., 1999. An evaluation of the inorganic and organic geochemistry of the San Vicente Mississippi Valley-type zinc-lead district, central Peru; implications for ore fluid composition, mixing processes, and sulfate reduction. Economic Geology 94, 1067-1092.

Szekely, T.S., Grose, L.T., 1972. Stratigraphy of the carbonate, black shale, and phosphate of the Pucará Group (Upper Triassic—Lower Jurassic), Central Andes, Peru. Geological Society of America Bulletin 83, 407-428.

Takahashi, T., 1960. Supergene alteration of zinc and lead deposits in limestone. Economic Geology 55, 1083-1115.

Vega, I.M.R., 2018. Geologia y mineralizacion del deposito Mississipi Valley-type de Zn-Pb, proyecto Canon Florida, Norte de Peru. Universidad Nacional de Huancavelica, Huancavelica, Peru, p. 164.

4 Geology and Genesis of the Shalipayco evaporite-related Mississippi Valley-Type Zn–Pb deposit, Central Peru: geological and C–O–S isotopic constraints

Saulo B. de Oliveira[1,2], David L. Leach[3], Caetano Juliani[2], Lena V. S. Monteiro[2], Craig A. Johnson[4] and Marianna Gulman Nassif Caran[2]

[1]Nexa Resources, São Paulo, SP 04571-010, Brazil

[2]Institute of Geosciences, University of São Paulo, São Paulo, SP 05508-080, Brazil

[3]Center for Mineral Resources Science, Department of Geology and Geological Engineering, Colorado School of Mines, Golden CO 80401, USA

[4]U.S. Geological Survey, MS 963, P.O. Box 25046, Denver, CO 80225, USA

Abstract

The Shalipayco Zn–Pb deposit, located in central Peru, is composed of several stratabound orebodies. The most important of them, which represent the main subject of this study, are Resurgidora and Intermedios. The host rocks are carbonates from the Chambará Formation of the Pucará Group, including boundstones, mudstones and wackestones interdigitated with former evaporite levels interpreted as formed in supratidal-sabkha depositional systems. The Chambará Formation in Shalipayco deposit could be subdivided into four members, named Chambará I to IV from the base to the top, according to descriptive characteristics of carbonate and evaporite rocks. The presence of evaporites in the Pucará sequence has important implications for the generation of a diagenetic ground preparation stage for the subsequent mineralizing event. The replacement of calcium sulfate by dolomite in the presence of organic matter during burial diagenesis produced secondary porosity generating stratigraphic traps and sulfur source for later Zn–Pb sulfide precipitation. This diagenetic dolomitization is quite extensive laterally throughout the Chambará Formation but it is almost conditioned to Chambará II and III members, where it is so intense that partially or completely obliterated the previous sedimentary textures. The Shalipayco mineralogy is composed of a simple assemblage: two types of sphalerite (dark brown and pale yellow sphalerite) and galena, with pyrite, marcasite, dolomite, calcite, barite, chalcedony, and fluorite. Only one ore-stage was identified, and it is characterized by sphalerite and galena associated with late sparry dolomite and calcite as open-space infilling, including vuggs, porous and fractures. Cementation and breccia infills by sulfides also occur. The least altered carbonate rocks have

values of $\delta^{13}C$ between 1.1‰ and 1.9‰ and $\delta^{18}O$ between 27.1‰ and 30.8‰. The oxygen and carbon isotopic composition of burial diagenetic replacement dolomite indicated some organic matter involvement and low formation temperature ($\delta^{13}C$ = 0.2 to 2.1‰ and $\delta^{18}O$ = 20.9 to 26.2‰). Late calcite has lighter carbon compositions ($\delta^{13}C$ = –2.9 to –0.1‰ and $\delta^{18}O$ = 11.0 to 17.5‰) suggesting migration of fluids through organic-rich sequences, probably dark-colored dolostones of the Chambará Formation or rocks from the upper Aramachay Formation. The very negative values of the sulfur isotope in sulfides ($\delta^{34}S$ = –23.3 to –6.2‰) indicate a predominance of bacterial sulfate reduction process. The mixing of incoming metalliferous brines with trapped fluids rich in H_2S could represent an efficient mechanism for the ore deposition at Shalipayco deposit by changes in redox conditions.

Introduction

The Shalipayco Zn–Pb deposit is located in the central highlands of Peru, 170 km northeast of Lima, 35 km southeast of the city of Cerro de Pasco, in the departments of Pasco and Junin. The Zn–Pb sulfide stratabound orebodies are hosted in Late Triassic to Early Jurassic carbonatic rocks of Pucará Group. Ore sulfide showings occur along approximately 12 km in the deposit area following the general strike direction of NW–SE of the host rocks. These surface ore exposures were exploited in small-scale rudimentary shallow underground mines during the 1970s. More recently, after a joint-venture agreement with Pan American Silver in 2006, Votorantim Metais company (now Nexa Resources) and Milpo carried out mineral exploration work including extensive drillhole programs in the Shalipayco deposit. The mineral resources currently known are 23 million tons with grades of Zn 5.1%, Pb 0.5% and Ag 35 g/t (Robson et al. 2017). The Shalipayco deposit is composed of several Zn–Pb stratabound orebodies, but the most expressive are the Resurgidora and Intermedios levels, which contains most of the mineral resources and that is the focus of this work. The surface sulfide occurrences of Eddy with an apparently structural control and subsurface extension not been confirmed by the drillhole survey are also discussed. In the deposit district location several other Zn–Pb deposits are hosted by carbonatic rocks of the Pucará basin, with their genesis interpreted as similar to Shalipayco. as San Vicente (Fontbote and Gorzawski 1990), Cerro Pasco (Baumgartner et al. 2008), Colquijirca (Bendezú and Fontboté 2009), Atacocha and Milpo (Gunnesch and Baumann 1984) and Morococha (Catchpole et al. 2015) (Fig. 1).

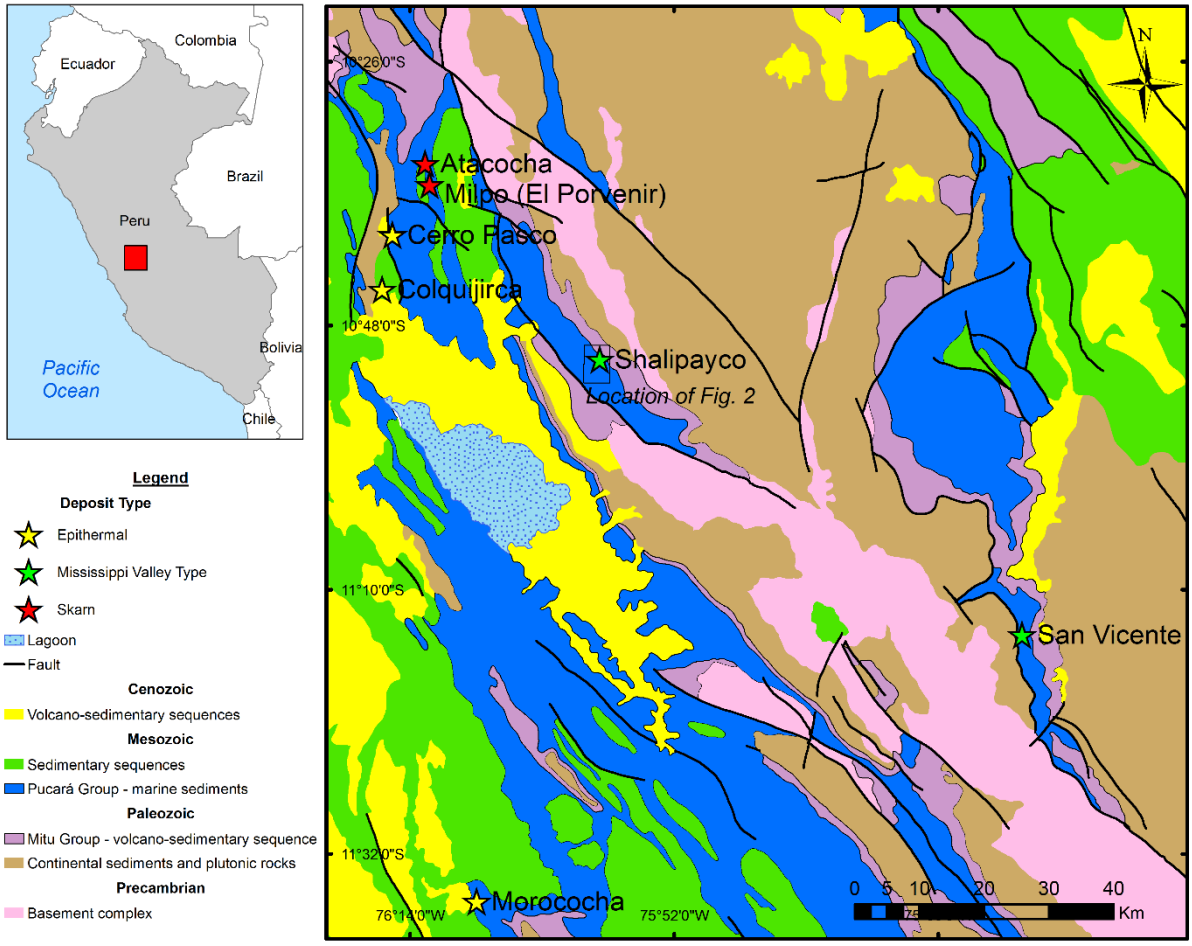

Fig. 1. Geological map from central Peru, simplified from INGEMMET (1999), with the location of Shalipayco deposit and of other selected deposits hosted in Pucará Group, and the study area location (box refers to Fig. 2).

Some aspects of the Shalipayco deposit are discussed by Fontboté (1990), Fontboté et al. (1990), Gunnesch et al. (1990), Soler and Lara (1990) and Moritz et al. (1996). However, there are no detailed geological description and ore characterization in the Shalipayco deposit, which is one of the purposes of this paper. This paper presents new observations of the mineral deposits and much of the geological knowledge accumulated by the geologists who worked on the exploration project, including the recent studies by Tuanama (2016). In addition, this paper addresses the question concerning the origin of the deposit considering the hypothesis of a Mississippi-Valley type (MVT) genetic model or a carbonate-replacement type (CRD) deposit with a distal magmatic source possibly related to the same magmatic source of the ore fluids for the Cerro de Pasco and Atacocha districts. For this, studies based on the geological observations and descriptions and the application of trace elements geochemistry, the stable C–O isotopic analysis in carbonates and S isotopic analysis in sulfides and sulfates were conducted. As results, this paper shows the local stratigraphic compartmentalization of the

Chambará Formation in the deposit and a discussion about its fluid origin, possible sulfur sources and the geological constraints of Zn–Pb mineralization.

Regional Geologic Setting

In the central region of the Andes, tectonic movements of the South American plate produced three different structural features: the Western Cordillera, which includes the magmatic arc resulting from subduction processes, the Eastern mountain range that represents an area of uplift and the region between these is a plateau called Andean Altiplano. Today features observed in the Andes are the result of three separate geodynamic events (Benavides-Cáceres 1999), occurring in the Precambrian, during the period between the Paleozoic and Mesozoic era (until the early Triassic) and between the upper Triassic until the present. The third geodynamic cycle, also known as Andean Cycle, began in the Triassic with the opening of the Atlantic Ocean (Mégard 1984; Mégard 1987; Benavides-Cáceres 1999). In this context, the back-arc zone was subjected to extensional tectonics, generating systems of horst-graben in the central portion of the Andes. The rocks of the Mitu Group formed in the early rift stage includes volcaniclastic and clastic sequences of the Permian-Triassic with thicknesses of 800 to 1,500 meters, and conglomerates, sandstones and polymictic breccias with provenance from andesitic volcanic rocks (Noble et al. 1978).

The extensional and subsidence efforts generated by the rifting process have been gradually fading and changing to a Mesozoic basin with marine deposition during the Pucará Basin evolution (Mégard 1987; Benavides-Cáceres 1999). Located in the Center-North of Peru, the Pucará Basin is bounded on the East by the Guyana Shield and to the West by the Peruvian Altiplano (Rosas et al. 2007). The basin is the first marine transgression of the Andean cycle covering the rocks of the Mitu Group. It is characterized by the predominance of rocks deposited in a shallow marine platform, such as limestone and dolostone, and organic matter-rich fine clastic rocks and evaporites. The rocks of the Pucará Group are described by Mégard (1968) and Szekely and Grose (1972) as a sequence of marine transgressive sediments deposited between the Late Triassic and the Early Jurassic. The Pucará Group is divided into three formations (Chambará, Aramachay, and Condorsinga), according to their lithotypes, fossil content, facies and geochemical aspects (Mégard 1968). The Chambará Formation is the basal unit of the carbonate basin and consists predominantly of dolostone and layers of limestone. Chert is present throughout in the form of nodules or centimeter-thick bands and has

great fossil content (Mégard 1968). Rosas et al. (2007) interpreted the rocks of the Chambará Formation as derived from carbonate platform sediments formed in the transition between the rift stage controlled by faults and the post-rift regional subsidence. The considerable variation of the thickness of unit from 25 meters in Tingocancha to 1,170 meters in San Vicente was considered as consequence of this tectonic evolution. The change in the rate of subsidence controlled not only the thickness of the formation but also the continuity of deep-water depositional facies (Rosas et al. 2007). Carbonatic shales with bituminous and sporadic silty levels with ammonites and other fossils compose the Aramachay Formation, indicated changes in depositional environment. This fossil content reflects a deep and restricted marine depositional environment. Despite being less exposed, this formation is laterally homogeneous and deposition is attributed to a stable platform (Rosas et al. 2007). Condorsinga Formation is composed predominantly of limestone with the presence of dolostone locally in its base that reflects the shallow platform environment. It differs from Chambará Formation by the rare amount of chert and dolostones that is restricted to the basal parts of the sequence. The presence of pseudomorphs after evaporitic minerals lenses indicates a secondary basin subdivision that would have generated hypersaline conditions in a lagoon environment. The age of this formation (Upper Sinemuriana–Toarcian) is indicated by the presence of ammonites (Mégard 1968). However, the rocks from this formation are not common in outcrops due to structural Andean inversion and erosion (Rosas et al. 2007).

Sampling and Analytical Procedures

For the characterization of host and mineralized rocks, 101 samples from seven drillholes (SH-56, SH-60, SH-70, SH-120, SH-180, SH-210, and SH-231) spatially distributed throughout the entire deposit were selected, including the deepest stratigraphic drillhole that cuts all the lithological units (SH-43). The location of the sampled drillhole is shown in the Figure 2. The sampling was done in order to select drillholes that intersect the Intermedios and Resurgidora mineralized levels. The selected samples were described macroscopically and in thin sections and polished thin sections were prepared for analysis under a Leica DM750P optical microscope (transmitted and reflected light). The samples were treated with a solution of potassium ferrocyanide and Alizarin-S in order to differentiate the carbonate minerals (calcite, dolomite and iron carbonates). Double-polished thin sections were observed for fluid inclusion petrographic studies in an Olympus BX51 research microscope in the Fluid Inclusion

Laboratory at the Colorado School of Mines, USA. However the fluid inclusions are very small (less than 5 μm in diameter) and difficult to obtain microthermometric measurements (Goldstein and Reynolds 1994).

The analytical results of Ag, As, Ba, Be, Bi, Cd, Co, Cr, Cu, Hg, In, Mn, Mo, Ni, Pb, Sb, Sr, Ti, V, W and Zn of 20,538 drill core whole-rock samples from the Votorantim Metais database were used. The samples comprise half drill cores sampled continuously at approximately 1 m intervals and were analyzed at ALS Chemex, Toronto, Canada, using an inductively coupled plasma atomic emission spectrometer (ICP-AES) after fine crushing (70 wt % <2 mm), pulverizing (85 wt % <75 μm) and four acid digestion.

Sulfur stable isotope analyses on sphalerite, galena, pyrite and barite were obtained in the Southwest Isotope Research Laboratory of the US Geological Survey in Denver, USA, following the procedures of Johnson et al. (2018). Isotopic compositions are reported in usual delta notation (in units of per mil ‰) relative to Vienna Cañon Diablo troilite (VCDT) for sulfur. For carbon and oxygen stable isotopes study a diamond-drill device with tungsten carbide tip of 2 mm (Dremel 3000) was used for a selective sampling of different carbonate generations. Powdered samples were directly forwarded to the Stable Isotope Laboratory, University of São Paulo, Brazil (LIESP-USP) for processing and analysis. Sample preparation for analysis involved approximately 100 micrograms of the sample that was placed in a 12 ml vial, heated to a temperature of 72 ºC and subjected to flush process. The ratios came for the reaction of the orthophosphoric acid with the carbonic gas from carbonate samples. The analysis was made in a Thermo Finnigan GasBench II coupled to a Delta V Advantage IRMS. The results are reported in usual notation (‰) relative to the international Vienna standards Pee Dee Belemnite (VPDB) and Standard Mean Ocean Water (VSMOW). All samples have been analyzed in duplicate. The instrumental precision for $\delta^{13}C$ was ±0.05‰ and for $\delta^{18}O$ was ±0.07 ‰ and the accuracy was of ±0.07 ‰ for $\delta^{13}C$ and ±0.06 ‰ for $\delta^{18}O$.

Geology of the Shalipayco Deposit

The host rocks of Shalipayco deposit are represented by the Chambará Formation, which is composed predominantly of carbonate and former evaporite-bearing rocks with different degrees of dolomitization, including partially dolomitized mudstones and oolitic wackestones to completely recrystallized dolostones. The Chambará Formation in the deposit can be divided into four members: Chambará I, II, III, and IV from base to top, according to the host rocks

characteristics and the type of mineralization (Fig. 3). The Chambará I member is the basal unit of the Chambará Formation (Fig. 3d) and lies in with an erosional contact with the Mitu Group (Fig. 3e). The rocks of the Mitu Group were intercepted by few drillholes in the deposit and occurs as poorly selected polymorphic conglomerates, arkose sandstones and amygdaloidal volcanic rocks (Fig. 3e). The Chambará I is composed of dark gray lime mudstones to wackestones, locally with millimetric dark rounded clasts of chalcedony and small calcite grains (Fig. 3d). Sparry calcite occurs in replacement texture on previous carbonates and fills cavities. This unit has centimeter-size porosity that is expressed as a vuggy texture with dolomite that fills fractures and contains non-economical occurrences of disseminated dark brown sphalerite and pyrite. Late veins are filled by sparry calcite, which is characteristic of these units. The second sequential member in the stratigraphy is the Chambará II that hosts the Zn–Pb mineralized Intermedios level (Fig. 3c). This member is mainly composed of a porous gray dolostone consisting of sparry planar dolomite that commonly obscures the original sedimentary textures of former evaporites (Fig. 3c). The dolomitization of carbonates is always associated with the deposition of late thin pyrite in the interstices of dolomite crystals. Late chalcedony occurs replacing nodules and medium-thick sparry calcite represents late crystallization between the dolomite crystals. All the Chambará sequence is interpreted as being formed in supratidal–sabkha depositional systems.

The Chambará III member hosts the Zn–Pb mineralized Resurgidora level that is characterized by the presence of a beige dolomitic boundstone composed by intercalation of micritic layers partially replaced by sparry dolomite and fine interlaminar micritic dolomite (Fig. 3a) at its top. Calcite nodules believed to be anhydrite pseudomorphs are common, as well as fractures filled by late calcite and or dolomite. Stylolites are common features in these rocks and are generally filled with pyrite and organic matter. The sulfides present in these dolomitic rocks include zoned dark and pale-brown sphalerite, galena, fine- to medium-grained (~1 mm size in diameter) pyrite and fine-grained marcasite occurring as breccia matrix and as open-space fill (filling cavities and fractures), sometimes resulting in evaporite breccia textures. In both members, Chambará II and III there are occurrences of metric intercalations of partially dolomitized mudstones and wackestones with some preserved sedimentary textures and former evaporitic levels. The least altered rocks are composed of millimeter-size ooids and oncoids with sub-concentric structures partially replaced by sparry dolomite. The matrix, when present, is micritic. Fine size dolomite fills vuggy porosities and is locally associated with barite crystals. Medium (~0.5 mm size) sparry calcite is associated with very minor to absent fluorite and

occurs as the final stage of porosity fill and as breccia matrix in these rocks. The Chambará IV is characterized by massive light gray lime mudstones (Fig. 3b) and wackestones with some fossils that includes pellets and bivalves. Some interlayered coarse-grained layers with greater porosity show partial dolomitization with limestone mud locally replaced by dolomite, resulting in the partial destruction of the sedimentary textures.

The Chambará formation in the Shalipayco deposit is composed of intercalations of limestone, dolostone, and former evaporites layers with similar appearance and lithological repetition throughout the stratigraphic column. Two stratigraphic markers with up to 10 meters thick are commonly used for the determination of the contacts of the Chambará members. A fossiliferous level with crinoids, bivalves, and corals mark the top of Chambará I and the base of the Chambará II, while a gray fetid dolomitic wackestone level with sulfide and organic matter defines the top of dolostones from Chambará III and the base of limestones of Chambará IV.

In summary, the Chambará Formation in the deposit is a basal member of mudstones and wackestones of predominantly limestone (Chambará I), two sequential members with composition with associated former evaporite layers hosting the significant stratabound Zn–Pb sulfide bodies: the lower is characterized by the porous dolomite (Chambará II) and the upper by the beige dolomite (Chambará III), and at the top sequence another member with the predominance of mudstones and wackestones with calcareous composition (Chambará IV). Tuanama (2016) presents a more detailed compartmentalization of the Shalipayco deposit stratigraphy than the one presented here, individualizing 10 lithological units and 5 levels of sulfide occurrences, however the lithological controls for mineralization are the same as presented – the stratabound Zn–Pb ore is hosted in dolostone levels with more developed porosity and permeability and in association with former evaporitic rocks. All the stratigraphic sequence in the Shalipayco deposit is tectonically positioned with dip direction of N225/30 (Fig. 4) that consequently determines the strike direction of the stratabound orebodies.

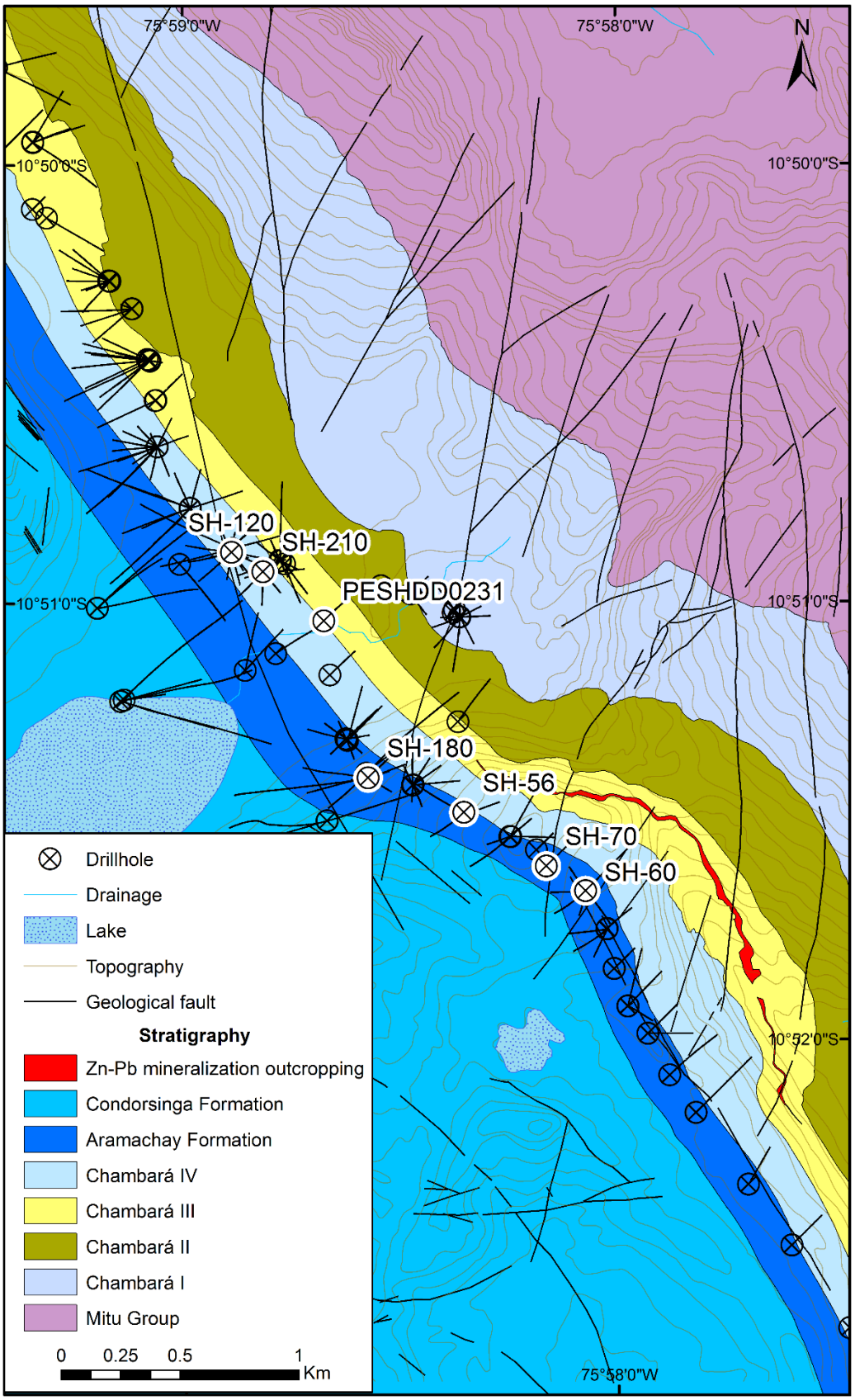

Fig. 2. Local geological map with the compartmentalization of Chambará Formation in the Shalipayco deposit and drillhole samples location.

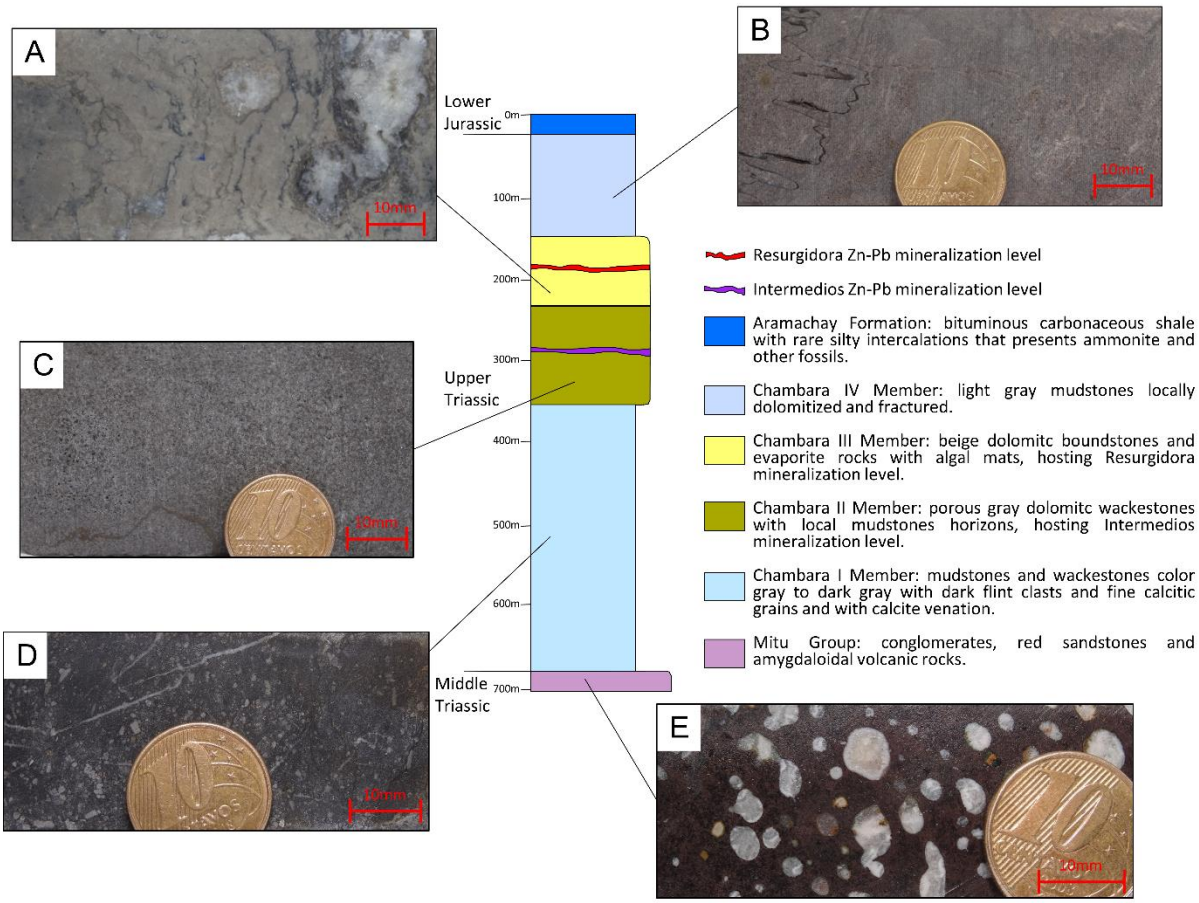

Fig. 3. Stratigraphic column on Shalipayco deposit with photos of characteristic drillcore hand samples: A) SH-180-189.70: Beige dolomitic boundstone with calcite pseudomorphs after halite from Chambará III Member. B) SH-43-147.60: Dark gray dolomitic mudstone with stylolites from Chambará IV Member. C) SH-43-359.30: Massive porous gray dolostone from Chambará II Member. D) SH-43-490.40: Black massive packstone from Chambará I Member. E) SH-43-688.80: Amygdaloidal andesite from Mitu Group.

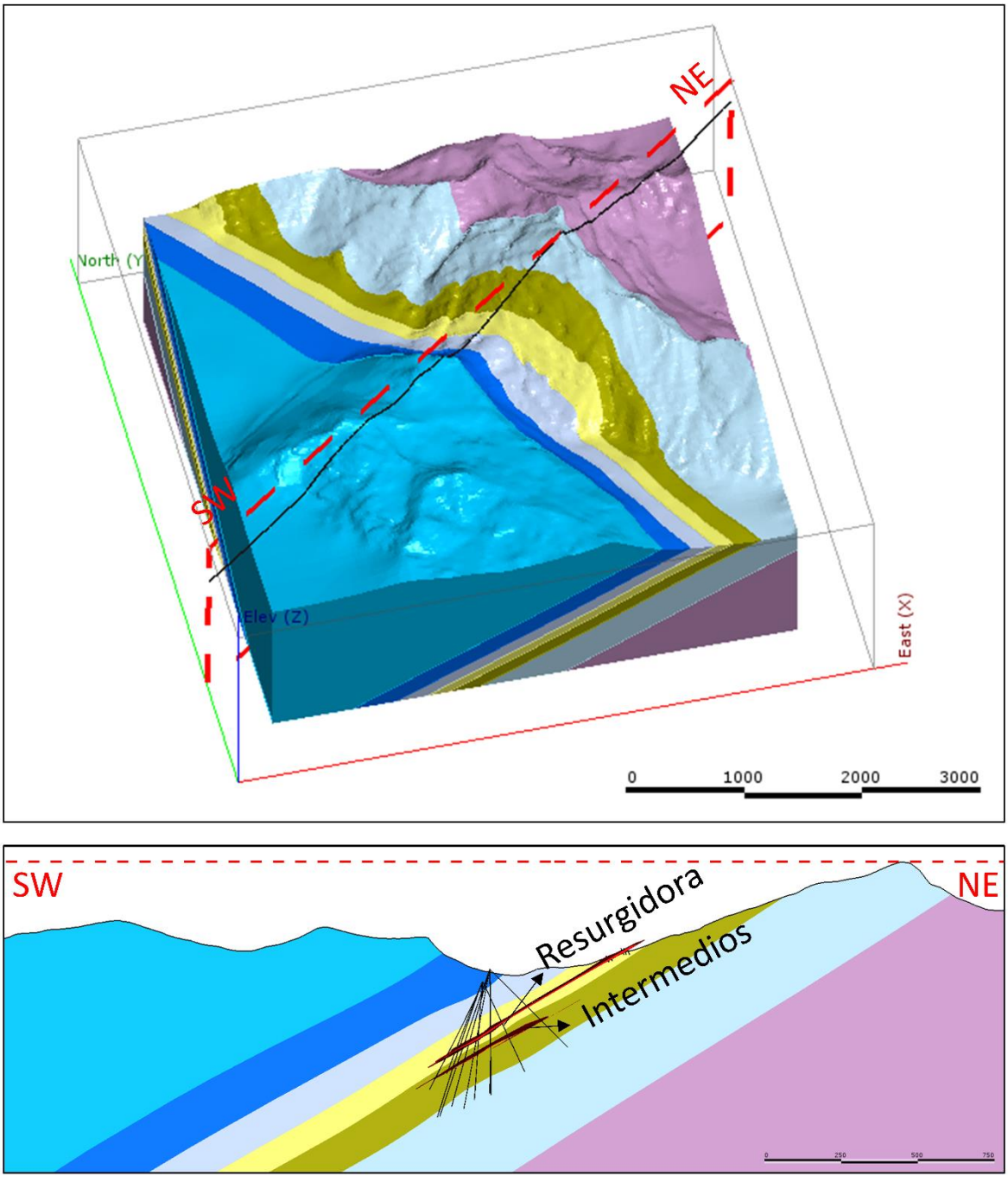

Fig. 4. A) 3D geological model of Shalipayco deposit. B) Geologic cross section with NE direction perpendicular to the main layers dip direction (N225/30) highlighting the Resurgidora and Intermedios layers. The legend color scheme is the same as in figures 2 and 3.

The Role of Evaporites

The Zn–Pb mineralization in the MVT Shalipayco deposit presents several evidences of a relationship with former evaporites also recognized and described in the MVT Florida Canyon deposit, hosted in the Pucará Group (De Oliveira et al. 2019), and other MVT deposits worldwide (Charef and Sheppard 1987; Bouabdellah et al. 2015; Bouabdellah et al. 2014; Bouhlel et al. 2016; Leach et al. 2017). Sabkha facies with evaporite presence is described in the Pucará Group sequence (Benavides 1968; Fontbote and Gorzawski 1990). In the Shalipayco deposit, vanished evaporites minerals and ghosts of evaporite facies (Warren 2006; Warren 2016) are present in Zn–Pb mineralization host rocks providing evidence of former evaporites. The main rock types associated with former evaporites: porous dolomite and evaporite breccia, as well as the pseudomorphs of evaporite minerals that compose the sabkha facies in Shalipayco are shown in Figure 5. The porous dolostone is a coarse massive dolostone in light brown to gray with significant secondary porosity sometimes with open pores (barren) (Fig. 5a) other times filled by sphalerite and galena (Fig. 5b). The evaporite breccia is a dolomitic rock sometimes with dark dolomite clasts in a white sparry dolomite matrix well defined, sometimes in a chaotic texture also with dark and white dolomite generations (Fig. 5d, e). The evaporite breccia was produced by dissolution and collapse of evaporites in the original sedimentary sequence. The replacement of gypsum or anhydrite by sparry dolomite in burial diagenesis conditions (Anderson and Garven 1987) generate open spaces due to the difference in volume between these minerals, which makes the breccia an excellent potential host-rock for mineralization. More detailed description of porous dolostone and evaporite breccias are given by Leach and Song (2018) and De Oliveira et al. (2019). In the boundstones, mudstones, and wackestones with less alteration, it is possible to observe preserved textures of former evaporites, such as acicular, fibrous and radiated evaporite pseudomorphs replaced by calcite (Fig. 5c). Rounded nodules of halite pseudomorphs replaced by calcite are present in the beige dolomitic boundstone (Fig. 3a). The former evaporite levels occur in both the Chambará II and the Chambará III members with highly variable thicknesses and spatial continuity, however, they occur more frequently in the Chambará III, where the largest sulfide orebody Resurgidora are also present.

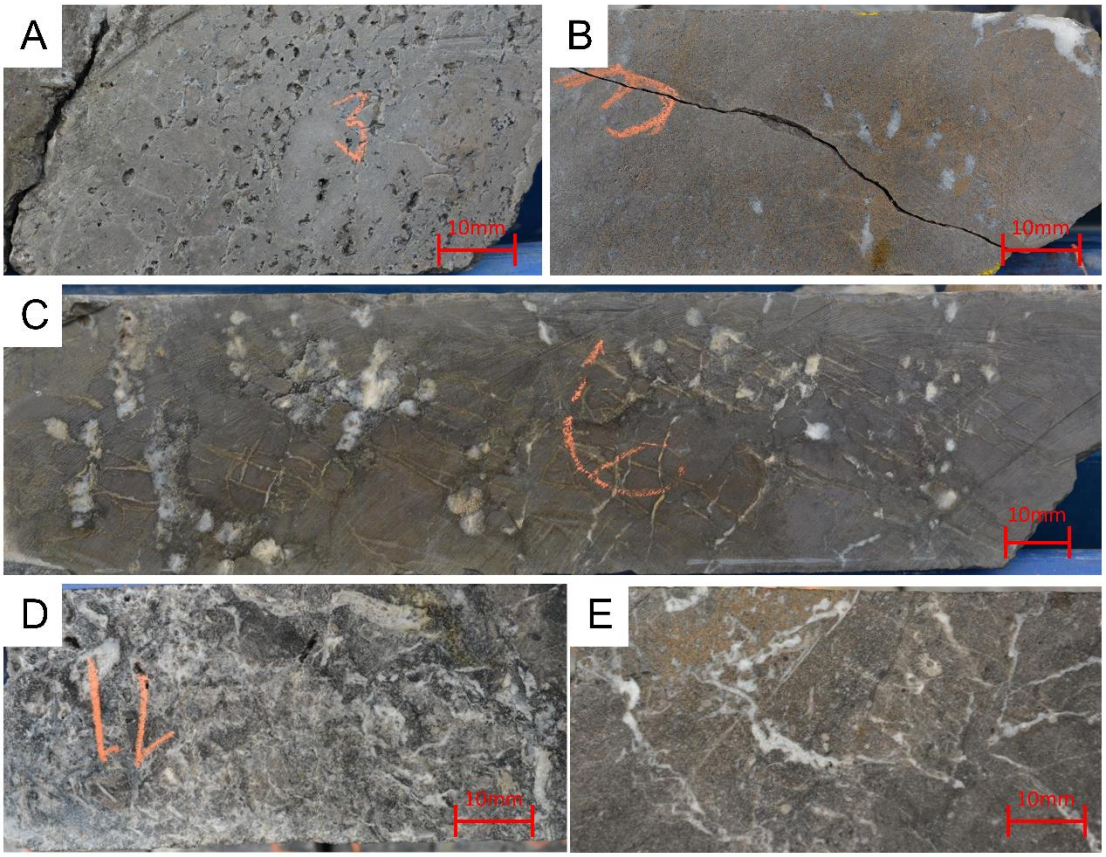

Fig. 5. Drillcore samples representative rock textures. A) SH-210-107.70: Barren porous dolostone with abundant vuggy (large pores). B) SH-56-287.60: Porous dolostone with vuggs filled by dark sphalerite and some white sparry dolomite. C) SH-43-173.30: Dolomitic mudstone with white calcite pseudomorph after halite. D) SH-43-540.30: Barren evaporite breccia with chaotic texture with dark and white dolomite. E) SH-43-571.10: Evaporite breccia with dark sphalerite in void-filling texture.

Characterization of Zn–Pb stratabound orebodies

The Zn–Pb mineralization is composed predominantly of pale yellow sphalerite, dark brown sphalerite, pyrite, galena and marcasite that form the main mineralization assemblage concentrations as stratabound orebodies (Fig. 6). The gangue minerals forming the host rocks are dolomite, calcite, barite, fluorite and quartz (Fig. 6). Open space filling in porous dolostone, cavities and fractures are the most common ore in the Resurgidora and Intermedios stratabound ore zones. These sulfide minerals also occur in non-economic concentrations and are less expressive in terms of the lateral extension, metal grades, and thickness as disseminated mineralization in restricted porous dolostone levels in Chambará I member. These zones are identified as Virgencita, San Luis and Pucará levels (Tuanama 2016). Besides these mineralized zones, some surface exposures of sulfides called Eddy Vein that include traces of chalcopyrite and iron oxides in addition to sphalerite, galena, and pyrite. The Eddy Vein has a structural control of N170 strike and 75E dip, with no subsurface extension confirmed by drillholes.

The Resurgidora Zn–Pb orebody

The Resurgidora level is the most significant orebody of the deposit in terms of tonnage and it outcrops along almost all deposit extension in brown colors (low surface oxidation) detaching in the landscape. The orebody has an average thickness of 4 meters, reaching locally a maximum of 11 meters, and with 4 kilometers of extension along with its main strike direction in the subsurface. The mineralization is predominantly hosted on dolostones and subordinately on partially dolomitized mudstones, wackestones and boundstones of Chambará III. The main ore is composed of coarse zoned sphalerite (dark and pale-brown color) associated with coarse sparry dolomite (Fig. 6h) and as evaporite breccia matrix (Fig. 6d). In the former evaporite-bearing rocks, the dark sphalerite is associated with sparry dolomite that fills spaces between euhedral barite crystals and in some cases replacing barite (Fig, 6a, b). In the boundstones and mudstones, the sulfides occur as fracture filling in association with sparry calcite and dolomite.

The Intermedios Zn–Pb orebody

The Intermedios orebody has a strike extension of 2 kilometers of known mineralization with an average thickness of 8 meters, reaching locally a maximum of 25 meters. The ore sulfides are hosted in porous dolostones mainly and in fewer amounts in the mudstones and wackestones levels of Chambará II. Sphalerite is the most abundant mineral of this orebody and occurs in several forms: medium-coarse size (~0.2 mm) as breccia matrix, disseminated near the sparry carbonate bands, forming breccia matrix of the clasts with dolomite intraclasts and zoned ranging from pale to dark sphalerite in colloform texture, indicating rapid deposition. In dolostones, medium-coarse size (<0.5 mm) euhedral zoned sphalerite occurs disseminated and in fractures of millimeter thickness, together with fine pyrite locally associated with hydrothermal dolomite and chalcedony. In general, the pale yellow sphalerite appears at the edges of the fractures, followed by the dark sphalerite, indicating that the last one was the first phase to precipitate. Locally the sulfides occur as network fractures and in breccias with massive concentrations of the two sphalerite generations, pyrite, and galena (Fig. 6f). In these cases, the sphalerite crystals are coarse, euhedral and zoned locally associated with stylolites. Sometimes the sphalerite appears fractured, indicating tectonic stresses after its precipitation

and, in a subordinate way, filling dissolution cavities associated with sparry calcite (Fig. 6e). Sparry calcite in vein occurs as the late phase cutting sulfide mineralization.

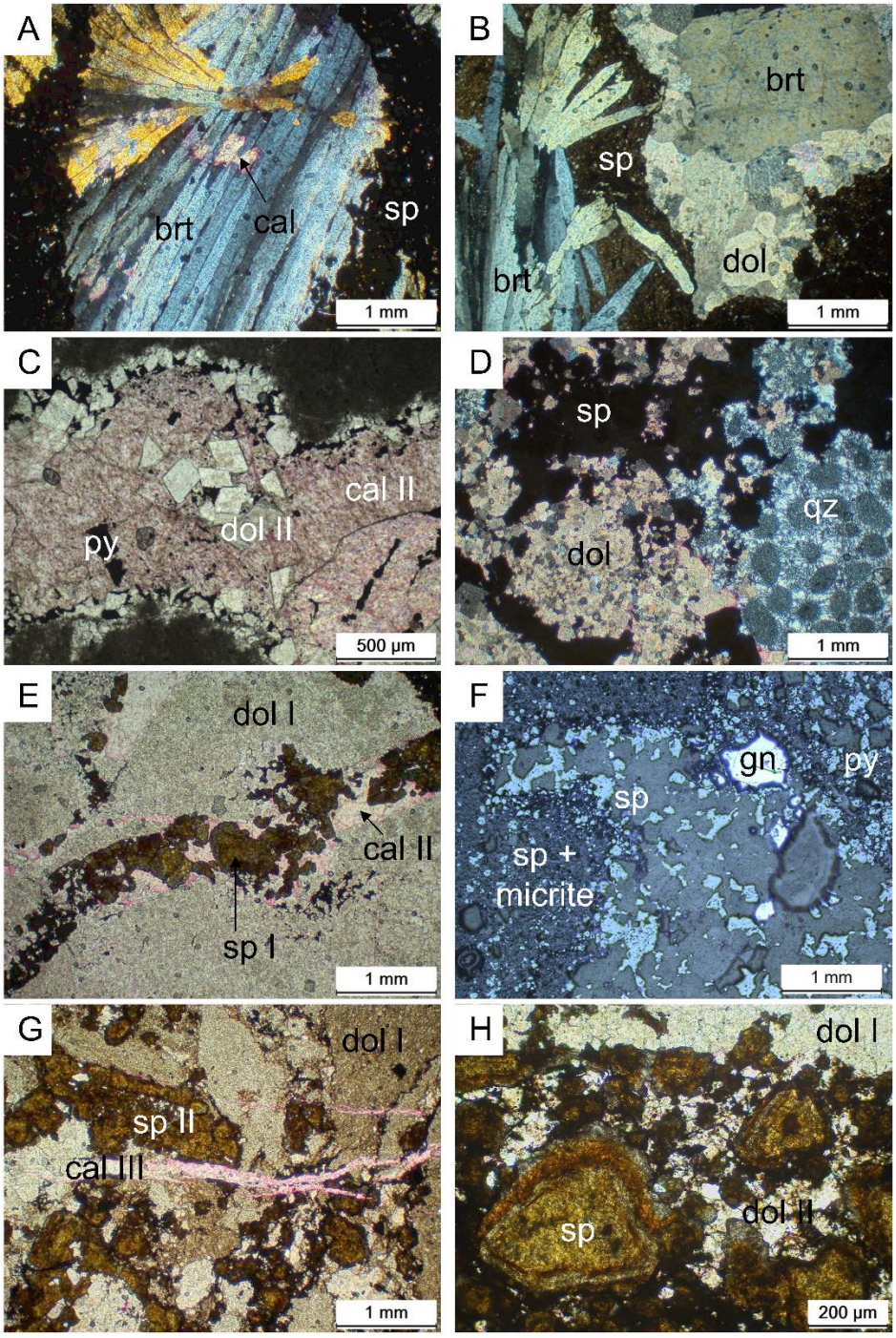

Fig. 6. Photomicrographs. A) SH-43-196.50: Barite within sphalerite with the late replacement of medium coarse calcite (cal II). B) SH-43-196.50: Barite associated with sparry white dolomite (dol II) in an open-space filling texture. C) SH-43-210.30: Fracture filled by dolomite at edges and then by calcite with pyrite (alizarin red-stained). D) SH-210-253.10: Dolostone with sphalerite (sp I) and late chalcedony. E) SH-120-182.70: Dolostone with fracture filled by sphalerite with calcite (alizarin red-stained). F) SH-231-140.00: Disseminated thin sphalerite as breccia matrix associated with galena and interstitial pyrite. G) SH-56-284.60: Fragments of sparry dolomite (dol II) cut by late calcite (cal II) (alizarin red-stained). H) SH-56-283.40: Coarse sphalerite with concentric color zoning within the dolomitic matrix.

Paragenetic sequence

The paragenetic sequence for the Shalipayco Zn–Pb deposit are divided into four major geological stages: (1) the initial sedimentary carbonate deposition of Chambará Formation rocks, (2) a diagenetic stage (pre-mineralization event) characterized by dolomitization, (3) the Zn–Pb sulfide mineralization stage and (4) a post-mineralization stage. A paragenetic sequence for the minerals at the Shalipayco is given in Figure 7.

Dolomitization results in the diagenetic replacement of the sedimentary micritic calcite and the calcite particles (cal I) of the original limestones and former evaporite minerals that formed the sparry dolomite (dol I) that resulted in predominantly replacement textures. The host rocks of the mineralization are intensely dolomitized in general, with few portions that have preserved original sedimentary textures. The light colored dolomites and boundstones of the Chambará III top levels are rocks that present little-advanced dolomitization, and have preserved sedimentary textures and allochemicals, such as oolites and oncoids, and their micritic matrix (cal I). It is possible to observe the intra-oolite concentric porosity that is replaced by fine-medium sparry dolomite (dol I), as well as the vuggy intraclastic porosity. In the mineralized Chambará II and III members, the texture of the original rock is completely obliterated, resulting in a crystalline texture composed of sparry dolomite (dol I).

The Zn–Pb mineralization stage begins with the precipitation of pyrite as fine crystals between the sparry dolomite crystals. The precipitation of pale yellow and dark brown sphalerite (possibly with a zoning between them), galena and new pyrite phases define this sulfide stage. The association with slightly late stage white sparry dolomite (dol II) is common (Fig. 6h). Marcasite occurs associated with pyrite and sphalerite in late stages. The second dolomite stage (dol II) occurs as open-space filling in fractures and as breccia matrix. In the rocks with micritic textures, barite occurs filling fractures earlier than the deposition of fine-medium zoned sphalerite (Fig. 6a), in larger crystals, and with a disordered arrangement and with euhedral habit as acicular crystals (Fig. 6b). Chalcedony occurs as a late phase in the mineralization stage, sometimes cutting ore sulfides and replacing cavities of original evaporite nodules. Finally, post-mineralization fine-medium calcite occurs as millimetric veins (Fig. 6g) and as open-space filling (Fig. 6c) and replacement texture.

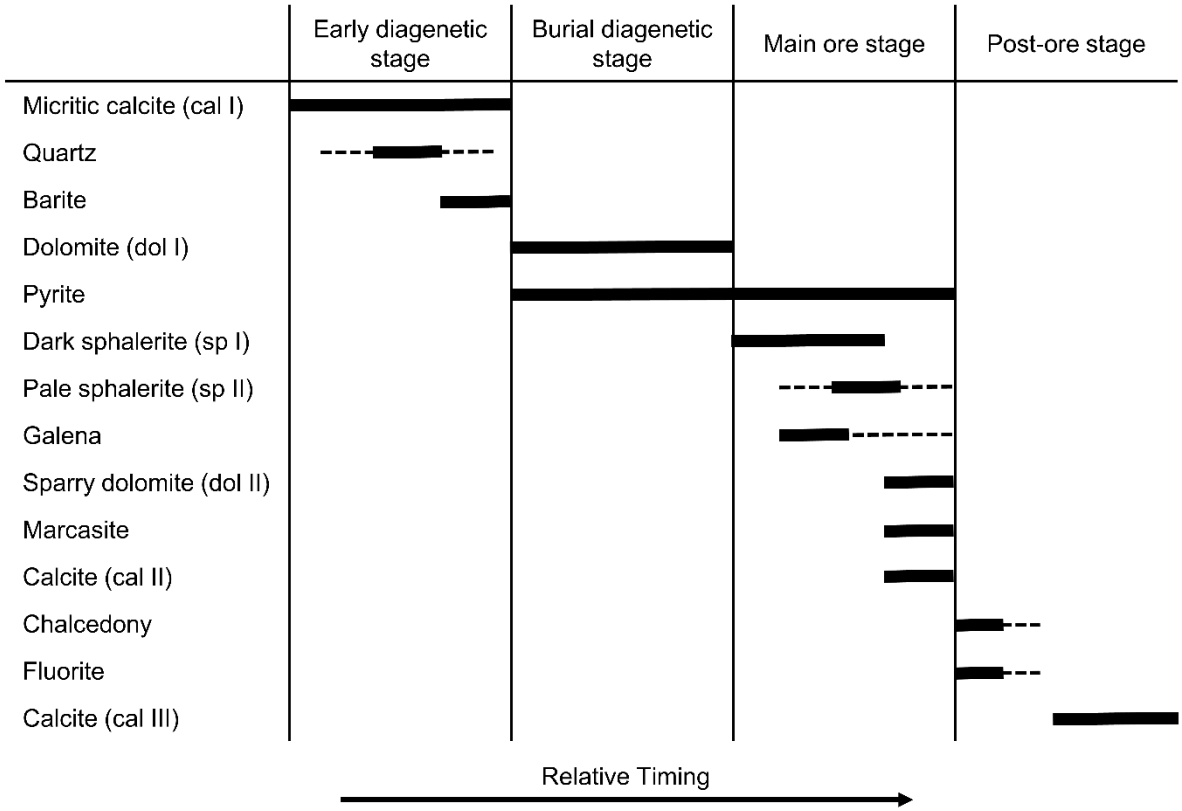

Fig. 7. The paragenetic sequence of Shalipayco deposit. Bars thicknesses reflect the abundance of minerals.

Trace elements

An analysis of 21 trace elements of whole-rock drill core samples at intervals of approximately one meter in length was provided by the Nexa Resources company (Table 1). Elements with concentrations below the detection limit in many samples (Be, Bi, and W) were not considered. The distribution of selected trace elements were observed considering samples divided into four groups: non-mineralized carbonate host rock (n = 19,023), Intermedios stratabound orebody (n = 858), Resurgidora stratabound orebody (n = 460) and Eddy vein occurrence (n = 197) (Table 1). The Co, Cr, Mo, Ni, Sr, V elements present no characteristic behavior in any of the four sample groups, with maximum, minimum and median values very close in the four domains. The Ba, Mn and Ti elements show very particular distributions, with higher maximum values in the carbonate host-rock samples (9,120; 14,750 and 28,100 ppm, respectively) in relation to the Intermedios orebody (440; 3,690 and 9,900 ppm, respectively), Resurgidora orebody (3,820; 10,200 and 1,300 ppm, respectively) and Eddy vein (330; 3,990 and 8,700 ppm, respectively) samples. The In maximum values tend to be higher also in the domains with sulfides (20.6 ppm for Intermedios and 12 ppm for Eddy vein) in relation to the non-mineralized host rocks (8.84 ppm), however, only the Resurgidora orebody has a maximum

value lower than the carbonate rocks (2.42 ppm). The Ag, As, Cd, Cu, Hg and Sb elements are also higher in the three domains with sulfides presence (Intermedios, Resurgidora and Eddy vein) than in the non-mineralized carbonate host rock. These six elements, in addition, also distinguish very well the Eddy vein sulfide occurrence related to NW structure, from the two main Zn–Pb stratabound sulfide bodies (Intermedios and Resurgidora) (Fig. 8). The medians of Ag, As, Cd, Cu, Hg and Sb elements are 124, 261, 452, 26, 42 and 93 ppm in the Eddy vein occurrence, while in the Intermedios and Resurgidora orebodies are 17, 138, 81, 18, 13 and 29 ppm, and 12, 132, 50, 2, 8 and 20 ppm respectively.

Table 1. Selected trace element ranges and median (ppm) of drillcore whole-rock samples in the carbonate host rock, Intermedios orebody, Resurgidora orebody and Eddy Vein occurrence on Shalipayco deposit.

	non-mineralized carbonate host rock n = 19,023	**Intermedios stratabound orebody** n = 858	**Resurgidora stratabound orebody** n = 460	**Eddy vein occurrence** n = 197
Ag	0.005–272 (**1.3**)	0.25–217 (**17**)	0.19–174 (**12**)	2.8–916 (**124**)
As	1–5,860 (**49**)	15–4,220 (**138**)	10–2,500 (**132**)	2.5–7,040 (**261**)
Ba	0.5–9,120 (**5**)	5–440 (**5**)	5–3,820 (**60**)	5–330 (**5**)
Be	0.025–3.9 (**0.3**)	0.025–0.8 (**0.3**)	0.18–0.9 (**0.3**)	0.025–1.3 (**0.3**)
Bi	0.005–12 (**1**)	0.005–6 (**1**)	0.005–4 (**1**)	0.005–20 (**1**)
Cd	0.01–971 (**1**)	0.21–1,310 (**81**)	0.18–791 (**50**)	0.25–3,140 (**452**)
Co	0.1–604 (**1**)	0.4–41 (**2**)	0.5–16 (**1**)	0.1–850 (**2**)
Cr	0.5–625 (**2**)	0.5–198 (**1**)	0.5–13 (**1**)	0.5–156 (**2**)
Cu	0.1–2,300 (**2**)	0.5–634 (**18**)	0.5–154 (**2**)	0.5–21,500 (**26**)
Hg	0.005–359 (**0.3**)	0.05–271 (**13**)	0.005–171 (**8**)	0.005–317 (**42**)
In	0.003–9 (**0.01**)	0.003–21 (**0.12**)	0.003–3 (**0.01**)	0.003–12 (**0.01**)
Mn	25–14,750 (**1,610**)	431–3,690 (**1,500**)	935–10,200 (**3,705**)	6–3,990 (**916**)
Mo	0.05–49 (**1**)	0.08–196 (**0.5**)	0.19–18 (**3**)	0.09–17 (**1**)
Ni	0.1–512 (**2**)	0.1–170 (**1**)	0.1–15 (**1**)	0.1–1,780 (**1**)
Pb	1–266,000 (**51**)	10–94,300 (**291**)	11–122,000 (**1,723**)	15–479,100 (**889**)
Sb	0.003–2,010 (**5**)	2.5–514 (**29**)	2.5–578 (**20**)	2.5–7,110 (**93**)
Sr	3–8,210 (**93**)	25–2,980 (**57**)	47–2,780 (**150**)	4–4,310 (**56**)
Ti	25–28,100 (**100**)	25–9,900 (**50**)	50–1,300 (**100**)	25–8,700 (**50**)
V	0.5–324 (**5**)	0.5–126 (**1**)	0.5–46 (**7**)	0.5–176 (**1**)
W	0.05–220 (**5**)	0.05–80 (**5**)	0.1–70 (**5**)	0.05–70 (**10**)
Zn	1–384,300 (**165**)	72–388,400 (**28,800**)	120–260,000 (**21,750**)	5–520,700 (**135,500**)

The median values are given in parentheses; n = number of samples

A spatial analysis of the trace elements distribution along the main faults was made in plan view maps (Fig. 8). In the Shalipayco deposit, two patterns of faults are recognized, the first is older with NW direction thrust faults with low angle dip (e.g. Eddy vein) and the other is characterized by secondary N direction steeply faults limited by the first ones (Figs. 2 and 8). The Ag, As, Cd, Cu, Hg and Sb elements show higher values around the Eddy vein N structure than in the Zn–Pb stratabound orebodies of Intermedios and Resurgidora with general dip direction of N225/30 (Figs. 4 and 8).

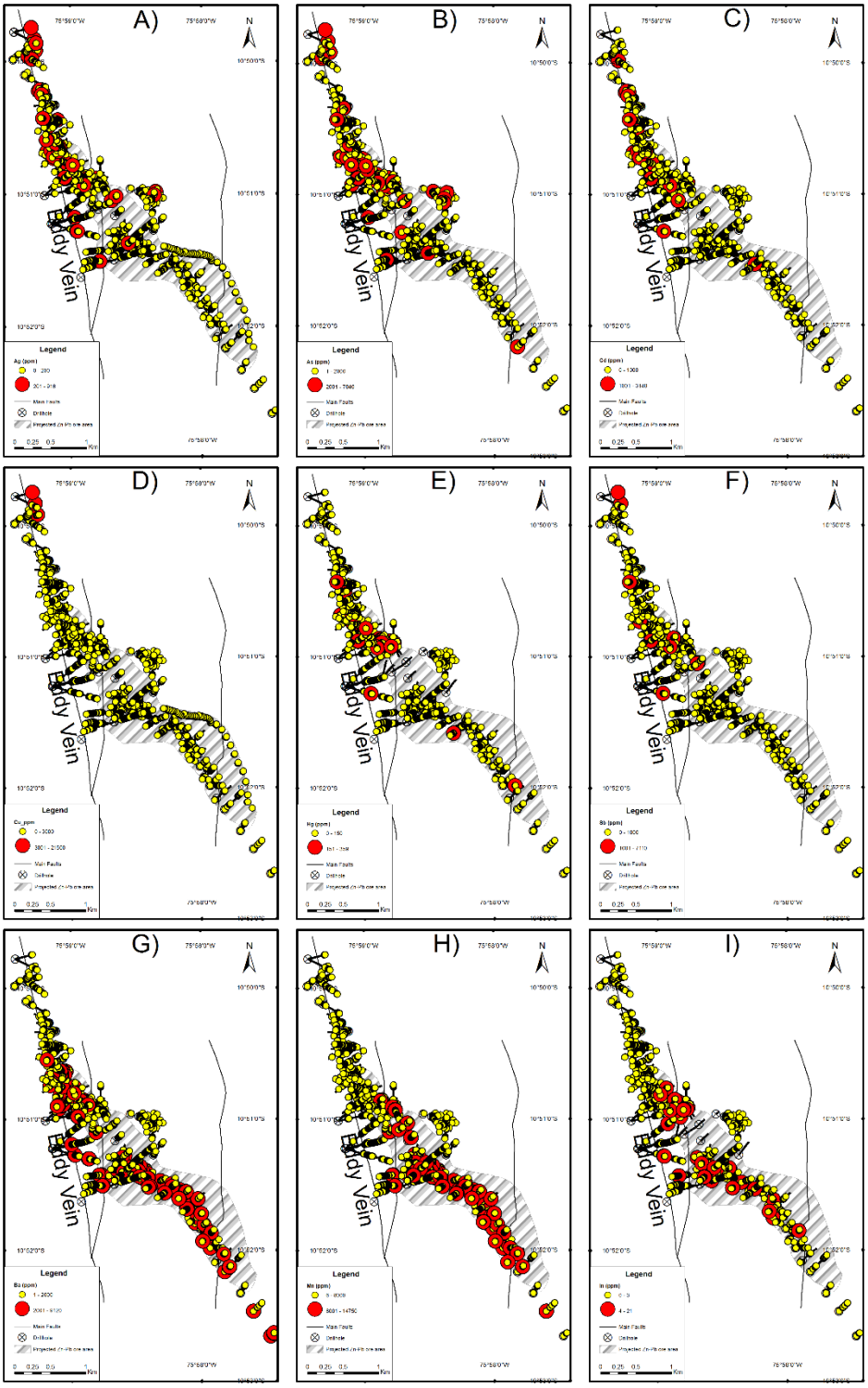

Fig. 8. Distribution of selected minor elements in drill core samples projected in the plan view of the Shalipayco deposit. A) Silver. B) Arsenic. C) Cadmium. D) Copper. E) Mercury. F) Antimony. G) Barium. H) Manganese. I) Indium.

Carbon, oxygen and strontium isotopes

The samples selected for C and O stable isotopes were made based on the petrographic and occurrence modes of the different carbonate generations and their relationship with sulfides. The results obtained for host rocks and carbonates are presented in Table 2. The previously published carbon and oxygen isotope data of Moritz et al. (1996) from Shalipayco deposit are included for comparison to the new data presented in this study. The carbonates exhibit a positive covariation in the δ13C versus δ18O plot clustering in three sample groups (Fig. 9). The isotopic variation in the different carbonate minerals also correlates with the paragenetic sequence with lighter δ13C and δ18O values also been the later stages.

The whole-rock samples analyzed comprise the three main lithotypes of ore host rocks: (1) mudstones/wackestones, (2) boundstones with former evaporite levels and (3) dolostones. Non-mineralized boundstones, mudstones, and wackestones have □13C values between 1.1‰ and 1.9‰ and □18O values between 27.1‰ and 30.8‰. These rocks were grouped and interpreted as the most preserved of the deposit (Fig. 9) and present the largest □18O values of the analyzed samples set. The group 1 samples plots entirely in the field of Triassic marine limestones (Veizer et al. 1999). The high values of □18O are consistent with the signature of marine carbonates and are indicative of conditions of high salinity, typical of evaporitic conditions, which is corroborated by the evaporite pseudomorphs in these rocks. The group 2 comprises samples from the sparry dolomite (dol II) and from the dolostones (dol I) that had interaction with mineralization fluid associated with the ore-stage sulfides, plotting partially in the Triassic limestones field (Veizer et al. 1999). This set of samples have δ13C values between -0.1 to 2.1‰ and of δ18O values between 17.5 to 26.2‰. The closer ranges between the host dolostone (dol I) and the ore-associated sparry dolomite (dol II) indicate that isotopic equilibrium was established between hydrothermal fluids and isotopically dominated by the host rock during the main stages of sulfide precipitation. The group 3 is composed almost entirely of calcite samples from late veins (cal II) related to sulfide ore (Figs. 6c, e). This last group shows the lighter values for both δ13C (–2.9 to –0.5‰) and δ18O (11.0 to 16.1‰) among all carbonates from the deposit. These lighter C and O isotopic signature may reflect the involvement of meteoric fluids during dedolomitization of host dolostones.

The carbonate samples of group 2 cluster samples from burial diagenetic replacement dolomite (dol I) and late void-filling sparry dolomite related to ore-stage (dol II). The same isotopic grouping was observed in the Florida Canyon deposit dolomites (De Oliveira et al.

2019). Nevertheless, when the two dolomite stages from spatially close samples are analyzed, slightly lighter values of C and O are observed for the late stage sparry dolomite (e.g. replacement dolostone in sample SH 43 519.80 with δ18O = 24.5‰ and δ13C = 0.2‰, and sparry dolomite in sample SH-43-571.10 with δ18O = 17.5‰ and δ13C = -0.1‰).

Strontium isotope data (Table 3, Fig. 10) also define distinct values for different carbonate stages in Shalipayco deposit, which are analogous to carbonates from the Florida Canyon deposit (De Oliveira et al. 2019). The strontium data for the Shalipayco deposit from Moritz et al. (1996) differentiate the limestones (cal I) with a range plotting inside the Triassic seawater (Koepnick et al. 1990; Korte et al. 2003); the burial diagenetic replacement dolomite (dol I) with a range plotting partially in the same field but slightly more radiogenic and the late coarse calcite (cal II) with the most radiogenic values. The three samples from Mitu Group alkali basalt show more radiogenic 87Sr/86Sr values (from 0.709654 to 0.719669) than all carbonate samples (from 0.707650 to 0.708980) in Shalipayco deposit.

Sulfur isotopes

Sulfur isotopic compositions were analyzed on eight samples of sphalerite (two generations), three of galena, three of pyrite and two of barite samples from the Resurgidora and Intermedios orebodies (Table 4, Fig. 11). The δ34S values for all sulfides minerals do not differ significantly between the different orebodies or show a relationship with depths or paragenetic position. The two samples of barite that are earlier in the paragenetic sequence have δ34S values of 13.7 and 17.3‰ that are closer to the values of Jurassic to Middle Triassic seawater sulfate (15 to 17‰, Claypool et al. 1980). The δ34S values for dark sphalerites range from -19.1 to -16.8‰ and for light sphalerites from -17.9 to -15.3‰ whereas the samples of galenas range from -23.0 to -10.4‰ and pyrite range from -23.3 to -6.2‰ with a slightly greater spread. The temperature of the sphalerite-galena isotopic pair for two sample pairs (SH-120-109.80 and SH-231-140.90, Table 3) was calculated using the equation from Ohmoto and Rye (1979). This geothermometer assumes isotopic equilibrium, contemporaneity and that the isotopic compositions of sphalerite and galena have been preserved. The 139 º and 159 ºC calculated temperatures values are consistent with fluid inclusion homogenization temperatures of 115 º to 162 ºC obtained by Moritz et al. (1996) for ore-related sparry dolomite (dol II) in Shalipayco deposit.

Table 2. Carbon and oxygen isotope composition of the carbonates of Shalipayco deposit.

Sample	Ore body / member	Material / mineral	Group	Petrographic description	$\delta^{18}O_{VSMOW}$(‰)	$\delta^{13}C_{VPDB}$(‰)	Reference
SH-60-171.50-R	Intermedios	limestone (cal I)	group 1	Beige boundstone	30.8	1.9	This study
SH-60-174.40-R	Intermedios	limestone (cal I)	group 1	Beige boundstone with gp	30.4	1.9	This study
SH-60-170.40	Resurgidora	limestone (cal I)	group 1	Wackestone with oncolites and oolites with calcite pseudomorphs after evaporite	30.7	1.7	This study
SH-70-217.60	Resurgidora	limestone (cal I)	group 1	Mudstone with sparry dol filling voids with gp, py and cal in fractures	27.8	1.8	This study
		limestone I	group 1		27.1	1.1	Moritz et al (1996)
		limestone I	group 2		24.5	0.7	Moritz et al (1996)
		limestone I	group 2		23.6	0.3	Moritz et al (1996)
		limestone I	group 2		23.6	0.8	Moritz et al (1996)
SH-43-519.80	Chambará I	dolostone (dol I)	group 2	Dolostone with intergranular cal	24.5	0.2	This study
SH-56-298.20-R	Intermedios	dolostone (dol I)	group 2	Dolomitic wackestone with oncolites and with cal vugs and veinlets	25.9	1.7	This study
SH-43-359.30	Intermedios	dolostone (dol I)	group 2	Beige dolomitic boundstone with laminated texture	20.9	1.5	This study
		replacement dolomite I	group 2		26.2	1.9	Moritz et al (1996)
		replacement dolomite I	group 2		26.0	1.8	Moritz et al (1996)
		replacement dolomite I	group 2		25.5	2.1	Moritz et al (1996)
		replacement dolomite I	group 2		25.4	1.9	Moritz et al (1996)
		replacement dolomite I	group 2		25.1	2.0	Moritz et al (1996)
		replacement dolomite I	group 2		24.4	1.1	Moritz et al (1996)
SH-70-220.00	Resurgidora	sparry dolomite (dol II)	group 2	Dolomitic wackestone with fractures filled by sparry dolomite	25.3	1.0	This study
SH-43-571.10	Chambará I	sparry dolomite (dol II)	group 2	Dolostone with cal veins	17.5	-0.1	This study
		sparry dolomite II	group 2		24.5	1.6	Moritz et al (1996)
		coarse calcite II	group 2		25.5	1.5	Moritz et al (1996)
SH-120-173.00	Intermedios	calcite (cal II)	group 3	Boundstone with cal pseudomorphs after evaporite nodules	14.8	-0.8	This study
SH-120-171.00	Intermedios	calcite (cal II)	group 3	Dolostone with local concentrations of sulfides and cal veins	13.4	-1.3	This study
SH-56-298.20-C	Intermedios	calcite (cal II)	group 3	Mudstone with dol, gp, py and cal in fractures	11.0	-1.0	This study

Sample	Ore body / member	Material / mineral	Group	Petrographic description	$\delta^{18}O_{VSMOW}$(‰)	$\delta^{13}C_{VPDB}$(‰)	Reference
SH-180-189.70	Resurgidora	calcite (cal II)	group 3	Mudstone with fibro-radiated brt, cal vugs with internal sediments and snow-on-roof texture with py, sp and gp	16.1	-0.5	This study
SH-120-109.80	Resurgidora	calcite (cal II)	group 3	Dolostone with local concentrations of sulfides and cal veins	14.7	-1.4	This study
		coarse calcite II	group 3		12.5	-2.9	Moritz et al (1996)
		coarse calcite II	group 3		12.4	-2.8	Moritz et al (1996)
SH-231-134.60	Intermedios	calcite vein (cal III)		Dolostone with some cal veins	13.3	-5.1	This study

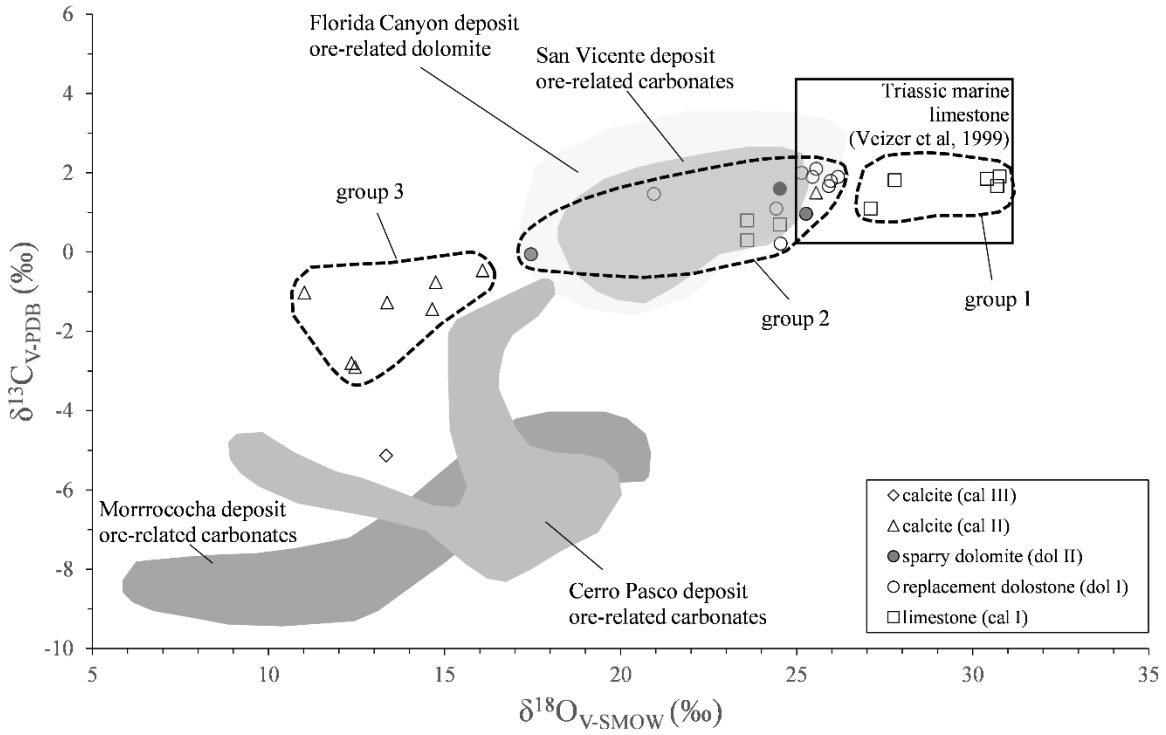

Fig. 9. Diagram $\delta^{13}C$ (‰VPDB) vs $\delta^{18}O$ (‰VSMOW) showing values for carbonate samples from Shalipayco deposit (data from Table 2) compared to ore-related carbonates data from Florida Canyon (De Oliveira et al. 2019), San Vicente (Spangenberg et al. 1996), Morococha (Catchpole et al. 2015) and Cerro Pasco (Baumgartner et al. 2008) deposits.

Table 3. Strontium isotopes compositions of Chambará Formation limestone and Mitu Group alkali basalt from Shalipayco deposit. Strontium data from limestone, replacement dolomite and coarse calcite from Moritz et al. (1996).

Sample	Mineral / Rock	$^{87}Sr/^{86}Sr$	2s	Reference
SH-56-298,20-N	Chambará Fm. limestone	0.708254	0.000020	This study
SH-70-217,60-N	Chambará Fm. limestone	0.708021	0.000038	This study
SH-60-170,40-N	Chambará Fm. limestone	0.708208	0.000015	This study
FSH-27	Limestone (I)	0.70788		Moritz et al (1996)
FSH-76	Limestone (I)	0.70790		Moritz et al (1996)
FSH-73	Limestone (I)	0.70765		Moritz et al (1996)
FSH-19	Limestone (I)	0.70799		Moritz et al (1996)
SH-43-683.90-M	Mitu Gp. alkali basalt	0.719669	0.000019	This study
SH-43-684.70-M	Mitu Gp. alkali basalt	0.709996	0.000017	This study
SH-43-685.90-M	Mitu Gp. alkali basalt	0.709654	0.000017	This study
FSH-13	Repl. Dol (I)	0.70857		Moritz et al (1996)
FSH-71	Repl. Dol (I)	0.70789		Moritz et al (1996)
FSH-72	Repl. Dol (I)	0.70786		Moritz et al (1996)
FSH-64	Repl. Dol (I)	0.70780		Moritz et al (1996)
FSH-68	Repl. Dol (I)	0.70773		Moritz et al (1996)
FSH-19	Coarse calcite (II)	0.70853		Moritz et al (1996)
FSH-71	Coarse calcite (II)	0.70898		Moritz et al (1996)
FSH-72	Coarse calcite (II)	0.70830		Moritz et al (1996)

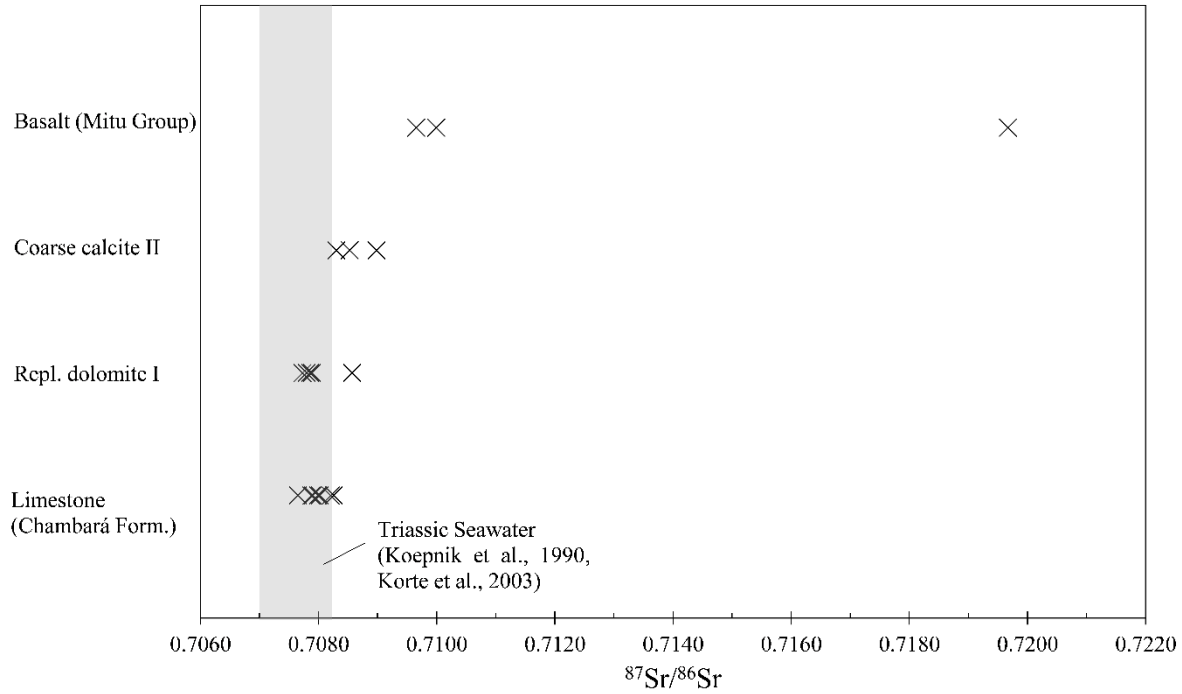

Fig. 10. Sr isotope compositions of the different stages carbonates from Chambará Formation of Shalipayco deposit and basalts from Mitu Group (data from Table 3). Data from limestone, replacement dolomite and coarse calcite from Moritz et al. (1996).

Table 4. Sulfur and oxygen isotopes compositions of sphalerite, galena, pyrite, and barite from Shalipayco deposit.

Sample	Sector	Mineral	$\delta^{34}S_{VCDT}$(‰)
SH-56-298.20-O	Intermedios	Barite	17.3
SH-70-220.00-O	Resurgidora	Barite	13.7
SH-120-109.80-G	Resurgidora	Galena	-23.0
SH-231-140.90-G	Intermedios	Galena	-22.2
SH-43-221.70-G	Resurgidora	Galena	-10.4
SH-210-219.70-H	Intermedios	Pyrite	-21.3
SH-43-221.70-H	Resurgidora	Pyrite	-6.2
SH-43-248.60-H	Intermedios	Pyrite	-23.3
SH-120-109.80-E	Resurgidora	Sphalerite I	-19.1
SH-120-113.80-E	Resurgidora	Sphalerite I	-18.0
SH-120-175.60-E	Intermedios	Sphalerite I	-16.8
SH-56-287.60-E	Intermedios	Sphalerite I	-17.0
SH-120-175.60-F	Intermedios	Sphalerite II	-15.3
SH-231-140.90-F	Intermedios	Sphalerite II	-17.9
SH-231-44.30-F	Resurgidora	Sphalerite II	-16.1
SH-60-171.50-F	Resurgidora	Sphalerite II	-16.4

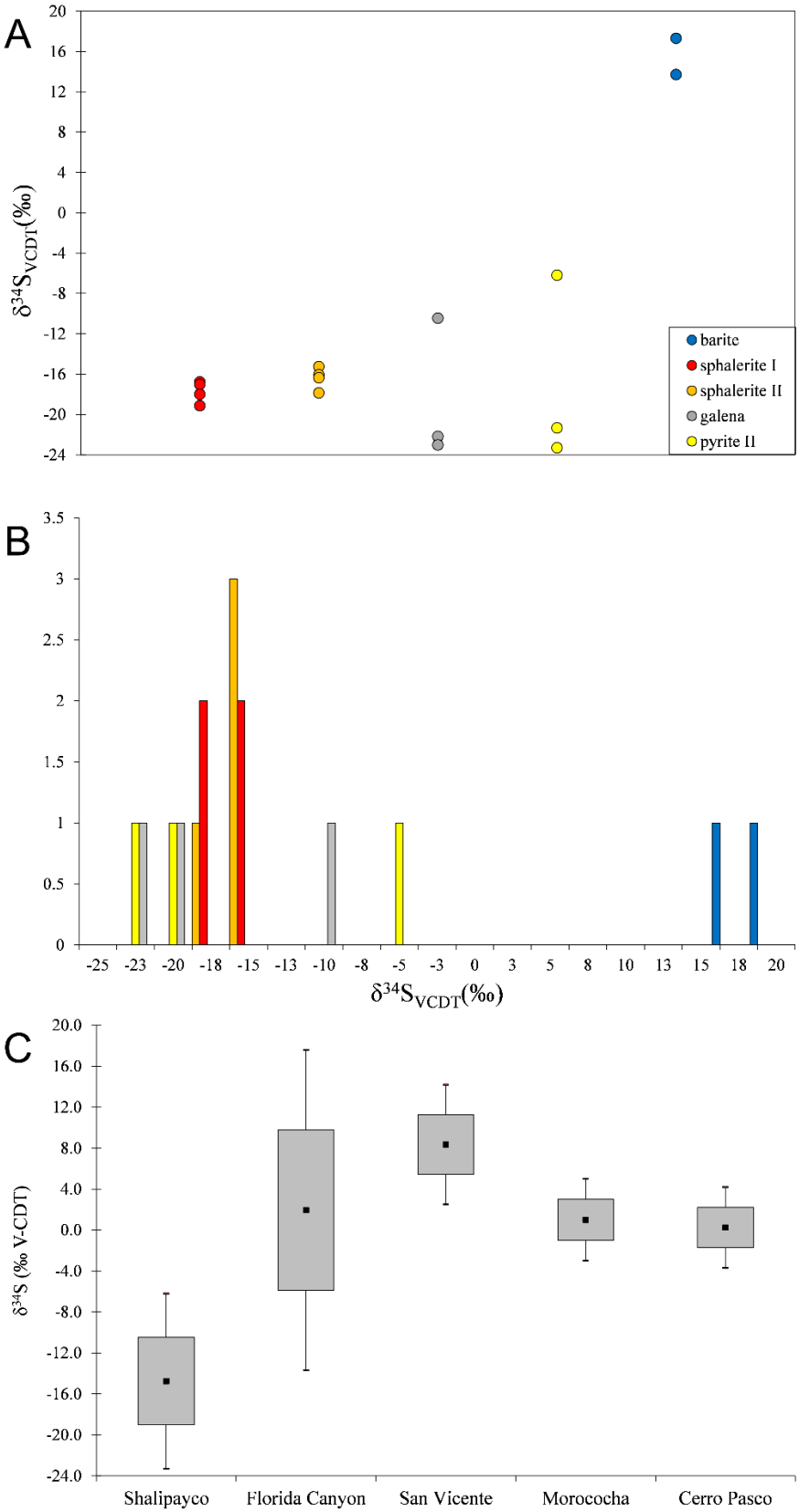

Fig. 11. A) δ34S values for sphalerite, galena, pyrite and barite from Shalipayco deposit. B) Histogram of the δ34S values for sphalerite, galena, pyrite and barite. C) Box plot of δ34S values for sulfides from Shalipayco (data from Table 4), Florida Canyon (De Oliveira et al. 2019), San Vicente (Fontbote and Gorzawski 1990; Spangenberg et al. 1999; Schütfort 2001), Morococha (Kouzmanov et al. 2008) and Cerro Pasco (Baumgartner et al. 2008) deposits

Discussion

Litho-stratigraphic constraints

The main Zn–Pb stratabound orebodies (Resurgidora and Intermedios) in the Shalipayco deposit are hosted in the most porous and permeable units of the Chambará carbonate sequence, defined in this work as Chambará II and III members. These two members also reflect the levels where evaporite pseudomorphs are present whereas the Chambará III has the most extensive evidence of former evaporite occurrences and consequently the Resurgidora orebody has greater lateral and metalliferous contents. The former evaporite-bearing rocks of the Pucará Group are responsible for an essential ground preparation stage for subsequent sulfide mineralization. The distribution of mineralization was controlled in part by the dissolution of the former evaporites that produced extensive evaporite dissolution breccias and consequently zones of higher permeability for the ore fluids. In addition, the conversion of gypsum or anhydrite to carbonate higher permeability of the strata created when former evaporites were dissolved to form evaporite breccias. Furthermore, replacement of calcium sulfate by dolomite in the presence of organic matter provided a source of reduced sulfur (Anderson and Garven 1987). This process also generated H_2S reservoirs during burial diagenesis that would become a future sulfur source for Zn–Pb sulfide precipitation. In addition, the secondary porosity observed in the Chambará II and III porous dolostones was likely generated by the diagenesis of an evaporite- and organic-rich porous dolostone. The upper and lower adjacent Chambará I and Chambará IV members of sabkha sequence formed predominantly by mudstones and packstones also have had an important role in the deposit genesis acting as physical traps conditioning initially H_2S reservoirs and then the ore fluid in the most porous members. Considering a movement of an ascending fluid from the basis of the stratigraphic sequence and that the Chambará I member is poorly permeable and porous, the presence of vertical steeply deep structures are essential for the basinal fluid flow. The NNE faults that intersect the stratabound Zn–Pb orebodies (Figs. 2 and 8) are considered as the main channels for the ascending metal-bearing brines.

Origin of the ore fluid

The Shalipayco carbonate minerals present an overall positive covariance of the isotopic composition of carbon and oxygen, which indicates crystallization by different temperature

fluids or their interaction with isotopically light fluids. The tendency of decreasing values of $\delta^{13}C$ associated to lower values of $\delta^{18}O$ for late paragenetic carbonates suggests a different carbon source in relation to host rocks or mechanisms of reduction of sulfate-mediated by organic matter during the evolution of the deposit.

The Mississippi Valley-type (MVT) deposits fluid inclusion data typically indicate homogenization temperatures in the average range of 90 º to 150 ºC (Leach et al. 2005), while the Carbonate Replacement deposits (CRD) data indicate temperatures in the average range of 200 º to 500 ºC (Megaw et al. 1988). The $\delta^{18}O$ average value for ore-related sparry dolomite (dol II) in the Shalipayco deposit is 22.4‰ with a ranging from 17.5 to 25.3‰ (Fig. 9). The oxygen isotope composition of the fluid in equilibrium with carbonates at the above-mentioned temperatures intervals has been estimated using the respective dolomite-water fractionation equations of Zheng (1999). Considering the average temperature ranging of CRD deposits the $\delta^{18}O_{H2O}$ in the fluid that generated sparry dolomite (dol II) in Shalipayco would vary from 12.4‰ (at 200 ºC) to 19.9‰ (500 ºC) which will be inconsistent with the typically $\delta^{18}O_{H2O}$ interval of 5.5 to 10.0‰ of magmatic waters (Taylor 1974). However, a hypothesis of an originally magmatic fluid that undergoes a fluid mixing process with an isotopically lighter meteoric fluid could also generate a more negative oxygen isotopic signature and could not be ruled out. On the other hand, assuming the average temperature ranging for MVT deposits for the $\delta^{18}O_{H2O}$ in the fluid that generated sparry dolomite in Shalipayco would vary from 1.3‰ (at 90 ºC) to 9.8‰ (150 ºC) which will be in agreement with formational water compositions isotopic equilibrium with the host rocks.

The fluid inclusion assemblages in Shalipayco minerals indicate single-phase (liquid) inclusions for early replacement dolomite (dol I) and two-phase (liquid + vapor) inclusions for late sparry dolomite (dol II) and sphalerite. The homogeneous liquid system concludes entrapment below about 40–50 ºC, while two-phase system indicates higher temperature fluids (Goldstein and Reynolds 1994). These data are in agreement with the interpretation of early dolomite (dol I) generation during burial diagenesis, considering an average geothermal gradient of 25 ºC/km, and with the fluid inclusion data from Moritz et al. (1996) on sparry dolomite of Shalipayco deposit, which yielded a homogenization temperature range of 115 º to 162 ºC and salinities between 9.5 wt.% and 26 wt.% NaC1 equivalent. On the other hand, the reported fluid inclusion data for Morococha epithermal-related mineralization indicated an original brine (2–5 wt.% NaCl eq.) with latest fluid generation associated with abundant carbonate precipitation ranging from 220 º to 260 ºC (Catchpole et al. 2011).

The oxygen isotopic composition of the fluids that formed the Shalipayco Zn–Pb ores is similar to that of the San Vicente (Fontbote and Gorzawski 1990; Spangenberg et al. 1999) and Florida Canyon (De Oliveira et al. 2019) MVT deposits, but distinct from the Cerro de Pasco (Baumgartner et al. 2008) and Morococha (Catchpole et al. 2015) magmatic-related deposits (Fig. 9). Hydrothermal ore-related carbonates from Cerro de Pasco deposit have $\delta^{13}C$ values (–6.6 to –4.5‰) and $\delta^{18}O$ values (9.5 to 19.5‰) that differ from the $\delta^{13}C$ and $\delta^{18}O$ values of Pucará host rocks. The lower $\delta^{13}C$ values indicate a stronger contribution of magmatic carbon (Baumgartner et al. 2008). Similar lighter $\delta^{13}C$ values for the carbonate from the polymetallic vein and replacement deposits have been published for the Morococha (Catchpole et al. 2015). The low $\delta^{13}C$ values could result from fluid interaction with organic matter horizons in the Pucará Group carbonate rocks. However, sulfides in the Morococha district consistently yield $\delta^{34}S$ values close to zero (Catchpole et al. 2015) been more acceptable a magmatic fluid source than an organic matter source, which would have much lower negative $\delta^{34}S$ values (Hoefs and Hoefs 1980).

In contrast to the trend presented by the oxygen isotopes, impoverishment at $\delta^{13}C$ (Fig. 9) is attributed mainly to the change in the isotopic composition of the carbon reservoir, since the variation in temperature usually does not have a very significant effect on the carbon isotopes fractionation (Emrich et al. 1970). The tendency of decreasing values of $\delta^{13}C$ may indicate derivation of the carbonates associated with the oxidation stage of the organic matter. According to Carothers and Kharaka (1980), the degradation of organic matter is one of the known processes that result in the depletion of $\delta^{13}C$ values of a hydrothermal fluid. This negative isotopic carbon signature could also reflect the replacement of former evaporite minerals into dolomite (dol I) in the presence of organic matter. Therefore, it is reasonable to consider that there was a light carbon isotope reservoir generated through BSR process during diagenesis before Zn–Pb mineralization stage.

The burial diagenetic dolomite data show strontium isotopic ranges very closer to host rocks data suggesting a carbonate basin-restricted fluid involvement. The more radiogenic strontium isotopic composition of late-stage carbonates indicate an exogenous metalliferous brine forming-fluid for Zn–Pb mineralization stage. The late process of dedolomitization overprinted in the sparry dolomites (dol II) involving meteoric fluid could be probably inherited its radiogenic signature in the new-formed calcite.

Source of sulfur and mechanisms of sulfide precipitation

The reduce sulfur necessary for the precipitation of sulfide ore-minerals may originate from bacterial sulfate reduction (BSR) or thermochemical sulfate reduction (TSR). BSR is common in diagenetic settings with temperatures about 0 < T < 60–80 ºC, while TSR is common in the temperature range of 0–100 < T < 150–200 ºC (Machel et al. 1995). Previous evaporite minerals (gypsum and anhydrite) from the own Pucará Group sequence are the most probable local sulfur source for the Shalipayco deposit. The textures of porous dolostone, evaporite breccia and calcite after evaporite pseudomorphs before the sulfide stage in Shalipayco deposit suggest that the replacement occurred in burial diagenesis. During this stage, the evaporite sulfate minerals in presence of organic matter were replaced by carbonates (calcite or dolomite) producing also H_2S gas and formation water (Anderson and Garven 1987). Although the very small size (< 8 μm) of the fluid inclusions, as is common in carbonates from BSR settings (Machel et al. 1995), did not allow an accurate microthermometry study, the primary assemblages observed in burial diagenetic dolomite are liquid single-phase inclusions, which indicates entrapment temperatures below 40–50 ºC (Goldstein and Reynolds 1994). The precipitation of the ore occurred when the metalliferous brine reached porous zones of the lithological trap with H_2S gas reservoirs. The negative values and the wide range of $\delta^{34}S$ observed in the sulfides of Shalipayco deposit are compatible with bacterial sulfate reduction during burial diagenetic stages (Machel et al. 1995). The low temperature indicative observed in fluid inclusions from early replacement dolomite (< 40–50 ºC) is also consistent with reduced sulfur generated by bacteria (Machel et al. 1995) with sulfur trapped in porous rocks adjacent to impermeable cap rocks. The $\delta^{34}S$ values of barite (+13.7 and +17.3‰) partially matches of Jurassic to Middle Triassic marine sulfate range (+15 to +17‰, Claypool et al. 1980), suggesting it was a source of earlier barite sulfate.

The MVT deposits of San Vicente and Florida Canyon show sulfur isotope ratios in ore-sulfides from –0.7 to +14.2‰ (Fontbote and Gorzawski 1990; Spangenberg et al. 1999; Schütfort 2001) and from –13.7 to +17.6‰ (Basuki et al. 2008), respectively. These authors interpreted a TSR as the mechanism for sulfate reduction in both MVT deposits. The sulfur isotope compositions for sulfides from Cerro Pasco (–3.7 to +4.2‰, Baumgartner et al. 2008) and for Morococha (–3.0 to +5.0‰, Kouzmanov et al. 2008) epithermal deposits are compatible with a magmatic source for sulfur (Ohmoto 1986). For discussion purposes, considering the distal magmatic genesis (carbonate-replacement type) hypothesis for Shalipayco deposit would

expect a homogeneous and cluster sulfide isotope ratios around 0 ±4‰ $\delta^{34}S$, based on other carbonate-replacement deposits (Thompson and Beaty 1990; Beaty et al. 1990). The carbonate-replacement Santa Eulalia deposit shows a widespread with $\delta^{34}S$ ratios ranging from 4 to -11‰ at the East Camp and a narrower spread occurs with negative values from -8 to -15‰ in the West Camp (Megaw et al. 1988), however, the Shalipayco sulfides still reach much more negative values (-6.2 to -23.3‰), reinforcing nonmagmatic relation sulfur source.

Metal source

The strontium values from Chambará Formation limestones and from diagenetic replacement dolomite (dol I) exhibit similar $^{87}Sr/^{86}Sr$ ranges from 0.707650 to 0.708254 and from 0.70773 to 0.70857, respectively, and close to Norian seawater composition (0.7075–0.7082, Koepnick et al. 1990; Korte et al. 2003). These values suggest a carbonate basin restrict circulation of fluids without external strontium source during burial diagenetic stages (Fig. 10). The $^{87}Sr/^{86}Sr$ values (from 0.70830 to 0.70898) from ore-related coarse calcite (cal II) indicate an external basin source for strontium and analogously for metals. The $^{87}Sr/^{86}Sr$ ratios from Mitu Group alkali basalt (from 0.709654 to 0.719669) indicate it as a potential strontium and metal source, but not excluding a mixture from another source, as discussed by Moritz et al. (1996).

Fontboté et al. (1990) and Gunnesch et al. (1990) report lead isotope analyses of galena samples from the Shalipayco deposit. These data are compared to lead isotope ratios of galena from San Vicente, Atacocha, Milpo (El Porvenir), Morococha and Cerro Pasco deposits (Gunnesch et al. 1990; Mukasa et al. 1990) plotted in Figure 12. The isotopic composition of galena from all distinguished deposits hosted in Pucará rocks plot in a field above the orogen curve and almost all below the upper crustal evolution curve (Zartman and Doe 1981) indicating a continental crustal dominance for metal sources. It is possible to distinguish linear arrays very well defined for different deposits (Fig. 12). The almost vertical tight linear trends of Pb isotope data indicate mixtures with different source-rocks during fluid migration (Gulson 1986) in all deposits. However, such arrays could be analytical been related to mass discrimination errors caused by slight variations in filament temperatures present sometimes in old analyzes (Leach et al. 2005).

The MVT deposits of Shalipayco and San Vicente show different lead isotope signatures and this was interpreted as different source-rocks. The Mitu Group conglomerates of

Shalipayco present minor radiogenic lead isotope values relatively of Sarayaquillo Formation clastic sediments for San Vicente (Fontboté et al. 1990; Gunnesch et al. 1990). The Pb isotope data from Atachocha and Milpo skarn deposits (Gunnesch and Baumann 1984) and the epithermal Cerro Pasco (Baumgartner et al. 2008), which are spatially juxtaposed, are overlapped in the same trend suggesting the same source-rocks and even interrelated formation process with the same coeval magmatic-hydrothermal event. This relationship does not occur with the Shalipayco Pb isotope ratios suggesting that this deposit would not be related to the same magmatic process or even at different ages. As an example, the lead isotope ratios of galena from the deposits in Mexico are relatively homogeneous within individual mineral districts, and deposits of similar type exhibit similar isotope ratios (Cumming et al. 1979). The skarn and carbonate replacement deposits of Chihuahua region, Mexico have broadly similar Pb isotope signatures indicating a cogenetic origin (Ostendorf et al. 2017).

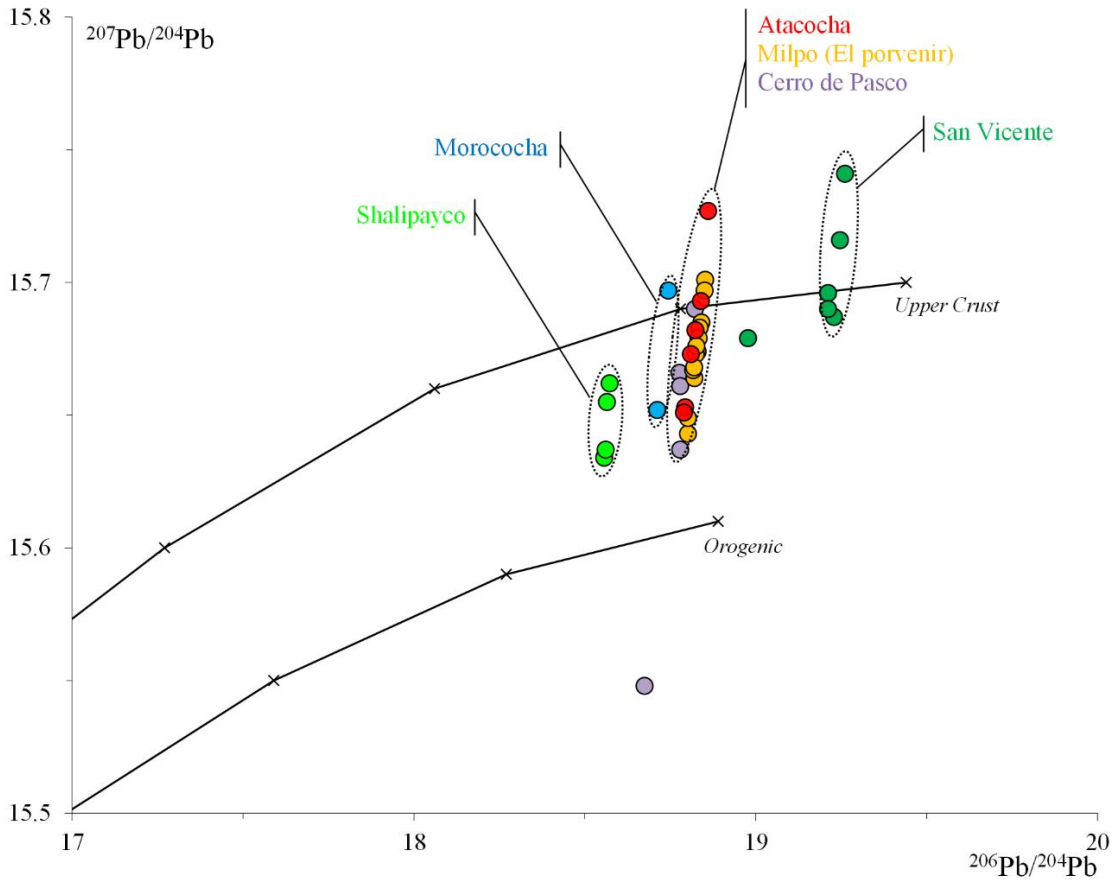

Fig. 12. Uranogenic diagram, with plumbotectonic model curves from Zartman and Doe (1981), showing the Pb isotopic compositions of galena samples. Shalipayco, San Vicente, Atacocha, Milpo and Morococha deposits data from Gunnesch et al. (1990), Cerro Pasco deposit data from Mukasa et al. (1990).

Conclusions

The Zn–Pb mineralization observed in the Shalipayco deposit accords with the majority of characteristics described for global MVT-style deposits (Leach and Sangster 1993; Leach et al. 2005): 1) the Chambará Formation host-rocks are platformal carbonates with evaporite sequences within the Andean orogenic foreland fold-and-thrust belt. 2) The sulfide mineralization occurs in dolostones and is clearly epigenetic and stratabound morphology. 3) The Shalipayco mineralogy is simple with sphalerite, galena, pyrite, quartz, dolomite, calcite, barite and fluorite. 4) Both isotopic composition from lead (metal) and reduced sulfur indicate crustal sources.

Carbonate-replacement deposits and MVT deposits exhibit many common characteristic, however, the main differences are the high temperatures and the association with magmatic sources in carbonate replacement systems. The fact of no such obvious spatial or genetic relationships with magmatism recognized for the Shalipayco deposit but its location close to other magmatically affiliated deposits hosted in the same carbonate sequence as skarn (Atacocha and Milpo) and epithermal (Cerro Pasco, Colquijirca and Morococha) awakens the question of its origin. However, the data obtained from sulfur isotopes in sulfides ($\delta^{34}S$ = -23.3 to -6.2‰) and carbon and oxygen isotopes ($\delta^{13}C$ = -0.1 to +1.6‰ and $\delta^{18}O$ = +17.5 to +25.3‰) in ore-related sparry dolomite do not corroborate this hypothesis not matching magmatic fluid sources. The temperature indicators from fluid inclusion data and sulfur isotope geothermometers obtained for Shalipayco deposit (<160º C) do not indicate the common high temperatures from the CRD deposits, but typical ones from MVT systems. The isotopic signatures of other nearby possible cogenetic deposits (Cerro Pasco and Morococha epithermal deposits and Atacocha and El Porvenir skarn deposits) also present distinguished lead, sulfur, carbon and oxygen isotopic signatures.

The Eddy vein occurrence shows a trace elements geochemistry signature with relative elevated Ag, As, Cd, Cu, Hg and Sb, which suggests a relationship with Cerro Pasco epithermal deposits and Atacocha and El Porvenir skarn deposits. Therefore, the sulfide occurrences of the Eddy vein and the Zn–Pb MVT orebodies of Resurgidora and Intermedios would be temporally distinct events with distinct structure controls. However, specific studies in the Eddy vein should be made to prove this hypothesis.

The Shalipayco deposit shows a very similar stratigraphic compartmentalization with Florida Canyon deposit also hosted in the base of Pucará Group, detached horizons with the

same ground preparation characteristics as porous dolostone, evaporite breccia and evaporite pseudomorphs. The Zn–Pb ore textures and form of occurrence are also very similar in both evaporite-related MVT deposits, leading to the conclusion of which they were formed by same basin metalliferous brine and by similar precipitation mechanisms, opening the possibility of discovering new deposits of this type in the Pucará Group.

References

Anderson GM, Garven G (1987) Sulfate-sulfide-carbonate associations in Mississippi Valley-type lead-zinc deposits. Economic Geology 82:482-488.

Basuki NI, Taylor BE, Spooner ETC (2008) Sulfur isotope evidence for thermochemical reduction of dissolved sulfate in Mississippi Valley-type zinc-lead mineralization, Bongara area, northern Peru. Economic Geology 103:783-799.

Baumgartner R, Fontboté L, Vennemann T (2008) Mineral zoning and geochemistry of epithermal polymetallic Zn-Pb-Ag-Cu-Bi mineralization at Cerro de Pasco, Peru. Economic Geology 103:493-537.

Beaty DW, Landis GP, Thompson TB (1990) Carbonate-hosted sulfide deposits of the Central Colorado mineral belt. Economic Geology Pub. Co.

Benavides-Cáceres V (1999) Orogenic evolution of the Peruvian Andes: the Andean cycle. Geology and ore deposits of the Central Andes 7:61-107.

Benavides V (1968) Saline deposits of South America International Conference on Saline Deposits. pp 249-290.

Bendezú R, Fontboté L (2009) Cordilleran epithermal Cu-Zn-Pb-(Au-Ag) mineralization in the Colquijirca district, central Peru: Deposit-scale mineralogical patterns. Economic Geology 104:905-944.

Bouabdellah M, Castorina F, Bodnar RJ, Banks D, Jébrak M, Prochaska W, Lowry D, Klügel A, Hoernle K (2014) Petroleum migration, fluid mixing, and halokinesis as the main ore-forming processes at the peridiapiric Jbel Tirremi fluorite-barite hydrothermal deposit, northeastern Morocco. Economic Geology 109:1223-1256.

Bouabdellah M, Niedermann S, Velasco F (2015) The Touissit-Bou Beker Mississippi Valley-type district of northeastern Morocco: relationships to the Messinian salinity crisis, Late Neogene-Quaternary alkaline magmatism, and buoyancy-driven fluid convection. Economic Geology 110:1455-1484.

Bouhlel S, Leach DL, Johnson CA, Marsh E, Salmi-Laouar S, Banks DA (2016) A salt diapir-related Mississippi Valley-type deposit: the Bou Jaber Pb-Zn-Ba-F deposit, Tunisia: fluid inclusion and isotope study. Mineralium Deposita 51:749-780.

Carothers WW, Kharaka YK (1980) Stable carbon isotopes of HCO3− in oil-field waters—implications for the origin of CO2. Geochimica et Cosmochimica Acta 44:323-332.

Catchpole H, Kouzmanov K, Fontboté L, Guillong M, Heinrich CA (2011) Fluid evolution in zoned Cordilleran polymetallic veins—Insights from microthermometry and LA-ICP-MS of fluid inclusions. Chemical Geology 281:293-304.

Catchpole H, Kouzmanov K, Bendezú A, Ovtcharova M, Spikings R, Stein H, Fontboté L (2015) Timing of porphyry (Cu-Mo) and base metal (Zn-Pb-Ag-Cu) mineralisation in a magmatic-hydrothermal system—Morococha district, Peru. Mineralium Deposita 50:895-922.

Charef A, Sheppard SMF (1987) Pb-Zn mineralization associated with diapirism: fluid inclusion and stable isotope (H, C, O) evidence for the origin and evolution of the fluids at Fedj-El-Adoum, Tunisia. Chemical Geology 61:113-134.

Claypool GE, Holser WT, Kaplan IR, Sakai H, Zak I (1980) The age curves of sulfur and oxygen isotopes in marine sulfate and their mutual interpretation. Chemical Geology 28:199-260.

Cumming GL, Kesler SE, Krstic D (1979) Isotopic composition of lead in Mexican mineral deposits. Economic Geology 74:1395-1407.

De Oliveira SB, Leach DL, Juliani C, Monteiro LVS, Johnson CA (2019) The Zn–Pb mineralization of the Florida Canyon, an evaporite-related Mississippi Valley-type deposit in the Bongará District, Northern Peru. Economic Geology:under review.

Emrich K, Ehhalt DH, Vogel JC (1970) Carbon isotope fractionation during the precipitation of calcium carbonate. Earth and Planetary Science Letters 8:363-371.

Fontbote L, Gorzawski H (1990) Genesis of the Mississippi Valley-type Zn-Pb deposit of San Vicente, central Peru; geologic and isotopic (Sr, O, C, S, Pb) evidence. Economic Geology 85:1402-1437.

Fontboté L (1990) Stratabound ore deposits in the Pucará basin In: Fontboté L, Amstutz G. C., Cardozo M., Cedillo E, Frutos J (eds) Stratabound Ore Deposits in the Andes. Springer-Verlag Berlin Heildelberg, pp 253-266.

Fontboté L, Gunnesch KA, Baumann A (1990) Metal sources in stratabound ore deposits in the Andes (Andean Cycle)—lead isotopic constraints Stratabound Ore Deposits in the Andes. Springer, pp 759-773.

Goldstein RH, Reynolds TJ (1994) Systematics of fluid inclusions in diagenetic minerals. SEPM.

Gulson BL (1986) Lead isotope in mineral exploration. Elsevier, Netherlands.

Gunnesch KA, Baumann A (1984) The Atacocha district, central Peru: some metallogenetic aspects Syngenesis and Epigenesis in the Formation of Mineral Deposits. Springer, pp 448-456.

Gunnesch KA, Baumann A, Gunnesch M (1990) Lead isotope variations across the central Peruvian Andes. Economic Geology 85:1384-1401.

Hoefs J, Hoefs J (1980) Stable isotope geochemistry. Springer.

INGEMMET (1999) Mapa geológico del Perú, Escala 1:1,000,000. Instituto Geológico Minero y Metalúrgico, Lima, Peru.

Johnson CA, Stricker CA, Gulbransen CA, Emmons MP (2018) Determination of $\delta^{13}C$, $\delta^{15}N$, or $\delta^{34}S$ by isotope-ratio-monitoring mass spectrometry using an elemental analyzer US Geological Survey Techniques and Methods. pp 19.

Koepnick RB, Denison RE, Burke WH, Hetherington EA, Dahl DA (1990) Construction of the Triassic and Jurassic portion of the Phanerozoic curve of seawater $^{87}Sr/^{86}Sr$. Chemical Geology: Isotope Geoscience section 80:327-349.

Korte C, Kozur HW, Bruckschen P, Veizer J (2003) Strontium isotope evolution of Late Permian and Triassic seawater. Geochimica et Cosmochimica Acta 67:47-62.

Kouzmanov K, Bendezú A, Catchpole H, Ageneau M, Pérez JA, Fontboté L (2008) The Miocene Morococha district, central Peru: Large-scale epithermal polymetallic overprint on multiple intrusion-centered porphyry systems Australasian Institute of Mining and Metallurgy, Pacific Rim Congress. pp 117-121.

Leach D, Song Y (2018) Sediment-hosted zinc-lead and copper deposits in China In: Chang Z, Goldfarb R (eds) Mineral deposits of China. pp in press.

Leach DL, Sangster DF, Kelley KD, Ross RL, Garven G, Allen CR (2005) Sediment-hosted Pb-Zn deposits: a global perspective. Economic Geology 100:561-608.

Leach DL, Song Y-C, Hou Z-Q (2017) The world-class Jinding Zn–Pb deposit: ore formation in an evaporite dome, Lanping Basin, Yunnan, China. Mineralium Deposita 52:281-296.
Machel HG, Krouse HR, Sassen R (1995) Products and distinguishing criteria of bacterial and thermochemical sulfate reduction. Applied geochemistry 10:373-389.
Mégard F (1968) Geología del cuadrángulo de Huancayo 25-m-[Boletín A 18] INGEMMET Boletín, Serie A: Carta Geológica Nacional. Servicio de Geología y Minería, Lima, Peru, pp 123.
Mégard F (1984) The Andean orogenic period and its major structures in central and northern Peru. Journal of the Geological Society 141:893-900.
Mégard F (1987) Structure and evolution of the Peruvian Andes In: Schaer JP, Rodgers J (eds) The Anatomy of Mountain Ranges. Princeton University, Princeton, New Jersey, United States, pp 179-210.
Megaw PKM, Ruiz J, Titley SR (1988) High-temperature, carbonate-hosted Ag-Pb-Zn (Cu) deposits of northern Mexico. Economic Geology 83:1856-1885.
Moritz R, Fontboté L, Spangenberg J, Rosas S, Sharp Z, Fontignie D (1996) Sr, C and O isotope systematics in the Pucará basin, central Peru. Mineralium Deposita 31:147-162.
Mukasa SB, Vidal C CE, Injoque-Espinoza J (1990) Pb isotope bearing on the metallogenesis of sulfide ore deposits in central and southern Peru. Economic Geology 85:1438-1446.
Noble DC, Silberman ML, Megard F, Bowman HP (1978) Comendite (peralkaline rhyolite) and basalt in the Mitu Group, Peru: evidence for Permian-Triassic lithospheric extension in the central Andes. US Geological Survey Journal of Research 6:453-457.
Ohmoto H, Rye RO (1979) Isotopes of sulfur and carbon. Geochemistry of Hydrothermal Ore Deposits (Barnes, HL, ed.), 509-567. John Wiley & Sons Inc., New York.
Ohmoto H (1986) Stable isotope geochemistry of ore deposits. Reviews in mineralogy 16:491-560.
Ostendorf J, Henjes-Kunst F, Schneider J, Melcher F, Gutzmer J (2017) Genesis of the Carbonate-Hosted Tres Marias Zn-Pb-(Ge) Deposit, Mexico: Constraints from Rb-Sr Sphalerite Geochronology and Pb Isotopes. Economic Geology 112:1075-1088.
Robson DM, Carlsson JT, Altman KA, Theben S (2017) NI 43-101 Technical Report on the Preliminary Economic Assessment of the Shalipayco Project, Junin Region, Peru. Roscoe Postle Associates Inc (RPA), Toronto, Canada, pp 194.
Rosas S, Fontboté L, Tankard A (2007) Tectonic evolution and paleogeography of the Mesozoic Pucará Basin, central Peru. Journal of South American Earth Sciences 24:1-24.
Schütfort EG (2001) The genesis of the San Vicente lead zinc rhythmite deposit, Peru: a petrologic, geochemical, and sulfur isotope study. Oregon State University, pp 136.
Soler P, Lara MA (1990) Minor and Trace Elements in the Polymetallic Stratabound Ore Deposits of the Central Peruvian Andes In: Fontboté L, Amstutz GC, Cardozo M, Cedillo E, Frutos J (eds) Stratabound Ore Deposits in the Andes. Springer, Berlin, pp 735-748.
Spangenberg J, Fontboté L, Sharp ZD, Hunziker J (1996) Carbon and oxygen isotope study of hydrothermal carbonates in the zinc-lead deposits of the San Vicente district, central Peru: a quantitative modeling on mixing processes and CO_2 degassing. Chemical Geology 133:289-315.
Spangenberg JE, Fontboté L, Macko SA (1999) An evaluation of the inorganic and organic geochemistry of the San Vicente Mississippi Valley-type zinc-lead district, central Peru; implications for ore fluid composition, mixing processes, and sulfate reduction. Economic Geology 94:1067-1092.
Szekely TS, Grose LT (1972) Stratigraphy of the carbonate, black shale, and phosphate of the Pucará Group (Upper Triassic—Lower Jurassic), Central Andes, Peru. Geological Society of America Bulletin 83:407-428.

Taylor HP (1974) The application of oxygen and hydrogen isotope studies to problems of hydrothermal alteration and ore deposition. Economic geology 69:843-883.
Thompson TB, Beaty DW (1990) Geology and the origin of ore deposits in the Leadville District, Colorado: Part II. Oxygen, hydrogen, carbon, sulfur, and lead isotope data and development of a genetic model. Carbonate-hosted sulfide deposits of the Central Colorado mineral belt Econ Geol Monog 8:156-179.
Tuanama N (2016) Controles geológicos del manto intermedio y su relación con la génesis del yacimiento tipo Mississippi Valley en Shalipayco, Junín, Perú Facultad De Ingeniería Geológica, Minera Metalúrgica Y Geográfica. Universidad Nacional Mayor San Marcos Lima, Peru, pp 158.
Veizer J, Ala D, Azmy K, Bruckschen P, Buhl D, Bruhn F, Carden GAF, Diener A, Ebneth S, Godderis Y, Jasper T, Korte C, Pawellek F, Podlaha OG, Strauss H (1999) $^{87}Sr/^{86}Sr$, $\delta^{13}C$ and $\delta^{18}O$ evolution of Phanerozoic seawater. Chemical Geology 161:59-88.
Warren JK (2006) Evaporites: sediments, resources and hydrocarbons. Springer Science & Business Media.
Warren JK (2016) Evaporites: A geological compendium. Springer.
Zartman RE, Doe BR (1981) Plumbotectonics—the model. Tectonophysics 75:135-162.
Zheng Y-F (1999) Oxygen isotope fractionation in carbonate and sulfate minerals. Geochemical Journal 33:109-126.

5 Structural control and timing of evaporite-related Mississippi Valley-type Zn–Pb deposits in Pucará Group, Northern Central Peru

Saulo B. de Oliveira[1,2], Caetano Juliani[2], Lena V. S. Monteiro[2], and Colombo Tassinari[2]

[1]Nexa Resources, São Paulo, SP 04571-010, Brazil

[2]Institute of Geosciences, University of São Paulo, São Paulo, SP 05508-080, Brazil

Abstract

The South America MVT belt comprises the deposits of San Vicente, Florida Canyon and Shalipayco and some minor Zn–Pb occurrences in an extension of more than a thousand kilometers the carbonates and evaporites hosts of the Pucará Group, in central–northern Peru. Structural constraints of the MVT Peruvian deposits are conditioned by deep sub-vertical secondary extension structures with general N, NNE or NNW direction related to strike-slip movements superimposed on previous Andean NW thrust structures. Recent studies on Shalipayco and Florida Canyon deposits point to same processes of rock formation, diagenesis and mineralization genesis acting in province scale. Based on a compilation of available data for the evaporite-related MVT deposits and studies on the structural and tectonic evolution of the Peruvian Andes, and new isotopic data of Pb-Pb and Rb-Sr in sulfides allowed to establish correlations of local process of the deposits to the regional Andean tectonic events. The Florida Canyon dome structure was attributed to Juruá Orogeny (157–152 Ma). The stage of dolomitization forming the porous dolostone and evaporite breccia during burial diagenesis is attributed to the period between Juruá and Mochica Stages. The oil migration to these reservoir rocks occurred probably during Mochica event (100–95 Ma). The Rb-Sr dating of sphalerite from the Florida Canyon deposit together with temporal field relations indicated that the sulfide ore formed in or just after Peruvian Orogeny (86-83 Ma).

Introduction

The evaporite-related Mississippi Valley-type (MVT) Zn–Pb deposits host in the carbonate rocks of Pucará Group form one of the world most important belt of this deposit type in South America. The MVT belt is defined from the northern to central Peru including the

deposits of San Vicente, Florida Canyon and Shalipayco, and the minor Zn–Pb occurrences of Maino, Florcita, Ulcumayo, Piñon, Sillapata, Huacrash–Aynamayo, Puntayacu, Pichita Caluga, Cascas, Ninabamba, Raymondi Sur, Tambo María, Pampa Seca, San Roque, Bolívar and Soloco (Carlotto et al., 2009). This paper forms part of a regional multidisciplinary study of the evaporite-related MVT deposits in Peruvian Andes, that include the Florida Canyon deposit (De Oliveira et al., 2018) in the northern Peru and Shalipayco deposit (De Oliveira et al., in prep.) in central Peru.

The main aim of this work is to correlate the structural data and the evolution stages recognized in the MVT deposits with the major structural-tectonic events of the northern central Andes in Peru. We present new structural insights based on the 3D geological model, new lead isotopic analysis for Florida Canyon and Shalipayco deposits discussing metal source for ore-genesis and the age obtained through the Rb-Sr method in sphalerite for Florida Canyon deposit.

Geologic Setting

In northern and central Andes of Peru, where are located the evaporite-related MVT belt, three morphotectonic units can be defined (Fig. 1): the Western Cordillera, the Eastern Cordillera and the Sub-Andean Zone (Mathalone and Montoya, 1995; Benavides-Cáceres, 1999; Hermoza et al., 2005; Eude et al., 2015). Mégard (1984) defined two main thrust and fold belts where most of the shortening in the Andes are apparently concentrated: the ENE-vergent Marañon thrust and fold belt (MTFB) that bounds the Western Cordillera formed in Eocene, and the NE-vergent Sub-Andean thrust and fold belt (STFB) in the contact of Eastern Cordillera formed in Neogene (Fig. 1). Recent tectonic studies carried out in northern central Peru, detailed the eastern part of the Western Cordillera (including Marañon trust and fold belt) (Scherrenberg et al., 2012; Scherrenberg et al., 2014) and the eastern wedge (Eastern Cordillera and Sub-Andean Zone) (Hermoza et al., 2005; Eude et al., 2015). The Florida Canyon MVT deposit (De Oliveira et al., 2018) is located on Sub-Andean Zone in STFB. The San Vicente (Fontbote and Gorzawski, 1990) and Shalipayco (De Oliveira et al., in prep.) MVT deposits are located in Eastern Cordillera also in the STFB context (Fig. 1).

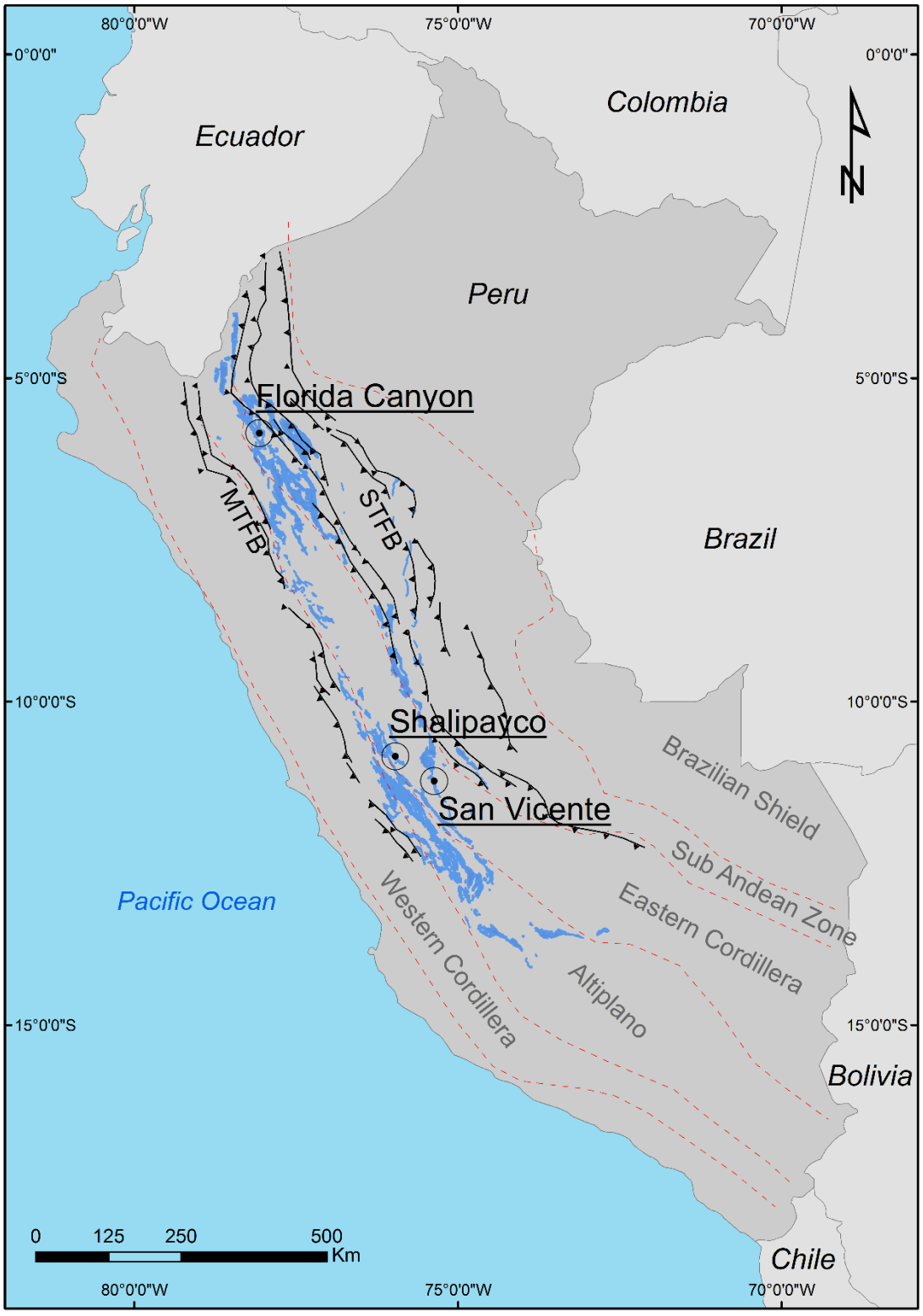

Fig. 1. Location of the Florida Canyon, Shalipayco and San Vicente evaporite-related MVT deposits and the main surface exposition of Pucará Group (Palacios, 1995). Morphostructural units of Peru after Benavides-Cáceres (1999). Location of the Marañon (MTFB) and Sub-Andean (STFB) thrust and fold belts after Mégard (1984).

Andean Cycle in Northern Central Peru

The Andean period is characterized by relatively short tectonic phases and by longer intervals of relative tectonic quiescence (Mégard, 1984; Benavides-Cáceres, 1999). The tectonic evolution of the Andes in Peru could be divided into three major cycles: a pre-Andean Cycle (Precambrian–Paleozoic), a transitional extensional period which the Pucará Basin developed (Late Triassic to Early Jurassic) and the properly Andean Cycle (Early Jurassic–present) (Mégard, 1987; Benavides-Cáceres, 1999). In the late Jurassic, a paleogeographic pattern was established in central and northern Peru lasting until the late Cretaceous. The paleogeographic consisted in two arcs: Paracas (West) and Marañon (East), thereabout where actually are the Western and Eastern Cordilleras, respectively, so separated by the W and E Peruvian basins (Mégard, 1984). The Late Triassic to Early Jurassic period is characterized by extension tectonics along grabens with NW–SE trends with marine transgressions and coeval bimodal alkaline magmatism (Jaillard et al., 2000). The sequence of red sandstones and conglomerates beds with evaporite intercalations of Permian–Triassic Mitu Group filled fault-controlled grabens with the association of peralkaline rhyolite and basalts (Mégard, 1978; Noble et al., 1978). A marine transgression overlaps the Mitu volcano-sedimentary sequence during Late Triassic and Early Jurassic resulting in the deposition of the carbonate and evaporitic sequence of Pucará Group (Szekely and Grose, 1972; Mégard, 1978; Loughman and Hallam, 1982; Rosas et al., 2007). Locally alkaline lava flows occur interbedded in Pucará marine sediments, which indicate dominance of extensional tectonic regime during this period (Schaltegger et al., 2008). The subduction during the Late Jurassic to Late Cretaceous is inferred mainly from the calc-alkaline magmatic arcs. Subsequent deposition of continental clastic sediments of the Sarayaquillo Formation sandstones (Middle-Upper Jurassic) and of the Goyllarisquizga conglomerates (Lower Cretaceous) resulted in a burial depth of Pucará Group rocks exceeding 2,000 m (Fontbote and Gorzawski, 1990) before late Miocene tectonic deformation (Mégard, 1984).

Andean Structural Evolution in Northern Central Peru

The structural evolution of the Peruvian Andes is characterized by regionally succession of orogenic deformation phases summarized on Table 1. The evolution is interpreted as a sequence of deformation eastward from the cost to the Sub-Andean Zone (Steinmann, 1929;

Mégard, 1978, 1984, 1987; Benavides-Cáceres, 1999; Jaillard et al., 2000; Pfiffner and Gonzalez, 2013). Four structural phases named Mochica (Cenomanian), Peruvian (Santonian–Campanian), Incaic (mid to late Eocene) and Quechua (Miocene–Pliocene) was defined by Steinmann (1929). New seismic data made possible the recognition of the Nevadan orogenic event (Kimmeridgian) recorded in the Pucará Group rocks (Mathalone and Montoya, 1995; Caputo, 2014; Eude et al., 2015). This deformational stage is also described in Peru by Benavides-Cáceres (1999) who named it Vicusian orogeny. Caputo (2014) proposed the name of Juruá orogeny for this the South American regional deformation event also correlated to other synchronous events described in Argentina, Bolivia, Brazil and Chile (Sempere et al., 1999; Sempere et al., 2002).

The seismic sections indicated that Juruá related faults in affected Middle to Early Late Jurassic stratas, indicating a latest Jurassic age for the tectonism (Mathalone and Montoya, 1995; Jaillard et al., 2000; Bump et al., 2008; Caputo, 2014). The NW–SE seismic sections present deep subvertical faults with apparent general dip for NW, sometimes they were reactivated affecting more recent (Cretaceous–Cenozoic) superimposed sequences. During the Middle to Late Jurassic, a transtensional tectonic regime, probably sinistral, prevailed in the NW–SE trend of northern central Peru with some localized basin uplift and alternation of marine sedimentation. Based on authigenic illite K–Ar age in Carboniferous oil and gas reservoir beds of the Solimões Basin (Elias et al., 2007), Caputo (2014) dates the Juruá Orogeny as old as Kimmeridgian.

The Mochica phase is defined by open, upright and parallel folds trend NW–SE sometimes with straight limbs and relatively sharp hinges, most often described in the extreme west of the Western Cordillera (Mégard, 1984; Pfiffner and Gonzalez, 2013). The folds generated during Mochica phase trend in two directions: a mainly direction is oblique to general Andean trend, while the second early direction is normal to it (Benavides-Cáceres, 1999). The folds are sharply cut by the Coastal Batholith with ages of 95–91 Ma (Mukasa, 1986), bracketing the age of Mochica stage younger than this magmatism (Pfiffner and Gonzalez, 2013). The Coastal Batholith emplacement occurred after the formation of the Mochica phase folds and is coeval with strike-slip faulting (Pfiffner and Gonzalez, 2013). The Mochica phase is in part coincided with the opening of the South Atlantic during the late Albian (Silver et al., 1998).

The Peruvian phase is characterized by folding affected an elongated area with a NW trend in the Eastern Cordillera, and a basin uplift with possible compression in the Western

Cordillera, being attributed Santonian to Campanian age (Mégard, 1984; Benavides-Cáceres, 1999; Jaillard et al., 2000). The structures included isoclinal and recumbent folds inclined to NE or E and tangential deformation indicatives as ramps and duplex (Benavides-Cáceres, 1999).

The Incaic phase is featured by tight extensive chevron-folding, thrust and reverse faulting in Western Cordillera and open folding and steep thrust faulting in Eastern Cordillera (Benavides-Cáceres, 1999; Jaillard et al., 2000; Pfiffner and Gonzalez, 2013). The Marañon fold-and-thrust belt (MTFB) can be attributed to the Incaic phase deformation (Mégard, 1984; Jaillard et al., 2000; Pfiffner and Gonzalez, 2013). The unconformity of volcanic rocks (about 40 Ma) with the Upper Cretaceous rocks of Casapalca Formation gives a minimum age for the Incaic tectonism (Noble et al., 1979).

The Quechua deformation stage occurs predominantly in the Sub-Andean Zone and Eastern Cordillera and it is subdivided into three episodes (Mégard, 1984; Jaillard et al., 2000). The Quechua 1 encompasses reactivation of Incaic phase structures and wide-open folds and reverse thrusts in Western Cordillera during 17–15 Ma (Mégard, 1984; Jaillard et al., 2000; Pfiffner and Gonzalez, 2013). Because of superimposition of Quechua 1 folding over Peruvian folding, the folds are tighter and commonly coaxially refolded in the Eastern Cordillera (Mégard, 1984). The Quechua 2 pulse caused primarily dextral slip along the many longitudinal NW–SE trending faults (Mégard, 1984). The thrusting to NE direction restricting the sedimentation to the margins of the orogen in the time span 9–8 Ma (Pfiffner and Gonzalez, 2013). The upper limit on Quechua 2 contractional deformation is constrained by the $^{40}Ar/^{39}Ar$ isotopic age of 8.6 Ma in a Puchcas tuff unit that lies in unconformity over the deformed rocks of Huanta Formation (Wise et al., 2008). Different from the earlier Mochica, Peruvian, Incaic and Quechua 1 phases, where the shortening direction was NE–SW, the Quechua 2 movement was related to N–S trending sub-horizontal shortening (Mégard, 1984). By the other hand, the Quechua 3 shortening is dominantly E–W direction and dated at about 6 Ma in Sub-Andean Zone where it generated the Sub-Andean fold-and-thrust belt (SFTB) (Mégard, 1984). The Quechua 3 pulse in northern central Peru is characterized by folding and reverse and strike-slip faulting (Jaillard et al., 2000).

Table 1. Summary of Andean deformation events in north–central Peru.

Deformational event	Period	Age	Predominant zone	Shortening direction	Structures and main characteristics
Quechua III	Miocene–Pliocene	<6 Ma	Sub-Andean zone	E–W	- folding and reverse and sinistral strike-slip faulting
Quechua II	Miocene	9–8 Ma	Eastern Cordillera Sub-Andean zone	N–S	- dextral strike-slip along the longitudinal NW–SE trending faults - tectonic inversion of pre existing normal faults
Quechua I	Miocene	17–15 Ma	Western Cordillera Eastern Cordillera Sub-Andean zone	NE–SW	- open folds and reverse thrusts in WC - tight and commonly coaxial refolding in the EC
Incaic	Eocene	<40 Ma	Western Cordillera Eastern Cordillera	NE–SW	- tight folding and thrust faulting WC - open folding and steep thrust faulting EC
Peruvian	Upper Cretaceous (Santonian–Campanian)	86–83 Ma	Western Cordillera Eastern Cordillera Sub-Andean zone	NE–SW	- isoclinal and recumbent folds inclined to NE or E - tangential deformation indicatives as ramps and duplex
Mochica	Lower Cretaceous (Cenomanian)	100–95 Ma	Western Cordillera Eastern Cordillera	NE–SW	- open, upright and parallel folds - dextral strike-slip faulting related to oblique folding
Juruá (Nevadan)	Upper Jurassic (Kimmeridgian)	157–152 Ma	Sub-Andean zone	NE–SW	- subvertical faults with apparent general dip for NW

Tectonic settings and MVT deposits

Most of world's Mississippi Valley-type (MVT) zinc–lead deposits are linked to major orogenic belts (Bradley and Leach, 2003; Leach et al., 2005; Leach et al., 2010). Bradley and Leach (2003) highlight that the majority of MVT deposits of the world are situated in orogenic forelands, defining three tectonic settings of occurrence: arc–continent collision, Andean-type subduction, or basin inversion. The authors also emphasize that not all MVT deposits are formed in forelands, and some deposits are formed in an extension setting or within thrust belts. The main three MVT deposits host in the Pucará Group (San Vicente, Florida Canyon and Shalipayco) are within the thrust belt setting of the Andes. Other examples of MVT deposits in the same context are the Picos da Europa, Spain (Fernández et al., 2000) and Robb Lake, Canada (Smethurst et al., 1999), in this last example the Zn–Pb mineralization postdate the thrusting.

Geology of the Evaporite-Related MVT Deposits of Peru

Host rocks and stratigraphy on the evaporite-related MVT deposits

The evaporite-related MVT deposits of Peru are hosted in the carbonates and former evaporites of Pucará Group. This sedimentary sequence extends along approximately 1,000 km in the direction NW–SE from the central to northern of the country (Fig. 1). Although Pucará outcrops occur predominantly in the Eastern Cordillera and northern Altiplano (Fig. 1), stratigraphic columns based on seismic and wells data present their occurrence from Western Cordillera to Sub-Andean Zone (Pfiffner and Gonzalez, 2013; Eude et al., 2015).

The Triassic–Jurassic Pucará Group is subdivided, from the base towards the top, in the Chambará, Aramachay, and Condorsinga formations (Szekely and Grose, 1972; Mégard, 1978; Loughman and Hallam, 1982; Rosas et al., 2007). The Pucará Group is dominated by shallow-water platform interbedded limestones and dolostones with evaporite facies from the Chambará and Condorsinga formations. The Aramachay Formation intermediate unit is composed by deeper-water bituminous calcareous shales (Szekely and Grose, 1972; Rosas et al., 2007). Intercalations of basaltic flows occur within the Aramachay Formation (Rosas et al., 2007).

The Florida Canyon and Shalipayco Zn–Pb ore bodies are hosted in the Chambará Formation that lies with angular unconformities with the Mitu Group volcanic-sedimentary

sequence (Moritz et al., 1996; Basuki et al., 2008; Oliveira et al., 2018a, 2018b). The San Vicente Zn–Pb ore bodies is hosted either in the Chambará as in the Condorsinga formations (Fontbote and Gorzawski, 1990; Spangenberg et al., 1996; Spangenberg et al., 1999). The basement rocks in the Bongará Province where Florida Canyon is located is the Marañon Complex comprising Neoproterozoic to Early Paleozoic orthogneisses and metasedimentary sequences (Mégard, 1978). In central Peru, the basement rocks of San Vicente and Shalipayco deposits is the phyllites and quartzitic beds of the Lower to Middle Paleozoic Excelsior Group (Mégard, 1978).

The three evaporite-related MVT deposits of the Chambará Formation present subdivisions with local identifications (Fig. 2). In the Florida Canyon deposit, the Chambará Formation is subdivided in three members from the stratigraphy base to the top, Chambará 1, 2, and 3 (Reid, 2001; Basuki et al., 2008). The intermediate member Chambará 2 is a dolostone of sabkha facies, while the members Chambará 1 and 3 are predominantly limestones (De Oliveira et al., 2018). The Shalipayco deposit presents a very similar subdivision with Chambará I, II, III and IV members, where the top and base (Chambará I and IV) are massive or laminated limestones and the two intermediate members (Chambará II and III) are composed mainly of dolostones (De Oliveira et al., in prep.). In the San Vicente deposit, the Chambará Formation is subdivided in Basal Series, San Judas dolostone, Neptuno limestone and San Vicente dolostone (Fontbote and Gorzawski, 1990; Spangenberg et al., 1996; Spangenberg et al., 1999). The Uncush limestone and the Alfonso dolostone are equivalent to Aramachay and Condorsinga Formations, respectively (Spangenberg et al., 1996; Spangenberg et al., 1999). In all three MVT deposits, the Zn–Pb ore bodies are hosted in the dolostone members (Fig. 2).

Paragenetic Sequence of the MVT deposits of Peru

In all three most studied MVT deposits of Peru the same paragenetic mineral phases are described with: i) an early replacement dolomite stage prior to Zn–Pb mineralization; ii) the ore stage with sulfides (two sphalerite phases; an early dark brown and a late light brown, galena, pyrite and marcasite) in association with sparry dolomite, mainly in void-filling texture, and iii) a late calcite vein stage (Fontbote and Gorzawski, 1990; Moritz et al., 1996; Spangenberg et al., 1996; Spangenberg et al., 1999; Reid, 2001; Basuki et al., 2008; De Oliveira et al., 2018; De Oliveira et al., in prep.). However, they receive different interpretations according to the geological events, which they are assigned. In Table 2, the paragenetic sequence of carbonate

minerals from each deposit are summarized according to recent interpretations for Florida Canyon (De Oliveira et al., 2018) and Shalipayco deposits (De Oliveira et al., in prep.).

Fontboté and Gorzawski (1990) assumed all the carbonate phases and the sulfide ore formed during burial diagenesis for San Vicente deposit. Spangenberg et al. (1996); Spangenberg et al. (1999) and Moritz et al. (1996) interpreted all San Vicente and Shalipayco carbonate generations formed in a single event in association with ore with hydrothermal origin. Reid (2001) and Basuki et al. (2008) described the dolomitization in Florida Canyon deposit as an ore-related alteration also hydrothermal in origin. In the studies of De Oliveira et al. (2018) for Florida Canyon deposit and of De Oliveira et al. (in prep.) for Shalipayco deposit two distinct paragenetic stages are recognized: the extensive dolomitization that replaces evaporite sulfates is attributed to burial diagenesis, while the ore-related sparry dolomite commonly in void-filling texture is assigned to posterior hydrothermal incoming brine. Early calcite veins attributed to early diagenesis are only described in the Florida Canyon deposit (De Oliveira et al., 2018).

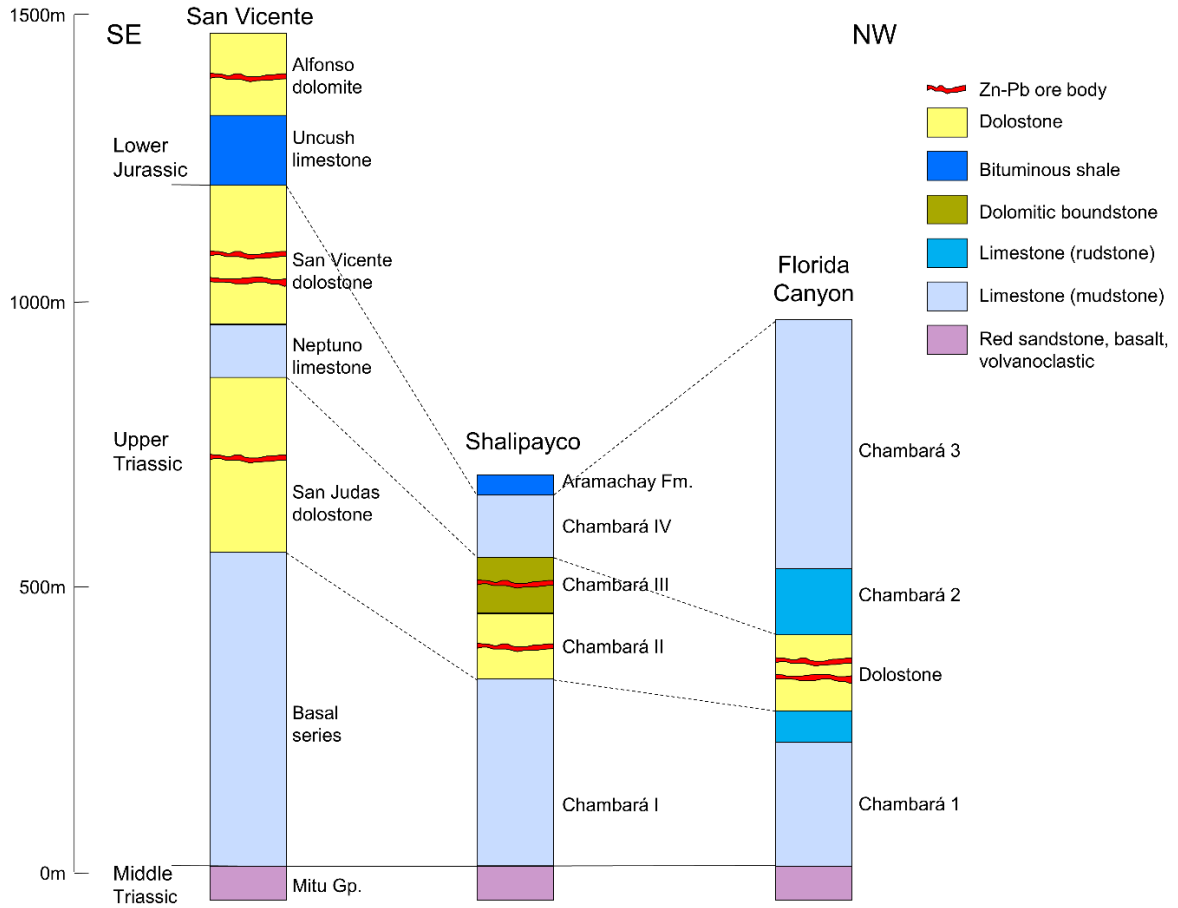

Fig. 2. The stratigraphic sequence and subdivisions of the Chambará Formation in the Florida Canyon (De Oliveira et al., 2018), Shalipayco (De Oliveira et al., in prep.) and San Vicente evaporite-related MVT deposits (Fontboté and Gorzawski, 1990).

Table 2. Summary of paragenetic sequence for San Vicente (Fontbote and Gorzawski, 1990; Spangenberg et al., 1996; Spangenberg et al., 1999), Shalipayco (Moritz et al., 1996; De Oliveira et al., in prep.), and Florida Canyon deposits (Reid, 2001; Basuki et al., 2008; De Oliveira et al., 2018).

Source	Fontboté and Gorzawski (1990)	Spangenberg et al. (1996); Spangenberg et al. (1999)	Moritz et al. (1996); De Oliveira et al. (in prep.)	Reid (2001); Basuki et al. (2008)	De Oliveira et al. (2018)
MVT Deposit	San Vicente	San Vicente	Shalipayco	Florida Canyon	Florida Canyon
Burial diagenesis		calcite / dolomite replacing evaporite sulfate (EPC / EPD)			calcite as evaporite pseudomorph (cal III)
	diagenetic crystallization rhythmite (DCR): black dolomite I and white dolomite II	dark replacement dolomite (DRD)	replacement dolomite I	early dolomite (D1)	replacement dolomite (dol II)
					porous dolostone (dol II)
					evaporite breccia (dol II)
Sulfide mineralization	sparry dolomite	white sparry dolomite (WSD)	sparry dolomite II	late dolomite (D2)	white sparry dolomite (dol III)
	calcite	late void-filling calcite / dolomite (LFC / LFD)	coarse calcite II	calcite (C1) and calcite (C2)	late void-filling calcite (cal IV)

The San Vicente deposit has a general bedding with north direction with a dip of ~25-30°W that follow the main thrust faults in the area, as the Utcuyatu fault that defines the local upper contact of Pucará Group with Tarma Granodiorite (Fontbote and Gorzawski, 1990; Badoux et al., 2001). San Vicente lies on the western limb of an anticline trending 170° (Fontbote and Gorzawski, 1990). The stratabound Zn–Pb orebodies are both parallel and subparallel to the bedding as a parallel of the thrusts (Dávila et al., 2000). A series of normal faults mainly striking 50° and 140° cut the carbonate units in the proximity to the orebodies (Fontbote and Gorzawski, 1990; Spangenberg et al., 1996). The faults were formed during simple dextral shearing and the displacement along these faults is centimetric to decimetric-long for both eastward and westward (Badoux et al., 2001). The general north direction faults in San Vicente deposit were interpreted as main channel ways of the Zn–Pb mineralizing fluids (Dávila et al., 2000).

The Florida Canyon deposit is characterized by a dome structure defined by drilling with general northwest trending along which the main stratabound Zn–Pb ore bodies are hosted. The deposit is limited by the steeply deep north-northeast Sam Fault with a displacement over tens of meters on the west side and by the extensive Tesoro thrust fault striking northwest in the eastern portion (De Oliveira et al., 2018). The two main known mineral bodies hosted in subvertical halokinetic evaporite breccia are located in the Sam Fault and in another parallel fault with the general northward direction (Fig. 3). A right lateral strike-slip component and some splays off the main Sam Fault occur in the northern part of the Florida Canyon deposit (Reid, 2001).

The general bedding and the stratabound Zn–Pb orebodies in Shalipayco deposit strike 145° with a dip ~30°SW (De Oliveira et al., in prep.). A series of normal steep faults with a northward strike occur along all the deposit (Fig. 4). The 3D perspective images show the distribution of the sum of zinc and lead grades along the stratabound ore, highlighting the high grades closer to the faults with the general northward direction (Fig. 3). Apparently this faults did not shift the orebodies, however, they could have small displacements, as the ones described in San Vicente deposit, that could not be noticed in geological interpretation due of a large drilling spacing (>25 m). A major fault named Eddy Vein with strike 170° and dip ~70°NE cut the orebodies and apparently limits their southern continuity. This structure was systematically

tested by drilling and is barren (De Oliveira et al., 2018). Until now, the known sulfide orebodies in Shalipayco deposit are concordant with bedding.

A common aspect in the structural pattern of the Shalipayco and Florida Canyon deposits is the higher values of the sum of zinc and lead grades around secondary steeply structures, indicating them as ore-fluid channels (Fig. 3). These secondary structures, in general, make a low angle with the major Andean thrusts fault planes with direction northwestward. Epigenetic mineralization is typically localized along low displacement faults and extensional fracture systems (Cox, 2010). The MVT fluid migration is ineffective within thrust faults, however, transitions from thrusting to transpressional deformation or tectonic uplift could form large dilational zones within bounding strike-slip faults during large-scale contractional events (Bradley and Leach, 2003; Leach and Song, 2018). Within a strike-slip regime, these extension structures are identified as T-fractures (Petit, 1987). The kinematics of the strike-slip component on northwestern Andean thrust fault would be dextral in both the Shalipayco and Florida Canyon deposit (Fig. 3).

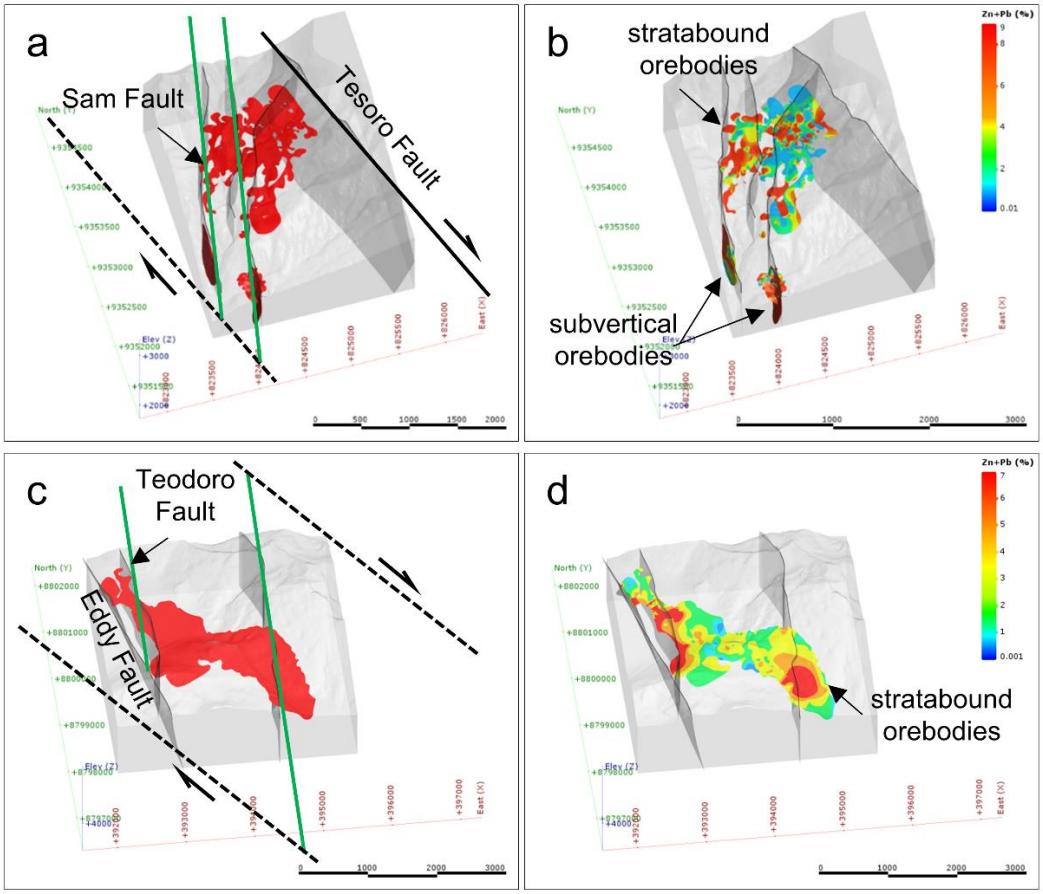

Fig. 3. Oblique views to the NW of 3D geological model of Shalipayco and Florida Canyon deposits. a) Structural pattern with strike-slip faults in black, T-fractures in green and Zn–Pb orebodies of the Florida Canyon deposit. b) Distribution of the sum of zinc and lead grades within the orebodies along the Florida Canyon deposit. c) Structural pattern with strike-slip faults in black, T-fractures in green and Zn–Pb orebodies of the Shalipayco deposit. d) Distribution of the sum of zinc and lead grades within the orebodies along the Shalipayco deposit.

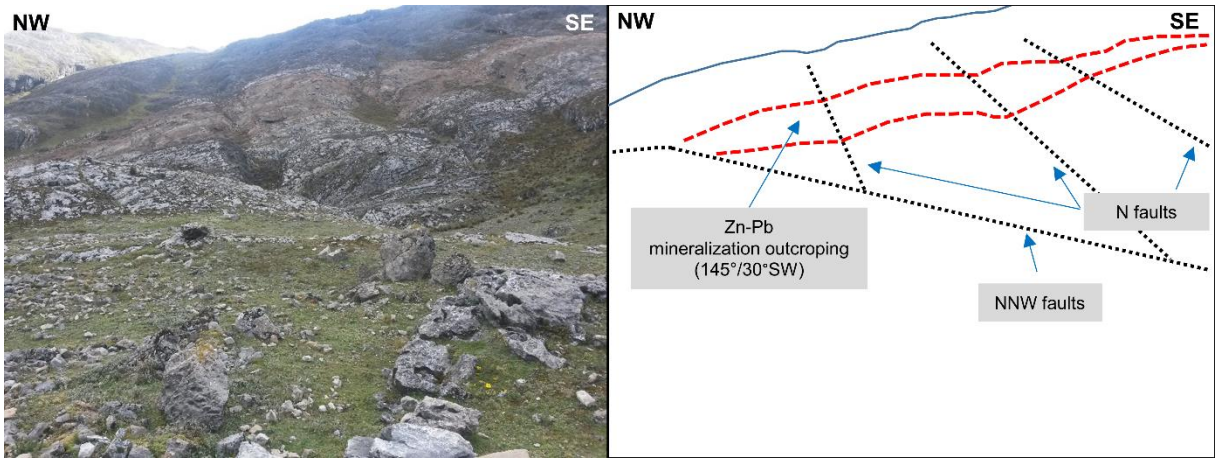

Fig. 4. Outcrop in the mineralized zone in Shalipayco showing secondary ore-related steeply dipping faults with north direction limited by north-northwest faults.

Age of evaporite-related MVT deposits belt of Peru

Various authors proposed different mineralization ages for the MVT deposits of Peru, but there is no precisely geochronological data available so far for the main ore bodies. Fontbote and Gorzawski (1990) interpreted that the genesis of the pre-ore extensive dolomitization and the Zn–Pb sulfide mineralization in San Vicente deposit was formed in a single-stage event during burial diagenesis at the end of the Jurassic. Moritz et al. (1996), in their study on Shalipayco and San Vicente deposits, assumed that both MVT deposits are cogenetic and the ore-formation brine migration was driven by tectonic compression during the Incaic phase (40 Ma), through steeply dipping faults pumping fluids from the depth. A regional hydrothermal system with tectonic interconnected ore-fluid plumbing for the different MVT occurrences in the San Vicente area is also suggested by Spangenberg et al. (1999). Badoux et al. (2001) based on the San Vicente deposit location on Sub-Andean Zone and structural data, proposed that the San Vicente mineralization is syntectonic in origin and younger than Late Miocene Quechua 3 phase. Carlotto et al. (2009) assumed the Eocene to Miocene age to the MVT belt of Peru.

In the Bongará Province, Reid (2001) identified in the Maino and Florcita MVT occurrences areas, that the Zn–Pb mineralization occurred post-Cretaceous unconformity after the deposition of the sandstone of Goyllarizquisga Formation attributed to Lower Cretaceous (Valanginian-Aptian, Jacay, 2005). This would date the ore event as less than 80–70 Ma and therefore the author and Basuki et al. (2008) correlated the MVT mineralization in the Florida Canyon deposit and occurrences nearby to the Peruvian (Campanian) tectonic compressive event or younger.

Analytical Procedures

For Pb isotope analysis separates of ore sulfide minerals (galena and sphalerite) and Mitu Group (volcanoclastic) and Chambará Formation (limestones) whole-rock samples from Shalipayco and Florida Canyon deposits were carried out at Geochronological Research Center, University of São Paulo, Brazil. Galena and sphalerite crystals for Pb isotope analyses were selected by handpicking under a binocular microscope. Galena samples were leached and separated using standard cation-exchange procedures. The procedural blank for lead was 99 pg for Mitu Group samples and 43 pg for Chambará Formation samples. Lead isotope ratios were corrected relative to the values of the NBS-981 standard by: $^{206}Pb/^{204}Pb$ = 16.894 ±0.006; $^{207}Pb/^{204}Pb$ = 15.433 ±0.008 and $^{208}Pb/^{204}Pb$ = 36.516 ±0.025; value ± standard deviation (1σ).

For Rb–Sr isotope analysis, the Florida Canyon sphalerite samples were handpicked under a binocular microscope. Sphalerite Rb-Sr analytical procedures were modified from Nakai et al. (1990), Brannon et al. (1992), and Christensen et al. (1995). The analyses were performed in one sample (V_297-250.10-I) by stepwise leaching procedure, briefly described below, and in another three sphalerite separates (V_297-227.70-I; FC-17-198.70-I and V_329-167.20-I) by standard procedure (Nakai et al., 1990; Brannon et al., 1992; Christensen et al., 1995). The leaching sample was initially dissolved in 1 N HCl and the first leaching (L1) went to rubidium separation using standard cation exchange columns, and the residue to the second leaching stage (L2). In the subsequent leaching, the previous residue was attacked with 3 N HCl (L2) and then with 6 N HCl (L3), successively. All the leachates and the final residue were spiked with ^{87}Rb-^{84}Sr spikes. The procedural blank was 137 pg. The $^{87}Sr/^{86}Sr$ isotopic ratios were normalized to $^{87}Sr/^{86}Sr$ = 0.1144. During this study, the average measured $^{87}Sr/^{86}Sr$ ratio for NBS987 standard was 0.710239 ± 0.000016. Isotopic analyses were performed on a thermal ionization mass spectrometer (TIMS) Finnigan MAT 262.

Results

Rb-Sr Results

The results of Rb–Sr isotope analysis on the Florida Canyon deposit samples are presented in Table 3. All samples in $^{87}Rb/^{86}Sr$ vs. $^{87}Sr/^{86}Sr$ plot show a linear correlation but with a high scatter around the initial $^{87}Rb/^{86}Sr$ values and a high MSWD of 23 (model-3 fit of

Ludwig, 2012). This does not represent an isochron regression with geochronological meaning for the entire sample set a priori, indicating a mixing, a heterogeneous isotopic composition or both. Rb–Sr dating assumes that the sphalerite was formed from a homogeneous fluid and the system remained closed after its deposition. As previously discussed, the deposit of Florida Canyon does not present any indication that the ore-forming sphalerite has experienced any deformation or metamorphism after deposition. In some MVT deposits formed during the extensive dissolution of the host rocks and with the mixing of two or more fluids, an isotopic homogeneity may not occur (Brannon et al., 1996). In this case, the sphalerite isotopic composition could be heterogeneous because of incomplete mixing of diverse fluids (Brannon et al., 1996). Another problem that may occur in Rb–Sr dating on sphalerite is a natural contamination by small amounts of clays relatively rich in strontium (Brannon et al., 1996). The selected crystals of sphalerite from Florida Canyon are slow-growing euhedral crystals in open-space filling texture (De Oliveira et al., 2018) so with less likely to incorporate microscopic quantities of clay (Brannon et al., 1996). However, we do not have high-resolution images that safely discard this hypothesis. By the other hand, the previous S isotopic analyses for sphalerite from Florida Canyon ($\delta^{34}S$ = –2.8 to +6.8‰, De Oliveira et al. (2018) also characterize an isotopic heterogeneity in the mineralized system that could indicate an incomplete mixing of fluids (Brannon et al., 1996).

Table 3. Rb–Sr isotope analyses of sphalerite samples from Florida Canyon deposit.

Sample	Fractions	Rb (ppm)	Sr (ppm)	$^{87}Rb/^{86}Sr$	1σ	$^{87}Sr/^{86}Sr$	2σ
V_297-227.70-I	Total	0.09	2.48	0.11	0.001	0.710291	0.000181
FC-17-198.70-I	Total	1.21	15.98	0.22	0.005	0.709553	0.000240
V_329-167.20-I	Total	0.06	5.70	0.03	0.000	0.709476	0.000128
V_297-250.10-I	Total	0.77	9.66	0.23	0.003	0.710233	0.000071
	Leachate 1	0.32	75.11	0.01	0.002	0.709720	0.000274
	Leachate 2	0.69	62.05	0.03	0.001	0.710281	0.000118
	Leachate 3	0.33	7.96	0.12	0.001	0.710274	0.000117
	Residue	0.44	0.40	3.18	0.027	0.713957	0.000085

We thus adopt that the Sr isotopic composition in fluids during the time of mineralization was highly variable. Although there may be heterogeneity in the mineralized system, the Rb–Sr isotopic data can still bring some age indicators for the mineralization in the Florida Canyon MVT deposit. The samples are clustering into two groups (Fig. 5). The first cluster is defined by L1, V_329-167.20-I and FC-17-198.70-I samples, which present an isochron regression line with the Residue sample with a 0.70946 ±0.00056 initial $^{87}Sr/^{86}Sr$ value and age of 99.0 ±23 Ma (dashed line in Fig. 5). The second cluster considering the L2, L3, V_297-227.70-I and V_297-250.10-I samples presents an isochron regression line with the Residue sample with a

0.71012 ±0.00021 initial $^{87}Sr/^{86}Sr$ value and age of 84.7 ±9.9 Ma (continuous line in Fig. 5). The points near the origin are not collinear probably because in one of the sets must have the presence of solid inclusions of other minerals, such as apatite, clays, etc, that were not homogenized isotopically with the hydrothermal fluids during the formation of sphalerite..

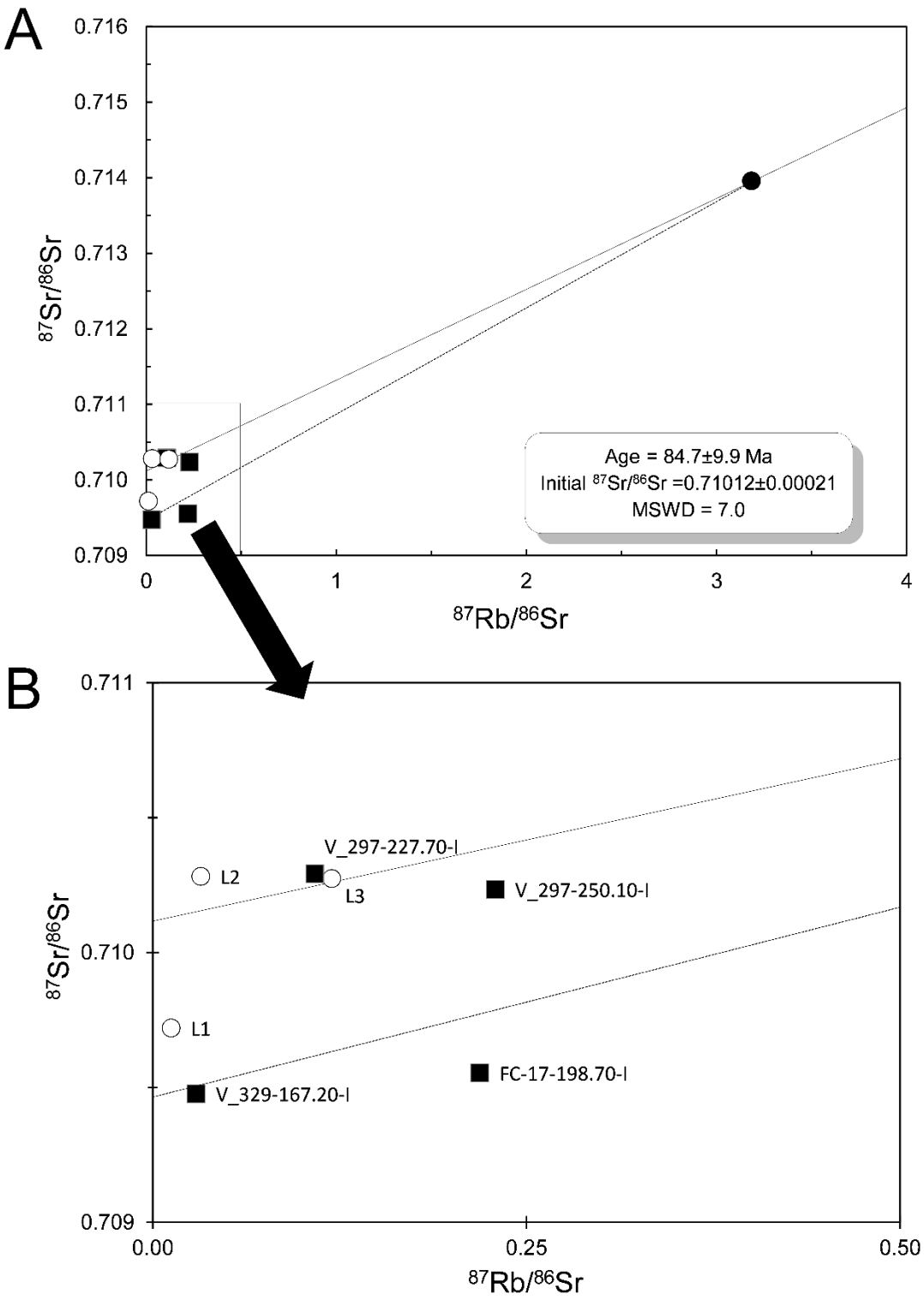

Fig. 5. . 87Rb/86Sr vs. 87Sr/86Sr diagram for sphalerite (sp I) samples from Florida Canyon deposit. The age was calculated from Table 3 data, discarding the samples L1, FC-17-198.70-I and V_329-167.20-I.

Pb-Pb Results

The Pb isotope analyses are reported in Table 4. A Stacey and Kramers (1975) model age considering galena and sphalerite samples from Florida Canyon is shown in Figure 6. Gunnesch et al. (1990) have determined lead isotope ratios of galena from San Vicente and Shalipayco (FYA-56 and FSH-19 samples, Table 4). Their data are compared to those for Florida Canyon and Shalipayco in Figure 7.

The $^{207}Pb/^{204}Pb$–$^{206}Pb/^{204}Pb$ galena (n = 5) and sphalerite (n = 3) data from Florida Canyon plot close to the Stacey and Kramers (1975) model Pb-growth curve and have a model age of 74 Ma (Fig. 6). This model age is in agreement with Rb–Sr geochronological age of 84.7 ±9.9 Ma, indicating a clustering of ages at 74–95 Ma for the Zn–Pb mineralization event in Florida Canyon MVT deposit.

The lead isotopes ratios of the three main evaporite-related MVT deposits in north-central Peru (San Vicente, Shalipayco and Florida Canyon) are characterized by radiogenic linear arrays that cross the standard lead evolution models (Fig. 7), which is typical for MVT deposits (Gulson, 1986). The vertical trends in the plumbotectonic diagram (Fig. 7) indicates heterogeneous Pb sources for the three MVT deposits, typical of Pb derived from sedimentary rocks, which are also heterogeneous. The three deposit have relatively high $^{207}Pb/^{204}Pb$ and $^{208}Pb/^{204}Pb$ ratios typical of the upper continental crust (Zartman and Doe, 1981). The Shalipayco and Florida Canyon galena and sphalerite samples overlap in the $^{207}Pb/^{204}Pb$ and $^{206}Pb/^{204}Pb$ graph (Fig. 7) and are distinct from the San Vicente data suggesting different source rocks. Unfortunately, there is no isotopic lead data available in the literature for host rocks or the basement of San Vicente deposit. Some Shalipayco and Florida Canyon data, which plot below the orogene curve (Fig. 7), probably indicate contamination of ore lead by upper crustal lead derived from the host-rock dolomite and from the Mitu Group basement rocks immediately below in stratigraphy. However, the largest data arrays for Shalipayco and Florida Canyon galenas and sphalerites indicate that the rocks of the Mitu Group would not be the unique metal sources but a mixture with other basement rocks.

Table 4. Pb isotope compositions of whole-rock and sulfide separate samples from Florida Canyon and Shalipayco deposits. All San Vicente and two Shalipayco galena sample data with a * are from Gunnesch et al. (1990).

Sample	Deposit	Mineral / Rock	$^{206}Pb/^{204}Pb$	2σ	$^{207}Pb/^{204}Pb$	2σ	$^{208}Pb/^{204}Pb$	2σ
V_46-284.40-N	Florida Canyon	Chambará Fm. limestone	18.852	0.007	15.658	0.006	38.699	0.016
V_46-589.40-N	Florida Canyon	Chambará Fm. limestone	18.806	0.006	15.653	0.006	38.673	0.018
V_46-665.05-N	Florida Canyon	Chambará Fm. limestone	18.973	0.005	15.663	0.005	38.676	0.015
SH-56-298,20-N	Shalipayco	Chambará Fm. limestone	18.718	0.010	15.739	0.010	38.911	0.027
SH-70-217,60-N	Shalipayco	Chambará Fm. limestone	18.779	0.029	15.649	0.025	38.557	0.060
SH-60-170,40-N	Shalipayco	Chambará Fm. limestone	19.138	0.006	15.664	0.006	38.556	0.021
V_46-737.80-M	Florida Canyon	Mitu Gp. volcanoclastic	18.842	0.007	15.663	0.007	38.853	0.019
V_46-738.80-M	Florida Canyon	Mitu Gp. volcanoclastic	23.075	0.010	15.883	0.009	39.148	0.029
V_46-748.50-M	Florida Canyon	Mitu Gp. volcanoclastic	18.677	0.006	15.638	0.005	39.140	0.012
SH-43-683.90-M	Shalipayco	Mitu Gp. volcanoclastic	18.803	0.008	15.656	0.007	38.894	0.020
SH-43-684.70-M	Shalipayco	Mitu Gp. volcanoclastic	18.837	0.008	15.669	0.007	38.865	0.019
SH-43-685.90-M	Shalipayco	Mitu Gp. volcanoclastic	18.797	0.006	15.662	0.007	38.830	0.020
V_297-227.70-I	Florida Canyon	Sphalerite	18.659	0.043	15.718	0.060	38.875	0.184
FC-17-198.70-I	Florida Canyon	Sphalerite	18.623	0.015	15.681	0.013	38.738	0.037
V_329-167.20-I	Florida Canyon	Sphalerite	18.680	0.023	15.694	0.023	38.819	0.074
V_329-165.60-K	Florida Canyon	Galena	18.611	0.014	15.642	0.016	38.639	0.052
FC-17-170.85-K	Florida Canyon	Galena	18.600	0.006	15.657	0.007	38.652	0.019
V_214-80.60-K	Florida Canyon	Galena	18.641	0.007	15.657	0.006	38.699	0.018
V_312-45.00-K	Florida Canyon	Galena	18.597	0.008	15.624	0.006	38.561	0.016
V_329-167.20-K	Florida Canyon	Galena	18.628	0.007	15.661	0.006	38.703	0.017
SH-43-221.70-K	Shalipayco	Galena	18.627	0.021	15.684	0.025	38.714	0.079
FYA-56*	Shalipayco	Galena	18.556		15.634		38.529	
FSH-19*	Shalipayco	Galena	18.572		15.662		38.630	
SV-M37*	San Vicente	Galena	19.260		15.741		39.348	
SV-M31*	San Vicente	Galena	19.246		15.716		39.502	
SV-M44*	San Vicente	Galena	19.228		15.687		39.346	
SV-5*	San Vicente	Galena	19.211		15.696		39.171	
SV-6*	San Vicente	Galena	19.211		15.690		39.150	
SV-1*	San Vicente	Galena	18.977		15.679		38.915	

Discussion

The mineralogy, textures and paragenesis of the three main deposits of the Peruvian evaporite-related MVT belt (San Vicente, Shalipayco and Florida Canyon) were recently studied, compared and discussed (De Oliveira et al., 2018; De Oliveira et al., in prep.). The authors assumed therefore that the same similar ore-forming processes occurred in the three deposits. In this section, these processes and structures in the evaporite-related MVT belt are organized in geologic time and correlated with the main tectonic events described in the Peruvian Andes (Steinmann, 1929; Mégard, 1984, 1987; Benavides-Cáceres, 1999; Jaillard et al., 2000; Pfiffner and Gonzalez, 2013) (Fig. 8).

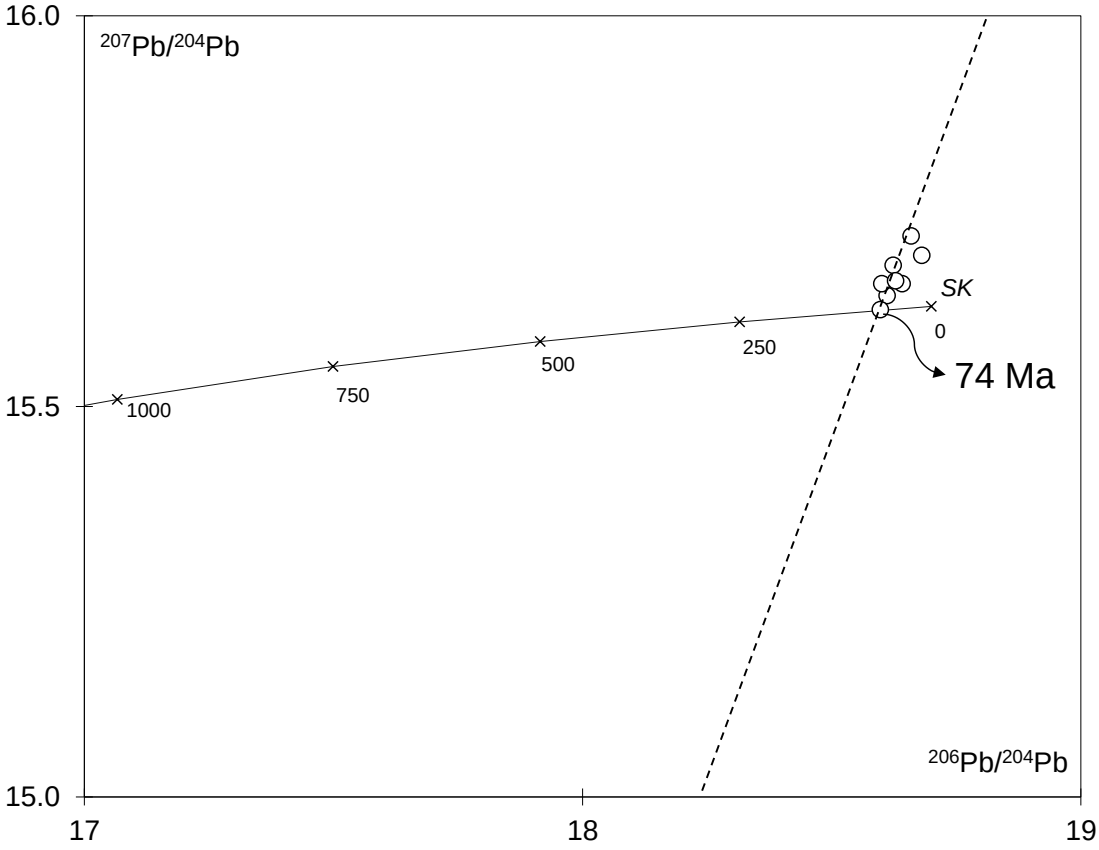

Fig. 6. 207Pb/204Pb vs. 206Pb/204Pb diagram showing Stacey and Kramers (1975) model age isochron (SK) for Florida Canyon sphalerite and galena samples.

The carbonate and former evaporite sequence of Pucará Group age is attributed to the Upper Triassic and Lower Jurassic, based on Chambará Formation fossils assign to Norian (Sánchez, 1995) and precise $^{206}Pb/^{238}U$ zircon ages of 201.58 ±0.17 Ma (Rhetian–Hettangian) from volcanic ash layers within Aramachay Formation (Schaltegger et al., 2008).

After deposition, the Pucará rocks have undergone an interval of relative tectonic quiescence lasting about 50 Ma until the Juruá Orogeny (Caputo, 2014). The precipitation of

early diagenetic dolomite and calcite veins described in Florida Canyon deposit (De Oliveira et al., 2018) could be attributed to this period. Mathalone and Montoya (1995) interpreted the earliest Cretaceous (Nevadan/Juruá Orogeny) structures of Pucará base thrusting to the southwest based on seismic data as formed by salt movement. The dome structure defined on the Florida Canyon deposit is also interpreted as the product of salt movement from evaporite sabkha facies on Chambará Formation (De Oliveira et al., 2018) or from the evaporite levels from Mitu Group (Petersen, 1965; Benavides, 1968). The evaporite presence as thick saline beds has a favorability to serve as incompetent or lubricating layers to décollements and fold-thrust structures during Andean thrust (Petersen, 1965; Mégard, 1987). The salt movement would be related to Juruá Orogeny because this is the first tectonic event after its deposition, but prior non-tectonic salt movement during the initial diagenesis should not be ruled out.

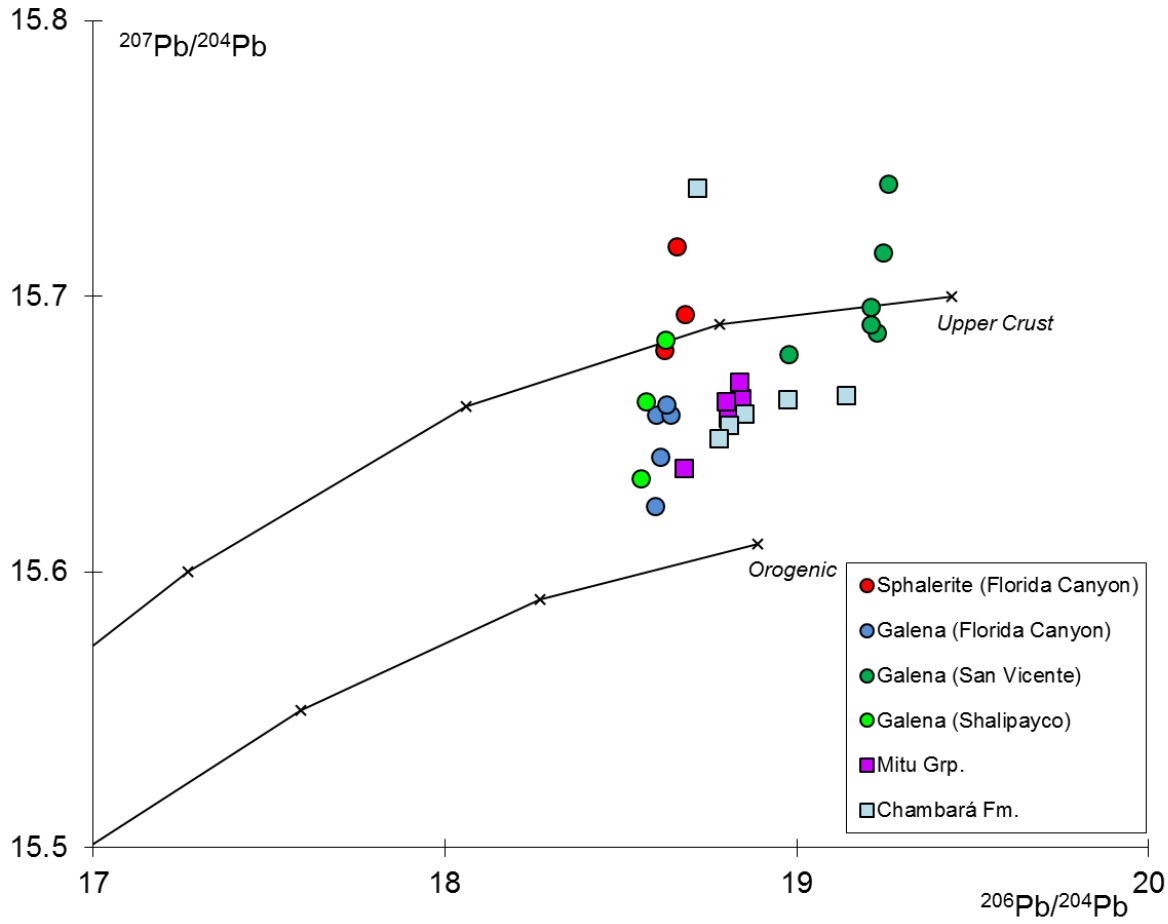

Fig. 7. 207Pb/204Pb vs. 206Pb/204Pb diagram with lead isotope compositions of galena ore from Florida Canyon, Shalipayco and San Vicente deposits compared with those of Pucará carbonate host rocks and potential metal source rocks of Mitu, along with the evolution curves for upper crust and orogenic reservoirs from Zartman and Doe (1981). Galena data of San Vicente deposit and two galena samples of Shalipayco from Gunnesch et al. (1990).

After the Juruá thrusting and the deposition of continental sediments overlying the Pucará sequence at the end of Jurassic a burial depth about 2 to 3.5 km possibly may have been reached (Fontbote and Gorzawski, 1990). This burial condition would generate a geothermal gradient with temperatures about 50–100 °C that is consistent with the oil generation and replacement of calcium sulfate (gypsum) by sparry dolomite in the presence of organic matter (Anderson and Garven, 1987). The origin of burial diagenetic dolomite that comprises the evaporite breccias and porous dolostone and the calcite after evaporite pseudomorphs described in Florida Canyon (De Oliveira et al., 2018) and Shalipayco (De Oliveira et al., in prep.) could be correlated to this second period of quiescence between the end of Juruá stage (157–152 Ma) and the beginning of the Mochica stage (100–95 Ma).

The black shales from Aramachay Formation have been identified as an oil source rock by many authors (Fontbote and Gorzawski, 1990; Mathalone and Montoya, 1995; Klein et al., 2011; Eude et al., 2015). The bitumen identified in the porous and interstices of evaporite breccia and porous dolostone from sabkha facies of Chambará Formation (stratigraphically below Aramachay Formation) are paragenetically after these rocks formation and before the Zn–Pb sulfide ore in Florida Canyon and Shalipayco deposits (De Oliveira et al., 2018; De Oliveira et al., in prep.). In the San Vicente deposit, the bitumen generation is interpreted after sphalerite and galena precipitation (Fontbote and Gorzawski, 1990; Spangenberg et al., 1999). An alternative oil source rock that could generate the bitumen in Chambará Formation stratigraphically below the Pucará sequence is the Copacabana Formation (Mathalone and Montoya, 1995; Sempere et al., 2002; Eude et al., 2015). Tectonic movements and basin uplift probably promoted the hydrocarbon migration. A probable tectonic stage for the oil and gas migration was the Mochica Orogeny because this is the first compression event after the generation of porous dolostone and evaporite breccia rocks with the presence of bitumen filling porous present in the Florida Canyon and Shalipayco deposits.

The ore textures in evaporite breccia and evaporite breccia in Florida Canyon and Shalipayco show the precipitation of sphalerite and galena filing porous and open spaces after bitumen (De Oliveira et al., 2018; De Oliveira et al., in prep.). The metalliferous brine migration should happen after Mochica event. The distribution of zinc and lead sum in the Florida Canyon and Shalipayco deposits follow a structural pattern. The high grades are related to north secondary structures generated from primary dextral north-northwest strike-slip structures (Fig. 3). These secondary structures are steeply dipping faults with distentional perpendicular component, equivalent to the T-fractures from Riedel's clay model (Petit, 1987; Fossen, 2016),

that allowed the upraise of metal-bearing brines from Mitu Group rocks or even basement rocks. The Mitu Group rocks are likely sources of radiogenic lead (Fig. 7) and radiogenic strontium for Zn-–Pb mineralization in Shalipayco and Florida Canyon as discussed by De Oliveira et al. (2018); De Oliveira et al. (in prep.). The northwestern strike-slip motion was generated over pre-existing thrusting faults and the secondary northern structures immediately after in a subsequent stage of structural accommodation. Mégard (1984) suggests the possibility of strike-slip motion along faults sub-parallel to the trench should be considered during Triassic to early Cretaceous although the strain regime was dominantly extensional. Strike-slip structures are also described in other Andean portions (Cembrano et al., 2002; Ramos, 2010). The strike-slip faulting results in fault jog formation and the resulting rupture-related dilation will instantaneously reduce pressure to such an extent that a fluid could move (Robb, 2004).

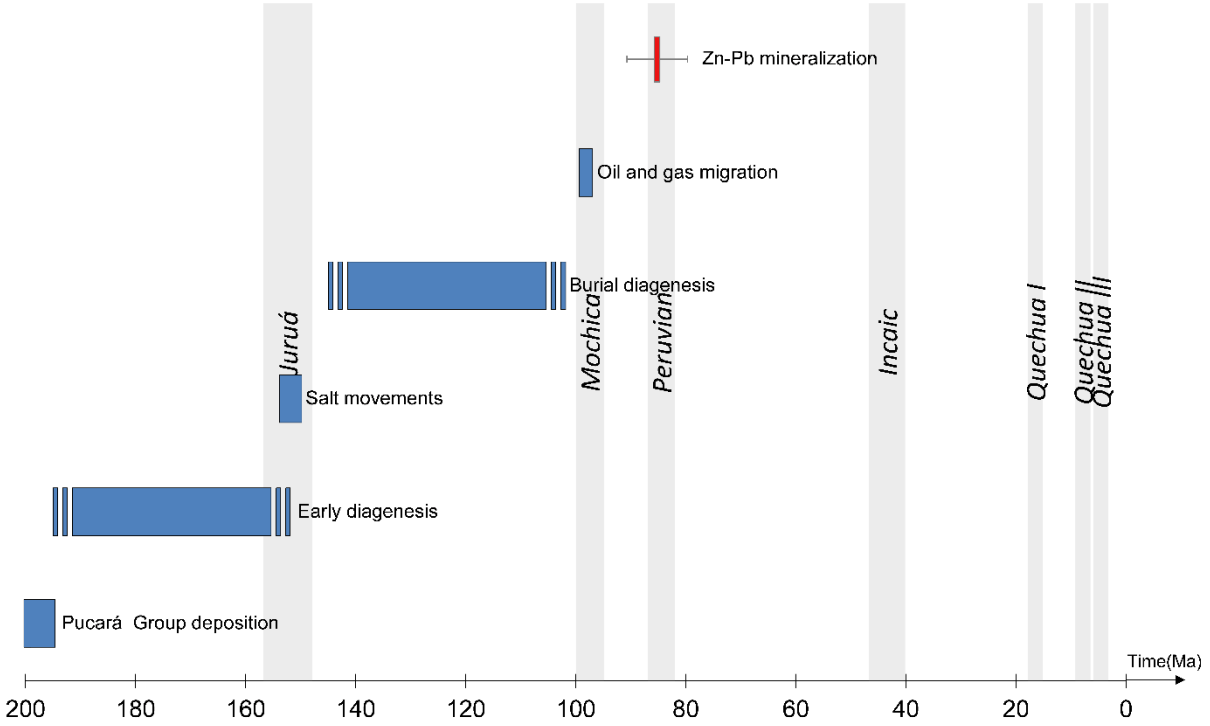

Fig. 8. Timeframe for the evaporite-related MVT Zn–Pb mineralizations (85 Ma) hosted in the Pucará Group rocks with the Andean tectonic deformation evolution main stages in north-central Peru.

The 84.7 ±9.9 Ma age obtained from Rb–Sr analysis in sphalerite and the Pb–Pb model age of 74 Ma for galena from Florida Canyon deposit is consistent with this interpretation of ore precipitation at end of Peruvian Orogeny (86–83 Ma). The Santonian age is also concordant with the fields observations of Reid (2001) that describe MVT ore mineralization occurring after Lower Cretaceous Goyllarizquisga Formation deposition.

Concluding Remarks

1. The MVT Zn–Pb deposits of Shalipayco, Florida Canyon and San Vicente present similar lithologies, stratigraphy, mineralogy, paragenesis and structural control, so, we assume that the processes of rock formation and mineralization genesis were the same in these deposits.

2. The structural control of the Shalipayco and Florida Canyon MVT Zn–Pb deposits is conditioned by deep sub-vertical secondary extension structures with general N, NNE or NNW direction related to strike-slip movements superimposed on previous Andean NW thrust structures.

3. The dome structure from Florida Canyon interpreted as the product of salt movement from evaporite levels from Pucará and Mitu Groups acting as incompetent or lubricating layers to décollements during Juruá Orogeny (157–152 Ma).

4. The genesis of ground preparations stage of dolomitization forming the porous dolostone and evaporite breccia during burial diagenesis is attributed to the period between Juruá and Mochica stages. The oil migration to these reservoir rocks occurred probably during Mochica event (100–95 Ma).

5. The Rb–Sr analysis of sphalerite from the Florida Canyon deposit together with temporal relations observed in the field reveal that the sphalerite ore formed in or just after Santonian time during Peruvian Orogeny (86–83 Ma).

References

Anderson, G.M., Garven, G., 1987. Sulfate-sulfide-carbonate associations in Mississippi Valley-type lead-zinc deposits. Economic Geology 82, 482-488.

Badoux, V., Moritz, R., Fontboté, L., 2001. The Mississippi Valley-type Zn-Pb deposit of San Vicente, Central Peru: an Andean syntectonic deposit. Mineral deposits at the beginning of the 21th Century. Proceed Joint 6th Biennial SGA-SEG Mtg, Krakow, Poland, 191-195.

Basuki, N.I., Taylor, B.E., Spooner, E.T.C., 2008. Sulfur isotope evidence for thermochemical reduction of dissolved sulfate in Mississippi Valley-type zinc-lead mineralization, Bongara area, northern Peru. Economic Geology 103, 783-799.

Benavides-Cáceres, V., 1999. Orogenic evolution of the Peruvian Andes: the Andean cycle. Geology and ore deposits of the Central Andes 7, 61-107.
Benavides, V., 1968. Saline deposits of South America, International Conference on Saline Deposits, pp. 249-290.
Bradley, D.C., Leach, D.L., 2003. Tectonic controls of Mississippi Valley-type lead-zinc mineralization in orogenic forelands. Mineralium Deposita 38, 652-667.
Brannon, J., Podosek, F., Cole, S., 1996. Radiometric dating of Mississippi Valley-type ore deposits. Carbonate-hosted lead-zinc deposits: SEG special volume 4, 536-545.
Brannon, J.C., Podosek, F.A., McLimans, R.K., 1992. Alleghenian age of the Upper Mississippi Valley zinc–lead deposit determined by Rb–Sr dating of sphalerite. Nature 356, 509.
Bump, A., Kennan, L., Fallon, J., 2008. Structural history of the Andean foreland, Peru, and its relation to subduction zone dynamics, American Association of Petroleum Geologists Annual Convention and Exhibition: San Antonio, Texas, American Association of Petroleum Geologists, search and discovery article.
Caputo, M.V., 2014. Juruá Orogeny: Brazil and Andean Countries. Brazilian Journal of Geology 44, 181-190.
Carlotto, V., Quispe, J., Acosta, H., Rodríguez, R., Romero, D., Cerpa, L., Mamani, M., Díaz-Martínez, E., Navarro, P., Jaimes, F., 2009. Dominios geotectónicos y metalogénesis del Perú. Boletín de la Sociedad Geológica del Perú 103, 1-89.
Cembrano, J., Lavenu, A., Reynolds, P., Arancibia, G., López, G., Sanhueza, A., 2002. Late Cenozoic transpressional ductile deformation north of the Nazca–South America–Antarctica triple junction. Tectonophysics 354, 289-314.
Christensen, J.N., Halliday, A.N., Leigh, K.E., Randell, R.N., Kesler, S.E., 1995. Direct dating of sulfides by Rb-Sr: A critical test using the Polaris Mississippi Valley-type Zn-Pb deposit. Geochimica et Cosmochimica Acta 59, 5191-5197.
Cox, S., 2010. The application of failure mode diagrams for exploring the roles of fluid pressure and stress states in controlling styles of fracture-controlled permeability enhancement in faults and shear zones. Geofluids 10, 217-233.
Dávila, D., Febres, O., Fontboté, L., Oldham, L., 2000. Exploración y geología del yacimiento San Vicente, Yacimientos minerales peruanos, Primer volumen de monografias. Instituto Ingenieros de Minas del Perú, Lima, pp., p. 305-328.
De Oliveira, S.B., Leach, D.L., Juliani, C., Monteiro, L.V.S., Johnson, C.A., 2018. The Zn–Pb mineralization of the Florida Canyon, an evaporite-related Mississippi Valley-type deposit in the Bongará District, Northern Peru. Economic Geology, under review.
De Oliveira, S.B., Leach, D.L., Juliani, C., Monteiro, L.V.S., Johnson, C.A., Caran, M.G.N., in prep. Geology and Genesis of the Shalipayco evaporite-related Mississippi Valley-Type Zn–Pb deposit, Central Peru: geological and C–O–S isotopic constraints. Mineralium Deposita.
Elias, A.D., De Ros, L.F., Mizusaki, A.M., Kawashita, K., 2007. Isotopic evidence on the diagenetic evolution of coastal sabkha reservoirs from the Solimões Basin, northern Brazil. Gondwana Research 11, 553-567.
Eude, A., Roddaz, M., Brichau, S., Brusset, S., Calderon, Y., Baby, P., Soula, J.-C., 2015. Controls on timing of exhumation and deformation in the northern Peruvian eastern Andean wedge as inferred from low-temperature thermochronology and balanced cross section. Tectonics 34, 715-730.
Fernández, F., Both, R., Mangas, J., Arribas, A., 2000. Metallogenesis of Zn-Pb carbonate-hosted mineralization in the southeastern region of the Picos de Europa (central northern Spain) province: geologic, fluid inclusion, and stable isotope studies. Economic Geology 95, 19-40.

Fontbote, L., Gorzawski, H., 1990. Genesis of the Mississippi Valley-type Zn-Pb deposit of San Vicente, central Peru; geologic and isotopic (Sr, O, C, S, Pb) evidence. Economic Geology 85, 1402-1437.

Fossen, H., 2016. Structural geology. Cambridge University Press.

Gulson, B.L., 1986. Lead isotope in mineral exploration. Elsevier, Netherlands.

Gunnesch, K.A., Baumann, A., Gunnesch, M., 1990. Lead isotope variations across the central Peruvian Andes. Economic Geology 85, 1384-1401.

Hermoza, W., Brusset, S., Baby, P., Gil, W., Roddaz, M., Guerrero, N., Bolaños, R., 2005. The Huallaga foreland basin evolution: Thrust propagation in a deltaic environment, northern Peruvian Andes. Journal of South American Earth Sciences 19, 21-34.

Jacay, J., 2005. Análisis de la sedimentación del sistema cretáceo de los Andes del Perú Central. Revista del Instituto de Investigación de la Facultad de Ingeniería Geológica, Minera, Metalurgica y Geográfica 8, 49-59.

Jaillard, E., Hérail, G., Monfret, T., Díaz-Martínez, E., Baby, P., Lavenu, A., Dumont, J.F., 2000. Tectonic evolution of the Andes of Ecuador, Peru, Bolivia and northernmost Chile, Tectonic Evolution of South America. 31st International Geological Congress, Publications Rio de Janeiro, pp. 481-559.

Klein, G.D., Zúñiga y Rivero, F.G., Hay-Roe, H., Alvarez-Calderon, E., 2011. A Reappraisal of the Mesozoic/Cenozoic Tectonics and Sedimentary Basins of Peru. Search and Discover Article (AAPG); AAPG/Datapages, Inc.: Tulsa, OK, USA.

Leach, D., Song, Y., 2018. Sediment-hosted zinc-lead and copper deposits in China, In: Chang, Z., Goldfarb, R. (Eds.), Mineral deposits of China, p. in press.

Leach, D.L., Bradley, D.C., Huston, D., Pisarevsky, S.A., Taylor, R.D., Gardoll, S.J., 2010. Sediment-hosted lead-zinc deposits in Earth history. Economic Geology 105, 593-625.

Leach, D.L., Sangster, D.F., Kelley, K.D., Ross, R.L., Garven, G., Allen, C.R., 2005. Sediment-hosted Pb-Zn deposits: a global perspective. Economic Geology 100, 561-608.

Loughman, D.L., Hallam, A., 1982. A facies analysis of the Pucara Group (Norian to Toarcian carbonates, organic-rich shale and phosphate) of central and northern Peru. Sedimentary Geology 32, 161-194.

Ludwig, K., 2012. User's manual for Isoplot version 3.75–4.15: a geochronological toolkit for Microsoft. Excel Berkley Geochronological Center Special Publication.

Mathalone, J.M.P., Montoya, M.R., 1995. Petroleum geology of the sub-Andean basins of Peru, In: Tankard, A.J., Suarez Soruco, R., Welsink, H.J. (Eds.), Petroleum Basins of South America. AAPG Special Volumes, pp. 423-424.

Mégard, F., 1978. Etude géologique des Andes du Pérou central: contribution à l'étude géologique des Andes n 1. Institut français d'études andines, Paris.

Mégard, F., 1984. The Andean orogenic period and its major structures in central and northern Peru. Journal of the Geological Society 141, 893-900.

Mégard, F., 1987. Structure and evolution of the Peruvian Andes, In: Schaer, J.P., Rodgers, J. (Eds.), The Anatomy of Mountain Ranges. Princeton University, Princeton, New Jersey, United States, pp. 179-210.

Moritz, R., Fontboté, L., Spangenberg, J., Rosas, S., Sharp, Z., Fontignie, D., 1996. Sr, C and O isotope systematics in the Pucará basin, central Peru. Mineralium Deposita 31, 147-162.

Mukasa, S.B., 1986. Zircon U-Pb ages of super-units in the Coastal batholith, Peru: Implications for magmatic and tectonic processes. Geological Society of America Bulletin 97, 241-254.

Nakai, S.i., Halliday, A.N., Kesler, S.E., Jones, H.D., 1990. Rb–Sr dating of sphalerites from Tennessee and the genesis of Mississippi Valley-type ore deposits. Nature 346, 354.

Noble, D.C., McKee, E.H., MÉGard, F., 1979. Early Tertiary "Incaic" tectonism, uplift, and volcanic activity, Andes of central Peru. Geological Society of America Bulletin 90.
Noble, D.C., Silberman, M.L., Megard, F., Bowman, H.P., 1978. Comendite (peralkaline rhyolite) and basalt in the Mitu Group, Peru: evidence for Permian-Triassic lithospheric extension in the central Andes. US Geological Survey Journal of Research 6, 453-457.
Palacios, O., 1995. Geología del Perú. Dirección de Geología Regional (INGEMMET). Carta Geológica Nacional, INGEMMET, Perú. Boletín 55, 156.
Petersen, U., 1965. Regional geology and major ore deposits of central Peru. Economic Geology 60, 407-476.
Petit, J.P., 1987. Criteria for the sense of movement on fault surfaces in brittle rocks. Journal of Structural Geology 9, 597-608.
Pfiffner, O., Gonzalez, L., 2013. Mesozoic–Cenozoic evolution of the Western margin of South America: case study of the Peruvian Andes. Geosciences 3, 262-310.
Ramos, V.A., 2010. The tectonic regime along the Andes: Present-day and Mesozoic regimes. Geological Journal 45, 2-25.
Reid, C.J., 2001. Stratigraphy and mineralization of the Bongara MVT zinc-lead district, northern Peru. University of Toronto, Toronto, Canada, p. 179.
Robb, L., 2004. Introduction to ore-forming processes. Blackwell publishing.
Rosas, S., Fontboté, L., Tankard, A., 2007. Tectonic evolution and paleogeography of the Mesozoic Pucará Basin, central Peru. Journal of South American Earth Sciences 24, 1-24.
Sánchez, A., 1995. Geología de los cuadrángulos de Bagua Grande, Jumbilla, Lonya Grande, Chachapoyas, Rioja, Leimebamba y Bolívar: hojas 12-g, 12-h, 13-g, 13-h, 13-i, 14-hy 15-h. Instituto Geológico Minero y Metalúrgico Peru.
Schaltegger, U., Guex, J., Bartolini, A., Schoene, B., Ovtcharova, M., 2008. Precise U–Pb age constraints for end-Triassic mass extinction, its correlation to volcanism and Hettangian post-extinction recovery. Earth and Planetary Science Letters 267, 266-275.
Scherrenberg, A.F., Holcombe, R.J., Rosenbaum, G., 2014. The persistence and role of basin structures on the 3D architecture of the Marañón Fold-Thrust Belt, Peru. Journal of South American Earth Sciences 51, 45-58.
Scherrenberg, A.F., Jacay, J., Holcombe, R.J., Rosenbaum, G., 2012. Stratigraphic variations across the Marañón Fold-Thrust Belt, Peru: Implications for the basin architecture of the West Peruvian Trough. Journal of South American Earth Sciences 38, 147-158.
Sempere, T., Carlier, G., Carlotto, V., Jacay, J., Jiménez, N., Rosas, S., Soler, P., Cárdenas, J., Boudesseul, N., 1999. Late Permian-early Mesozoic rifts in Peru and Bolivia, and their bearing on Andean-age tectonics, IV International Symposium on Andean Geodynamics, Göttingen, Abstracts, pp. 680-685.
Sempere, T., Carlier, G., Soler, P., Fornari, M., Carlotto, V.c., Jacay, J., Arispe, O., Néraudeau, D., Cárdenas, J., Rosas, S., Jiménez, N., 2002. Late Permian–Middle Jurassic lithospheric thinning in Peru and Bolivia, and its bearing on Andean-age tectonics. Tectonophysics 345, 153-181.
Silver, P.G., Russo, R.M., Lithgow-Bertelloni, C., 1998. Coupling of South American and African plate motion and plate deformation. Science 279, 60-63.
Smethurst, M., Sangster, D., Symons, D., Lewchuk, M., 1999. Paleomagnetic age for Zn-Pb mineralization at Robb Lake, northeastern British Columbia. Bulletin of Canadian Petroleum Geology 47, 548-555.
Spangenberg, J., Fontboté, L., Sharp, Z.D., Hunziker, J., 1996. Carbon and oxygen isotope study of hydrothermal carbonates in the zinc-lead deposits of the San Vicente district, central Peru: a quantitative modeling on mixing processes and CO_2 degassing. Chemical Geology 133, 289-315.

Spangenberg, J.E., Fontboté, L., Macko, S.A., 1999. An evaluation of the inorganic and organic geochemistry of the San Vicente Mississippi Valley-type zinc-lead district, central Peru; implications for ore fluid composition, mixing processes, and sulfate reduction. Economic Geology 94, 1067-1092.

Stacey, J.t., Kramers, J., 1975. Approximation of terrestrial lead isotope evolution by a two-stage model. Earth and planetary science letters 26, 207-221.

Steinmann, G., 1929. Geologie von Peru, 448 pp. Carl Winters Universitätsbuchhandlung.

Szekely, T.S., Grose, L.T., 1972. Stratigraphy of the carbonate, black shale, and phosphate of the Pucará Group (Upper Triassic—Lower Jurassic), Central Andes, Peru. Geological Society of America Bulletin 83, 407-428.

Wise, J.M., Noble, D.C., Zanetti, K.A., Spell, T.L., 2008. Quechua II contraction in the Ayacucho intermontane basin: Evidence for rapid and episodic Neogene deformation in the Andes of central Perú. Journal of South American Earth Sciences 26, 383-396.

Zartman, R., Doe, B., 1981. Plumbotectonics—the model. Tectonophysics 75, 135-162.

.

6 Discussões e Conclusões Finais

A presente tese em linhas gerais teve como principal objetivo melhor compreender a geologia e gênese dos depósitos de Zn–Pb de Florida Canyon e Shalipayco, e pode-se afirmar que tal resultado foi alcançado, gerando novas contribuições e interpretações para a formação desta classe de depósitos hidrotermais de metais base.

Algumas das perguntas inicialmente propostas foram respondidas e as hipóteses colocadas no início desta tese foram testadas. A seguir são resumidas as conclusões alcançadas com o estudo de cada um dos dois depósitos separadamente em escala local em um primeiro momento, e depois em escala regional analisando-se o cinturão de depósitos MVT peruano como um todo.

Para o depósito Florida Canyon:

– A mineralização sulfetada no depósito de Florida Canyon apresenta um controle estrutural principal dado por um domo definido por sondagem e apresenta dois diferentes estilos: i) um primeiro predominantemente *stratabound* hospedado em dolomitos porosos e brechas de dissolução evaporíticas, que acompanham a estrutura dômica, e ii) um segundo, discordante das camadas e de mais alto teor de Zn e Pb, associado a brechas evaporíticas diapíricas.

– A distribuição de teores dentro da estrutura dômica está associada a falhas de alto ângulo secundárias de direção N–NE delimitadas por falhas de cavalgamento regionais andinas de direção geral NW.

– Antes da mineralização, a diagênese das rochas da plataforma carbonática e evaporítica da sequência de Pucará desempenhou um papel fundamental condicionando onde iria ocorrer a precipitação dos sulfetos de Zn e Pb. A diagênese das rochas carbonáticas e evaporíticas iniciais produziu novas fases de carbonatos, modificou e criou novas vias de circulação de fluidos e gerou armadilhas estruturais e de hidrocarbonetos que determinaram onde o depósito mineral se formou.

– As fases de carbonatos diagenéticos são muito mais abundantes do que fases mais tardias associadas a mineralização sendo distinguíveis através das assinaturas isotópicas de Sr e imagens de catodoluminescência. Dolomita e calcita diagenéticas ocorrem predominantemente em texturas de substituição enquanto que dolomita hidrotermal associada a esfalerita e galena ocorre principalmente em texturas de preenchimento de espaços vazios.

– A mineralização sulfetada de Zn e Pb é posterior a migração de hidrocarbonetos. Esfalerita e galena preenchem poros que anteriormente foram preenchidos por hidrocarbonetos, atualmente betume.

– No depósito de Florida Canyon são encontradas diversas evidências de evaporitos pretéritos, totalmente substituídos e/ou transformados, tais como texturas de pseudomorfos de minerais evaporíticos (gipsita e halita), brechas de dissolução evaporíticas e dolomitos porosos. Estruturas como o próprio domo que define o depósito e corpos de minério subverticais sugerem movimentação de sal (halocinese) anterior a formação da mineralização sulfetada, durante a diagênese inicial e de soterramento.

– A mineralogia não-sulfetada em Florida Canyon consiste em smithsonita (principalmente), hemimorfita, cerussita e goethita. A gênese desta mineralização está associada com falhas de pequeno rejeito que permitiram a circulação de água meteórica atingindo profundidades de centenas de metros, oxidando a mineralização hipogênica sulfetada em substituição direta. A assembleia mineralógica supergênica é um indicador paleoclimático sugerindo clima úmido durante sua formação. Em analogia ao depósito de Zn não-sulfetado Cristal, localizado também no Distrito de Bongará, a idade do Mioceno Superior é atribuída a mineralização supergênica de Florida Canyon.

Para o depósito de Shalipayco:

– O depósito Shalipayco apresenta uma compartimentação estratigráfica muito semelhante à do depósito Florida Canyon, também hospedado na Formação Chambará, destacando-se horizontes com mesmas características pré-mineralização, como brecha evaporítica, dolomito poroso e pseudomorfos de minerais evaporíticos.

– As mineralizações de Zn–Pb de Shalipayco apresentam diversas características comuns a depósitos MVT, sendo claramente epigenéticas, morfologia *stratabound*, mineralogia simples com esfalerita, galena e pirita, e composições isotópicas de chumbo e enxofre indicando fontes crustais.

– O depósito de Shalipayco encontra-se geograficamente localizado em um distrito com diversos outros depósitos com associação magmática hospedados nas rochas do Grupo Pucará, como os depósitos *skarn* de Atacocha e Milpo, e epitermais de Cerro Pasco, Colquijirca e Morococha, levando a hipótese de uma origem do tipo *carbonate-replacement* (CRD). Depósitos CRD apresentam muitas semelhanças com depósitos MVT, no entanto, as principais diferenças são altas temperaturas e fonte magmática de fluidos e do enxofre. Os dados de

isótopos de enxofre em sulfetos ($\delta^{34}S$ = –23,3 a –6,2‰) e isótopos de carbono e oxigênio em dolomita esparítica associada a mineralização ($\delta^{13}C$ = –0,1 a +1,6‰ e $\delta^{18}O$ = +17,5 a +25,3‰) não corroboram essa hipótese não coincidindo com fontes de fluido derivados da consolidação de magmas. As assinaturas isotópicas de carbono, oxigênio e chumbo dos depósitos hidrotermais próximos com associação magmática como Cerro Pasco, Morococha, Atacocha e El Porvenir também são distintas dos valores obtidos para Shalipayco, que são mais próximos dos valores de depósitos MVT de San Vicente e Florida Canyon. Indicadores de temperatura de inclusões fluidas e geotermômetros de isótopos de enxofre obtidos para Shalipayco (<160 ºC) não indicam altas temperaturas típicas de depósitos CRD (200 ° a 500 °C), mas sim de depósitos MVT (90 ° a 180 °C).

– A ocorrência sulfetada denominada Veta Eddy, associada a um sistema de falhas NW que limita o depósito de Shalipayco em sua porção sul, apresenta assinatura geoquímica de elementos traço distinta, com valores relativamente elevados de Ag, As, Cd, Cu, Hg e Sb, o que sugere uma associação distal com sistemas tipo epitermais. No entanto, estudos específicos direcionados a esta ocorrência não-econômica devem ser conduzidos para confirmar esta hipótese.

Para o cinturão de depósitos MVT hospedados no Grupo Pucará.

– Os depósitos MVT de Zn–Pb de Florida Canyon, Shalipayco e San Vicente apresentam semelhanças quanto a litologia, mineralogia, estratigrafia, paragênese e controle estrutural, assim, assume-se que os processos de formação das rochas hospedeiras e da mineralização foram os mesmos nestes depósitos.

– O controle estrutural dos depósitos de Shalipayco e Florida Canyon é condicionado por estruturas extensionais secundárias sub-verticais com direção N, NNE e NNW, prévias a mineralização, relacionadas a movimentos *strike-slip* posteriores a estruturação geral andina de falhas de empurrão de direção geral NW.

– A estrutura dômica do depósito Florida Canyon é interpretada como produto de movimentos de sal de níveis evaporíticos do Grupo Pucará e do Grupo Mitu, que atuaram como níveis incompetentes e plásticos que permitiram a movimentação de camadas superiores durante a orogênese Juruá (157–152 Ma).

– A gênese do estágio pré-mineralização de dolomitização que formou brechas evaporíticas e dolomito poroso durante diagênese de soterramento é atribuído ao período entre

orogêneses Juruá e Mochica. A migração de óleo para estas rochas reservatórios ocorreu provavelmente durante o evento Mochica (100–95 Ma).

– As análises de Rb–Sr em esfalerita do depósito Florida Canyon, conjuntamente com relações temporais de campo revelam que a mineralização de Zn e Pb se formou durante ou logo após o Santoniano durante a orogênese Peruvian (86–83 Ma).